

Copyright
By
Gun Up Kwon
2008

**The Dissertation Committee for Gun Up Kwon certifies that this is the approved
version of the following dissertation:**

**Strengthening Existing Steel Bridge Girders
by the Use of Post-Installed Shear Connectors**

Committee:

Michael D. Engelhardt, Supervisor

Richard E. Klingner, Co-Supervisor

Karl H. Frank

John L. Tassoulas

Stelios Kyriakides

**Strengthening Existing Steel Bridge Girders
by the Use of Post-Installed Shear Connectors**

by

Gun Up Kwon, B.S., M.S.

Dissertation

Presented to the Faculty of the Graduate School of

The University of Texas at Austin

in Partial Fulfillment

of the Requirements

for the Degree of

Doctor of Philosophy

The University of Texas at Austin

December 2008

Dedication

To my father and mother,
for their constant support of my dream, and
to Yanghyun,
for her unconditional support and love.

Acknowledgements

First of all, I would like to express my deep gratitude to my academic advisors Prof. Michael D. Engelhardt and Prof. Richard E. Klingner, for their guidance, support, patience, and encouragement throughout this research study. I also thank Jon Kilgore, Clara Carbajal, and Joseph Rohmer at the Texas Department of Transportation for their financial support and technical assistance. I must also extend my gratitude to Hulya Kayir for her immense assistance in this research project.

The experimental work conducted in the Phil M. Ferguson Structural Engineering Laboratory would not have been possible without the help of the laboratory staff: Blake Stasney, Dennis Phillip, Eric Schell, Mike Wason, Barbara Howard, Ella Schwartz, and Cari Billingsley. I would also like to thank Lauren Morton, Ty Womble, and Austin Evetts for their assistance in the laboratory.

I consider myself to be a very lucky person to have been associated with such a great program at the University of Texas at Austin. I would like to thank Professors, Karl H. Frank, Todd Helwig, James O. Jirsa, Loukas F. Kallivokas, Lance Manuel, John L. Tassoulas, Eric B. Williamson, Sharon L. Wood, Oguzhan Bayrak, Stelios Kyriakides, Krishnaswa Ravi-Chandar, and Clint N. Dawson for providing me with a solid background in structural engineering. I also thank Prof. Sang Whan Han, Dr. Sungjin Bae, and Dr. Oh-Sung Kwon for their encouragement to come to the U.S. Most of all, I thank my friends in the U.S. as well as in Korea for their support from start to finish.

December, 2008

Gun Up Kwon

**Strengthening Existing Steel Bridge Girders
by the Use of Post-Installed Shear connectors**

Publication No. _____

Gun Up Kwon, Ph.D.

The University of Texas at Austin, 2008

Supervisor: Michael D. Engelhardt

Co-Supervisor: Richard E. Klingner

A number of older bridges built before the 1970's were constructed with floor systems consisting of a non-composite concrete slab over steel girders. Many of these bridges do not satisfy current load requirements and may require replacement or strengthening. A potentially economical means of strengthening these floor systems is to connect the existing concrete slab and steel girders to permit the development of composite action. This dissertation describes a research program investigating methods to develop composite action in existing non-composite floor systems by the use of post-installed shear connectors.

Three types of post-installed shear connection methods were investigated. These methods are referred to as the double-nut bolt, the high tension friction grip bolt, and the adhesive anchor. These post-installed shear connectors were tested under static and fatigue loading, and design equations for ultimate strength and fatigue strength were developed. These post-installed shear connectors showed significantly higher fatigue strength than conventional welded shear studs widely used for new construction. The superior fatigue strength of these post-installed shear connectors enables strengthening of existing bridge girders using partial composite design, thereby requiring significantly fewer shear connectors than possible with conventional welded shear studs.

Five full-scale non-composite beams were constructed and four of these were retrofitted with post-installed shear connectors and tested under static load. The retrofitted composite beams were designed as partially composite with a 30-percent shear connection ratio. A non-composite beam was also tested as a baseline specimen. Test results of the full-scale composite beams showed that the strength and stiffness of existing non-composite bridge girders can be increased significantly. Further, excellent ductility of the strengthened partially composite girders was achieved by placing the post-installed shear connectors near zero moment regions to reduce slip at the steel-concrete interface.

Parametric studies using the finite element program ABAQUS were also conducted to investigate the effects of beam depth, span length, and shear connection ratio on the system behavior of strengthened partially composite beams. The studies showed that current simplified design approaches commonly used for partially composite beams in buildings provide a good prediction of the strength and stiffness of partially composite bridge girders constructed using post-installed shear connectors.

Table of Contents

CHAPTER 1 Introduction	1
1.1 General	1
1.2 Objective	2
1.3 Scope of this dissertation	3
CHAPTER 2 Background and Literature Review	5
2.1 Introduction.....	5
2.2 Conventional Welded Shear Studs.....	6
2.2.1 Static Behavior of Welded Shear Studs	6
2.2.2 Fatigue Behavior of Welded Shear Studs	11
2.2.3 AASHTO Design Provisions for Welded Shear Studs	13
2.2.3.1 AASHTO Standard Specifications for Highway Bridges	13
2.2.3.2 AASHTO LRFD Bridge Design Specifications.....	15
2.3 Design of Composite Beams.....	16
2.3.1 Shear Connection Ratio (Composite Ratio).....	16
2.3.2 Structural Behavior of Partially Composite Beams	17
2.3.2.1 Stiffness of Partially Composite Beams under Service Load	17
2.3.2.2 Ultimate Load-Carrying Capacity of Composite Beams	20
2.3.3 Predicting Maximum Slip at the Interface of Composite Beams	22
2.4 Finite Element Modeling of Composite Beams.....	26
2.4.1 Simulation of Push-out Tests	26
2.4.2 Simulation of Composite Beam Tests.....	26
2.5 Load Rating of existing Bridge Structures.....	28
2.5.1 Load-Rating using ASD and LFD Methods	28
2.5.2 Load-rating using LRFR.....	29
2.6 Previous Research on Post-Installed Shear Connectors.....	31

2.6.1	Use of High-Strength Bolts as Shear Connectors	31
2.6.2	Texas Department of Transportation Project 0-4124.....	32
2.6.2.1	Types of Post-Installed Shear Connectors Investigated.....	32
2.6.2.2	Selection of Post-Installed Shear Connectors	34
2.6.2.3	Summary of Test Results for Post-installed Shear Connectors..	36
2.7	Approaches for Design of Composite Bridge Girders with Post-Installed Shear Connectors	37

CHAPTER 3 Single Shear Connector Tests..... 39

3.1	Introduction.....	39
3.2	Test Program on Single Shear Connectors	40
3.2.1	Description of Test Specimens	40
3.2.2	Description of post-installed shear connectors	42
3.2.2.1	Double-Nut Bolt (DBLNB).....	42
3.2.2.2	High-Tension Friction-Grip Bolt (HTFGB).....	45
3.2.2.3	Adhesive Anchor (HASAA)	47
3.2.3	Specimen Designations.....	48
3.2.4	Material Properties.....	49
3.2.4.1	Concrete and Grout	49
3.2.4.2	HIT HY 150 Adhesive	49
3.2.4.3	Steel Plate.....	50
3.2.4.4	Shear Connector Materials.....	52
3.2.5	Test Setup and Instrumentation	54
3.2.6	Test procedure.....	56
3.3	Single Shear Connector Test Results.....	56
3.3.1	Static Behavior of Post-Installed Shear Connectors	56
3.3.1.1	Double-Nut Bolt (DBLNB).....	59
3.3.1.2	High-Tension Friction-Grip Bolt (HTFGB).....	60
3.3.1.3	Adhesive Anchor (HASAA)	61

3.3.2	Fatigue Behavior of Post-Installed Shear Connectors	62
3.4	Connectors in Lightly Reinforced Concrete Blocks	64
3.4.1	Details of Test Specimens.....	64
3.4.2	Static Test Results.....	65
3.4.3	Fatigue Test Results.....	68
3.5	Discussion of Test Results	69
3.5.1	Static Tests	69
3.5.1.1	Strength and Stiffness under Static Loading	69
3.5.1.2	Slip Capacity under Static Loading.....	72
3.5.2	Fatigue Tests	73
3.5.2.1	Comparison with Previous Research.....	73
3.5.2.2	Predicting Fatigue Strength.....	75
3.5.3	Shear Connectors in Lightly Reinforced Concrete Blocks	76
3.6	Summary	78

CHAPTER 4 Full-Scale Beam Tests and Analytical Modeling..... 81

4.1	Introduction.....	81
4.2	Test Program.....	82
4.2.1	Test Specimens	82
4.2.1.1	Non-Composite Beam (NON-00BS)	82
4.2.1.2	Design of Partially Composite Specimens (DBLNB-30BS, HTFGB-30BS, HASAA-30BS, HASAA-30BS1).....	85
4.2.1.3	Installation of Post-Installed Shear Connectors (DBLNB, HASAA, HTFGB).....	86
4.2.1.3.1	Installation of the DBLNB Connectors for Specimen DBLNB-30BS	87
4.2.1.3.2	Installation of the HTFGB connector for Specimen HTFGB- 30BS	90

4.2.1.3.3	Installation of the HASAA Connector for Specimen HASAA-30BS and HASAA-30BS1	92
4.2.2	Material Properties.....	94
4.2.2.1	Concrete, Grout, and Adhesive	94
4.2.2.2	Steel Beams and Reinforcing Bars.....	96
4.2.2.3	Shear Connectors.....	97
4.2.3	Test Setup.....	98
4.2.3.1	Details of Test Setup	98
4.2.3.2	Instrumentation.....	101
4.3	Test Results.....	102
4.3.1	Specimen NON-00BS.....	107
4.3.2	Specimen DBLNB-30BS	110
4.3.3	Specimen HASAA-30BS	113
4.3.4	Specimen HTFGB-30BS	115
4.4	Discussion of First Four Full-scale beam tests	118
4.4.1	Stiffness and Strength	118
4.4.2	Failure Modes	121
4.4.3	Interface Slip and Neutral Axis Locations.....	124
4.4.4	Constructability.....	128
4.4.4.1	Double-Nut Bolt (DBLNB) Method	128
4.4.4.2	High-Tension Friction-Grip Bolt (HTFGB) Method	129
4.4.4.3	Adhesive Anchor (HASAA) Method.....	130
4.5	Numerical Modeling of the Four Beam Test Specimens.....	131
4.5.1	Finite Element Model	131
4.5.1.1	Material Modeling.....	131
4.5.1.2	Element Selections	133
4.5.1.3	Analysis Procedure.....	136
4.5.2	Analysis Results.....	136
4.5.2.1	Non-Composite Specimen NON-00BS.....	136

4.5.2.2	Composite Specimens DBLNB-30BS and HASAA-30BS.....	139
4.5.2.3	Composite Specimen HTFGB-30BS	143
4.6	Improving Deformation Capacity of Retrofitted Composite Beams ..	145
4.6.1	Effect of Locating Shear Connectors near Supports.....	145
4.6.2	Test Results of Partially Composite Beam with Shear Connectors Concentrated near Supports	149
4.6.2.1	Test Results for Specimen HASAA-30BS1	150
4.6.2.2	Discussion of the Test Results (Specimen HASAA-30BS1)...	155
4.7	Summary	157

CHAPTER 5 Parametric Finite Element Study 159

5.1	Introduction.....	159
5.2	Parametric Study of Composite Beams	159
5.3	Results of Parametric Study.....	162
5.3.1	Composite Beams with Different Geometries	162
5.3.1.1	Comparisons with Current Design Provisions (Strength and Stiffness).....	166
5.3.1.2	Deformation Capacity of Composite Beams with Post-Installed Shear Connectors	169
5.3.2	Effect of Oversized Holes.....	173
5.4	Summary	175

**CHAPTER 6 Strengthening an Existing Bridge with Post-Installed Shear
Connectors – Case Study..... 177**

6.1	Introduction.....	177
6.2	Description of the Case Study Bridge.....	177
6.3	AASHTO Load-Rating for Existing Non-Composite Bridge Girders	181
6.3.1	General AASHTO Load Rating Approach.....	181
6.3.2	Load Rating based on Finite Element Analysis.....	182

6.4	Strengthening the Hondo Bridge by Post-Installed Shear Connectors	189
6.4.1	General design approach.....	189
6.4.2	Load Rating of Retrofitted Hondo Bridge based on Finite Element Analysis.....	197
6.5	Summary.....	200
CHAPTER 7 Summary, Conclusions, and Design Recommendations.....		203
7.1	Summary.....	203
7.2	Conclusions.....	204
7.3	Preliminary Design Recommendations.....	208
7.4	Recommendations for Further Research.....	212
Appendix A Analysis Results of Composite Beams		215
Appendix B Load Rating For Hondo Bridge		223

List of Tables

Table 2.1: Coefficients for static stiffness of a shear connector per Equation 2.5	11
Table 3.1: Material properties for single shear connector tests	51
Table 3.2: Test results for single shear connector specimens.....	57
Table 3.3: Test results of single shear connectors under fatigue loading.....	63
Table 3.4: Material properties of the HASAA connectors with wider spacing of transverse reinforcement.....	65
Table 3.5: Test results of the HASAA connectors with wide reinforcing bar spacing (Static loading).....	66
Table 3.6: Test results of the HASAA connectors under fatigue loading	68
Table 3.7: Stiffness of single shear connector specimens.....	72
Table 4.1: Concrete slump and compressive strength	96
Table 4.2: Steel coupon test results.....	97
Table 4.3: Reinforcing bar test results (#4 bars).....	98
Table 5.1: Analysis results for composite beams with 30-ft span	163
Table 5.2: Analysis results of composite beams with 40-ft long span.....	164
Table 5.3: Analysis results of composite beams with 50-ft long span.....	165
Table 5.4: Analysis results of composite beams with oversized holes in the beam flange	175
Table 6.1: Load rating of Hondo bridge (non-composite bridge girders).....	182
Table 6.2: Load rating results before retrofitting.....	189
Table 6.3: Connector force (kips) under cyclic loading	196
Table 6.4: Load rating of strengthened composite bridge girders	199

Table B.1: Connector shear forces for Case I loading	232
Table B.2: Connector shear forces for Case II loading.....	234
Table B.3: Shear connector force for several truck locations (kips).....	236

List of Figures

Figure 2.1: Non-composite versus Composite Action.....	6
Figure 2.2: Conventional push-out test specimen (Kayir 2006).....	7
Figure 2.3: Behavior of shear connector in composite beam.....	9
Figure 2.4: Load-slip curves for conventional welded shear stud	9
Figure 2.5: S-N data for shear studs (Kayir 2006).....	12
Figure 2.6: Initial stiffness of composite beams (AISC 2005)	19
Figure 2.7: Plastic cross-section analysis for composite beams (Viest et al. 1997)	21
Figure 2.8: Ultimate load-carrying capacity of a composite beam.....	21
Figure 2.9: Predicting maximum slip at the steel-concrete interface.....	23
Figure 2.10: Simply supported beam with different shear connector distribution	24
Figure 2.11: Strain distribution in composite beam.....	25
Figure 2.12: Investigated shear connectors.....	34
Figure 2.13: S-N Plot for Test Specimens (Kayir 2006)	35
Figure 3.1: Single shear connector test specimen.....	40
Figure 3.2: Reinforcing bar layout of single shear connector test specimens	41
Figure 3.3: Concrete formwork and reinforcing bar layout before concrete casting.....	42
Figure 3.4: Double-Nut Bolt (DBLNB) connector	43
Figure 3.5: Installation of the DBLNB connector for single shear connector test	44
Figure 3.6: High-Tension Friction-Grip Bolt (HTFGB) connector	46
Figure 3.7: Concrete surface after installation of High-Tension Friction-Grip Bolt (HTFGB).....	46
Figure 3.8: Adhesive Anchor (HASAA)	47
Figure 3.9: Injecting adhesive (HASAA)	48
Figure 3.10: Specimen designations used in this study	49
Figure 3.11: Shear and tension testing apparatus for connectors.....	53

Figure 3.12: ASTM A193 B7 rods after shear and tension tests	54
Figure 3.13: Direct-shear test setup for single shear connector tests (Kayir 2006).....	55
Figure 3.14: Instrumentation for single shear connector tests	55
Figure 3.15: Static test results of single shear connectors (DBLNB).....	57
Figure 3.16: Static test results of single shear connectors (HTFGB)	58
Figure 3.17: Static test results of single shear connectors (HASAA).....	58
Figure 3.18: Typical failed section of DBLNB connector (DBLNB-07ST)	59
Figure 3.19: Cracks in the concrete block and deformed connector (HTFGB-05ST).....	60
Figure 3.20: Failed section of HASAA connector (HASAA-07ST)	61
Figure 3.21: Fatigue test results of single shear connectors, compared with AASHTO equation for welded shear studs.....	63
Figure 3.22: Failed shear connector installed in lightly reinforced concrete block (HASAA-11ST)	66
Figure 3.23: Static test results of single shear connectors	67
Figure 3.24: Static test results of single shear connectors	68
Figure 3.25: Failed shear connectors after tests.....	70
Figure 3.26: Comparison of load ratio for post-installed shear connectors.....	71
Figure 3.27: Failed shear connectors after the tests.....	73
Figure 3.28: Fatigue test results of post-installed shear connectors	75
Figure 3.29: Cracks in concrete block (HASAA-12ST).....	78
Figure 4.1: Details of specimen cross-section	83
Figure 4.2: Reinforcement layout	84
Figure 4.3: Concrete formwork.....	84
Figure 4.4: Predicted load capacity of test specimens versus shear connection ratio.....	86
Figure 4.5: Coring and drilling into the specimen	88
Figure 4.6: Drilling through beam flange	89
Figure 4.7: Drilled holes for DBLNB installation	89
Figure 4.8: Use of “Squirter” Direct Tension Indicating (SDTI) washer	90

Figure 4.9: Drilling and coring into the concrete slab	91
Figure 4.10: Shear connectors installed in hole (HTFGB)	92
Figure 4.11: Installation of HASAA shear connectors	94
Figure 4.12: Test setup for full-scale beam tests (Pictures).....	99
Figure 4.13: Test setup for full-scale beam tests (Drawing).....	100
Figure 4.14: Linear potentiometers for measuring slip at the end of the specimen.....	101
Figure 4.15: Strain gage locations	102
Figure 4.16: Load vs. deflection curves (Specimen NON-00BS)	103
Figure 4.17: Load vs. slip curves (Specimen NON-00BS).....	103
Figure 4.18: Load vs. deflection curves (Specimen DBLNB-30BS).....	104
Figure 4.19: Load vs. slip curves (Specimen DBLNB-30BS).....	104
Figure 4.20: Load vs. deflection curves (Specimen HASAA-30BS)	105
Figure 4.21: Load vs. slip curves (Specimen HASAA-30BS).....	105
Figure 4.22: Load vs. deflection curves (Specimen HTFGB-30BS).....	106
Figure 4.23: Load vs. slip curves (Specimen HTFGB-30BS)	106
Figure 4.24: Load vs. midspan deflection curves for test specimens NON-00BS, DBLNB-30BS, HTFGB-30BS and HASAA-30BS	107
Figure 4.25: Specimen NON-00BS - Cracks in the slab and beam local buckling	108
Figure 4.26: Specimen NON-00BS – Overall view of specimen at end of test (11.5-in. deflection)	109
Figure 4.27: Specimen DBLNB-30BS - Cracks on the bottom of the concrete slab (3.25-in deflection)	112
Figure 4.28: Specimen DBLNB-30BS - Flange and web local buckling (8-in. deflection)	112
Figure 4.29: Specimen HASAA-30BS - Cracks on the bottom of the concrete slab (4.25-in deflection)	114
Figure 4.30: Specimen HASAA-30BS - Failed shear connectors	114
Figure 4.31: Specimen HASAA-30BS – Concrete cracks and beam local buckling (10-in. deflection)	115

Figure 4.32: Specimen HTFGB-30BS – Whitewash flaking (6.5-in. deflection)	117
Figure 4.33: Specimen HTFGB-30BS – Concrete crushing on the top of the slab (10-in. deflection)	118
Figure 4.34: Test results compared with theoretical values of stiffness and strength	120
Figure 4.35: Specimen HTFGB-30BS – shear connectors after the test (slab bottom) ..	121
Figure 4.36: Specimen HTFGB-30BS – concrete crushing on the top (10.5-in. deflection)	122
Figure 4.37: Specimen NON-00BS – Typical beam local flange and web buckling at large displacements	123
Figure 4.38: Specimen HTFGB-30BS – flange local buckling (11.0-in. deflection)	124
Figure 4.39: Slip at the ends of test specimens	125
Figure 4.40: Slip at the ends of Specimen HTFGB-30BS	126
Figure 4.41: Neutral axis locations of test specimens	127
Figure 4.42: Concrete model in ABAQUS	132
Figure 4.43: Connector load-slip relationship	132
Figure 4.44: Finite element model for full-scale beam specimen	134
Figure 4.45: Finite element model for single shear connector specimen	135
Figure 4.46: Load vs. midspan deflection curves (Specimen NON-00BS)	137
Figure 4.47: Deflection vs. end slip curves (Specimen NON-00BS)	138
Figure 4.48: Longitudinal stress distribution (Specimen NON-00BS)	138
Figure 4.49: Load-slip behavior of the DBLNB connector (ABAQUS)	139
Figure 4.50: Load vs. midspan deflection curves (Specimen DBLNB-30BS)	141
Figure 4.51: Load vs. midspan deflection curves (Specimen HASAA-30BS)	141
Figure 4.52: Deflection vs. end slip curves (Specimen DBLNB-30BS)	142
Figure 4.53: Deflection vs. end slip curves (Specimen HASAA-30BS)	142
Figure 4.54: Longitudinal stress distribution (Specimen DBLNB-30BS)	143
Figure 4.55: Load vs. midspan deflection curves (Specimen HTFGB-30BS)	144
Figure 4.56: Deflection vs. end slip curves (Specimen HTFGB-30BS)	144
Figure 4.57: Concentrating shear connectors	147

Figure 4.58: Load-deflection relations for the composite beam with concentrated shear connectors	148
Figure 4.59: End slip for the composite beam with concentrated shear connectors.....	148
Figure 4.60: Load vs. deflection curves (Specimen HASAA-30BS1)	149
Figure 4.61: Deflection vs. slip curves (Specimen HASAA-30BS1).....	150
Figure 4.62: Load-deflection relations for Specimen HASAA-30BS1	151
Figure 4.63: Specimen HASAA-30BS1 - Flange white wash flaking (5.75-in. deflection)	153
Figure 4.64: Specimen HASAA-30BS1 - Cracks around shear connector (8.5-in. deflection)	153
Figure 4.65: Specimen HASAA-30BS1 - Concrete cracks and gap at the interface near the north support (11.25-in. deflection)	154
Figure 4.66: Deflection vs. end slip curves for test specimens.....	156
Figure 4.67: Neutral axis locations of test specimens.....	156
Figure 5.1: Idealized load-slip behavior of a shear connector with an initial gap	161
Figure 5.2: Load-deflection relations of composite beams (W36x160 beam, 50-ft span)	162
Figure 5.3: Comparison of strength of composite beams	168
Figure 5.4: Comparison of stiffness of composite beams.....	168
Figure 5.5: Definition of ductility factor.....	170
Figure 5.6: Ductility of composite beams.....	172
Figure 5.7: Load-deflection graphs considering the effects of oversized holes	174
Figure 6.1: The Hondo case-study bridge.....	179
Figure 6.2: Top view of a typical span of the Hondo Bridge	180
Figure 6.3: Section details for the Hondo Bridge	180
Figure 6.4: Cross-section dimensions of W26x85 bridge girder	181
Figure 6.5: ABAQUS model of the Hondo Bridge.....	183

Figure 6.6: Standard design truck locations for load rating using ABAQUS.....	185
Figure 6.7: Load-deflection relations for the Hondo Bridge (before retrofiting)	186
Figure 6.8: Longitudinal stress distribution of the Hondo Bridge (non-composite).....	186
Figure 6.9: Longitudinal stress distribution due to dead load.....	188
Figure 6.10: Load-carrying capacity vs. shear connection ratio for Hondo Bridge	191
Figure 6.11: shear connector layout for Hondo Bridge	191
Figure 6.12: Connector force calculation for fatigue loading.....	194
Figure 6.13: Analytically predicted load-deflection relations for Hondo Bridge (after retrofitting).....	198
Figure 6.14: Longitudinal stress distribution of the Hondo Bridge (after retrofit).....	198
Figure 7.1: Design procedure using post-installed shear connectors.....	211
Figure A.1: Load-deflection relations of composite beams (W27x94, 30-ft span)	215
Figure A.2: Load-deflection relations of composite beams (W27x94, 40-ft span)	215
Figure A.3: Load-deflection relations of composite beams (W27x94, 50-ft span)	216
Figure A.4: Load-deflection relations of composite beams (W30x99, 30-ft span)	217
Figure A.5: Load-deflection relations of composite beams (W30x99, 40-ft span)	217
Figure A.6: Load-deflection relations of composite beams (W30x99, 50-ft span)	218
Figure A.7: Load-deflection relations of composite beams (W33x130, 30-ft span)	219
Figure A.8: Load-deflection relations of composite beams (W33x130, 40-ft span)	219
Figure A.9: Load-deflection relations of composite beams (W33x130, 50-ft span)	220
Figure A.10: Load-deflection relations of composite beams (W36x160, 30-ft span)	221
Figure A.11: Load-deflection relations of composite beams (W36x160, 40-ft span)	221
Figure A.12: Load-deflection relations of composite beams (W36x160, 50-ft span)	222
Figure B.1: Steel beam section	223
Figure B.2: Composite beam section (unit: in.).....	227
Figure B.3: Shear connector numbering.....	230
Figure B.4: Truck wheel locations.....	230

Figure B.5: Shear force diagram.....	230
Figure B.6: Truck wheel locations.....	233
Figure B.7: Shear force diagram.....	233

CHAPTER 1

Introduction

1.1 GENERAL

A number of older bridges are constructed with floor systems consisting of a non-composite concrete slab over steel girders. A significant number of these bridges were designed based on smaller loads than the standard design loads currently used for new bridges, as specified by the American Association of State Highway and Transportation Officials (AASHTO). The inadequate strength of these bridges can result in the need to limit truck loads on the bridge through load posting, or may require replacement of the bridge. Alternatively, strengthening measures can be undertaken to increase the load rating of the bridge.

A potentially economical means of strengthening these floor systems is to connect the existing concrete slab and steel girders to permit the development of composite action. Composite action permits the existing steel girder and concrete slab to act together more efficiently than in the original non-composite condition. Connecting the steel girders and the concrete slab using shear connectors can increase the load-carrying capacity of the girders by more than 50 percent, compared to that of the non-composite girders in which the two structural components act separately in flexure.

To achieve the benefits of composite action, the existing steel girder must be connected to the existing concrete slab to permit the transfer of shear forces at the steel-concrete interface. For new bridges, composite action is achieved by welding shear studs to the top of the steel girder prior to casting the concrete slab. In the case of an existing bridge, however, this approach is not possible, since the concrete slab is already in place. Consequently, to take advantage of composite action in existing bridges, economical and practical methods for post-installing shear connectors are needed. The objective of this research study was to identify structurally efficient and practical ways to post-install

shear connectors in existing bridges, and to develop performance data and methods for design of a girder strengthening system using post-installed shear connectors.

1.2 OBJECTIVE

The research study described here is the final phase of a multi-phase research program on post-installed shear connectors, funded by the Texas Department of Transportation (TxDOT). In the earlier phases of this program, an extensive series of tests on individual shear connectors was conducted under static, high-cycle fatigue, and low-cycle fatigue loads to identify shear connectors with advantageous structural performance characteristics (Hungerford 2004, Schaap 2004, Kayir 2006). These earlier tests considered eleven different types of post-installed shear connectors. Out of these eleven types of shear connectors, three were recommended for use in strengthening bridges (Kayir 2006). The study reported in this dissertation builds on the research conducted in the earlier phases of the research program. The research conducted as part of this dissertation includes the following major tasks:

- ✓ Conduct static loading tests on post-installed shear connectors to provide additional data on their strength, stiffness, and slip capacity.
- ✓ Conduct high-cycle fatigue loading tests on post-installed shear connectors to provide additional data on their fatigue strength.
- ✓ Conduct tests on full-scale composite beams retrofitted with post-installed shear connectors to obtain information on load-deformation response, ultimate strength, and constructability.
- ✓ Develop a finite element model to simulate the behavior of both non-composite beams and composite beams retrofitted with post-installed shear connectors.
- ✓ Conduct parametric studies using the developed finite element model to investigate the effects of various parameters including beam depth, span length, and shear connection ratio.

- ✓ Evaluate the feasibility of strengthening existing non-composite bridges with post-installed shear connectors by developing a detailed retrofit design for a case study bridge.
- ✓ Provide design recommendations for strengthening existing non-composite bridge girders by the use of post-installed shear connectors.

1.3 SCOPE OF THIS DISSERTATION

This dissertation is a continuation of the research work conducted by Schaap (2004), Hungerford (2004), and Kayir (2006) as a part of TxDOT Project 0-4124 and 5-4124. The previous work focused on the individual behavior of various types of post-installed shear connectors under static and fatigue loads. This study focused on the behavior of three types of post-installed shear connectors recommended by the previous research.

This dissertation consists of seven chapters. Chapter 2 provides background information on composite design. Behavior of conventional welded shear studs is reviewed and previous research on post-installed shear connectors is summarized. In Chapter 3, the test results are presented for individual shear connectors under static and high-cycle fatigue loading. Based on the single-shear connector tests, design equations for static and fatigue loads are recommended. Chapter 4 summarizes test results of full-scale composite beams retrofitted with post-installed shear connectors. A finite element model is also developed based on the test results. In Chapter 5, using the finite element model, parametric studies are conducted to evaluate the behavior of various composite beams and to develop design recommendations. In Chapter 6, design procedures to strengthen existing non-composite bridges using post-installed shear connectors are presented and applied to a case-study bridge. Finally, in Chapter 7, this dissertation concludes with a summary of the research work and design recommendations for strengthening existing non-composite bridge girders using post-installed shear connectors.

CHAPTER 2

Background and Literature Review

2.1 INTRODUCTION

The research described in this dissertation was conducted to develop efficient and practical methods to increase the load-carrying capacity of existing non-composite steel bridge girders by using post-installed shear connectors. As background for this research, this chapter starts with a brief review of previous research and current design provisions for conventional welded shear studs and composite beams. This chapter also presents methods to load-rate existing bridges according to the American Association of State Highway and Transportation Officials (AASHTO) *Manual for Condition Evaluation of Bridges* (2003) and *AASHTO Guide Manual for Condition Evaluation and Load and Resistance Factor Rating (LRFR) of Highway Bridges* (2005). This is followed by a review of previous research on post-installed shear connectors to strengthen existing non-composite steel girder bridges.

Throughout this dissertation, reference will be made to AASHTO design specifications for bridges. The *AASHTO Standard Specifications for Highway Bridges* (2002) provides design requirements using Allowable Stress Design (ASD) and Load Factor Design (LFD) formats. The *AASHTO LRFD Bridge Design Specifications* (2007) uses the Load and Resistance Factor Design (LRFD) format.

2.2 CONVENTIONAL WELDED SHEAR STUDS

Composite action between a concrete slab and a steel girder can be achieved by connecting the two structural components to permit transfer of horizontal shear force at the steel-concrete interface (Figure 2.1). For new construction, welded shear studs are commonly used to transfer the horizontal shear. The shear studs are normally welded to the beam flange using a stud welding gun. After welding the shear studs, the concrete slab is cast and composite action is achieved.

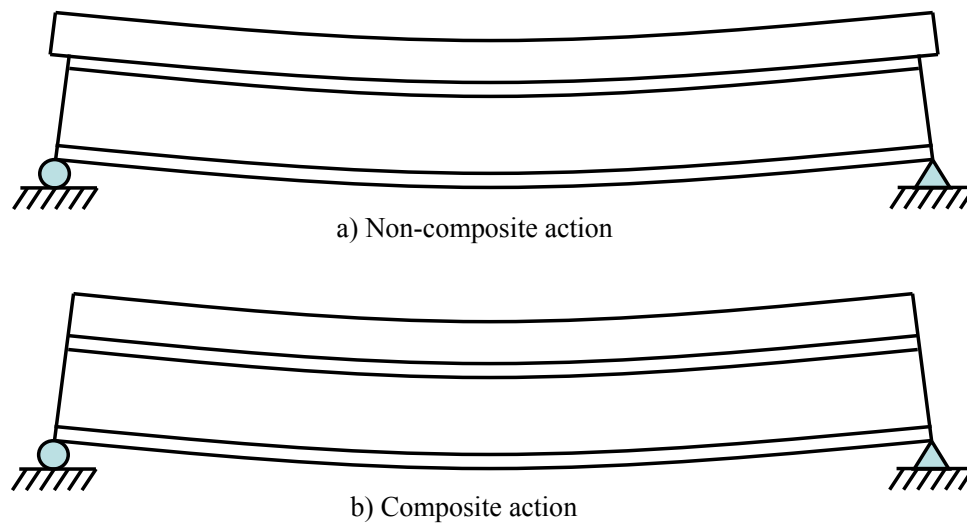


Figure 2.1: Non-composite versus Composite Action

2.2.1 Static Behavior of Welded Shear Studs

One of the most extensive studies to predict the ultimate strength of welded shear studs was conducted by Ollgaard *et al.* (1971), who tested forty-eight push-out specimens. Push-out test specimens, as shown in Figure 2.2, are commonly used to evaluate structural behavior of shear connectors under static and fatigue loading. The compressive strength and modulus of elasticity of concrete, stud diameter, type of

aggregate, and the number of connectors per slab were selected as variables in their tests. The connector tensile strength, slab reinforcement, and geometry were not considered as variables. The authors considered that the compressive strength and modulus of elasticity of concrete are controlling variables and proposed a design equation to predict the ultimate strength of welded shear studs as shown in Equation 2.1. The equation is capped by the tensile strength of the connector material.

$$Q_u = 0.5A_{sc}\sqrt{f'_c E_c} \leq A_{sc}F_u \quad (2.1)$$

where, Q_u = ultimate strength of shear connector (kips)

A_{sc} = area of cross section (in.²)

f'_c = compressive strength of concrete (ksi)

E_c = modulus of elasticity of concrete (ksi)

F_u = minimum specified tensile strength of shear connector (ksi)

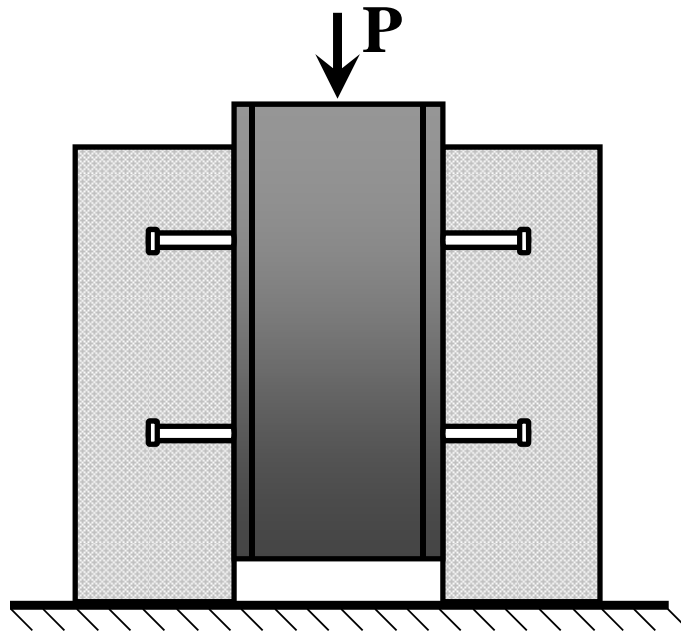


Figure 2.2: Conventional push-out test specimen (Kayir 2006)

Equation 2.1 is a function of only the concrete properties and the diameter of the connector (except for the cap in strength defined by $A_{sc} F_u$). Oehlers and Johnson (1987) proposed an equation for mean connector strength that also accounts for the constitutive properties of the connector:

$$Q_u = 5.0 \times A_{sc} \times F_u \times \left(\frac{E_c}{E_s} \right)^{0.4} \times \left(\frac{f_{cu}'}{F_u} \right)^{0.35} \quad (2.2)$$

where: E_s = modulus of elasticity of shear connector

f_{cu}' = specified cube compressive strength of concrete

Consistent units must be used.

As shear connectors do not have infinite stiffness, slip at the steel-concrete interface is unavoidable (Figure 2.3). The slip can be defined as the displacement at the steel-concrete interface. The slip occurs due to the local crushing of the concrete around the lower shank of the connector and bending of the shear connector (Viest 1997). Most welded shear stud tests showed a slip capacity of at least 0.2 in., which is considered to be sufficient to ensure ductile behavior of the entire system (Viest 1997). Therefore, current design provisions (AISC 2005, AASHTO 2007) do not specify a required slip capacity for shear connectors (Viest *et al.* 1997).

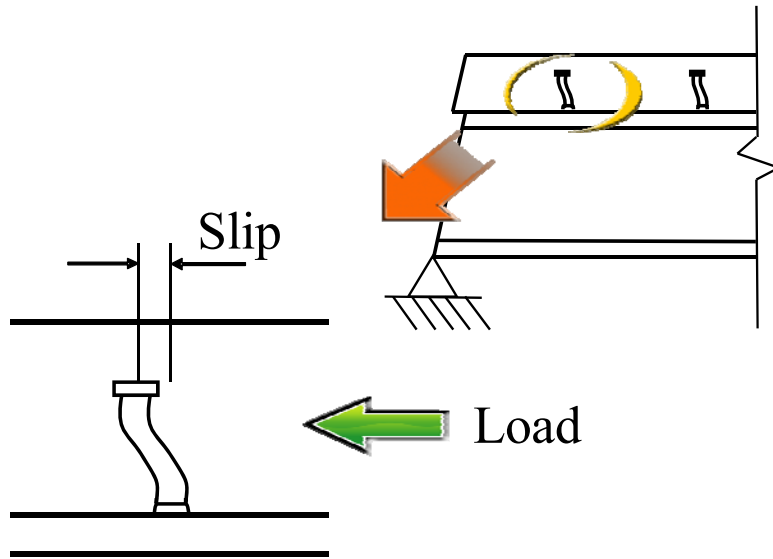


Figure 2.3: Behavior of shear connector in composite beam

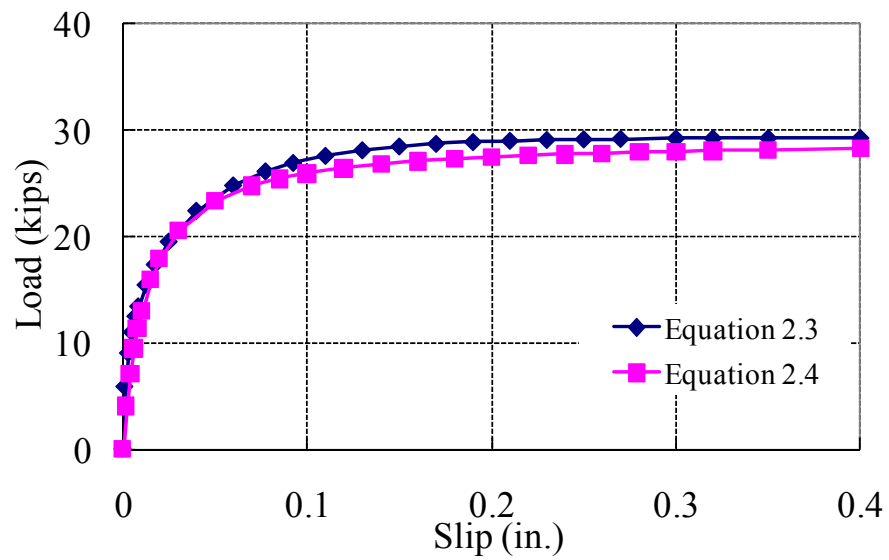


Figure 2.4: Load-slip curves for conventional welded shear stud

Ollgaard *et al.* (1971) proposed equations to predict load-slip behavior of conventional welded shear studs for continuously loaded specimens and for the reloading condition as shown in Equation 2.3 and 2.4, respectively.

$$Q = Q_u \left(1 - e^{-18\Delta}\right)^{2/5} \quad (2.3)$$

$$Q = Q_u \frac{80\Delta}{1 + 80\Delta} \quad (2.4)$$

where, Δ = slip of shear connector (in.)

Equation 2.3 is for shear connectors without any previous loading and Equation 2.4 was developed based on the specimens previously loaded to 10 kips per connector. Figure 2.4 shows load-slip relations of conventional welded shear studs according to Equation 2.3 and Equation 2.4. As shown in the figure Equation 2.3 shows a little higher stiffness than Equation 2.4.

Oehlers and Coughlan (1986) derived a static load-slip curve using linear regression analyses from the results of 42 test results with 19-mm and 22-mm diameter shear studs. Equation 2.5 shows their proposed load-slip relationship as the ratio of the slip to the connector diameter.

$$\Delta = (A + B \cdot f_{cu}') \cdot d \quad (2.5)$$

where, d = diameter of shear connector (*mm*)

The coefficients A and B are listed in Table 2.1, and f_{cu}' is in N/mm^2 .

Oehlers and Sved (1995) observed that the fracture of the connector occurs at about $0.95 \times Q_u$ on the descending branch of the load-slip curve. They proposed that the ultimate slip, s_u , be estimated as:

$$s_u = (0.45 - 0.0021 \cdot f_c') \times d \quad (2.6)$$

where, f_c' is in N/mm^2 and consistent unit should be used for s_u and d .

Table 2.1: Coefficients for static stiffness of a shear connector per Equation 2.5

Q/Q_u	$A (10^{-3})$	$B (10^{-5})$	Q/Q_u	$A (10^{-3})$	$B (10^{-5})$
0.1	22	20	0.85	138	72
0.2	40	37	0.9	156	70
0.3	52	48	0.95	223	119
0.4	63	55	0.99	319	170
0.5	80	73	1.0	371	208
0.6	102	96	1.0	406	251
0.7	120	102	0.99*	475	356
0.8	143	108	0.95*	453	178

*: descending branch after maximum load

2.2.2 Fatigue Behavior of Welded Shear Studs

Fatigue tests of composite beams were conducted by various researchers (Thurlimann 1959, Toprac 1965, Daniels and Fisher 1966). However, it is generally not possible from beam tests to evaluate the load acting on individual shear connectors.

Slutter and Fisher (1966) used push-out test specimens to investigate the behavior of welded shear studs under fatigue loading. They examined the effects of stress range, minimum stress, and load reversal on the fatigue life of welded shear studs. They found that stress range is the most important variable affecting the fatigue life of welded shear studs. Asserting that the lower limit of shear connector fatigue life determined from beam tests is about equal to the average results of the push-out tests, they developed an equation to predict fatigue life of welded shear studs as shown in Equation 2.7.

$$\log N = 8.072 - 0.1753 S \quad (2.7)$$

where, S = stress range (ksi)

N = number of cycles to failure

Slutter and Fisher (1966) found that the strength of the concrete surrounding the shear studs does not have a significant effect on the fatigue strength of the shear studs. Test results of Lehman *et al.* (1965) also showed no significant difference in the fatigue life of shear studs in lightweight concrete compared to the shear studs in normal weight concrete.

Fatigue strength of shear connectors can be represented by the number of cycles (N) of loading to failure under a certain stress range (S). Test results can be plotted on an S-N graph. Kayir (2006) summarized fatigue test results of 3/4-in. and 7/8-in. diameter welded shear studs published by several previous researchers as shown in Figure 2.5.

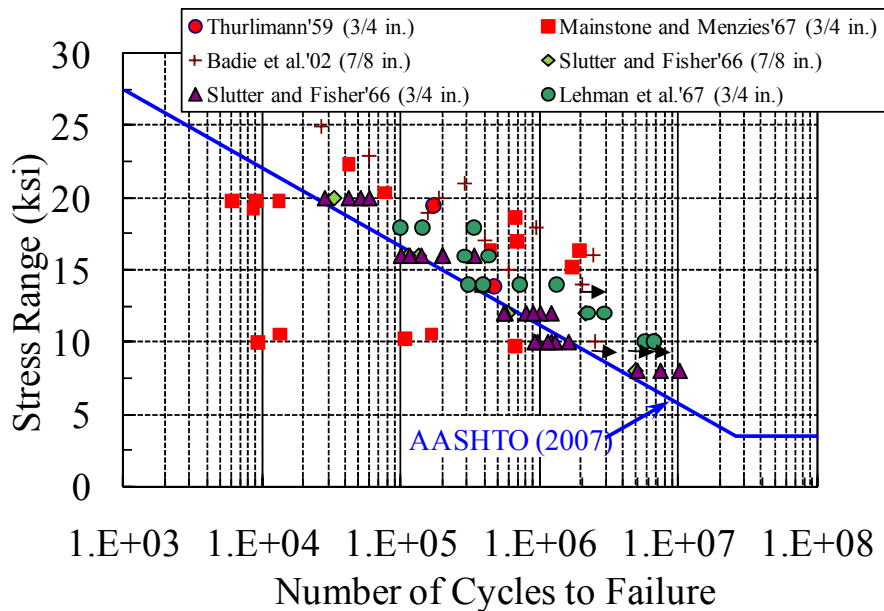


Figure 2.5: S-N data for shear studs (Kayir 2006)

2.2.3 AASHTO Design Provisions for Welded Shear Studs

Design requirements for conventional welded shear studs are provided in *AASHTO Standard Specifications for Highway Bridges (2002)*, hereafter referred to as the *AASHTO Standard Specifications*, and *AASHTO LRFD Bridge Design Specifications (2007)*, hereafter referred to as the *AASHTO LRFD Specifications*. Both specifications require that shear connectors be checked both for fatigue and for ultimate strength. Since fatigue is considered at service load levels, elastic analysis is applied to calculate the response of the structure (Kayir 2006). Simple plastic analysis is used to calculate ultimate strength.

2.2.3.1 AASHTO Standard Specifications for Highway Bridges

Design requirements of shear connector for steel-concrete composite beams are described in Section 10.38.2.1 and Section 10.38.5.1 of the *AASHTO Standard Specifications*. The horizontal shear force range under fatigue loading is determined using the HS20 design truck. Structural response is calculated including a distribution factor and an impact factor. The horizontal shear force range at the steel-concrete interface, S_r (kips/in.), is calculated under service load as shown in Equation 2.8.

$$S_r = \frac{V_r Q}{I} \quad (2.8)$$

Where: V_r = range of vertical shear due to live and impact loads (kips)

Q = first moment of the area of the portion of the transformed section above the steel-concrete interface, taken about the elastic neutral axis of the transformed section (in.³)

I = Moment of inertia of the transformed composite section (in.⁴)

The allowable range of horizontal shear, Z_r (kips) under fatigue load is determined according to Equation 2.9.

$$Z_r = \frac{\alpha d^2}{1,000} \quad (2.9)$$

where: $\alpha =$ 13,000 for 100,000 fatigue cycles
 10,600 for 500,000 fatigue cycles
 7,850 for 2,000,000 fatigue cycles
 5,500 for over 2,000,000 fatigue cycles
 $d =$ diameter of stud (in.)

The required spacing of shear connectors can be determined using Equation 2.10, but is not to exceed 24 in.

$$s = \frac{\sum Z_r}{S_r} \leq 24 \text{ in.} \quad (2.10)$$

Where: $s =$ required spacing of shear connectors (in.)

$\sum Z_r =$ the sum of the allowable range of horizontal shear at one transverse girder cross-section (kips)

$\sum Z_r$ can be determined multiplying the allowable range of horizontal shear of a shear connector by the number of shear connectors in a row on the beam flange.

The number of shear connectors so determined to resist fatigue under service load is then checked for ultimate strength. Since current AASHTO provisions do not allow partially composite design, the strength of shear connectors must satisfy fully composite design. The number of shear connectors can be calculated using Equation 2.11.

$$N_1 = \frac{P}{\phi Q_u} \quad (2.11)$$

where: $N_1 =$ number of shear connectors in a shear span

$P =$ force at the steel-concrete interface (lesser of Equation 2.19 or Equation 2.20) (kips)

$\phi =$ reduction factor = 0.85

Ultimate strength of shear connectors, Q_u (kips) can be calculated using Equation 2.12.

$$Q_u = 0.4d^2 \sqrt{f_c' E_c} \leq 60 \cdot A_{sc} \quad (2.12)$$

where: d = diameter of stud (in.)

f_c' = specified 28-day compressive strength of concrete (ksi)

E_c = modulus of elasticity of concrete

A_{sc} = area of shear connector (in.²)

2.2.3.2 AASHTO LRFD Bridge Design Specifications

The *AASHTO LRFD Specifications* provide design requirements for shear connectors in Section 6.10.10. Structural response under fatigue load is determined using a design truck with a uniform spacing of 30 ft between the 32-kip axles. A dynamic load allowance is included with the design truck. Similar procedures are used to determine the shear force range for fatigue and the maximum interface shear for ultimate strength in the *AASHTO LRFD Specifications* as are used in the *AASHTO Standard Specifications*.

The fatigue resistance of an individual shear connector, Z_r , can be determined according to Equation 2.13.

$$Z_r = \alpha \cdot d^2 \geq \frac{5.5 \cdot d^2}{2} \quad (2.13)$$

$$\alpha = 34.5 - 4.28 \cdot \log N \quad (2.14)$$

where: d = diameter of stud (in.)

N = number of fatigue load cycles specified in the *AASHTO LRFD Specifications Section 6.6.1.2.5* for a bridge with a design life of 75 years.

The ultimate static strength of a shear connector is shown in Equation 2.15.

$$Q_u = 0.5A_{sc}\sqrt{f_c'E_c} \leq A_{sc}F_u \quad (2.15)$$

where: F_u = specified minimum tensile strength of a stud (ksi)

2.3 DESIGN OF COMPOSITE BEAMS

2.3.1 Shear Connection Ratio (Composite Ratio)

Composite action between concrete slab and steel girders results in an increase in strength and stiffness of the bridge girders compared to non-composite girders. There exist two levels of composite design, fully composite and partially composite, according to the amount of shear force transferred at the steel-concrete interface (Schaap 2004, Hungerford 2004).

Fully composite can be achieved by providing enough shear connectors to transfer the interface shear force when the steel girder is fully yielded or when the concrete slab reaches its full compression capacity. A simple procedure to determine the number of shear connectors required to develop fully composite strength, N_f , is provided in the *AASHTO Standard Specifications* and the *AASHTO LRFD Specifications*. The same procedure is also provided in the *Specification for Structural Steel Buildings* published by the American Institute of Steel Construction (AISC 2005). This procedure computes the force at the steel-concrete interface when the fully composite cross-section reaches its plastic capacity. In typical design practice, the transformed section is used to calculate deflection under service loads ignoring slip at the steel-concrete interface.

A composite beam can be defined *Partially composite* when the number of shear connectors is less than required for fully composite design, so that the interface shear force is limited by the strength of the shear connectors. Thus, the ultimate strength of a partially composite beam is controlled by the strength of the shear connectors. In contrast

to fully composite beams, slip at the steel-concrete can be significant and results in a decrease in the elastic stiffness of partially composite beams.

The shear connection ratio, N/N_f (or η) can be defined as the ratio of the number of shear connectors at the steel-concrete interface (N) to the number of shear connectors required for fully composite design (N_f). A shear connection ratio of zero corresponds to zero shear connectors at the steel-concrete interface, and hence to a non-composite beam.

2.3.2 Structural Behavior of Partially Composite Beams

Current AASHTO provisions require composite beams to be designed as fully composite, and have no provisions for partially composite design. In a retrofit situation, however, post-installed shear connectors are likely to be more costly and time-consuming to install than the welded shear studs used in new construction. Because of those higher installation costs, it is preferable to use the minimum number of post-installed shear connectors needed to achieve a desired level of strengthening. This, in turn, suggests the need to design such systems for partially composite action.

2.3.2.1 Stiffness of Partially Composite Beams under Service Load

The stiffness of a steel-concrete composite beam can be represented by its vertical deflection under service load. A mathematical expression of the load-deflection relationship for partially composite beams was derived by Viest *et al.* (1958). However, this closed form solution is very complex and impractical for design purposes.

A more practical solution for predicting deflection of a composite beam considering slip at the steel-concrete interface was proposed by Johnson and May (1975). For a composite beam with a shear connection ratio of η , a convenient design equation was proposed by a linear interpolation approach. The equation is:

$$v_{part} = v_{full} + \alpha \cdot (v_{steel} - v_{full}) \cdot (1 - \eta) \quad (2-16)$$

where: v_{part} = deflection of partially composite beam

v_{full} = deflection of fully composite beam

v_{steel} = deflection of bare steel beam

α = non-dimensional deflection parameter, 0.4 recommended

(Oehlers 1995)

η = shear connection ratio (N / N_{full})

N = number of shear connector in a shear span

N_f = number of shear connectors required for full shear connection

This equation was compared with the results from theoretical composite beam analysis by McGarraugh and Baldwin (1971). This comparison showed that the above equation provides a conservative prediction of deflections for partially composite beams.

The commentary of the *AISC Specification for Structural Steel Buildings* (AISC 2005), hereafter referred to as the *AISC Specification*, provides an equation for the effective moment of inertia to estimate elastic deflections of partially composite beams. This equation results in the deflection of fully composite beams and bare beams, when $\eta = 1$ and $\eta = 0$, respectively. The equation is shown below.

$$I_{eff} = I_s + \sqrt{(\sum Q_n / C_f)} (I_{tr} - I_s) \quad (2.17)$$

where: I_s = moment of inertia of the bare steel beam

I_{tr} = moment of inertia of the fully composite beam

$\sum Q_n$ = summation of the shear strengths of shear connectors between the point of maximum positive moment and the point of zero moment to either side

C_f = compression force in concrete slab for fully composite beam, equal to the smaller of $A_s F_y$ and $0.85 f'_c A_c$

A_c = area of concrete slab within the effective width

Figure 2.6 shows the elastic stiffness of a composite beam with different shear connection ratios derived from Equation 2.17.

As shown in Figure 2.6, partially composite beams are much stiffer than non-composite beams. This indicates that a significant decrease in deflection under service load is expected when even a small number of post-installed shear connectors are installed in existing non-composite steel bridge girders.

A similar equation is also provided for the effective section modulus, S_{eff} , for the tension flange of the steel section. The equation is shown below.

$$S_{eff} = S_s + \sqrt{\left(\sum Q_n / C_f\right)}(S_{tr} - S_s) \quad (2.18)$$

where: S_s = section modulus of the steel beam

S_{tr} = section modulus of the fully composite beam

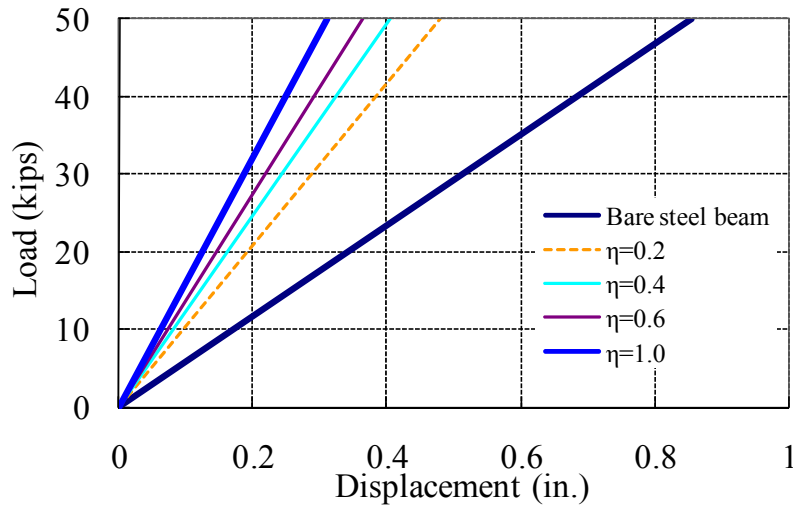


Figure 2.6: Initial stiffness of composite beams (AISC 2005)

2.3.2.2 Ultimate Load-Carrying Capacity of Composite Beams

The flexural strength of fully and partially composite beams can be calculated by simple plastic cross-sectional analysis assuming full yielding in the steel beam and an equivalent rectangular stress block in the concrete slab (Viest 1997). The plastic stress distribution on the cross-section of a composite beam is shown in Figure 2.7. The contribution of the longitudinal reinforcement to the flexural strength of the cross-section is normally very small, and is typically neglected.

The compression force C in the concrete slab is the smallest value among the following three equations below.

$$C_1 = A_s F_y \quad (2.19)$$

$$C_2 = 0.85 f_c' A_c \quad (2.20)$$

$$C_3 = \sum Q_n \quad (2.21)$$

where, A_s = area of steel beam

A_c = effective area of concrete slab

Flexural capacity of the composite beam cross-section can then be calculated by computing the moment of the resultant forces in Figure 2.7. For partially composite beams, Equation 2.21 controls the compression force in the concrete slab. For the design of composite beams according to current AASHTO provisions, using Equation 2.21 for the compression force is not allowed. Consequently, partially composite beams are implicitly prohibited by both the *AASHTO Standard Specifications* and the *AASHTO LRFD Specifications*.

The ultimate load-carrying capacity of a composite beam with different shear connection ratios is shown in Figure 2.8. The composite beam used in Figure 2.8 has the same geometry with the full scale beam test specimens described in Chapter 4. A

partially composite beam with a low shear connection ratio shows much higher strength than a non-composite beam. For example, a shear connection ratio as low as 30 percent results in a strength increase of about 50 percent.

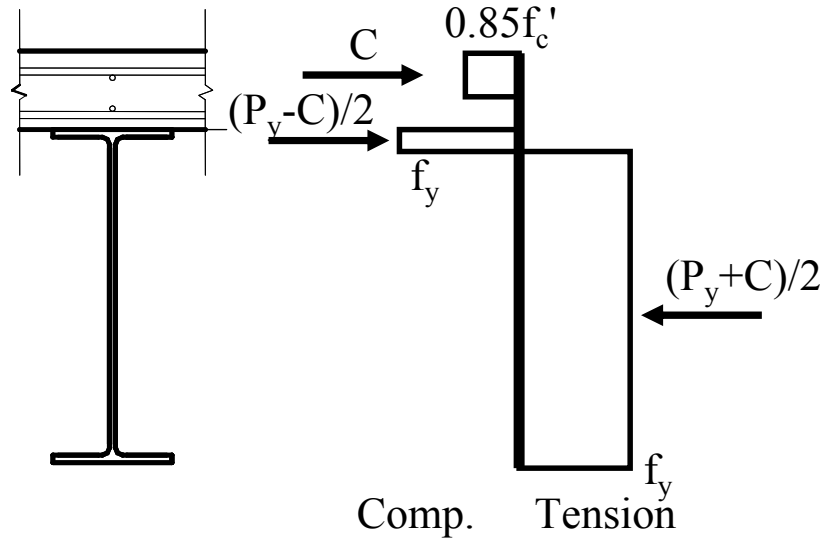


Figure 2.7: Plastic cross-section analysis for composite beams (Viest et al. 1997)

($C = \text{minimum of Equation 2.19 to 2.21}$, $P_y = A_s F_y$)

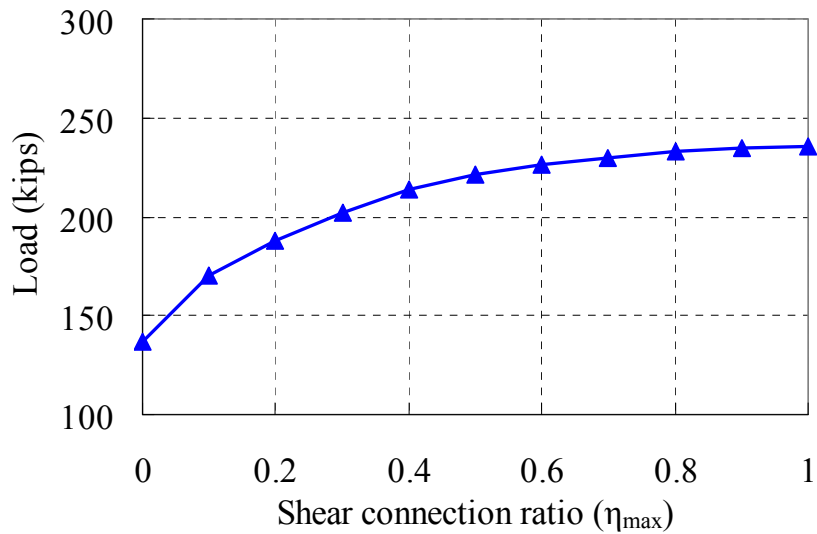


Figure 2.8: Ultimate load-carrying capacity of a composite beam

2.3.3 Predicting Maximum Slip at the Interface of Composite Beams

Oehlers and Sved (1995) developed equations to predict maximum slip at the steel-concrete interface for a simply supported, composite beam when it reaches its maximum strength. It is assumed that the steel beam and concrete slab remain linear elastic and that the shear connectors are plastic. The authors justified these assumptions by the fact that the steel and concrete elements are plastic in only small portion of the beam and most of the shear connectors are beyond the elastic range when the beam reaches its maximum strength.

For a concentrated load at midspan,

$$s_{\max} = \frac{M_{\max} LK_1}{4} - \frac{P_{sh} LK_2}{4} \quad (2.22)$$

For a uniformly distributed load,

$$s_{\max} = \frac{M_{\max} LK_1}{3} - \frac{P_{sh} LK_2}{4} \quad (2.23)$$

where, M_{\max} = maximum applied moment

L = span length

P_{sh} = sum of shear connector strengths in a shear span

$$K_1 = \frac{h_s + h_c}{(EI)_s + (EI)_c}, \quad K_2 = \frac{(h_s + h_c)^2}{(EI)_s + (EI)_c} + \frac{1}{(EA)_s} + \frac{1}{(EA)_c}$$

h_s = distance from centroid of steel slab to the steel-concrete interface

h_c = distance from centroid of concrete beam to the steel-concrete

interface

$(EI)_s$ = flexural stiffness of bare steel beam

$(EI)_c$ = flexural stiffness of concrete slab

$(EA)_s$ = axial stiffness of bare steel beam

$(EA)_c$ = axial stiffness of concrete slab

The above two equations can be generalized as shown in Equation 2.24 (Oehlers and Sved 1995). The areas of A_m and A_{sh} are shown in Figure 2.9.

$$s_{\max} = A_m K_1 - A_{sh} K_2 \quad (2.24)$$

where, A_m = Area under moment diagram in a shear span

A_{sh} = Area under interface shear force diagram in a shear span

The interface shear force at a composite section can be obtained as the sum of the shear connector strengths over the distance between the section under consideration and the support in the same shear span, as shown in Figure 2.9. Note that Figure 2.9 assumes fully loaded shear connectors along the span of the composite beam.

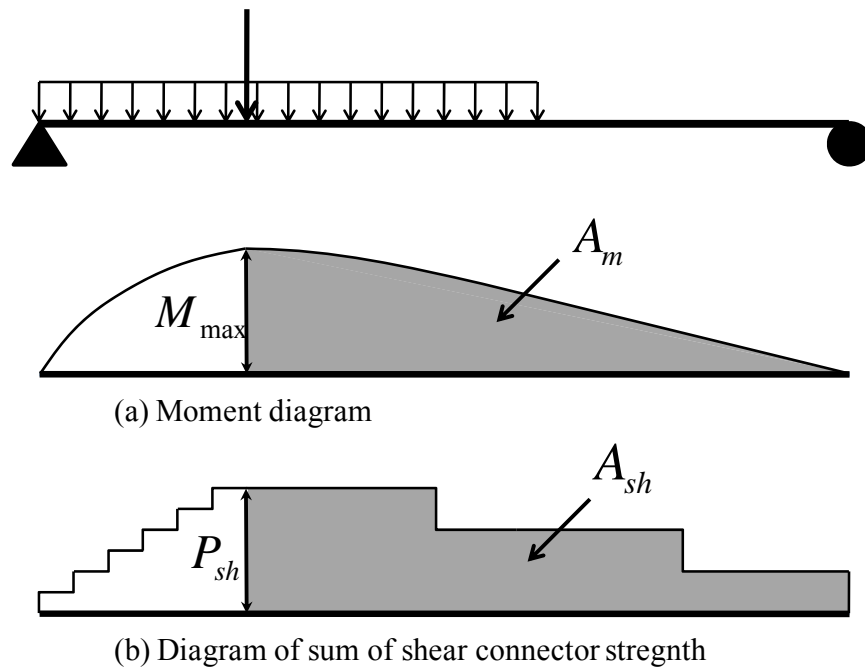


Figure 2.9: Predicting maximum slip at the steel-concrete interface

(Oehlers and Sved 1995)

Equation 2.24 indicates that slip at the steel-concrete interface can be reduced if shear connectors are concentrated near the supports. Figure 2.10 shows a simply supported beam with a concentrated load at mid-span of the beam. The moment diagram of the beam can be plotted with maximum moment at the loading point (Figure 2.10(a)). When the shear connectors are uniformly distributed along the span, the interface shear force diagram can be plotted as shown in Figure 2.10(b). If all of the shear connectors are moved adjacent to the supports, the interface shear force diagram doubles in size (Figure 2.10(c)), which results in a decrease of slip at the steel-concrete interface by doubling the second parameter of Equation 2.24.

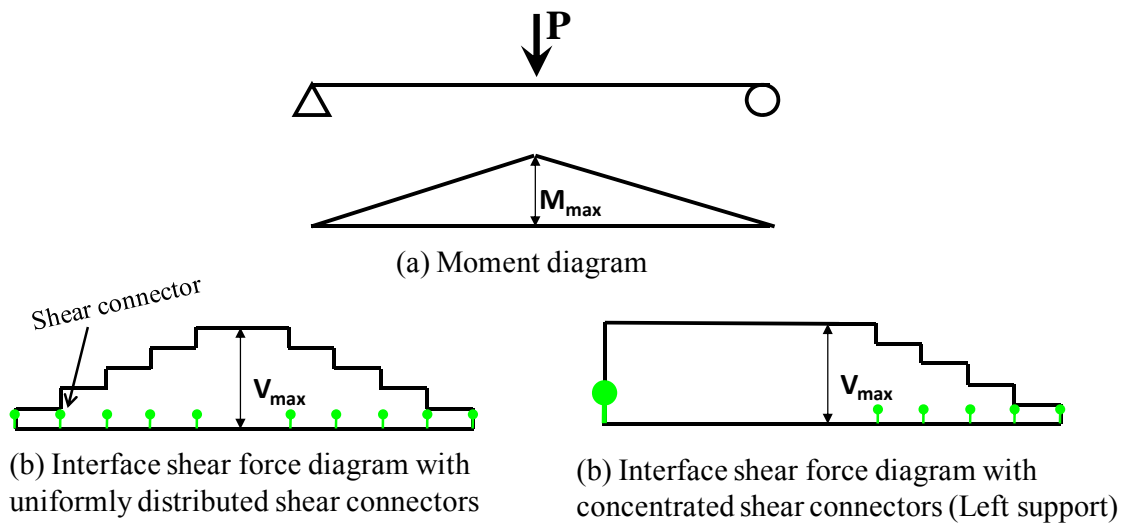


Figure 2.10: Simply supported beam with different shear connector distribution

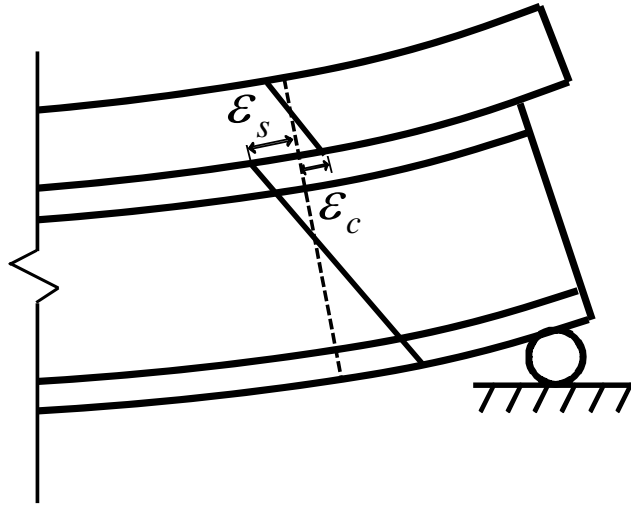


Figure 2.11: Strain distribution in composite beam

This analysis can be clarified by considering the shear force transferred at the steel-concrete interface. Figure 2.11 shows the strain distribution in a composite beam section. The strain discontinuity at the steel-concrete interface can be defined as the difference between strain at the bottom of the slab (ϵ_c) and strain at the top of the steel beam (ϵ_s). The maximum slip at the steel-concrete interface is the integral of the strain discontinuity at the interface over the shear span considered, as shown in Equation 2.25.

$$s_{\max} = \int (\epsilon_c - \epsilon_s) dx \quad (2.25)$$

The strain discontinuity can be reduced if more shear force is transferred at the interface. With uniformly distributed shear connectors, more interface shear can be transferred near the center of the beam than the support. The amount of interface shear that can be transferred in a section is proportional to the number of shear connectors from the section to the support in the same shear span. If all the connectors in a shear span are placed near the support, however, all of the sections can transfer the same amount of shear force, so the slip at the interface can be reduced.

2.4 FINITE ELEMENT MODELING OF COMPOSITE BEAMS

2.4.1 Simulation of Push-out Tests

Kalfas *et al.* (1997) developed a numerical model to simulate push-out tests using the finite element method (FEM). In their numerical model, shear connectors were modeled using beam elements. Each shear connector was modeled using four elements along its length. Rigid bar elements and three-dimensional solid elements were used for the steel beam and the concrete slab, respectively. The stress-strain relations of concrete in tension and the contribution of the reinforcing bars, however, were not taken into account.

Another numerical model to simulate push-out tests was developed by Lam and El-Lobody (2005) using the finite element program ABAQUS to predict maximum strength and modes of failure of shear connectors in a composite slab. They used various three-dimensional solid elements to model the concrete slab, the steel beam, and the shear connectors. They also conducted parametric studies with variables such as shear connector diameter and concrete strength. They asserted that current design provisions may overestimate the ultimate strength of 22-mm diameter welded shear studs.

2.4.2 Simulation of Composite Beam Tests

El-Lobody and Lam (2003) also developed finite element models for composite beams with solid slabs and with precast hollow-core slabs. They used the three-dimensional solid element (C3D8) in ABAQUS for both the concrete slab and the steel beam. The shear connectors were modeled using a non-linear spring element with the load-slip relationship obtained from push-out tests by the authors (El-Lobody and Lam 2003). To simulate the concrete behavior, strain softening after peak stress was considered in the material model both in compression and tension. An elastic-plastic material model was used to simulate the stress-strain behavior of the steel. The authors

validated their numerical models by comparing the analysis results with the test results of previous research by Chapmand and Balakrishnan (1964).

Queiroz *et al.* (2006) investigated the behavior of simply supported, steel-concrete composite beams using the finite element program ANSYS. The shear connectors were modeled using non-linear spring elements. Three-dimensional solid elements (SOLID65) were used for the concrete slab, and shell elements (SHELL43) were used for the steel beam. The shear connectors were modeled non-linear spring elements (COMBIN39) connecting the bottom of the concrete slab and the top of the steel beam. Only half of the span was modeled due to its symmetry in the model. Strain hardening of the steel beam was modeled using the equation proposed by Gattesco (1999). Concrete plasticity was modeled using multilinear isotropic hardening, but strain softening of the concrete was not included. Load-slip relationships of shear connectors from available pushout tests were used for the non-linear spring elements which simulate shear connectors in the model. Parametric studies were conducted to evaluate the effects of continuing the shear connection beyond the support, concrete strength, steel strength, and partial shear connection.

Lam *et al.* (2000) developed a finite element analysis model to predict the behavior of composite beams with steel girders and precast hollow-core slabs. In their study, two-dimensional plane stress elements were used for the concrete slab and the steel beam. Nonlinear spring elements were used for the shear connectors. The validity of the finite element model was demonstrated by comparison with test results, and parametric studies were conducted. The variables for the parametric studies included the size of transverse reinforcement, the slab thickness, the number of shear connectors, and the size of the steel section.

2.5 LOAD RATING OF EXISTING BRIDGE STRUCTURES

AASHTO provides standard procedures to evaluate the load-carrying capacity of existing bridge structures. The *AASHTO Manual for Condition Evaluation of Bridges* (2003), hereafter referred to as the *AASHTO Manual for Condition Evaluation*, defines load rating as “the determination of the live load carrying capacity of an existing bridge using existing bridge plans supplemented by information gathered from a field inspection.” The specific load ratings are necessary to determine the actual load-carrying capacity of existing bridges and to identify the need for load posting or bridge strengthening (AASHTO 2005). Load rating methods are briefly reviewed below, because these are pertinent to determining the number of post-installed shear connectors needed to strengthen an existing bridge to achieve a desired rating.

2.5.1 Load-Rating using ASD and LFD Methods

Bridge load-rating calculations are required based on a recent field inspection to maintain the safety of existing bridges (AASHTO 2003). The *AASHTO Manual for Condition Evaluation* provides two levels of load-rating for existing bridges: the Inventory rating level and the Operating rating level. The Inventory rating level evaluates structural capacity corresponding to the design of a new structure, and results in a live load that can be applied for an indefinite period of time. The Operating rating level give the maximum permissible live load for the structures. An unlimited number of cycles of vehicles at the Operating rating level may shorten the life of the bridge (AASHTO 2003).

The *AASHTO Manual for Condition Evaluation* offers two methods for load rating, the allowable stress method and the load factor method. The allowable stress method limits the stress level in a structure for the actual loadings applied, and the load factor method limits the effect of the factored loads to less than the strength of the structure and the serviceability limits.

To load-rate a bridge, the following procedure is used. The rating factor (RF) is a scale factor which gives the rating of the structure as a fraction of the rating vehicle weight. The load-rating result is usually expressed as the rating vehicle in tons multiplied by the rating factor. For example, if an HS 20 truck loading were used for the load rating and the rating factor were 0.8, the bridge load rating would be $0.8 \times HS\ 20 = HS16.0$. The rating factor is calculated using the following equation:

$$RF = \frac{C - A_1 D}{A_2 L(1 + I)} \quad (2.26)$$

where, C = the capacity of the member

D = the effect of dead load

L = the effect of live load

I = the impact factor for live load

A_1 = factor for dead loads

A_2 = factor for live load

For the allowable stress method, A_1 and A_2 are equal to 1.0 for both the Inventory rating level and the Operating rating level. For the load factor method, A_1 is equal to 1.3 and A_2 is equal to 2.17 for the Inventory rating level, and A_1 and A_2 are both equal to 1.3 for the Operating rating level.

2.5.2 Load-rating using LRFR

AASHTO also provides load rating procedures using the Load and Resistance Factor Rating method in the *Guide Manual for Condition Evaluation and Load and Resistance Factor Rating (LRFR) of Highway Bridges* (AASHTO 2005), hereafter referred to as the *AASHTO LRFR Manual for Condition Evaluation*. There are three different load-rating procedures according to the live-load model used for the load-rating: Design load rating, Legal load rating, and Permit load rating.

The Design load rating is based on the HL-93 loading and checks the strength of the structure using LRFD-based calculations. HL-93 loading consists of the design truck and design lane loads. Bridges with a Design load rating factor $RF \geq 1.0$ at the Inventory rating level have satisfactory load rating for all legal loads (AASHTO 2005). The Legal load rating is the load rating for AASHTO and State legal loads. Finally, the Permit load rating evaluates the structure for safety and serviceability for vehicles above the legally established weight limitations (AASHTO 2005).

To load-rate a bridge, the following equation is used for the LRFR load rating method.

$$RF = \frac{C - (\gamma_{DC})(DC) - (\gamma_{DW})(DW) \pm (\gamma_p)(P)}{(\gamma_L)(LL + IM)} \quad (2.27)$$

For the strength limit states: $C = \phi_c \phi_s \phi R_n$

For the service limit states: $C = f_R$

where, f_R = allowable stress in the *AASHTO LRFD Specifications*

R_n = nominal member resistance

DC = dead load effect due to structural components and attachments

DW = dead-load effect due to wearing surface and utilities

P = permanent loads other than dead loads

LL = live-load effect

IM =dynamic load allowance

γ_{DC} = LRFD load factor for structural components and attachments

γ_{DW} = LRFD load factor for wearing surfaces and utilities

γ_p = LRFD load factor for permanent loads

γ_L = evaluation live-load factor

ϕ_c = condition factor

ϕ_s = system factor

ϕ = LRFD resistance factor

The load and resistance factors are specified in the *AASHTO LRFR Manual for Condition Evaluation*. The load rating result is also reported as the product of a rating truck multiplied by the rating factor.

2.6 PREVIOUS RESEARCH ON POST-INSTALLED SHEAR CONNECTORS

2.6.1 Use of High-Strength Bolts as Shear Connectors

Dallam (1970) conducted an extensive research program on ASTM A325 high-strength bolts used as shear connectors for new construction, and developed design recommendations. Holes were drilled in the top flange of the steel beam and the high-strength bolts were held in place using a wire “chair” on the steel beam flange as the concrete was cast. At the end of 28 days after casting the concrete slab, the bolts were pretensioned by the “turn-of-nut” method. High-strength bolts showed about twice the ultimate strength of conventional welded shear studs. For fatigue, an endurance limit of 12 kips for 3/4-in. diameter high-strength bolts was proposed. Dallam (1970) also recommended fully composite design of composite beams with high-strength bolt shear connectors.

Dedic and Klaiber (1984) also used ASTM A325 high-strength bolts as shear connectors for composite construction. They post-installed shear connectors to increase the shear strength of the steel-concrete interface for existing composite bridge girders which were retrofitted by post-tensioning. The authors proposed two shear connection methods, the Double-Nutted High Strength Bolt and the Epoxied High Strength Bolt, which were modified and were investigated in the study reported in this dissertation. The study of Dedic and Klaiber (1984), however, focused on retrofitting existing composite bridge girders by post-tensioning. They recommended using the equation for conventional welded shear studs developed by Ollgaard *et al.* (1971) to calculate the

strength of the post-installed shear connectors. They did not investigate the structural behavior of post-installed shear connectors under fatigue loading.

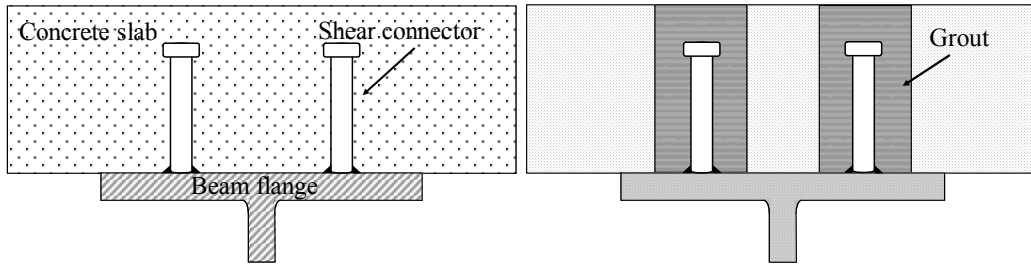
2.6.2 Texas Department of Transportation Project 0-4124

This dissertation is a continuation of Texas Department of Transportation (TxDOT) Research Project 0-4124, on *Methods to Develop Composite Action in Non-Composite Bridge Floor Systems*. Previous researchers on this project evaluated the performance of individual, post-installed, 3/4-in diameter shear connectors under static and fatigue loading. Results of the previous work on this project are reported by Hungerford (2004), Schaap (2004), and Kayir (2005).

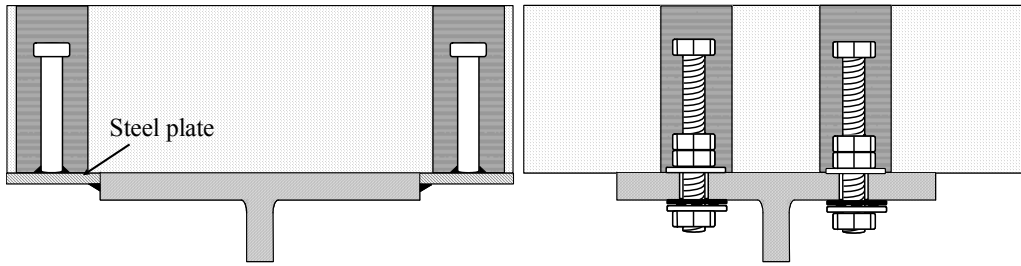
2.6.2.1 Types of Post-Installed Shear Connectors Investigated

Eleven types of post-installed shear connectors and conventional welded shear studs were investigated for their structural performance and constructability by Hungerford (2004), Schaap (2004), and Kayir (2006). Shear connectors investigated in their research are shown in Figure 2.12, along with the designations and abbreviations assigned to each shear connector in this project. Installation processes and material properties of shear connectors, grout, and adhesive are described in detail in Hungerford (2004) and Schaap (2004).

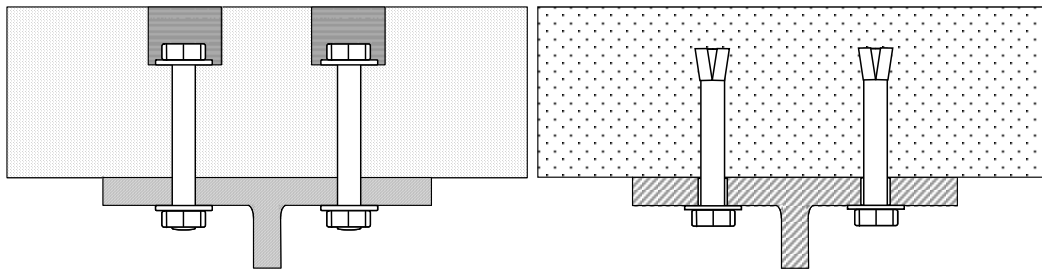
A direct shear test setup was used to evaluate the static and fatigue properties of the shear connectors in this study, instead of the more conventional push-out test setup. The direct shear test was used to reduce the eccentricity of loading and the sensitivity of test results to boundary conditions (Gattesco and Giuriani 1996). Details of the test setup for single shear connector tests are described in Chapter 3.



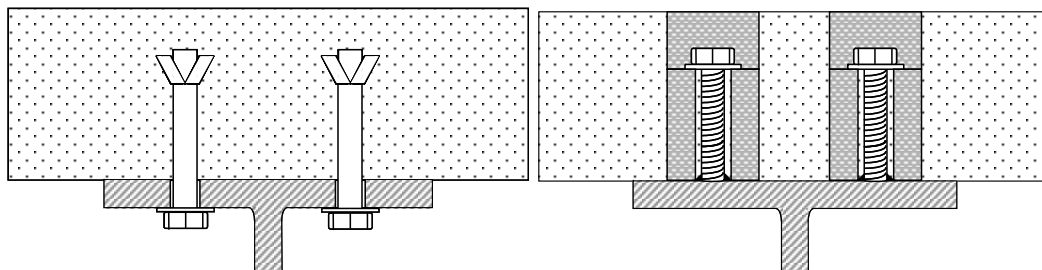
(a) Cast-in-Place Welded Stud (CIPST) (b) Post-Installed Welded Stud (POSST)



(c) Stud Welded to Plate (STWPL) (d) Double-Nut Bolt (DBLNB)



(e) High-Tension Friction Grip Bolt (HTFGB) (f) Expansion Anchor (KWIKB)



(g) Undercut Anchor (MAXIB) (h) Welded Threaded Rod (POSTR)

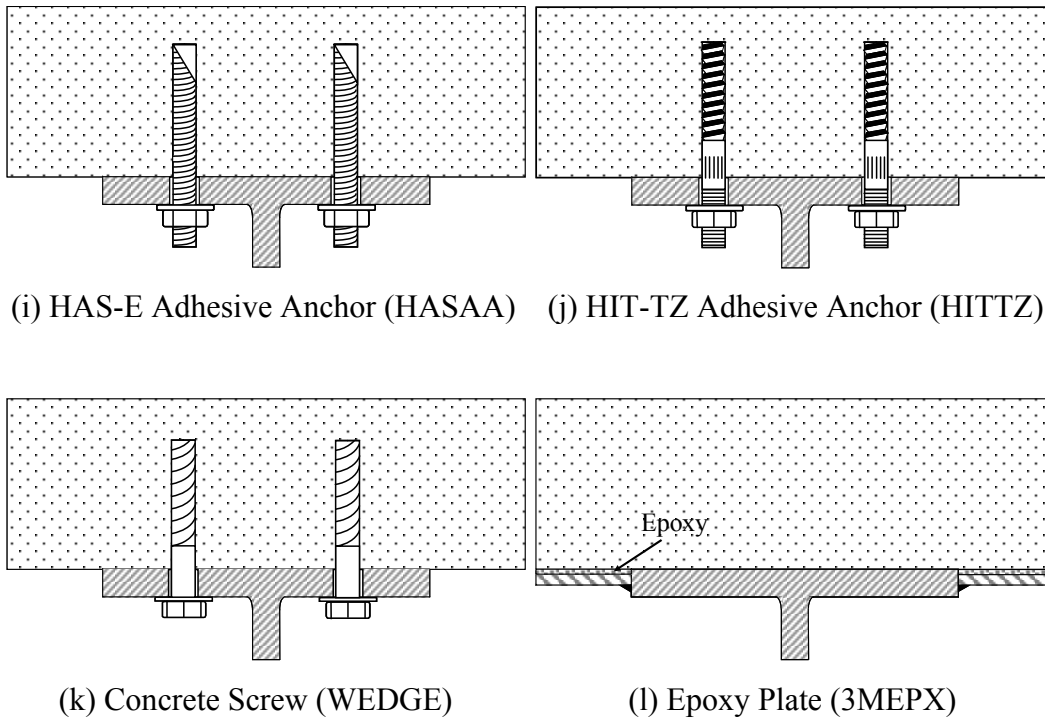


Figure 2.12: Investigated shear connectors

2.6.2.2 Selection of Post-Installed Shear Connectors

In the previous phases of this project, post-installed shear connectors were tested under static and fatigue loading. Three criteria were considered in evaluating the structural performance of the post-installed shear connectors under static loading: strength, stiffness, and slip capacity. High strength of post-installed shear connectors is desirable to reduce the number of connectors needed to strengthen a bridge due to the high installation cost and construction time. Even if a shear connector has high strength, however, the strength developed at large slips may not be useful due to the potentially large deflections of the retrofitted composite beams. Shear connectors are also required to have sufficient slip capacity to permit redistribution of shear force among shear connectors and to provide adequate deformation capacity of the retrofitted composite beam.

Based on the evaluation of the static behavior of the shear connectors, five types of post-installed shear connectors were selected for further testing under fatigue loading: POSST, DBLNB, HTFGB, HASAA, and WEDGB. First, high-cycle fatigue tests were conducted under various stress ranges. The results of those high-cycle fatigue tests are plotted in Figure 2.13 along with the corresponding test results for conventional welded shear studs. For those shear connectors which did not fail under five million or more cycles of loading, testing was stopped prior to failure. In Figure 2.13, these points are plotted with arrows adjacent to them. These tests showed that the post-installed shear connectors which do not require welding (DBLNB, HTFGB, HASAA and WEDGB) have significantly higher fatigue strength than welded shear studs (Kayir 2006). The low-cycle fatigue behavior of selected post-installed shear connectors was also investigated and the test results compared with test results of conventional welded studs.

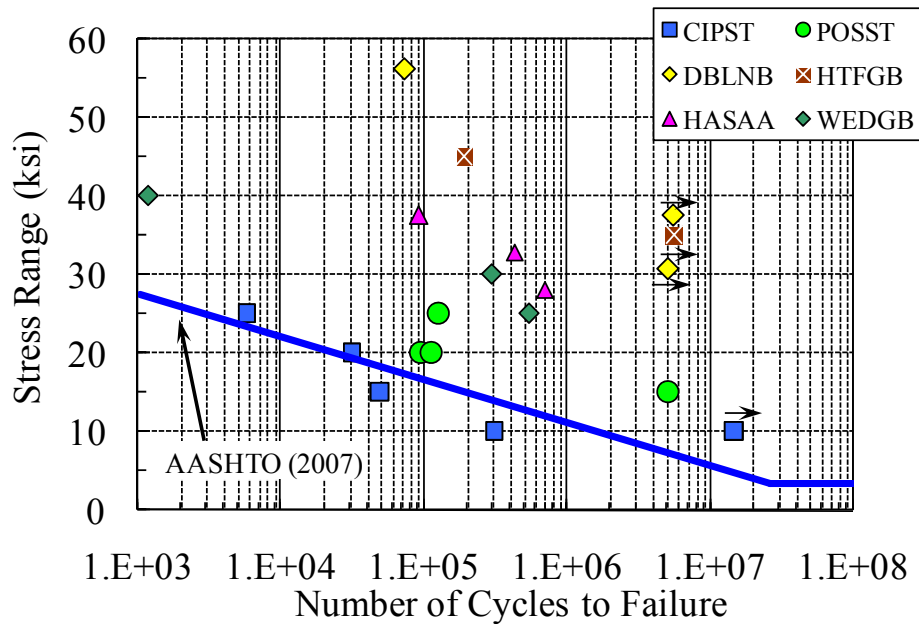


Figure 2.13: S-N Plot for Test Specimens (Kayir 2006)

2.6.2.3 Summary of Test Results for Post-installed Shear Connectors

Kayir (2006) compared static test results with current design equations to predict the ultimate strength of conventional welded shear studs and concrete anchors (AASHTO 2007, ACI 2005). None of the equations conservatively predicted the ultimate strength of the post-installed shear connectors tested under static loading. Alternatively, Equation 2.28 was proposed to predict the ultimate strength of post-installed shear connectors, Q_u , under static loading.

$$Q_u = 0.5A_{sc}F_u \quad (2.28)$$

The effective shear area, A_{sc} , of threaded shear connectors can be calculated as 80 percent of gross area of unthreaded connectors. For the DBLNB, HTFGB, and HASAA connectors, the predicted strength according to Equation 2.28 is 10 to 25% lower than the experimentally measured values.

The *AASHTO Standard Specifications* and the *AASHTO LRFD Specifications* define the fatigue strength of welded shear studs as a function of the applied stress range. Due to the time and cost of high-cycle fatigue tests, only a limited number of post-installed shear connectors were tested under high-cycle fatigue loading (Kayir 2006). Due to the large scatter in fatigue test results, a large number of shear connectors must be tested to characterize their fatigue behavior. Consequently, as part of the work reported here, the tests conducted by Kayir (2006) were supplemented by additional high-cycle fatigue tests on selected post-installed shear connectors.

Kayir (2006) also evaluated the low-cycle fatigue behavior of post-installed shear connectors. In those tests, cyclic displacement ranges varying from 0.1 in. to 0.2 in. were applied to the connectors for up to 4000 cycles. None of the post-installed shear connectors failed under 4,000 cycles of loading except one HTFGB connector specimen which had been previously subjected to 5 million loading cycles under high-cycle fatigue testing.

Post-installed shear connectors that had not failed under fatigue loading were loaded statically to evaluate their residual strength. Tests conducted by Kayir (2006) showed that the ultimate strength of post-installed shear connectors is not significantly affected by previous fatigue loading.

2.7 APPROACHES FOR DESIGN OF COMPOSITE BRIDGE GIRDERS WITH POST-INSTALLED SHEAR CONNECTORS

The AASHTO composite beam design provisions are intended for new construction using welded shear studs, and are based on past research on these systems. Further, the current AASHTO specifications recognize fully composite design only, not partially composite design. The absence of provisions for partially composite design in AASHTO likely reflects the fact that fatigue design requirements for welded shear studs normally result in a large number of shear connectors that will typically lead to a fully composite beam for static strength calculations. Thus, partially composite design is not normally used for bridge girders. By contrast, partially composite design is used on a routine basis for composite beams in buildings, and the *AISC Specification* has included detailed design provisions for partially composite beams for many years. The popularity of partially composite beams in buildings reflects the great efficiency of partially composite design for both strength and stiffness, as illustrated in Figure 2.6 and Figure 2.8. The different approaches to composite beam design in bridges versus buildings (bridges normally use fully composite beams; buildings normally use partially composite beams) likely reflects the dominating influence of fatigue in design of the composite beams for bridges, and the absence of fatigue considerations in design of composite beams for buildings.

When considering the development of composite action in existing non-composite bridge girders, a number of changes from conventional bridge design practice are needed. The welded shear stud, commonly used in new construction, is not likely to be a practical alternative as a post-installed shear connector due to its relatively low fatigue strength.

Thus, the current practice of using welded shear studs must be changed to enable the use of unconventional shear connectors. Although there is a long history of research and testing of welded shear studs, there is little data on post-installed shear connectors. Consequently, much of this research project was aimed at developing concepts for post-installed shear connectors, and at conducting tests to determine the properties needed for design.

In addition to developing new types of shear connectors, economical strengthening of existing non-composite beams will almost certainly require adopting partially composite design. The cost of post-installed shear connectors for an existing bridge is likely to be higher than the cost of welded shear studs for new construction. Fully composite design will therefore likely be very costly for strengthening existing bridges. Thus, the economic viability of strengthening existing non-composite bridges by post-installing shear connectors will depend largely on the ability to implement partially composite design.

In the remainder of the study reported in this dissertation, three types of post-installed shear connectors were selected based on previous work on TxDOT Project 0-4124 and were further investigated using a direct-shear test setup. The post-installed shear connectors selected were the double-nut bolt (DBLNB), the high-tension friction grip bolt (HTFGB), and the adhesive anchor (HASAA). These shear connectors were tested under static and fatigue loadings. The feasibility of partially composite design using these post-installed shear connectors was then demonstrated in tests of full-scale composite beam specimens. Finally, a detailed case study was conducted on an existing non-composite bridge in the San Antonio area.

CHAPTER 3

Single Shear Connector Tests

3.1 INTRODUCTION

As discussed in Chapter 2, after a thorough review of the results of the single shear connector test results of Hungerford (2004), Schaap (2004), and Kayir (2006), three types of post-installed shear connectors were selected for further investigation in this study. Those were the Double-Nut Bolt (DBLNB), the High-Tension Friction-Grip Bolt (HTFGB), and the Adhesive Anchor (HASAA).

In the previous research on post-installed shear connectors, 3/4-in. diameter connectors were tested under static and fatigue loadings. Those previous studies showed that post-installed shear connectors are more costly and time-consuming to install than conventional welded shear studs. In this study, therefore, it was decided to use 7/8-in. diameter shear connectors to reduce the number of connectors needed to strengthen an existing bridge.

Although a limited number of static and fatigue tests had already been conducted on the DBLNB, HTFGB and HASAA shear connectors by Hungerford (2004), Schaap (2004), and Kayir (2006), the test database on these connectors was rather small, particularly for fatigue loading, and did not include any tests on 7/8-in diameter connectors. Consequently, supplemental static and fatigue tests were conducted on the DBLNB, HTFGB and HASAA connectors as part of this current study. The purpose of these supplemental tests was to collect data on the performance of 7/8-in. diameter connectors, and to supplement the previous static and fatigue test data on these connectors. This chapter describes the supplemental tests conducted on the DBLNB, HTFGB and HASAA connectors, and provides comparisons with the previous tests on 3/4-in. diameter connectors.

3.2 TEST PROGRAM ON SINGLE SHEAR CONNECTORS

3.2.1 Description of Test Specimens

The test specimen for the individual shear connector tests is illustrated in Figure 3.1. This testing arrangement was developed in the previous studies by Hungerford (2004), Schaap (2004), and Kayir (2006). The specimen consists of a 1-in. thick steel plate sitting on top of a concrete block. The plate (1- x 6- x 36-in.) is intended to represent the top flange of a steel beam, and the concrete block (7- x 24- x 24-in.) is intended to represent the concrete bridge deck. A shear connector is then installed to connect the plate to the block, and is loaded as shown in Figure 3.1. Stiffeners are welded to the side of the plate to minimize bending of the plate.

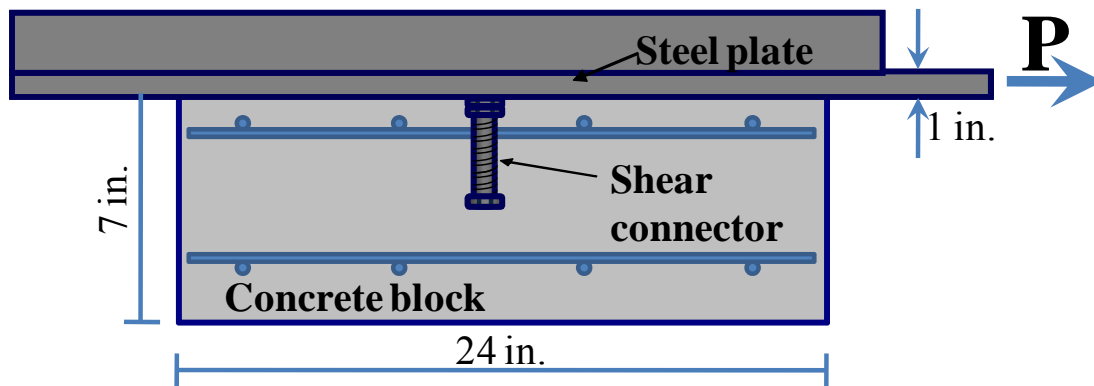


Figure 3.1: Single shear connector test specimen

As shown in Figure 3.2, the block was provided with two layers of deformed Grade 60 reinforcement (longitudinal and transverse directions, top and bottom), intended to represent the reinforcement typically found in the deck of older non-composite bridges. In the longitudinal direction of the block (the direction parallel to the applied load), #4 bars were placed at a 12-in. spacing. In the transverse direction, #5 bars were placed at a 6-in. spacing. A top clear cover of 1.5 in. (roadway side for real bridge slab) and a bottom clear cover 1 in. (bottom side for real bridge slab) were provided for the

specimens. Figure 3.3 also shows the bar layout in the concrete formwork before casting concrete.

The test specimens were cast with ready-mix concrete using a 1-cubic yard bucket. The maximum aggregate size was 3/4 in. and the specified 28-day design compressive strength was 3,000 psi, which is generally representative of the concrete used in older non-composite bridges. The inside surface of concrete formwork in Figure 3.3 was soaked with form oil before reinforcing bar cages were built to prevent the formwork from absorbing water from the fresh concrete. During the casting, the concrete was vibrated and screeded. Standard 4-x8-in. concrete cylinders were made along with the specimens and cured by the test specimens for compressive strength tests. After the casting, the exposed surface was covered with plastic sheeting for 5 days and sprayed with water twice a day for moist curing. Shear connectors were installed on the bottom side of the concrete block.

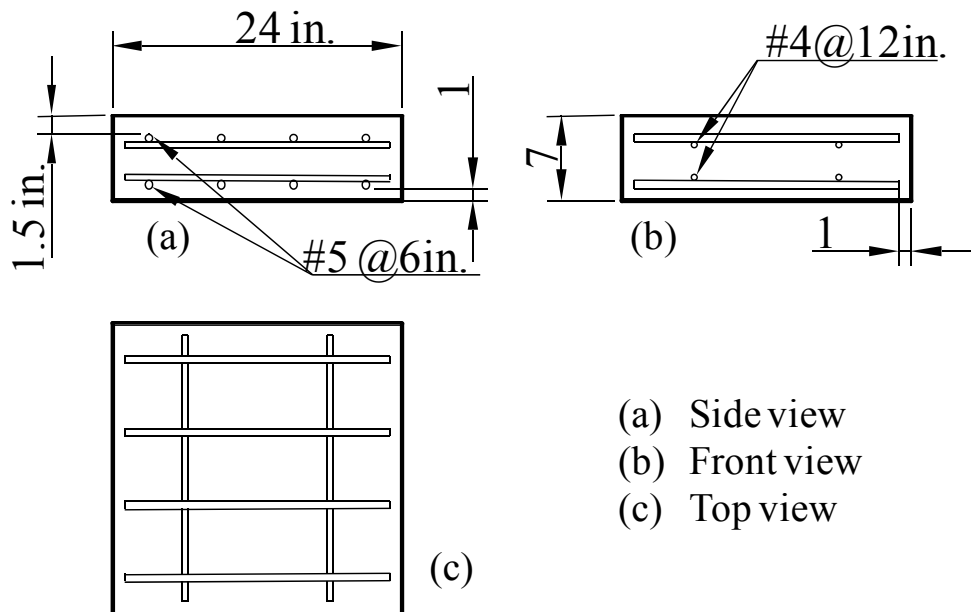


Figure 3.2: Reinforcing bar layout of single shear connector test specimens



Figure 3.3: Concrete formwork and reinforcing bar layout before concrete casting

3.2.2 Description of post-installed shear connectors

3.2.2.1 Double-Nut Bolt (DBLNB)

Early work on this shear connection method (Figure 3.4) was conducted at Iowa State University by Klaiber (1983), who investigated methods to increase the load capacity of existing composite girders by post-tensioning the steel girder. This post-tensioning resulted in an increased demand on the existing welded shear studs, and DBLNB connectors were used to supplement the existing studs.

In this study, the DBLNB connector used ASTM A193 B7 threaded rod instead of the SAE J429 - Grade 8 tap bolt which had been used in the single shear connector tests of Schaap (2004). ASTM A193 B7 threaded rod has rolled threads, which are believed to have better fatigue strength than the SAE J429 – Grade 8 tap bolt with cut threads (Benac 2007). The minimum specified ultimate strength of ASTM A193 B7 threaded rod is 125 ksi.

The DBLNB connector specimens were installed in the concrete blocks using procedures intended to simulate real construction procedures as much as possible. First, a 2-1/4-in. diameter hole was drilled through the concrete block using a rotary hammer drill as shown in Figure 3.5(a). Next, a 15/16-in. diameter hole was drilled through the steel plate using a portable drill with magnetic base. The connector was installed and tightened to a pretension of 39 kips with an impact wrench. “Squirter” Direct Tension Indicating (SDTI) washers were used to confirm the required pretension as shown in Figure 3.5(b). Finally the concrete block was placed on top of the steel plate and the hole was filled with a high-strength grout (Five Star[®] Highway Patch).

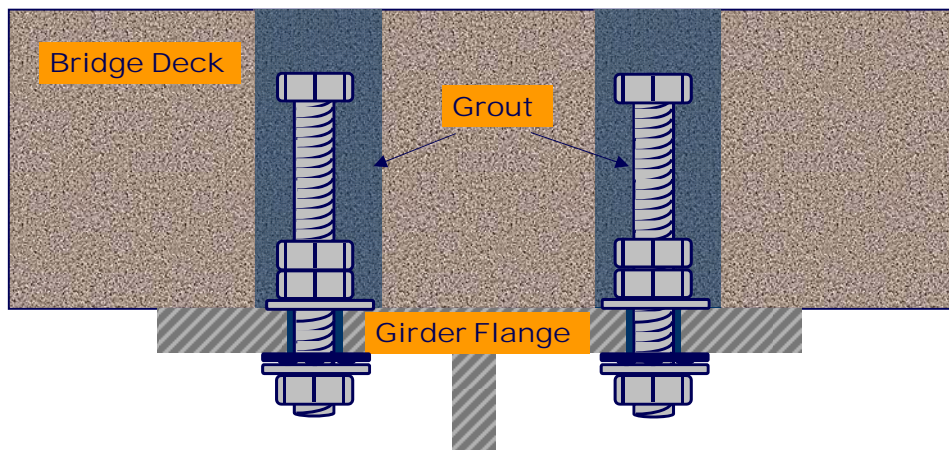


Figure 3.4: Double-Nut Bolt (DBLNB) connector



(a) Drilling hole through concrete block



(b) Installed shear connector

Figure 3.5: Installation of the DBLNB connector for single shear connector test

3.2.2.2 High-Tension Friction-Grip Bolt (HTFGB)

This shear connection method, shown in Figure 3.6, uses ASTM A325 high-strength bolts as the connector. The minimum specified ultimate strength of the connector material is 120 ksi. The HTFGB connector requires two different-size holes in the concrete block. First, a 1-in. diameter hole was drilled from one side of the concrete block to a depth of 5 in. From the other side of the block, a 2-in. diameter concentric hole was drilled to a depth of about 3 in. The two holes in the block were drilled from opposite sides to minimize spalling of concrete on the surface of the block during the drilling. For the actual installation of the HTFGB connectors in a bridge, both holes must be drilled from the top of the slab, as discussed in Chapter 4. Next, a 15/16-in. diameter hole was drilled through the steel plate using a portable magnetic drill. The connector was installed and tightened to a pretension of 39 kips with an impact wrench. “Squirter” Direct Tension Indicating (SDTI) washers were used to confirm the required pretension. Figure 3.7 shows the concrete surface after the installation. Finally, the hole on the surface of the concrete block was filled with high-strength grout (Five Star[®] Highway Patch).

Similar shear connection methods were investigated earlier at the University of Missouri and at Iowa State University. The high-strength bolt shear connector tested at the University of Missouri (Dallam, 1970), however, was intended for new construction. Klaiber (1983) at Iowa State University used epoxy to fill the gap between the oversized hole in the concrete slab and the connector shank, whereas in this study, to simplify installation, the gap was not filled.

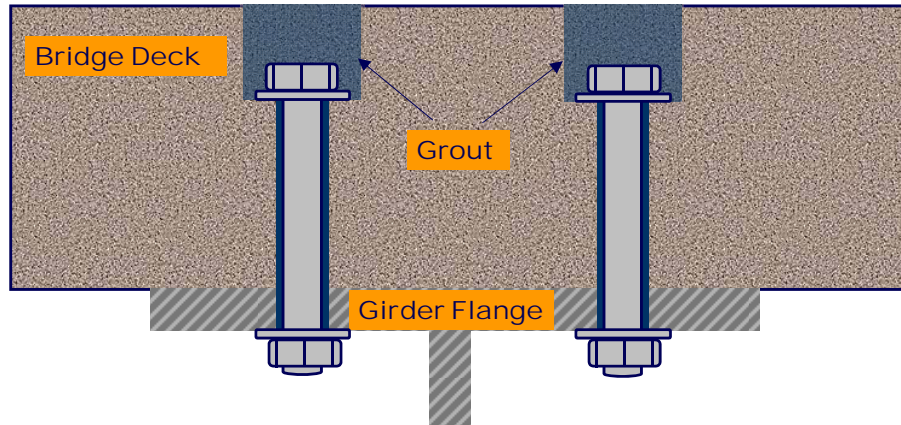


Figure 3.6: High-Tension Friction-Grip Bolt (HTFGB) connector



Figure 3.7: Concrete surface after installation of High-Tension Friction-Grip Bolt (HTFGB)

3.2.2.3 Adhesive Anchor (HASAA)

This shear connection method, shown in Figure 3.8, also uses ASTM A193 B7 threaded rod as the connector material. Hungerford (2004) and Kayir (2006) used ISO 898 Class 5.8 threaded rod (designated as HAS-E), which has a lower tensile strength than ASTM A193 B7 threaded rod. The higher strength B7 rod was used for this study to increase the capacity of the connector, and thereby reduce the number of connectors installed in a bridge. Adhesive used for this shear connection method was Hilti HY 150, a two-component adhesive.

The HASAA connector was the easiest to install of the three types of shear connectors tested in this study. First, 15/16-in. diameter holes were drilled through the steel plate and into the concrete block. After cleaning the hole in the concrete with a wire brush and compressed air, the adhesive was injected as shown in Figure 3.9. Then, the shear connector was inserted while twisting to an embedment depth of 5 in. Curing time of the adhesive is 50 min. at 60 °F. According to the adhesive manufacturer, the shear connector should not be disturbed during the curing time. After the adhesive was hardened, a nut was installed and tightened with a torque wrench to a torque of 150 lb-ft as recommended by the adhesive manufacturer.

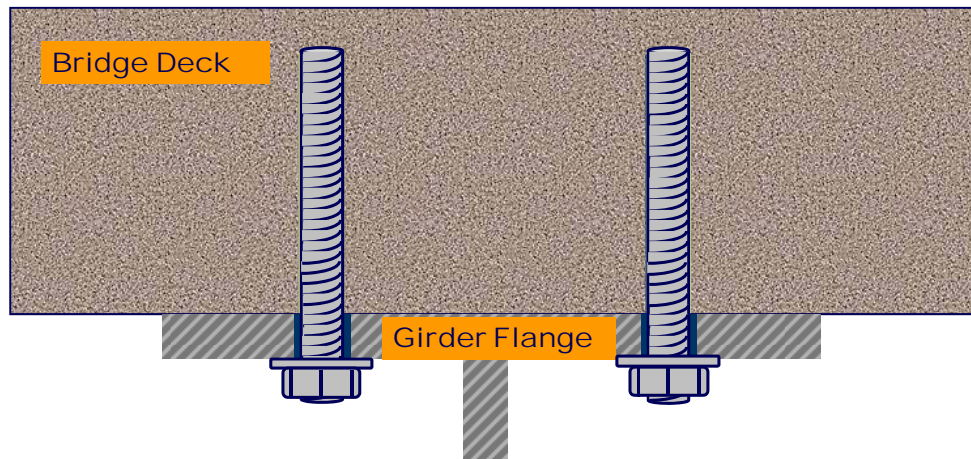


Figure 3.8: Adhesive Anchor (HASAA)



Figure 3.9: Injecting adhesive (HASAA)

3.2.3 Specimen Designations

Designations used for the single connector specimens start with the type of shear connector (DBLNB, HTFGB or HASAA), followed by a two-digit number. For static tests, this number represents the sequence of the tests. Since this number was counted from the tests conducted by Hungerford (2004), Schaap (2004), and Kayir (2006), it does not start from “01” in this dissertation. For high-cycle fatigue tests, the number is the stress range based on the estimated shear area. The last two letters represent the applied loading type. For full-scale beam tests described in Chapter 4, the two-digit number represents the shear connection ratio and the “BS” stands for Beam Static test. For duplicate specimens, a numeral is added at the end of the specimen name. Figure 3.10 describes the specimen designation system used in this study.

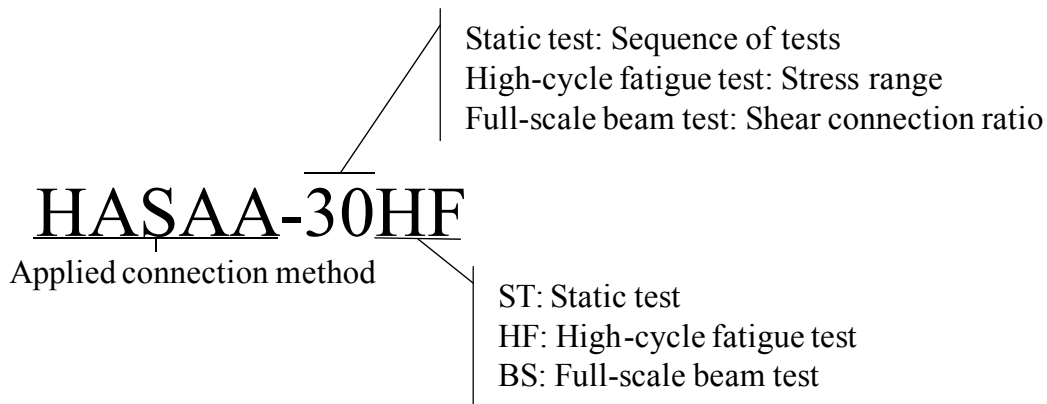


Figure 3.10: Specimen designations used in this study

3.2.4 Material Properties

3.2.4.1 Concrete and Grout

The concrete used for the test specimens had a specified 28-day compressive strength of 3,000 psi, and a maximum specified aggregate size of 3/4 in. The actual compressive strengths of the concrete at the time of each test were evaluated with 4- x 8-in. cylinders, and are summarized in Table 3.1.

Grout used for the DBLNB and HTFGB connectors was Five Star[®] Highway Patch, which is designed to provide high early strength. The manufacture specifies that roads can be opened to traffic 2 hours after application due to its high early strength. Its specified compressive strength at 2 hours is 2,000 psi. The compressive strength of the grout at the time of each test from 4- x 8-in. cylinders is also reported in Table 3.1.

3.2.4.2 HIT HY 150 Adhesive

The adhesive used for the HASAA connector was Hilti's HIT HY150, consisting of methacrylate resin, hardener, cement, and water. Its minimum specified compressive strength is 10,420 psi, and its minimum specified tensile strength is 2310 psi (Hilti 2006). Typical curing time at 68 °F is 50 minutes. The adhesive can be injected into the hole in

the concrete slab using a MD2000 dispenser, also manufactured by Hilti (Hilti 2006). The adhesive is viscous enough so that it can be used in overhead applications without the adhesive running out of the hole.

3.2.4.3 *Steel Plate*

The 1-in. thick steel plates used for the test specimens were ASTM A36 steel, with a yield strength of 48.1 ksi and an ultimate tensile strength of 71.9 ksi based on mill test reports (Kayir 2006).

Table 3.1: Material properties for single shear connector tests

Specimen	Concrete (psi)	Grout (psi)	Connector (ksi)		
			F_u	$0.6F_u$	F_v
DBLNB-05ST	3,020	3,670	147.0	88.2	91.1
DBLNB-06ST	3,020	3,670	147.0	88.2	91.1
DBLNB-07ST	3,020	3,670	147.0	88.2	91.1
HTFGB-05ST	3,550	-	148.6	89.1	87.7
HTFGB-06ST	3,550	-	148.6	89.1	87.7
HASAA-05ST	2,990	-	147.0	88.2	91.1
HASAA-06ST	2,990	-	147.0	88.2	91.1
HASAA-07ST	2,990	-	147.0	88.2	91.1
HASAA-20HF	3,840	-	173.6	104.2	105.1
HASAA-25HF	3,840	-	173.6	104.2	105.1
HASAA-25HF1	3,840	-	173.6	104.2	105.1
HASAA-30HF	3,840	-	173.6	104.2	105.1
HASAA-30HF1	3,410	-	147.0	88.2	91.1
HASAA-35HF	3,410	-	147.0	88.2	91.1
HASAA-40HF	3,410	-	147.0	88.2	91.1
DBLNB-45HF	6,040	6,360	173.6	104.2	105.1
HTFGB-35HF	6,230	-	148.6	89.1	87.7

F_u = ultimate tensile strength (ksi) F_v = ultimate shear strength (ksi)

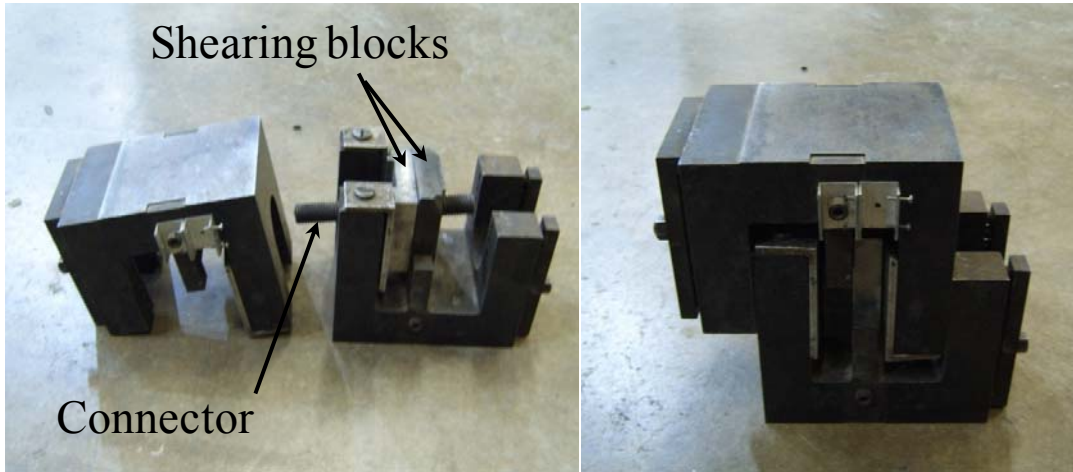
3.2.4.4 Shear Connector Materials

To determine the mechanical properties of the shear connector materials, tension and shear tests were conducted on the ASTM A193 B7 threaded rod used for the DBLNB and HASAA connectors and on the ASTM A325 high-strength bolts used for the HTFGB connectors. Tests were conducted using the specialized bolt-testing apparatus shown in Figure 3.11, and using 60-kip and 600-kip capacity Universal Testing Machines (UTM). Only ultimate strengths in shear and tension were determined from the tests.

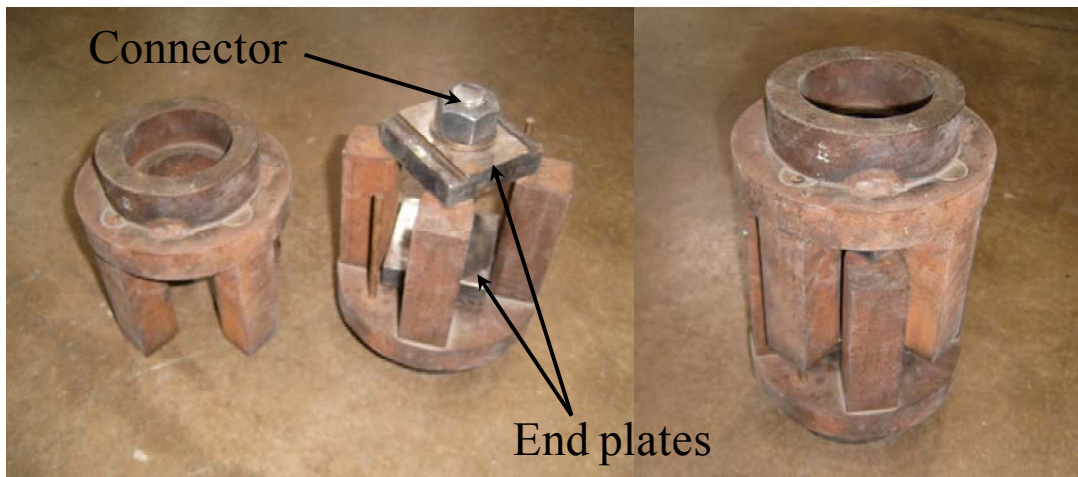
The shear test apparatus consists of two shearing plates and two blocks (Figure 3.11(a)). First, a shear connector was placed in the hole in the two shearing plates and one shearing plate was rested on the bottom block while the other plate was hung on the shear connector. Next, the top block was placed on the shearing plate and loaded to failure.

The tension test apparatus also has two plates and two blocks (Figure 3.11(b)). First, a connector was placed in the holes in the two plates and nuts were inserted on both sides of the connector. One plate was placed on the bottom block of the tension test apparatus and the other plate was hung on the other side of the bolt. Then, the top block was placed on the hung plate and loaded to failure.

Test results are listed in Table 3.1. The stress values reported in Table 3.1 were determined by dividing the failure loads by the effective area. The effective tension and shear areas of threaded part of the connector was taken as 75% and 80% of gross area of the unthreaded connector, respectively, as specified in the *AISC Specification*. Figure 3.12 shows typical failed sections of the connectors after the tests. Table 3.1 lists the tensile stress at fracture (F_u) and the shear stress at fracture (F_v). Also listed in the table is the value of $0.6F_u$, as this is often used as an estimate of F_v . Note from Table 3.1 that all of the shear connectors had a measured tensile strength significantly greater than the minimum specified values of 120 ksi for the A325 bolt, and 125 ksi for the B7 rod. The data in Table 3.1 also indicate that taking 60 percent of the measured tensile strength provides a very good estimate of the measured shear strength.



(a) Shear testing



(b) Tension testing

Figure 3.11: Shear and tension testing apparatus for connectors



(a) Failure sections in shear

(b) Failure sections in tension

Figure 3.12: ASTM A193 B7 rods after shear and tension tests

3.2.5 Test Setup and Instrumentation

The single shear connector tests were conducted using the direct-shear test setup shown in Figure 3.13. This is the same test setup that had been used by Kayir (2006). To hold the concrete block firmly in place during the tests, gaps between the reaction angles and the concrete block was filled with hydrostone (gypsum cement). A clamping rod was also used to prevent uplift of the steel plate. To minimize friction due to clamping, the clamping rod had strips of Teflon sheets on the plate washers clamping the steel plate.

For static tests, applied load and slip were measured at the steel-concrete interface. Load was applied with a 10,000-psi capacity pneumatic oil pump, manually operated. A 100-kip capacity load cell was attached between the clevis and the hydraulic ram. Two displacement transducers were installed on the test specimen to measure the slip at the steel-concrete interface as shown in Figure 3.14. Readings from these two transducers were averaged to determine the slip between the steel plate and the concrete block.

For fatigue tests, a hydraulic pump was connected to the hydraulic ram and the applied load was controlled by an MTS Model 407 controller (MTS 2000). The controller permits application of cyclic load between specified maximum and minimum loads with

automatic shutoff based on the specified loads. The slip at the steel-concrete interface was not measured for fatigue tests.

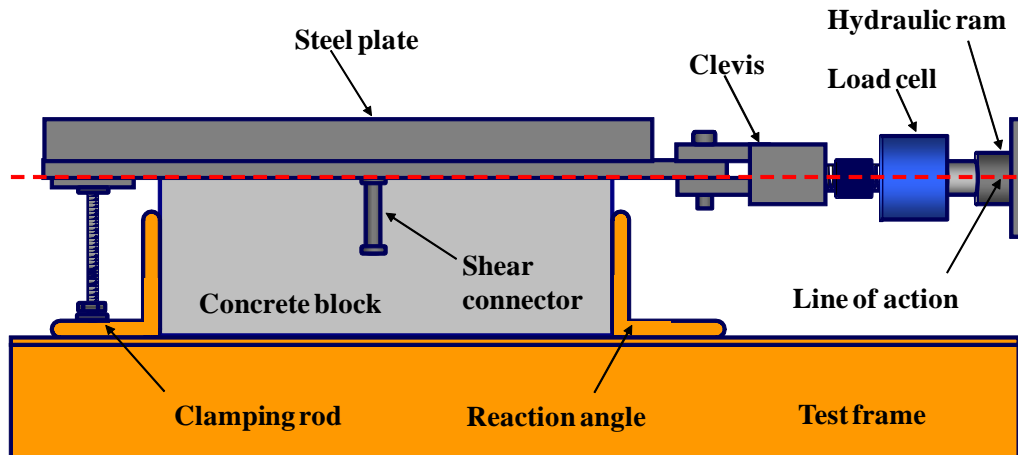


Figure 3.13: Direct-shear test setup for single shear connector tests (Kayir 2006)



Figure 3.14: Instrumentation for single shear connector tests

3.2.6 Test procedure

Static tests for single shear connectors were conducted to evaluate static strength, stiffness, and slip capacity of the post-installed 7/8-in. diameter shear connectors. Static tests were conducted using displacement control. Displacement and load were applied to the specimen with a 10,000-psi capacity pneumatic oil pump. For most of the specimens, displacement was increased monotonically until the shear connector failed.

For the fatigue tests, load control was used to apply a specified stress range to the test specimens. The specimens were loaded to the set point, which is the average between the maximum and minimum loads for a specified stress range. To prevent reversal of load a minimum load of 0.9 kips was set for each load range. Sinusoidal cyclic load was then applied until the connector failed or until 5 million cycles were applied. Test specimens which had not failed under 5 million cycles of loading were then loaded statically to failure to evaluate residual strength.

3.3 SINGLE SHEAR CONNECTOR TEST RESULTS

Three types of post-installed shear connectors, the DBLNB, HTFGB, and HASAA, were tested in this study. This section presents test results of single post-installed shear connectors under static and fatigue loading.

3.3.1 Static Behavior of Post-Installed Shear Connectors

Static tests were conducted to evaluate initial stiffness, ultimate strength, and slip capacity of post-installed shear connectors. The ultimate strength, Q_u , and maximum slip capacity, s_{\max} , of the shear connectors are listed in Table 3.2.

All specimens showed consistent load-slip behavior. Load-slip curves for each test specimen are shown in Figure 3.15 to Figure 3.17. All of the shear connectors except Specimen HTFGB-05ST showed connector failures at around $0.95Q_u$ on the descending

branch of the load-slip curve. This point was taken as the maximum slip capacity of the test specimens.

Table 3.2: Test results for single shear connector specimens

Specimen	DBLNB -05ST	DBLNB -06ST	DBLNB -07ST	HTFGB -05ST	HTFGB -06ST	HASAA -05ST	HASAA -07ST	HASAA -07ST
Q_u (kips)	43.77	39.57	40.45	55.33	50.67	37.07	34.69	36.79
s_{max} (in.)	0.45	0.40	0.31	1.45	1.54	0.41	0.42	0.39

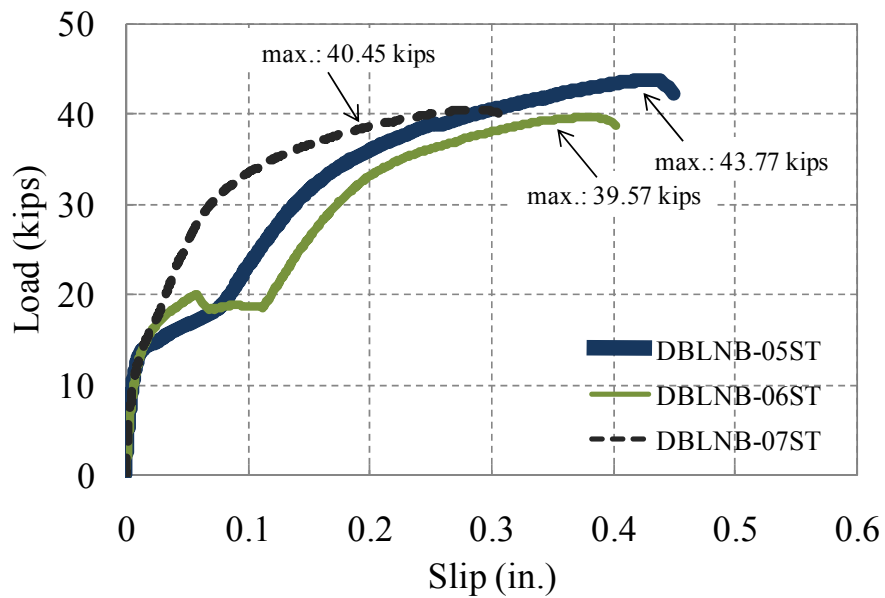


Figure 3.15: Static test results of single shear connectors (DBLNB)

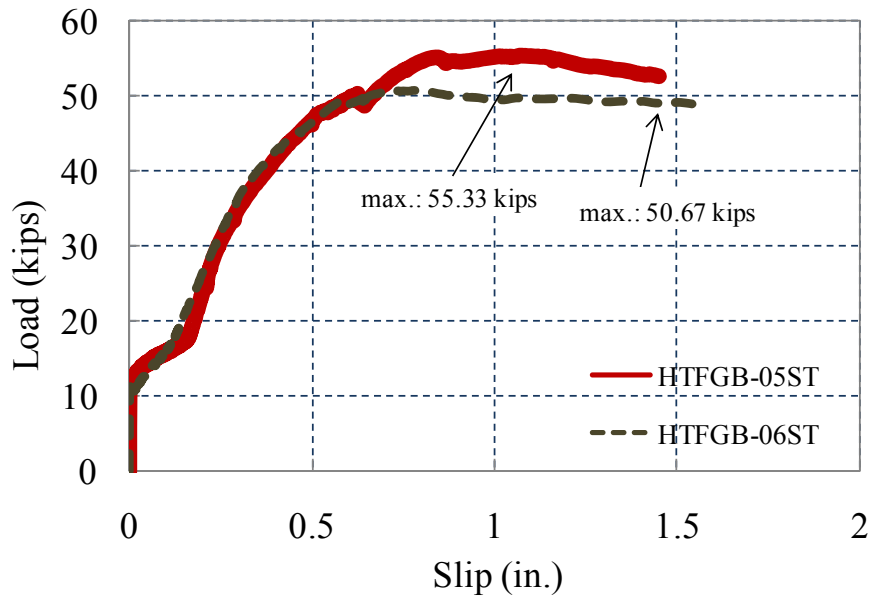


Figure 3.16: Static test results of single shear connectors (HTFGB)

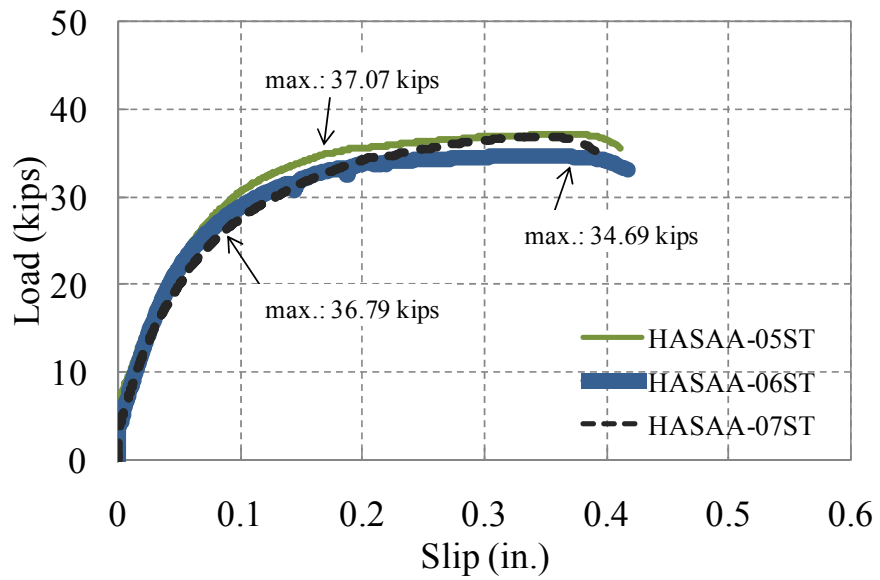


Figure 3.17: Static test results of single shear connectors (HASAA)

3.3.1.1 Double-Nut Bolt (DBLNB)

The three DBLNB connector specimens showed consistent ultimate strengths. The average strength of the three test specimens was 41.3 kip and the average slip capacity was 0.39 in. All of the DBLNB connector specimens showed connector failure at the steel-concrete interface. Figure 3.18 shows a typical failed connector section of Specimen DBLNB-07ST.

The specimens showed high stiffness in the elastic range. This may be due to the double nuts embedded in the concrete, which results in an increase of the bearing surface between the connector and the concrete. This increased bearing surface may also have helped to delay concrete crushing in front of the shear connector.

The specimens showed a sudden increase in slip at about 12 kips of loading due to slip of the shear connector in the oversized hole in the steel plate after friction was overcome (Figure 3.15). The amount of the slip varied according to the location of the connector in the oversized hole.



(a) Failed connector in the steel plate

(b) Failed connector in the concrete block

Figure 3.18: Typical failed section of DBLNB connector (DBLNB-07ST)

3.3.1.2 High-Tension Friction-Grip Bolt (HTFGB)

Only two HTFGB specimens were tested because the concrete block of the third specimen was damaged during installation. The average ultimate strength of the test specimens was 53.0 kips. For the HTFGB connector specimens, the threads were not in the shear plane, in contrast to the DBLNB and the HASAA connector specimens, which did have threads in the shear plane. The average ultimate slip of the HTFGB was 1.49 in., much larger than that of the DBLNB connectors. Note that the axes of the load-slip curves of Figure 3.16 (HTFGB) have different scales than those of Figure 3.15 (DBLNB).

The HTFGB connector specimens showed very high stiffness at low load levels because this connection method uses friction as a shear-transfer mechanism under initial loading. Both test specimens showed less than 0.01-in. slip at 11 kips of loading.

Specimen HTFGB-05ST was not loaded to connector failure due to significant cracking in the concrete block (Figure 3.19). The test was stopped at 1.83-in. slip. The load at this level of slip was 45.0 kips which was 80 percent of its maximum load on the descending branch. Similar cracks were also observed in Specimen HTFGB-06ST, even though the connector failed in shear.



Figure 3.19: Cracks in the concrete block and deformed connector (HTFGB-05ST)

3.3.1.3 Adhesive Anchor (HASAA)

Figure 3.17 shows load-slip curves for the HASAA connector specimens. These showed the most consistent behavior among the three shear connection methods. The average maximum strength and maximum slip capacity were 36.2 kips and 0.41 in., respectively.

The initial stiffness and average maximum strength of the HASAA connectors were less than for the DBLNB connector specimens. It is believed that the torque applied to this shear connector is not sufficient to create a large friction force at the interface. Therefore, the connectors resisted the applied shear primarily in bearing, starting at low load levels. However, very stable behavior without abrupt stiffness change was observed for these connectors. The abrupt stiffness change due to slip of the connector in the oversized hole in the steel plate was not observed since the annulus between the connector and the edge of the hole was filled with the adhesive during the installation as shown in Figure 3.20 (a). Figure 3.20 shows the failed section of Specimen HASAA-07ST.



(a) Failed connector in the steel plate



(b) Failed connector in the concrete block

Figure 3.20: Failed section of HASAA connector (HASAA-07ST)

3.3.2 Fatigue Behavior of Post-Installed Shear Connectors

Fatigue strength of a shear connector can be represented by the number of cycles of loading to failure under a specified stress range. Kayir (2006) evaluated fatigue strength of the three types of post-installed shear connectors as well as other types of shear connectors. In that study, DBLNB and HTFGB connector specimens showed very high fatigue strength compared to the HASAA connector specimens. In this study, ASTM A193 B7 threaded rod was used for the HASAA connectors instead of ISO 898 Class 5.8 threaded rod used by Kayir (2006).

Due to the long time duration needed to conduct a test, only a limited number of shear connectors was tested under fatigue loading. Test results for post-installed shear connector specimens under fatigue loading are listed in Table 3.3. The DBLNB and HTFGB connectors were tested under 45 ksi and 35 ksi stress ranges respectively, and did not fail after 5 million loading cycles. The HASAA connectors were tested under stress ranges varying from 20 ksi to 40 ksi, and all failed before reaching 5 million cycles. The fatigue strengths of the shear connector specimens show considerable scatter.

Specimens DBLNB-45HF and HTFGB-35HF1 did not fail after 5 million loading cycles. For these specimens, fatigue loading was continued. The specimens were then tested under static loading to determine if their static strength was substantially reduced as a result of the previous fatigue loading. The maximum residual strengths of Specimen DBLNB-45HF and HTFGB-35HF1 were 50.3 kips and 61.4 kips respectively. These high values suggest that the 5 million fatigue cycles had little effect on the residual static strength of the connectors.

Figure 3.21 shows the test results along with the AASHTO design equations for conventional welded shear studs. Data points for specimens that did not fail under 5 million cycles of loading are plotted with arrows adjacent to them, indicating that the number of cycles to failure would have exceeded the number recorded. The post-installed shear connectors investigated in this study showed much higher fatigue strength than the AASHTO equations for conventional welded shear studs.

Table 3.3: Test results of single shear connectors under fatigue loading

Specimen	DBLNB-45HF	HTFGB-35HF1	HASAA-40HF	HASAA-35HF	HASAA-30HF
Cycles to failure	5,111,963*	5,002,658*	56,054	210,318	341,574
Specimen	HASAA-30HF1	HASAA-25HF	HASAA-25HF1	HASAA-20HF	-
Cycles to failure	58,201	1,144,47	164,035	4,361,903	-

*: Specimen did not fail under the cycles of fatigue loading

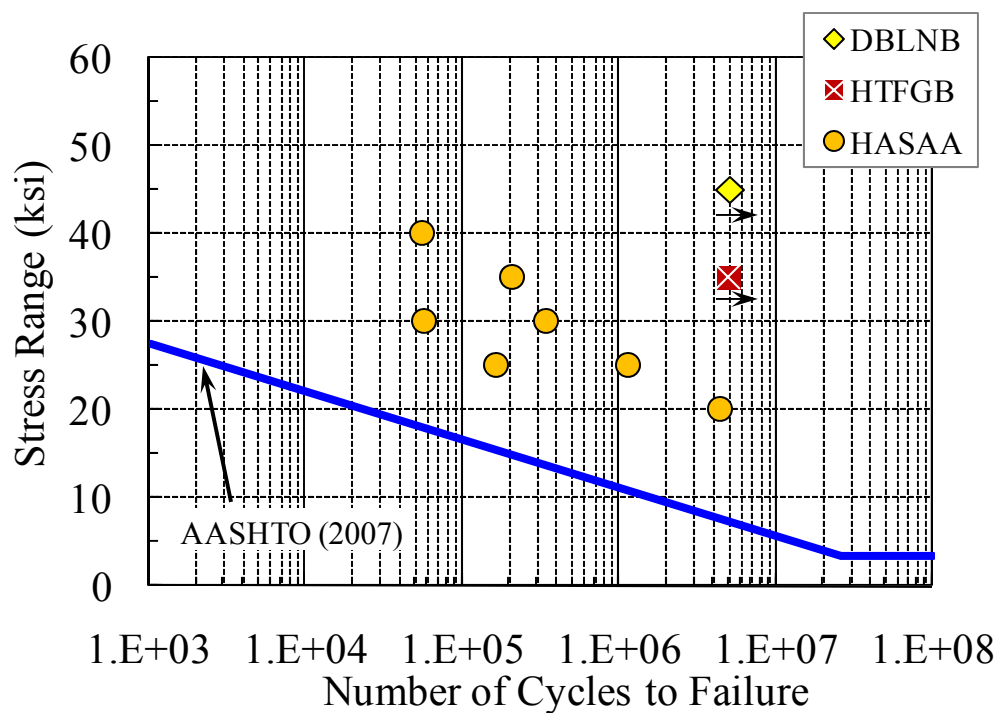


Figure 3.21: Fatigue test results of single shear connectors, compared with AASHTO equation for welded shear studs

3.4 CONNECTORS IN LIGHTLY REINFORCED CONCRETE BLOCKS

3.4.1 Details of Test Specimens

The shear connectors whose testing is described in the previous sections were installed in the concrete blocks with reinforcing details as shown in Figure 3.2. Spacing of the transverse reinforcing bars was 6 in. Those reinforcing details were recommended by a project advisor at Texas Department of Transportation (TxDOT), because that transverse bar spacing was commonly used for the concrete slabs of existing non-composite steel girder bridges.

To investigate the influence of transverse reinforcement spacing on shear connector performance, nine HASAA connectors were also installed in concrete blocks with transverse reinforcing bars spaced at 12 in. Six specimens were tested under static load and the other three specimens were tested under fatigue loading. Material properties of the nine HASAA connector specimens are listed in Table 3.4. Details of the specimens are identical to those of the HASAA specimens in the previous section except for the wider spacing of transverse reinforcing bars.

Table 3.4: Material properties of the HASAA connectors with wider spacing of transverse reinforcement

Specimen	Concrete (psi)	Connector (ksi)		
		F_u	$0.6F_u$	F_{shear}
HASAA-08ST	3450	147.0	88.2	91.1
HASAA-09ST	3450	147.0	88.2	91.1
HASAA-10ST	3450	147.0	88.2	91.1
HASAA-11ST	3450	147.0	88.2	91.1
HASAA-12ST	3450	147.0	88.2	91.1
HASAA-13ST	3450	147.0	88.2	91.1
HASAA-30HF2	3450	173.6	104.7	105.1
HASAA-30HF3	3450	173.6	104.7	105.1
HASAA-35HF1	3450	173.6	104.7	105.1

3.4.2 Static Test Results

Specimens HASAA-08ST to HASAA-13ST were installed in concrete blocks with a 12-in. transverse reinforcing bar spacing. The average maximum strength and slip capacity of the six HASAA specimens installed in the lightly reinforced concrete blocks were 30.9 kips and 0.73 in. respectively (Table 3.5). All of the six shear connector specimens were loaded until shear connector fracture and all of the concrete blocks showed longitudinal cracks as shown in Figure 3.22. These longitudinal cracks had not been observed for Specimens HASAA-05ST to HASAA-07ST, with transverse reinforcing bars spaced at 6 in.

Table 3.5: Test results of the HASAA connectors with wide reinforcing bar spacing (Static loading)

Specimen	HASAA-08ST	HASAA-09ST	HASAA-10ST	HASAA-11ST	HASAA-12ST	HASAA-13ST
Q_u (kips)	32.71	32.88	28.74	30.98	35.18	24.86
s_{max} (in.)	0.70	0.63	0.75	0.78	0.51	1.03



Figure 3.22: Failed shear connector installed in lightly reinforced concrete block (HASAA-11ST)

Test results of these specimens were not consistent with those of Specimen HASAA-05ST to HASAA-07ST, which had concrete blocks with 6-in. transverse reinforcing bar spacing. Figure 3.23 shows load-slip curves for the HASAA connector specimens installed in the lightly reinforced concrete blocks along with the load-slip curve for Specimen HASAA-05ST. Only two specimens showed initial stiffness similar

to that of Specimen HASAA-05ST; the other four specimens showed significantly lower stiffness than Specimen HASAA-05ST. All six specimens showed lower strength than Specimen HASAA-05ST. Specimen HASAA-13ST showed a maximum strength less than 70 percent of the average of the three HASAA connector specimens with 6-in. transverse reinforcing bar spacing.

All of the six HASAA connector specimens installed in the lightly reinforced concrete blocks showed larger slip capacity than Specimen HASAA-05ST. However, the slip capacity measured in the tests was also inconsistent.

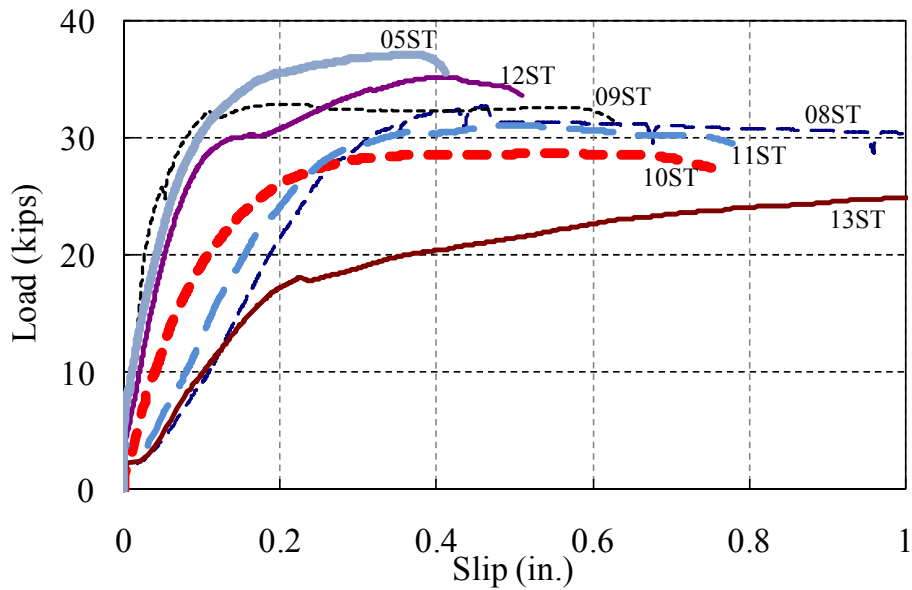


Figure 3.23: Static test results of single shear connectors (HASAA in lightly reinforced blocks)

3.4.3 Fatigue Test Results

Three HASAA connector specimens installed in lightly reinforced concrete blocks were also tested under fatigue loading, with the test results shown in Table 3.6. The HASAA connector specimens installed in lightly reinforced concrete blocks showed much lower fatigue strength than the otherwise identical specimens installed in concrete blocks with a 6-in. reinforcing bar spacing. Figure 3.24 shows the test results of all HASAA connector specimens under fatigue loading. As shown in the figure, it seems that the large reinforcing bar spacing is detrimental to the fatigue strength of shear connectors.

Table 3.6: Test results of the HASAA connectors under fatigue loading

Specimen	HASAA-30HF2	HASAA-30HF3	HASAA-35HF1
Number of Cycles to failure	9,841	21,499	101,842

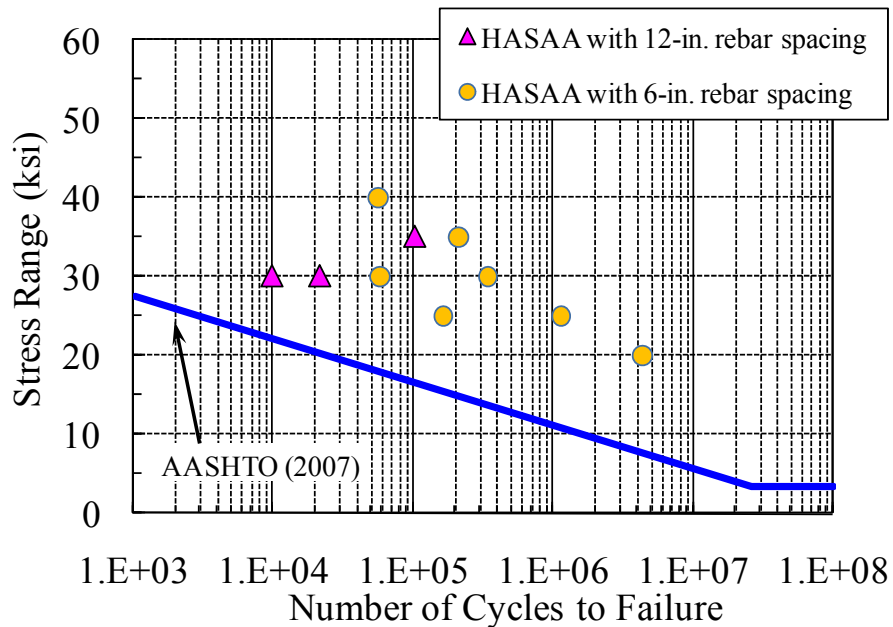


Figure 3.24: Static test results of single shear connectors

3.5 DISCUSSION OF TEST RESULTS

A total of 26 single shear connector specimens were tested under static and fatigue loads. Static strength, stiffness, and slip capacity of the shear connectors under static loading are discussed in this section. Next, design equations for the post-installed shear connectors under fatigue loading are proposed based on the test results in this study and the tests conducted by Kayir (2006). Finally, the effect of reinforcing details on the behavior of shear connectors is also discussed in this section.

3.5.1 Static Tests

3.5.1.1 Strength and Stiffness under Static Loading

In this study, high-strength connector materials were used for post-installed shear connectors to minimize the number of shear connectors needed for strengthening existing bridge girders. ASTM A193 B7 threaded rod was used for the DBLNB and HASAA connectors and ASTM A325 high-strength bolt was used for the HTFGB connector.

All shear connector specimens except Specimen HTFGB-05ST failed by fracture of the connector. Figure 3.25 shows failed connectors and concrete damage in front of the shear connectors. The DBLNB connector specimens showed less concrete crushing than the other two types of shear connector specimens, apparently due to the large bearing area of nuts embedded in the concrete block.

The high shear forces applied to the 7/8-in diameter high strength connectors in these tests caused significant cracks in the concrete blocks for the HTFGB connector specimens. Specimen HTFGB-05ST did not show connector fracture and the test was stopped after significant cracks developed in the concrete block. Only localized cracks were observed for the DBLNB and HASAA connector specimens with a 6-in. transverse reinforcing bar spacing. Note that in the large-scale beam tests described in Chapter 4, the beam specimen that was retrofitted with 7/8-in HTFGB connectors did not show the type of severe cracking observed in the single connector tests.



a. DBLNB-06ST

b. HTFGB-06ST

c. HASAA-06ST

Figure 3.25: Failed shear connectors after tests

Kayir (2006) developed Equation 2.28 to predict the maximum strength of post-installed shear connectors under static loading. The equation takes the ultimate shear strength of post-installed shear connectors as one-half of the tensile strength of the connector material. The effective shear area of the threaded rod can be estimated as 80 percent of the unthreaded area. The load ratio (observed maximum static strength divided by the predicted maximum strength from Equation 2.28) for each test specimen is plotted in Figure 3.26. For computing the predicted strength using Equation 2.28, the actual measured values of F_u of the connector material were used. With one possible exception, the post-installed shear connectors tested in this study showed a somewhat higher strength than that predicted using Equation 2.28. Specimen HASAA-06ST had a load ratio 0.98, only slightly less than unity. From Figure 3.26, it is apparent that Equation 2.28 underestimates the strength of several connectors, and comes very close for others. Based on the limited available data, Equation 2.28 appears to provide a simple and reasonable design basis for estimating the static strength of post-installed shear connectors.

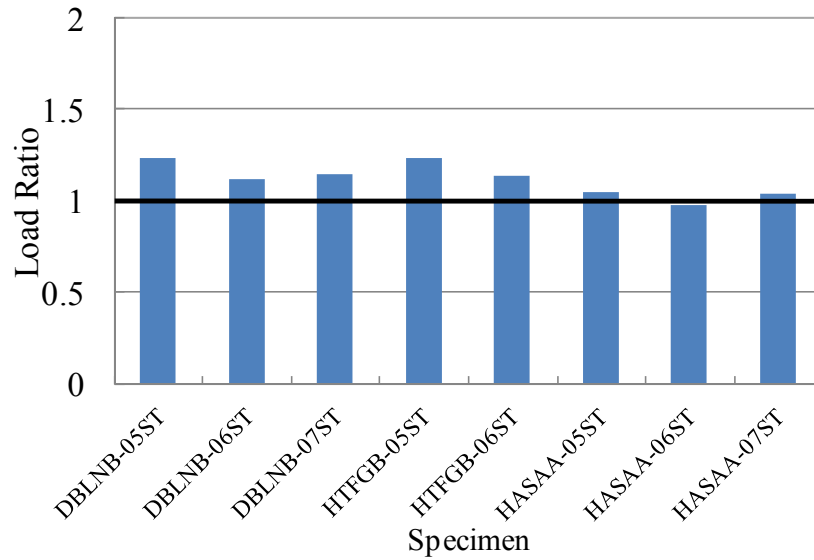


Figure 3.26: Comparison of load ratio for post-installed shear connectors

Among the three shear connection methods, the HTFGB connector showed the highest initial stiffness. The HTFGB connector initially transfers shear at the steel-concrete interface by friction. With the HTFGB connector, a composite beam can achieve full composite action without any slip at the steel-concrete interface before the friction is overcome. Friction is also an ideal shear transfer mechanism for fatigue load because the connector itself is not engaged in bearing and does not experience significant stress fluctuations. The DBLNB connector specimens also showed high initial stiffness due to the large bearing area of the embedded nuts.

To compare the overall stiffness of the post-installed shear connectors with that of conventional welded studs, the ratio of the load at 0.2-in. slip to the maximum load for each post-installed shear connector was compared with the same ratio for conventional welded shear studs. Ollgaard *et al.* (1971) developed equations to predict the load-slip behavior of the conventional welded shear studs as shown in Equations 2.3 and 2.4. These equations predict 99 percent and 94 percent of its ultimate load at 0.2-in. slip, respectively. Table 3.7 shows loads of shear connectors at 0.2-in. slip and the ratio of those loads to the ultimate strength.

The HASAA connector showed the highest load ratio (load at 0.2 in. slip / Max. load) among the three shear connection methods. It is believed that the oversized hole in the concrete slab for the HTFGB connector and in the steel beam flange for the HTFGB and DBLNB connectors reduce the strength of these connectors at low slip levels. The effect of oversized holes on the system behavior of composite beams retrofitted with post-installed shear connectors is investigated using finite element analysis in Chapter 5.

Table 3.7: Stiffness of single shear connector specimens

Specimen	DBLNB -05ST	DBLNB -06ST	DBLNB -07ST	HTFGB -05ST	HTFGB -05ST	HASAA -05ST	HASAA -07ST	HASAA -07ST
Load at 0.2 in.	35.98	33.10	38.69	23.93	26.45	35.52	33.84	34.21
Q_u	43.77	39.57	40.45	55.33	50.67	37.07	34.69	36.79
Ratio to Q_u (%)	82.2	83.6	95.6	43.2	52.2	95.8	97.5	93.0

3.5.1.2 Slip Capacity under Static Loading

Shear connectors are required to have enough slip capacity to redistribute shear force to adjacent shear connectors after yielding. Most conventional welded shear studs show slip capacities greater than 0.2 in., which is considered adequate to provide ductile behavior of the entire composite beam system (Viest et al. 1997). All post-installed shear connectors tested in this study showed more than 0.2-in. slip capacity. The DBLNB connector showed the least average slip capacity, 0.39 in.

From the single shear connector tests, the slip capacity of shear connectors appears to be significantly affected by the confinement of the connector. The HTFGB connector has a gap around the connector due to the oversized hole in the concrete block.

The DBLNB connector has a larger bearing area than the HASAA connector due to the embedded nuts which reduce concrete crushing in front of the connector. High-strength grout was also used to fill the gap in the concrete slab after the DBLNB connectors were installed. Figure 3.27 shows shear connectors extracted from the concrete blocks after the tests. Deformation of the shear connectors in Figure 3.27 indicates the amount of slip before the shear connectors failed.

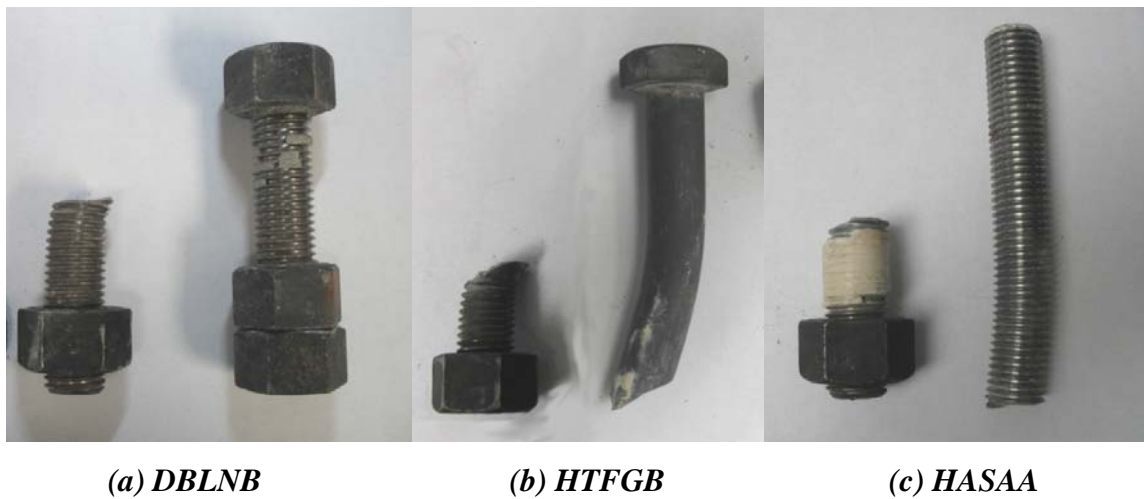


Figure 3.27: Failed shear connectors after the tests

3.5.2 Fatigue Tests

3.5.2.1 Comparison with Previous Research

Among the three types of post-installed shear connectors, the DBLNB and HTFGB connectors had much higher fatigue strength than the HASAA connector, and all post-installed shear connectors have higher fatigue strengths than the AASHTO curve for conventional welded studs.

In Figure 3.28, fatigue test results from this study are plotted along with the results of Kayir (2006). Test specimens which did not fail after 5 million cycles of

loadings are plotted with rightward arrows adjacent to the data points. It is clear that all of the post-installed shear connectors have significantly higher fatigue strength than the S-N curve for conventional welded shear studs given by AASHTO (2007).

The DBLNB and HASAA connectors used the same high-strength threaded rod for the connector material. As shown in Figure 3.28, the DBLNB connector specimens showed significantly higher fatigue strength than the HASAA connector specimens. The reason for this difference is not clear. However, the fatigue life of the DBLNB connectors may benefit from the double nuts at the steel concrete interface, which may reduce bending of the connector.

In contrast to the DBLNB and HTFGB connectors, all of the HASAA connector specimens failed before reaching 5 million cycles of loading. In this study, the HASAA connector specimens with ASTM A193 B7 threaded rod followed the trends of the test results for the HASAA connector specimens with ISO 898 Class 5.8 threaded rod tested by Kayir (2006). For the HASAA connector specimens, scatter in fatigue strength is evident in Figure 3.28. Because of this variability, additional fatigue tests would be desirable to better characterize the variability.

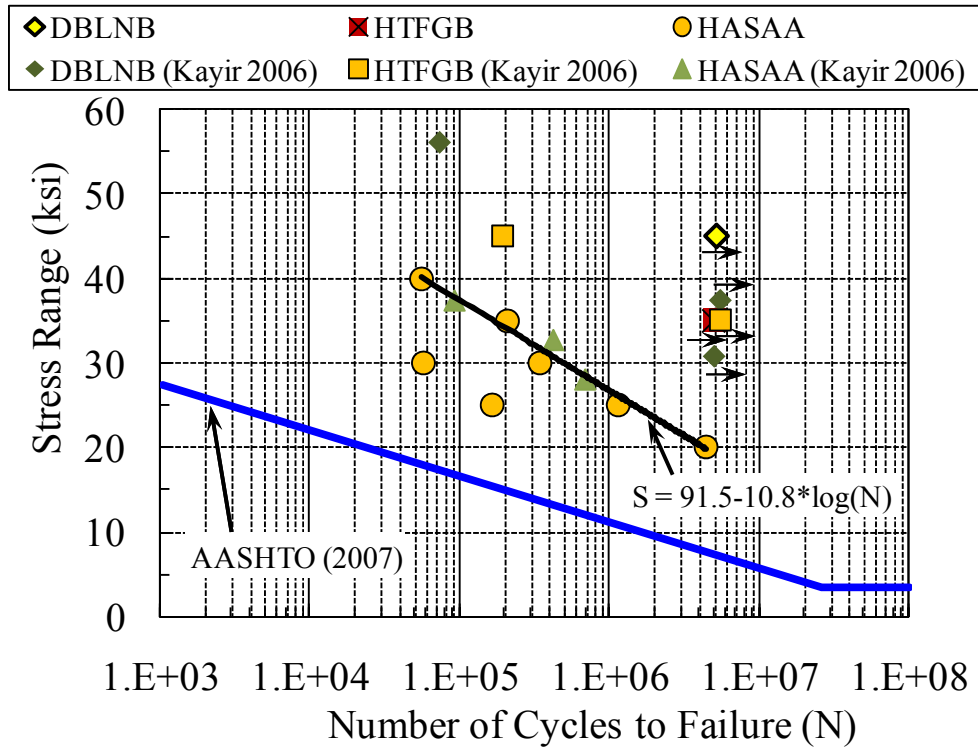


Figure 3.28: Fatigue test results of post-installed shear connectors

3.5.2.2 Predicting Fatigue Strength

Both the *AASHTO Standard Specifications* and the *AASHTO LRFD Specifications* define fatigue strength of conventional welded shear studs as a function of stress range. Slutter and Fisher (1966) report that the concrete strength does not significantly affect fatigue strength of the welded shear studs.

In this study, post-installed shear connectors showed superior fatigue strength compared to conventional welded shear studs. The number of fatigue test results for the HTFGB and DBLNB connectors under fatigue loading is not adequate to develop S-N curves to predict the fatigue strength of the shear connectors. However, it is possible to suggest a fatigue endurance limit for the HTFGB (ASTM A325 bolts) and DBLNB (ASTM A193 B7 threaded rods) connectors based on the test results in Figure 3.28. The

fatigue endurance limit for the HTFGB and DBLNB connectors is proposed to be a stress range of 35 ksi. Based on this stress range, Equation 3.1 can be used to define the endurance limit for the shear force range on the connector.

$$Z_r = 35ksi \times A_{sc} \quad (3.1)$$

where, Z_r = allowable range of shear force on the connector, kips

A_{sc} = effective shear area of the connector, in.²

The HASAA connector showed lower fatigue strength than the other two shear connection methods. Based on the test results, Equation 3.2 is recommended for the design of the HASAA connector under fatigue loading. Specimens HASAA-30HF1 and HASAA-25HF1 which showed significantly lower fatigue strength than the duplicate specimens with same stress ranges were not taken into account in the linear interpolation used to develop Equation 3.2 (Figure 3.28).

$$Z_r = (91.5 - 10.8 \log N) \times A_{sc} \quad (3.2)$$

where, N = number of cycles of fatigue loading

Since all HASAA shear connectors failed under the stress range tested in this study, more tests with a lower stress range should be conducted to determine the endurance limit of the HASAA connector. Equation 3.2 can be used for the HASAA connector with both ASTM A193 B7 threaded rod and ISO 898 Class 5.8 threaded rod.

3.5.3 Shear Connectors in Lightly Reinforced Concrete Blocks

In this research, nine HASAA connectors were installed in concrete blocks with 12-in. transverse reinforcing bar spacing. These specimens showed highly inconsistent test results under both static and fatigue loadings.

The shear connectors in the lightly reinforced concrete blocks had less confinement than the shear connectors installed in the blocks with 6-in. reinforcing bar

spacing. The low stiffness and strength of the shear connectors in the lightly reinforced blocks can be attributed to the lower confinement resulting from the larger reinforcing bar spacing. The low confinement of the shear connectors likely caused significant bending in the connectors in addition to shear stress, resulting in higher principal stress in the shear connectors. It is believed that this higher stress caused the HASAA shear connector specimens with 12-in. spacing of transverse reinforcing bar to have a lower maximum strength than those with a 6-in. spacing.

The HASAA connector specimens installed in the lightly reinforced concrete blocks showed large slip capacity. As shown in Figure 3.29, the longitudinal cracks in the concrete blocks are considered to be the result of the reduction in confinement around the shear connector. The HASAA connector specimens installed in the concrete blocks with 6-in. reinforcing bar spacing did not show longitudinal cracks in the concrete blocks.

The HASAA connectors installed in the concrete blocks with 12-in. reinforcing bar spacing showed significantly lower stiffness than the connectors in blocks with 6-in. reinforcing bar spacing. It is believed that large deformation of the shear connectors resulted in higher principal stresses due to the combination of shear and bending of the connectors, as noted above, and may have contributed to the lower fatigue life of these specimens.

As shown in the test results, a large transverse reinforcing bar spacing in the concrete slab seems to be detrimental to the behavior of the shear connectors under static and fatigue loading. However, typical existing bridges examined in this study have concrete slabs with closer transverse reinforcing bar spacing than the lightly reinforced concrete blocks in this study. Moreover, the confinement could be affected by the block size, so the concrete slab in existing bridges may have better confinement for the shear connectors than the concrete blocks used for the single shear connector tests. However, care should be taken to minimize cutting transverse reinforcing bars during installation of the DBLNB and HTFGB connectors since this may result in reduced confinement around the shear connectors.



Figure 3.29: Cracks in concrete block (HASAA-12ST)

3.6 SUMMARY

The behavior of individual post-installed shear connectors was evaluated using a single shear connector test setup. Three types of post-installed shear connectors (DBLNB, HTFGB, and HASAA) were tested under static and fatigue loading.

All of the three types of post-installed shear connectors showed consistent behavior under static loading. The shear strength of the connectors can be estimated as one-half their tensile strength. The effective area of the shear connectors with the thread in the shear plane can be calculated as 80 percent of the cross-section area of the unthreaded connector.

Design equations to predict the behavior under fatigue loading were also developed from the test results in this study and the test results conducted by Kayir (2006). For the HASAA connector, an S-N curve was proposed based on the test results under fatigue loading. An endurance limit was not determined since all shear connectors

failed before 5 million cycles of loading for the stress ranges selected in this study. The DBLNB and HTFGB connectors showed higher fatigue strength than the HASAA connector. An endurance limit of 35 ksi was proposed for the DBLNB and HTFGB connectors based on the test results. It is noteworthy that the post-installed shear connectors tested in this study showed significantly higher fatigue strength than the AASHTO curve for conventional welded shear studs.

CHAPTER 4

Full-Scale Beam Tests and Analytical Modeling

4.1 INTRODUCTION

In this chapter are described the full-scale beam tests that were conducted to evaluate the structural performance of non-composite beams retrofitted with post-installed shear connectors. In these tests, the stiffness, strength and ductility of retrofitted beams were examined under static loading. A total of five full-scale beam tests were conducted. The first specimen, a non-composite beam with no shear connectors, was tested to provide baseline data on the performance of an unretrofitted beam. The remaining four specimens were retrofitted with post-installed shear connectors. One specimen was retrofitted with the double nut bolt (DBLNB); one was retrofitted with the high tension-friction grip bolt (HTFGB) and two specimens were retrofitted with adhesive anchor (HASAA) shear connectors. As described in Chapter 2, these three types of connectors were chosen based on the results of static and fatigue tests conducted on individual shear connectors in earlier stages of this project, as well as on considerations of constructability.

During construction of the test specimens, the selected post-installed shear connectors were installed using procedures suitable for actual field application. Thus, in addition to evaluating the structural performance of the retrofitted beams, constructability issues for each type of post-installed shear connector were also evaluated.

This chapter provides a detailed description of the test setup, the test specimens, and the test results. Finite element analyses of the test specimens are also presented. These analyses provide further insight into the behavior of the retrofitted beams, and provide information on the capabilities and limitations of the finite element models for use in parametric studies described later in this study.

4.2 TEST PROGRAM

4.2.1 Test Specimens

Five full-scale specimens consisting of a steel beam and concrete slab were constructed and tested under static loading. Each specimen was a 38-ft long simply supported span, with a point load applied at midspan, and consisted of a W30x99 steel girder with an 84-in. wide by 7-in. thick reinforced concrete slab. The specimens were designed based on the configuration of bridges that were potential candidates for strengthening by the use of post-installed shear connectors, as reported in Hungerford (2004). The designation for each specimen starts with the name of the shear connection method, and is followed by the shear connection ratio in percentage. The specimen name ends with “BS” which stands for Beam Static test.

4.2.1.1 *Non-Composite Beam (NON-00BS)*

The first specimen was a non-composite steel girder with a concrete slab, intended to represent an existing unretrofitted bridge girder. A W30x99 section was used for the steel beam, and the concrete slab was 84-in. wide and 7-in. deep as shown in Figure 4.1. For the steel girder in the test specimens, ASTM A992 steel was used. Older steel bridges would typically have used ASTM A36 ($F_y = 36$ ksi) or ASTM A7 ($F_y = 33$ ksi) steel. These steels are no longer available in wide-flange shapes, however. ASTM A992 steel has a specified yield stress between 50 to 65 ksi and a minimum tensile strength 65 ksi. To simulate the prototype bridge, #4 and #5 Gr. 60 reinforcing bars were placed at a 6-in. spacing in the transverse direction. In the longitudinal direction, #4 bars were placed at a 12-in. spacing (Figure 4.1 and Figure 4.2). These reinforcement details were recommended by a project advisor at Texas Department of Transportation as being typical of existing bridges. Web stiffeners were welded at the center and both ends of the specimen to prevent local failures at the load and support points.

Concrete formwork was hung on the steel beam flanges to simulate unshored construction as shown in Figure 4.3. Before building reinforcing cages on the formwork, the top of the formwork was cleaned and coated with form oil. The concrete slab was cast with ready-mix concrete using a 1-cubic yard bucket. Concrete with a specified 28-day compressive strength of 3,000 psi was used. The concrete was vibrated and screeded. The 6- x 12-in. concrete cylinders were made for concrete cylinder tests, and the cylinders were placed by the test specimens to be cured in the same environment with the specimens. After casting, the exposed surface of the concrete was covered with plastic sheets for 5 days under moist conditions. The concrete formwork was removed from the specimen 7 days after the casting, and reused for the other specimens.

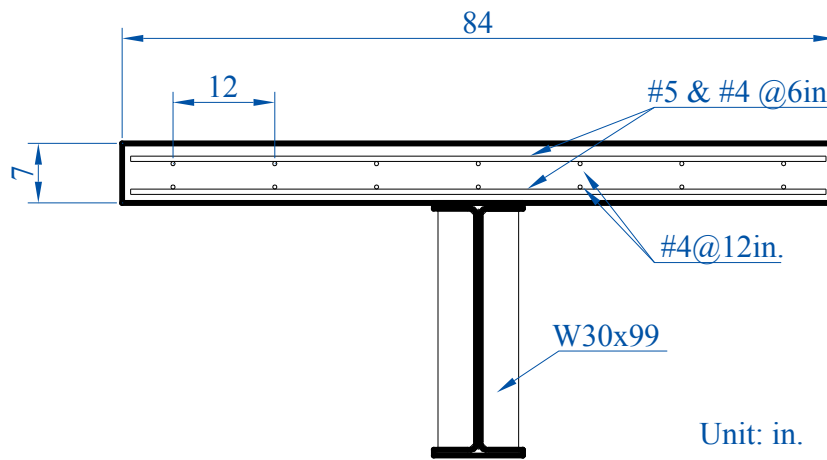


Figure 4.1: Details of specimen cross-section



Figure 4.2: Reinforcement layout



Figure 4.3: Concrete formwork

4.2.1.2 Design of Partially Composite Specimens (DBLNB-30BS, HTFGB-30BS, HASAA-30BS, HASAA-30BS1)

The four specimens retrofitted with post-installed shear connectors were designed as partially composite. Figure 4.4 shows the computed load-carrying capacity of the test specimens with respect to their shear connection ratio. These strength values were calculated using the minimum specified concrete strength ($f_c' = 3,000$ psi) and the minimum specified yield stress of the steel ($F_y = 50$ ksi). The contribution of the longitudinal reinforcing bars was neglected in the strength calculation. The minimum specified tensile strength of ASTM 193 B7 threaded rod, used for the DBLNB and HASAA connectors, is 125ksi. The ASTM A325 high-strength bolt used for the HTFGB connector has minimum specified tensile strength 120 ksi. For the full-scale beam tests, 7/8-in. diameter connectors were used as in the single shear connector tests in Chapter 3. Based on Equation 2.28, the ultimate shear capacity of each connector was computed as 30.1 kips for the DBLNB and HASAA connectors, and 28.9 kips for HTFGB connectors with threads in a shear plane. The effective shear area was taken as 80 percent of unthreaded gross area.

The ultimate strength of the partially composite beam was calculated using simple plastic analysis, as described in Chapter 2. Based on these calculations, the non-composite beam has a load-carrying capacity of 137 kips. The fully composite beam has a strength of 236 kips, approximately 70 percent greater than the non-composite beam. As shown in Figure 4.4, the ultimate strength of the non-composite beam can be increased significantly even with low shear connection ratios. Based on this analysis, it was decided to design the four test specimens with a 30-percent shear connection ratio. Even with only a 30-percent shear connection ratio, a 50-percent increase in the ultimate load-carrying capacity is predicted compared to the non-composite beam. To achieve a 30-percent shear connection ratio requires 16 shear connectors per shear span, or a total of 32 shear connectors in a beam.

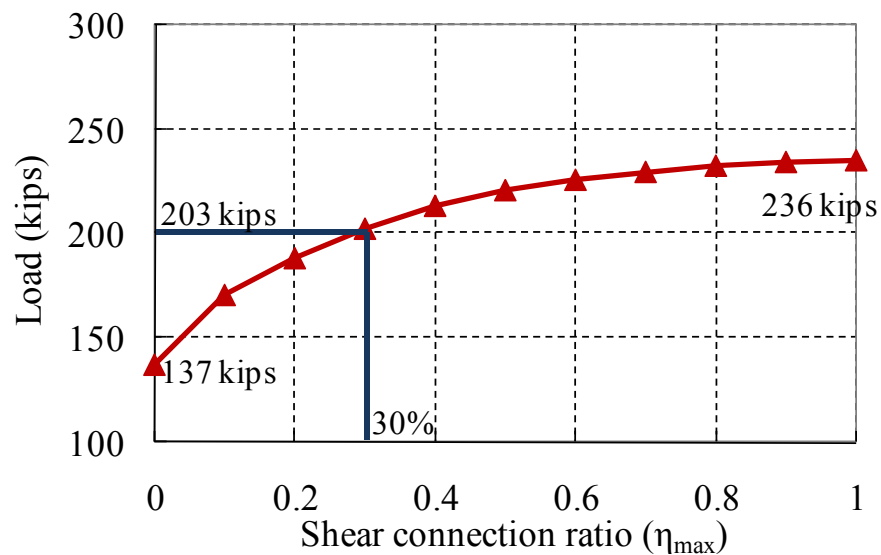


Figure 4.4: Predicted load capacity of test specimens versus shear connection ratio (based on minimum specified material properties)

4.2.1.3 Installation of Post-Installed Shear Connectors (DBLNB, HASAA, HTFGB)

For each of the retrofitted specimens, a non-composite beam was first constructed, as described for Specimen NON-30BS. Shear connectors were then installed in the specimen. Installation of the post-installed shear connectors in the full-scale beam specimens was different from the installation of the connectors in the concrete blocks used in the single connector tests described in Chapter 3. Installation procedures for the shear connectors in the full-scale beam specimens were chosen to be representative of installation procedures that could be used in actual field applications. A detailed description of the shear connector installation procedures is provided in the following sections.

4.2.1.3.1 Installation of the DBLNB Connectors for Specimen DBLNB-30BS

Installation of the DBLNB connectors requires access from both the top and bottom of the slab. Drilling through both the concrete slab and the steel beam flange was completed from the top and tightening of the connector was done underneath the slab using an impact wrench to reach the required pretension in the connector. Listed below is the procedure used to install the DBLNB connectors.

- 1) A 2.5-in. diameter hole was drilled into the concrete slab from the top using a Hilti DD200 coring machine. A DD-BL U4 diamond core bit was used for the coring operation (Figure 4.5). This core bit is designed for coring a wide range of concrete and medium steel reinforcement, and requires a constant supply of cooling water. It took 5 to 10 minutes to complete each hole through the 7-in. thick concrete slab.
- 2) A 15/16-in. diameter hole was drilled through the steel beam flange from the top side of the slab using a portable magnetic drill. A 10-in. long drill bit was used to drill the holes from the top of the slab. A hollow round bar was placed inside of the cored hole in the concrete to serve as a guide for the steel drill bit. This guide also helped to keep the inside surface of the concrete clean from cutting oil (Figure 4.6). To fix the coring machine and the magnetic drill to the concrete slab surface, a 1-in. thick steel plate was anchored to the concrete slab using four concrete anchors. In an actual field application, the drill and coring machine could be mounted on a truck or on a heavy steel plate attached to the slab with concrete anchors. Figure 4.7 shows the concrete surface after drilling.
- 3) A 7.25-in. long ASTM A193 B7 threaded rod was placed from the top to provide a 5-in. embedment depth. The connector was tightened to a pretension of 39 kips using an impact wrench. “Squirtter” Direct Tension Indicating (SDTI) washers were used to confirm the required pretension as shown in Figure 4.8. This proprietary washer has several bumps on its surface, under each of which has

embedded orange-colored silicone. As a bolt is tightened, the silicone material comes out and gives a visual indication of bolt tension. This washer was first tested using the Skidmore-Wilhelm Bolt-Tension Calibrator to check the amount of ejected silicone required to indicate that the specified pretension had been achieved.

- 4) The hole in the slab was then filled with Five Star[®] Highway Patch, a fast-setting, high-strength grout used for the repair of highways and bridges.



Figure 4.5: Coring and drilling into the specimen

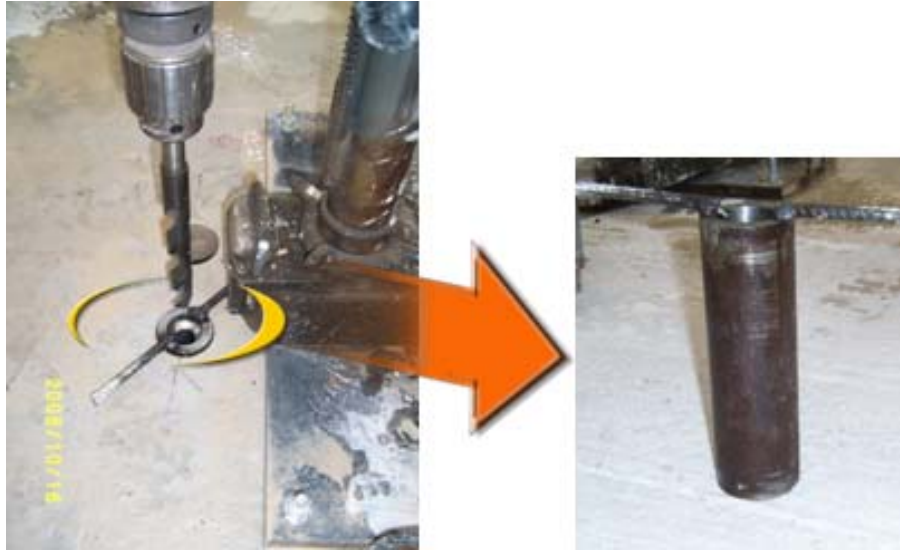


Figure 4.6: Drilling through beam flange



Figure 4.7: Drilled holes for DBLNB installation



Figure 4.8: Use of “Squirter” Direct Tension Indicating (SDTI) washer

4.2.1.3.2 Installation of the HTFGB connector for Specimen HTFGB-30BS

Installation of the HTFGB connector requires more steps than the DBLNB connector:

- 1) A 2.75-in. deep, 2-in. diameter hole was drilled into the concrete from the top using a Hilti TE-55 rotary hammer drill as shown in Figure 4.9.
- 2) A 1-in. diameter hole (concentric hole with the 2-in. diameter hole) was drilled through the concrete slab from the top using a Hilti DD200 coring machine (Figure 4.9). It took 5 to 10 minutes to complete each hole through the concrete slab. The coring bit wore rapidly and needed to be replaced after every 8 to 10 holes.
- 3) A 15/16-in. diameter hole was drilled through the steel beam flange from the top side of the slab using a portable magnetic drill and the same drill bit that had been used for the DBLNB connector. Care was taken not to let the drill bit touch the concrete surface inside the 1-in. diameter hole; otherwise, the drill bit wore out quickly.

- 4) A 7.25-in. long, ASTM A325 high strength bolt was inserted from the top of the slab into the hole, and was set to provide a 5-in. embedment depth. Figure 4.10 shows the concrete surface after inserting the connector. The connector was tightened with an impact wrench to a pretension of 39 kips, verified with SDTI washers.
- 5) The hole in the concrete slab was filled with Five Star[®] Highway Patch.



Figure 4.9: Drilling and coring into the concrete slab



Figure 4.10: Shear connectors installed in hole (HTFGB)

4.2.1.3.3 Installation of the HASAA Connector for Specimen HASAA-30BS and HASAA-30BS1

The same 7/8-in. diameter ASTM A193 B7 threaded rods used for the DBLNB connection method were also used for the HASAA shear connectors. Following is the procedure used to install the HASAA connector.

- 1) A 15/16-in. diameter hole was drilled through the steel beam flange from the bottom of the slab. A portable Jancy Slugger Cutter Mag Drill with magnetic base was used to drill the hole (Figure 4.11(a)).
- 2) A 5-in. deep hole was drilled into the concrete from the bottom using a 7/8-in. drill bit and a Hilti TE-55 rotary hammer drill as shown in Figure 4.11 (b). The 15/16-in. diameter hole is required to install the HASAA shear connector according to the installation manual provided by Hilti (Hilti 2006). A 15/16-in. diameter carbide-tipped drill bit did not fit into the 15/16-in. diameter hole

- through the steel beam flange. Therefore, a 7/8-in. diameter drill bit was used to drill the hole into the concrete, and was worked to make the hole larger.
- 3) The drilled hole was cleaned using a wire brush and compressed air before injecting adhesive.
 - 4) Hilti HIT HY 150 adhesive was injected into the hole using a Hilti HIT-MD 2000 manual dispenser. Eight to nine holes could be completed with an 11.1-fluid ounce cartridge pack. The adhesive was viscous enough not to run down during the overhead application (Figure 4.11 (c)).
 - 5) A connector rod was inserted with a twisting motion. According to information provided by Hilti, the rod can be adjusted during the specified gel time, but should not be disturbed between the gel time and cure time (6 min. and 50 min. at 68° F, respectively). Adhesive that overflowed was wiped off, leaving adhesive filling the gap between the oversized hole in the steel flange and the shear connector. The adhesive was viscous enough to hold the connector in the hole, so the connector did not have to be held in place during the cure time.
 - 6) After the cure time, the nut was tightened to the specified torque (150 lb-ft) using a torque wrench (Figure 4.11 (d)).



(a) Drilling through the steel flange



(b) Drilling into the concrete



(c) Injecting adhesive



(d) Tightening with torque wrench

Figure 4.11: Installation of HASAA shear connectors

4.2.2 Material Properties

4.2.2.1 Concrete, Grout, and Adhesive

Concrete for the full-scale beam tests was delivered by ready-mix truck from Capital Aggregates in Austin, Texas. The specified compressive strength was 3,000 psi with 3/4-in. river aggregate. Concrete slump tests were performed for each test specimen before casting concrete. Current TxDOT *Standard Specifications for Construction and*

Maintenance of Highways, Streets, and Bridges (TxDOT, 2004) require a slump of 4±1 in. for concrete for a bridge slab. The 3,000 psi concrete compressive strength was required for the test program to simulate older existing bridges, so that concrete with higher slump was accepted.

The concrete slump test and the compressive test results for each test specimens are listed in Table 4.1. The compressive strength of the concrete for Specimen NON-00BS was over 6,000 psi on the day of testing. However, it was considered that this did not significantly affect the test results for this non-composite specimen, because the contribution of concrete slab to the total flexural strength for non-composite beams is less than 5 percent.

Five Star[®] Highway Patch was used to fill the holes in the slab after installation of the DBLNB and HTFGB connectors. This is a fast setting, high-strength grout with a specified 2-hour compressive strength of 2,000 psi. Its measured compressive strength was 5,800 psi at 2 days, 7,000 psi at 7 days, and 7,570 psi on the test day for Specimen DBLNB-30BS. For Specimen HTFGB-30BS, the measured compressive strength on the test day was 9,130 psi.

The adhesive used for the HASAA connectors was Hilti HIT HY150, a two-part adhesive consisting of a methacrylate resin, hardener, cement, and water (Hilti 2006). The adhesive has a minimum specified compressive strength of 10,420 psi and a typical curing time at 68° F of 50 min.

Table 4.1: Concrete slump and compressive strength

Specimen	Slump (in.)	Compressive strength (f_c' , psi.)	
		28 days	Test day
NON-00BS	3	5,190	6,250
DBLNB-30BS	7	3,560	3,680
HASAA-30BS	4	3,500	3,610
HTFGB-30BS	5.5	3,850	4,060
HASAA-30BS1	7	2,590	3,220

4.2.2.2 Steel Beams and Reinforcing Bars

The W30x99 steel beams used for the full scale tests came from two different heats of steel. The W30x99 sections used for Specimens NON-00BS, DBLNB-30BS and HASAA-30BS came from one heat. The W30x99 sections used for Specimens HTFGB-30BS and HASAA-30BS1 came from a second heat. Tension tests were conducted on steel coupons taken from each heat of the W30x99 sections used for the test specimens. Four steel coupons were taken from each section, two from the beam web and two from the beam flange.

The Grade 60 reinforced bars used for the test specimens have a specified minimum yield stress of 60 ksi and a specified minimum ultimate tensile strength of 90 ksi. Tension tests were conducted on the #4 longitudinal reinforcing bars.

Three static yield stresses were measured in the yield plateau and averaged to determine the yield stress for both the steel girder coupons and the reinforcing bars. Test results are shown in Table 4.2 and Table 4.3. Note that the two different heats of steel used for the W30x99 beams had very similar measured yield and tensile strength values.

4.2.2.3 Shear Connectors

ASTM A193 B7 threaded rod used for the DBLNB and the HASAA connectors, and ASTM A325 high strength bolt used for the HTFGB connector have specified minimum tensile strengths of 125 ksi and 120 ksi, respectively.

The A193 B7 threaded rods used as shear connectors for the full-scale beam tests were all from the same production lot, and had measured ultimate shear and tensile strengths of 91.1 ksi and 147.0 ksi respectively. Similarly, the A325 bolts used for the full-scale beam tests were all from the same production lot, and had measured ultimate shear and tensile strengths of 87.6 ksi and 148.6 ksi, respectively.

Table 4.2: Steel coupon test results

Specimen	Section	Static yield stress (F_y , ksi)	Ultimate strength (F_u , ksi)	Elongation (%)
NON-00BS	Flange	56.9	77.4	38
DBLNB-30BS	Web	60.9	78.6	36
HASAA-30BS				
HTFGB-30BS	Flange	55.0	75.5	37
HASAA-30BS1	Web	59.3	77.5	36

Table 4.3: Reinforcing bar test results (#4 bars)

Specimen	Static yield stress (F_y , ksi)	Ultimate strength (F_u , ksi)	Elongation (%)
NON-00B	61.6	103.5	35
DBLNB-30B			
HASAA-30B	57.6	99.2	37
HTFGB-30BS	63.1	102.5	24
HASAA-30BS1			

4.2.3 Test Setup

4.2.3.1 Details of Test Setup

The full-scale beam specimens were 38-ft long, simply supported, with a point load applied at midspan. Details of the test setup are shown in Figure 4.12 and Figure 4.13. A roller support was provided at one end of the beam and a hinge support at the other end. Bracing was provided at each end of the beam to prevent the concrete slab from overturning due to unexpected loading eccentricity. These end braces were designed not to restrain longitudinal movement of the concrete slab.

Two 100-ton capacity hydraulic rams were used to apply a concentrated load at the midspan of the specimen. A load cell, placed at the loading point, measured the load applied by these hydraulic rams. The concentrated load was applied on a 10- x 20 x 1-in. steel plate to simulate a tire area of the standard AASHTO design truck. To prevent lateral torsional buckling of the beam during concrete casting and to provide for safety during testing of the specimen, the beam was braced laterally at midspan. Teflon sheets were used at the interface of the bracing and the steel beam to minimize frictional forces. For Specimen NON-00BS, four shear studs were installed on the beam flange at the

center of the beam, to help maintain safety of the setup during testing. Since they are located at the center of the beam, little or no composite action is expected to be developed as a result of these studs. To permit easy detection of yielding, the midspan portion of the steel beam was painted with whitewash.

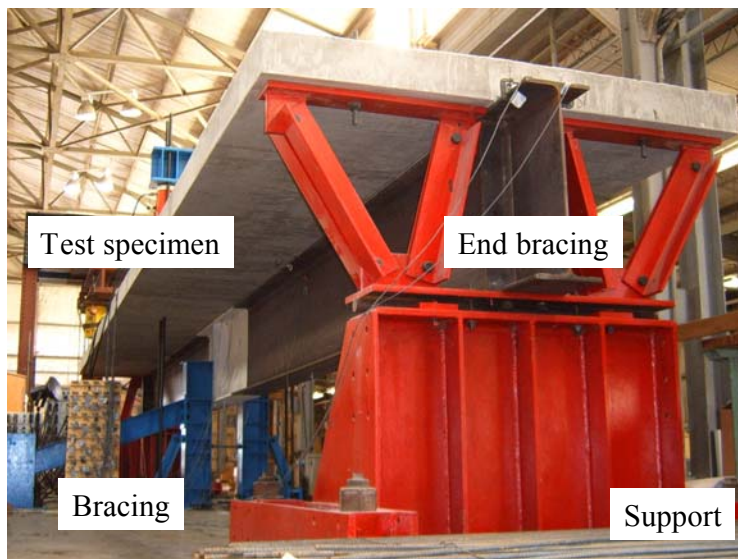
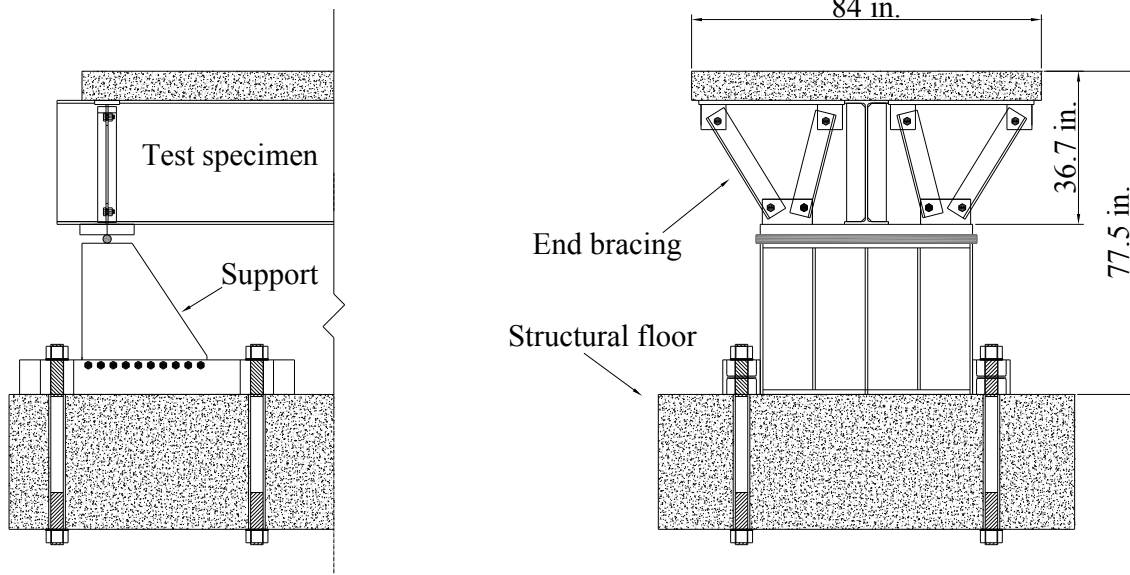
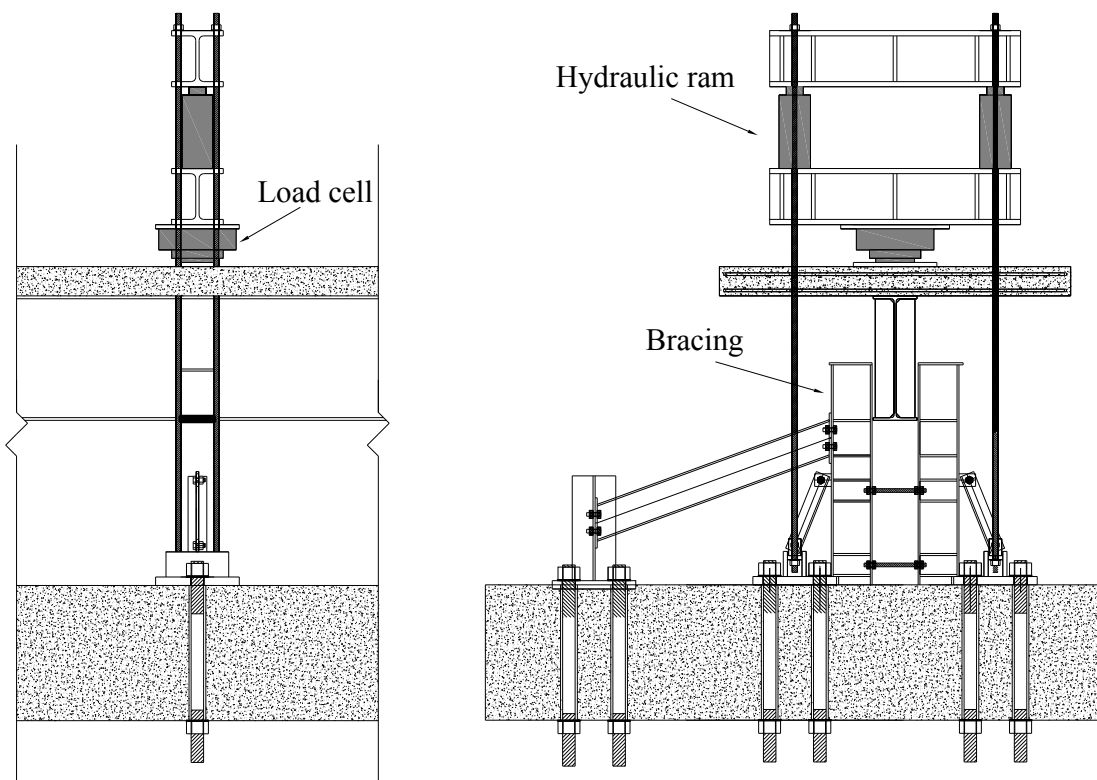


Figure 4.12: Test setup for full-scale beam tests (Pictures)



(a) Support details



(b) Loading frame details

Figure 4.13: Test setup for full-scale beam tests (Drawing)

4.2.3.2 Instrumentation

Vertical deflection, slip at the steel-concrete interface, and longitudinal strain in the steel beam were measured during each test. Displacement transducers at midspan and at quarter points measured vertical deflection. Slip at the interface between the concrete slab and the steel beam were also measured at the ends and quarter points of the beam. Figure 4.14 shows two linear potentiometers at the end of the beam to measure the slip at the steel-concrete interface. Strain gages were used to measure longitudinal strain of the steel beam at cross-sections located at midspan and at 6 in. from midspan. The location of the strain gages at the beam cross-section is shown in Figure 4.15.

Loading was applied by two 100-ton capacity hydraulic rams, driven by a 10,000-psi pneumatically driven oil pump, operated manually. Data readings were taken at 5-kip loading intervals in the elastic range. After the test specimen yielded, data were read at increments of 0.25-in. midspan deflection.

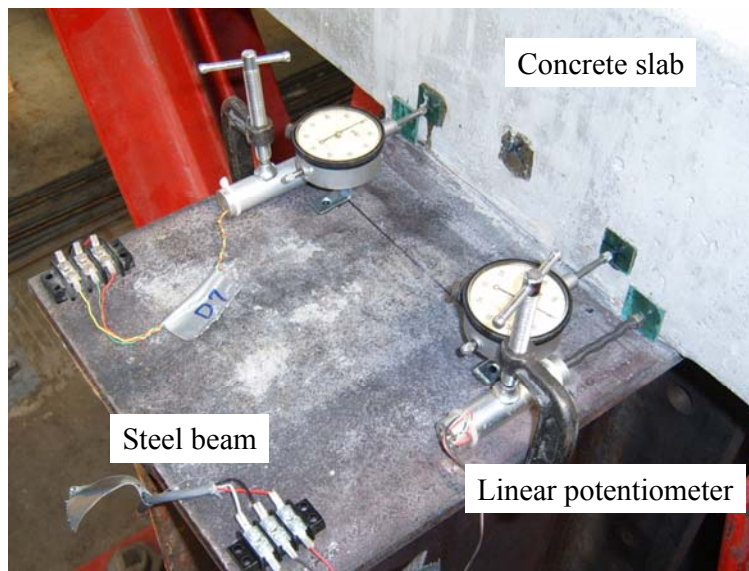


Figure 4.14: Linear potentiometers for measuring slip at the end of the specimen

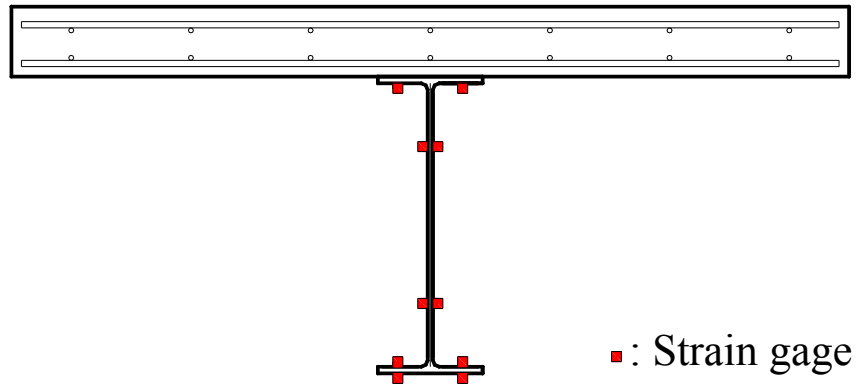


Figure 4.15: Strain gage locations

4.3 TEST RESULTS

During each test, in addition to electronically recording data, the specimens were visually examined for phenomena such as cracks in the concrete slab, yielding and local buckling in the steel beam, and failure of the post-installed shear connectors. In this section are presented the measured load-deflection and load-slip response of each specimen, along with a description of various phenomena observed during the tests.

Figure 4.16 and Figure 4.17 show the load-deflection and midspan deflection-slip response for the non-composite baseline Specimen NON-00BS. Load-deflection and load slip plots for the retrofitted Specimens DBLNB-30, HTFG-30BS and HASAA-30BS are shown in Figure 4.18 to Figure 4.23. Recall that each of these specimens was provided with 32 shear connectors per specimen to develop 30-percent shear connection ratio, and the connectors were uniformly spaced along the length of the beam. The load versus midspan deflection curves for each of the four specimens are plotted together in Figure 4.24. Results for Specimen HASAA-30BS1, which had shear connectors concentrated near beam ends, are described later in this chapter.

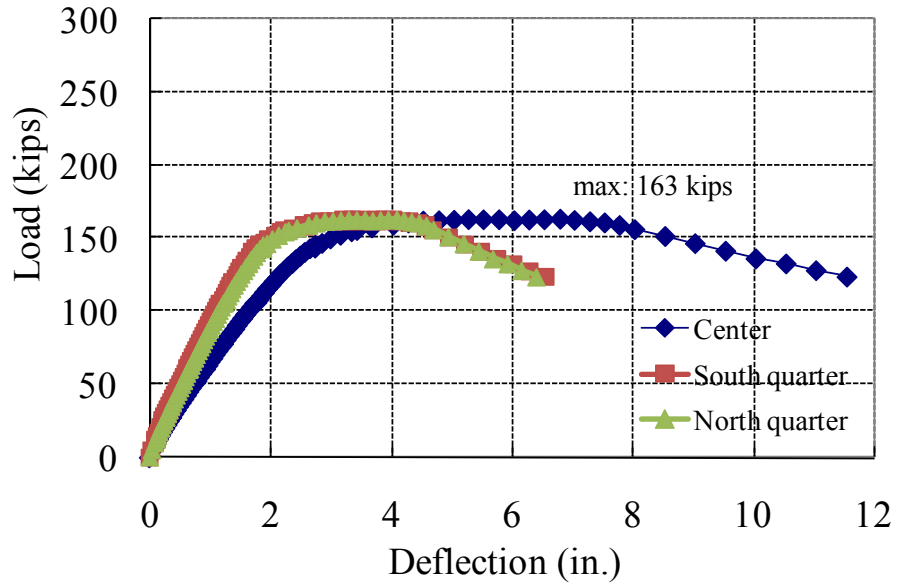


Figure 4.16: Load vs. deflection curves (Specimen NON-00BS)

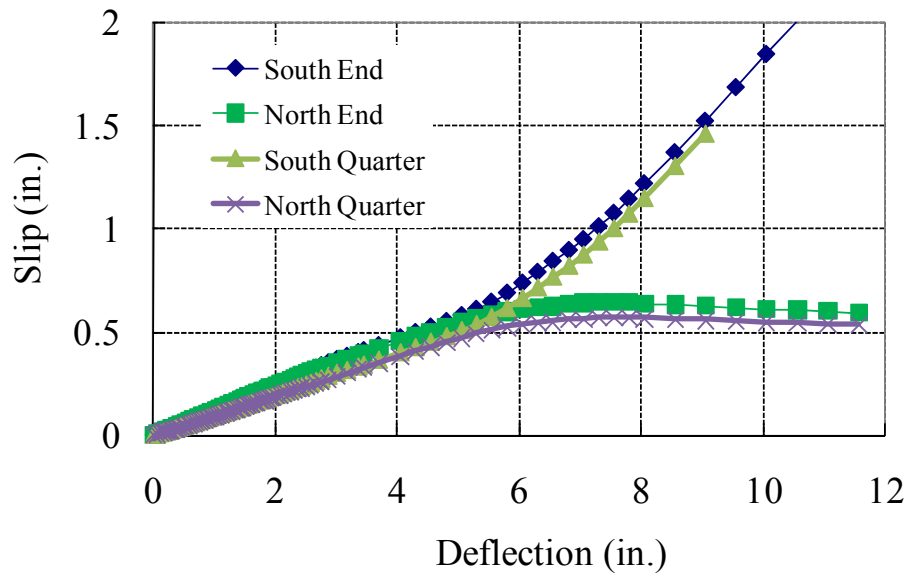


Figure 4.17: Load vs. slip curves (Specimen NON-00BS)

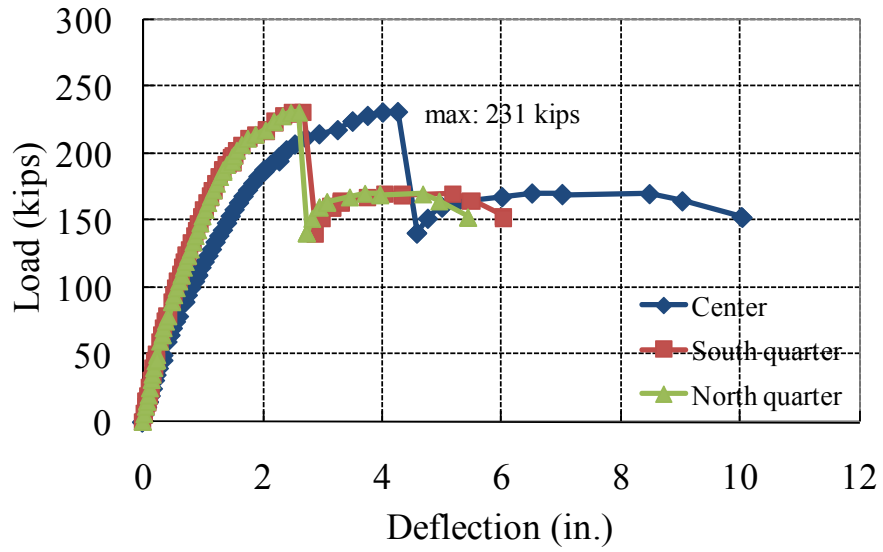


Figure 4.18: Load vs. deflection curves (Specimen DBLNB-30BS)

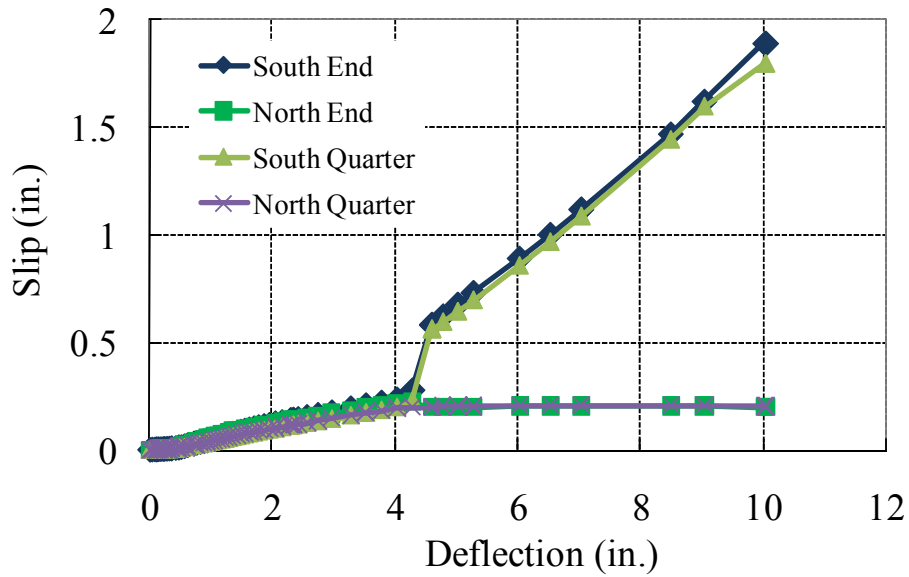


Figure 4.19: Load vs. slip curves (Specimen DBLNB-30BS)

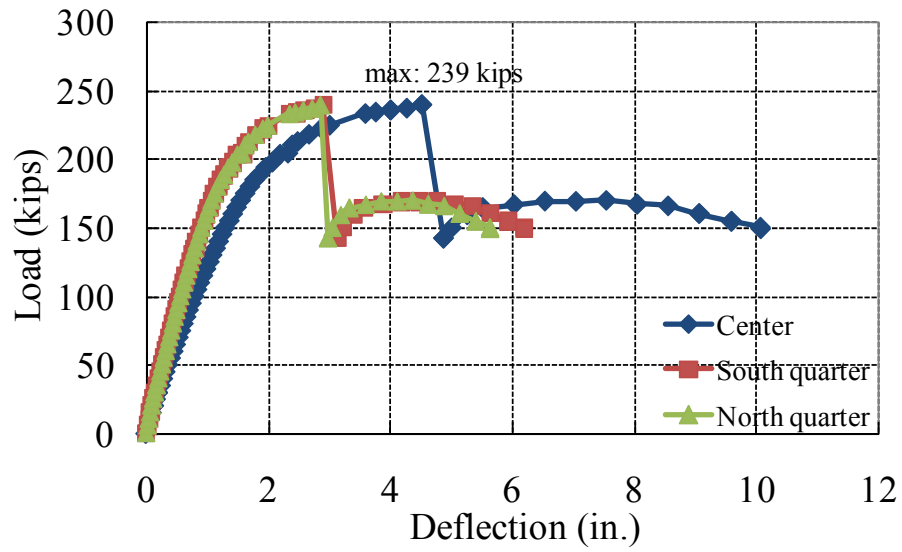


Figure 4.20: Load vs. deflection curves (Specimen HASAA-30BS)

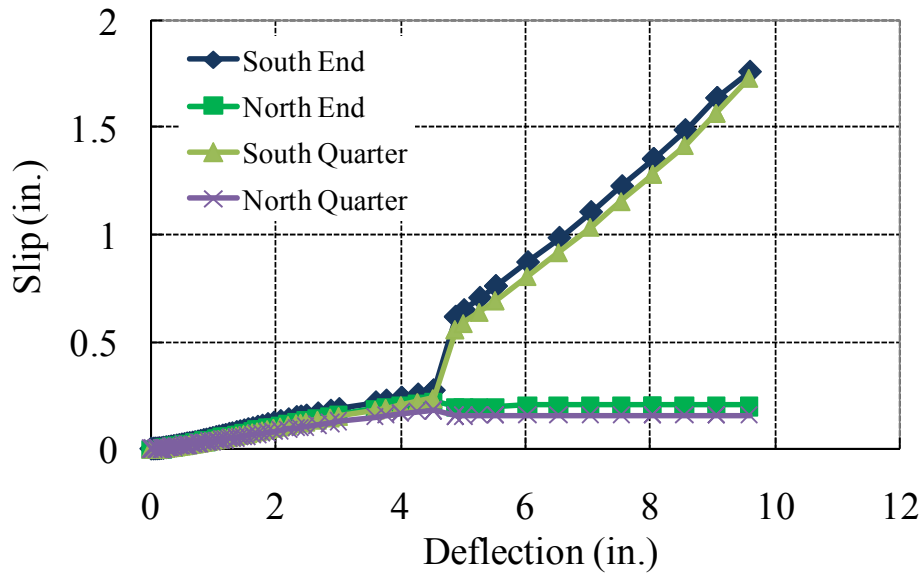


Figure 4.21: Load vs. slip curves (Specimen HASAA-30BS)

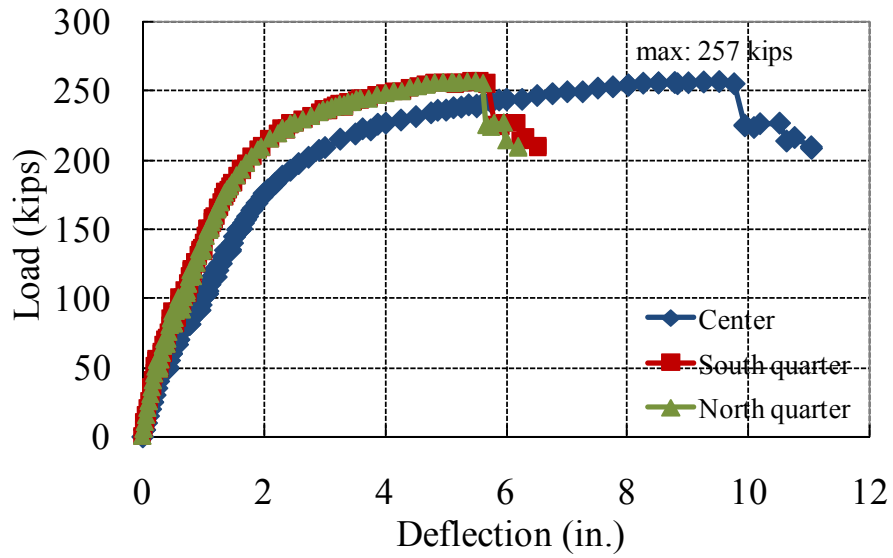


Figure 4.22: Load vs. deflection curves (Specimen HTFGB-30BS)

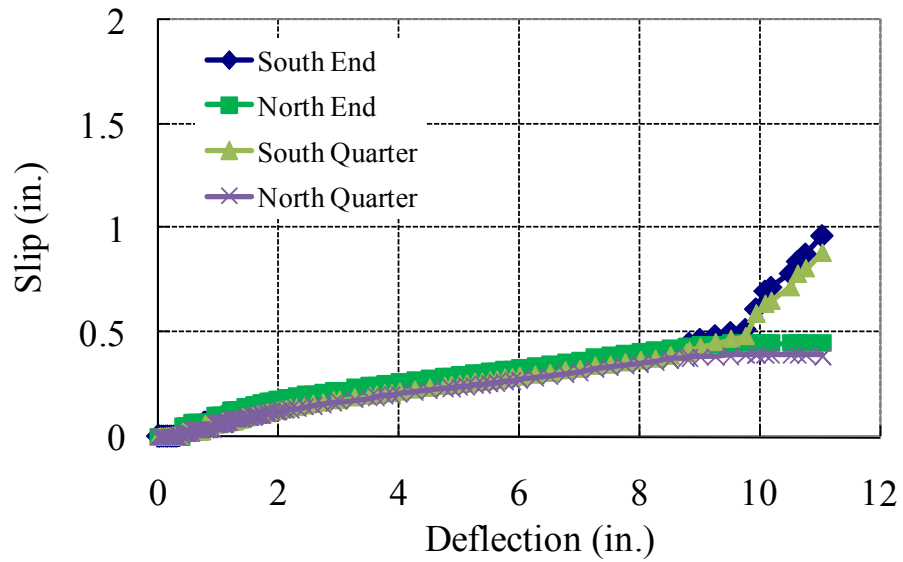


Figure 4.23: Load vs. slip curves (Specimen HTFGB-30BS)

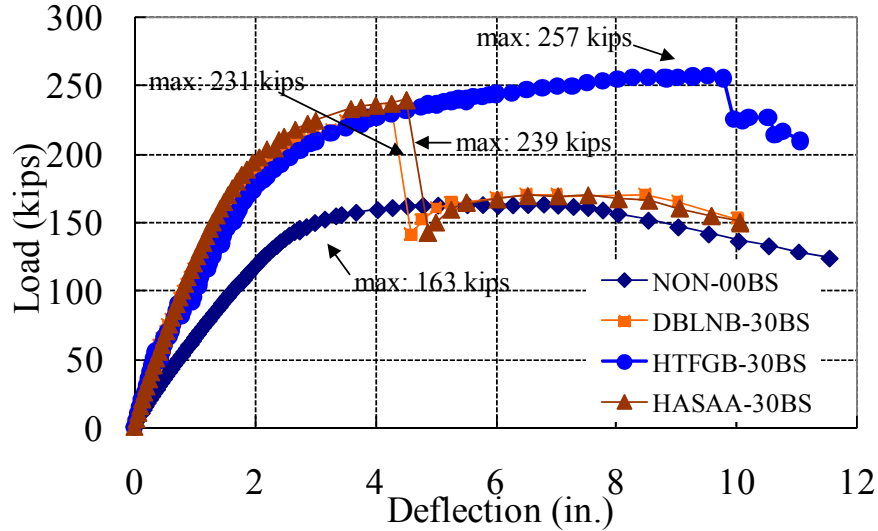


Figure 4.24: Load vs. midspan deflection curves for test specimens NON-00BS, DBLNB-30BS, HTFGB-30BS and HASAA-30BS

4.3.1 Specimen NON-00BS

Specimen NON-00BS was the baseline non-composite specimen. As indicated by the load-deflection plots in Figure 4.16 and Figure 4.24, this specimen showed highly ductile response, as might be expected for a compact, laterally supported steel beam.

The specimen showed a slight reduction in stiffness at a load of about 40 kips. Nonlinear behavior at this early stage might be attributed to the breaking of bond between the steel beam and the concrete slab, and possibly due to small movements at the supports. At 70 kips, the first cracks were observed on the bottom of the slab. At 90 kips, more cracks were detected on the bottom of the slab, spaced at 10 to 15 in. At 100 kips, whitewash began to flake off the bottom flange, although the load-deflection plot showed no indication of yielding. At 130 kips, flaking of whitewash from the top and bottom flanges indicated significant yielding of the beam. At 150 kips, Specimen NON-00BS started to lose stiffness, and the test was then switched from load control to displacement control.

At 4-in. deflection, more cracks were detected on the bottom of the slab between the existing cracks. Flaking of whitewash on the web was also observed. At 5-in. deflection, some cracks on the side of the concrete slab propagated horizontally, suggesting imminent crushing of the concrete at the top of the slab. At 6.5-in. deflection, both flange and web local buckling were observed in the steel beam. Flange buckling occurred only on one side and started about one-half the beam depth away from the midspan of the beam. Crack on the bottom of the concrete slab were about 1/16-in. wide. At about 6.8-in. deflection, Specimen NON-00BS reached its ultimate strength, 163.1 kips. Beyond 6.8-in. deflection, the strength of Specimen NON-00BS gradually decreased due to local flange and web buckling in the steel beam. At 7.5-in. deflection, flange buckling occurred on the other side of the beam flange. Figure 4.25 shows cracks in the slab, and local buckling of the steel beam at 11-in. deflection. The test stopped at 11.5-in. deflection for safety reasons. No crushing on the top of the concrete was observed after the test. An overall view of the specimen at 11.5-in. deflection is shown in Figure 4.26.

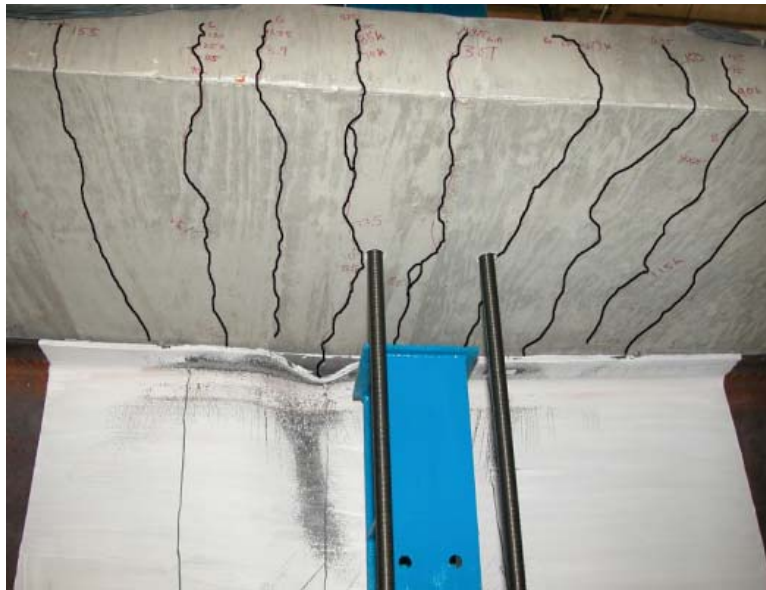


Figure 4.25: Specimen NON-00BS - Cracks in the slab and beam local buckling (11-in. deflection)



Figure 4.26: Specimen NON-00BS – Overall view of specimen at end of test (11.5-in. deflection)

4.3.2 Specimen DBLNB-30BS

Specimen DBLNB-30BS was strengthened with the DBLNB (double nut bolt) connectors. It was designed as 30 percent composite based on the specified strength of the concrete, the steel beam, and the DBLNB connector. A total of 32 shear connectors (16 connectors in each shear span) were installed in the beam, and were distributed uniformly along the length of the beam.

Figure 4.18 and Figure 4.24 shows the load-deflection response for Specimen DBLNB-30BS. Specimen DBLNB-30BS was much stronger and stiffer than Specimen NON-00BS, and showed a sudden strength drop after the peak load, due to the simultaneous failure of multiple shear connectors. After the strength drop, Specimen DBLNB-30BS behaved much like Specimen NON-00BS.

The initial stiffness of Specimen DBLNB-30BS was much higher than that of Specimen NON-00BS. At load levels past about 65 kips, Specimen DBLNB-30BS started losing stiffness. This reduction in stiffness may be due to the nonlinear behavior of the shear connectors near the supports, and due to friction being overcome between the connector and the steel beam, resulting in slip of the connectors within the oversize holes in the beam flange. At 130 kips, flaking of whitewash was detected on the bottom beam flange and on the beam web. The first crack on the concrete slab was detected at a load of 200 kips. The cracks were observed only on the edge of the slab and did not propagate across the bottom of the slab. Spacing of the cracks on the concrete slab edge was 5 to 8 in. At a load of 220 kips, some cracks on the concrete slab propagated across the bottom. At 220 kips, the stiffness of the specimen reduced significantly, and subsequent loading was applied by displacement control.

At 3.25-in. deflection, some cracks in the concrete slab propagated to the center of the slab. Most cracks propagated to the center, and were less than about 1/32 in. in width (Figure 4.27). At 4.25-in. deflection, one shear connector located near the south support failed with a loud noise. No sudden drop of load, however, was detected due to this failure. This can likely be attributed to the redistribution of shear force among the shear

connectors. When the shear connector failed, the maximum slip measured at the steel-concrete interface was 0.23 in., less than the average slip capacity of 0.39 in. measured for the DBLNB connectors in the single shear connector tests described in Chapter 3. At 4.5-in. deflection, more than 10 shear connectors fractured essentially simultaneously, and the strength of the specimen dropped suddenly. In addition, cracks on the side of the concrete slab propagated toward the top of the slab. There was no sign of crushing of concrete on the top of the slab, however.

After the simultaneous failure of multiple shear connectors, the structural behavior of Specimen DBLNB-30BS was similar to that of non-composite Specimen NON-00BS (Figure 4.24). At 5-in. deflection, top flange local buckling occurred at the first shear connector location from the center of the beam. At 6.0-in. deflection, beam flange buckling was detected on both sides of the flange, and web local buckling was also observed. Additional shear connector failures were observed at 8- and 8.5-in. deflections. Figure 4.28 shows slab cracks and steel beam local buckling at 8-in. deflection. The test was stopped at 10-in. deflection for safety reasons.

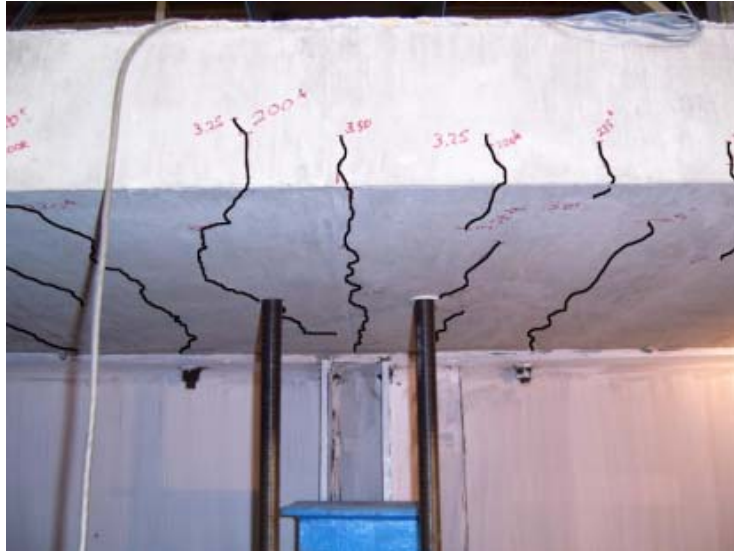


*Figure 4.27: Specimen DBLNB-30BS - Cracks on the bottom of the concrete slab
(3.25-in deflection)*



*Figure 4.28: Specimen DBLNB-30BS - Flange and web local buckling (8-in.
deflection)*

4.3.3 Specimen HASAA-30BS

Specimen HASAA-30BS was constructed with the HASAA (adhesive anchor) connectors. It was designed as 30 percent composite based on the specified strength of the concrete, the steel beam, and the HASAA connector. Sixteen shear connectors in a shear span, 32 shear connectors in total, were installed with uniform spacing along the beam. The number and location of shear connectors installed in Specimen HASAA-30BS was the same as for Specimen DBLNB-30BS.

This specimen behaved very much like Specimen DBLNB-30BS (Figure 4.24). Specimen HASAA-30BS was much stronger and stiffer than the non-composite beam specimen. A sudden drop in strength after the peak load was observed due to the failure of multiple shear connectors. After the strength drop, Specimen HASAA-30BS behaved very much like the non-composite Specimen NON-00BS.

A small amount of whitewash flaking was detected on the bottom beam web at a load of 120 kips. At 190 kips, flaking of whitewash was also observed on the bottom flange. At 200 kips, the first crack on the concrete slab was observed. At 210 kips, the crack propagated to the center of the slab. At 220 kips, several cracks were observed on the bottom of the concrete slab. Spacing of the cracks was 5 to 8 in. At 225 kips, the stiffness of the specimen reduced significantly, so subsequent testing was under displacement control instead of load control. Figure 4.29 shows concrete cracks at 4.25-in. deflection. Between 4.75- and 5.00-in. deflection, multiple connectors fractured consecutively. Thirteen shear connectors out of sixteen failed in the south shear span. Failed connectors are shown in Figure 4.30. The deflection of the beam after the failure of the shear connectors was 4.87 in.

After failure of multiple shear connectors, Specimen HASAA-30BS behaved very much like non-composite Specimen NON-00BS. Beam flange local buckling was first observed at 5.25-in. deflection, and web local buckling was detected at 6-in. deflection. Crack widths on the concrete slab were about 0.04 in. at 5.25-in. deflection. The test was

stopped at 10-in. deflection for safety reasons. Local buckling of the beam and cracks in the concrete slab are shown in Figure 4.31.

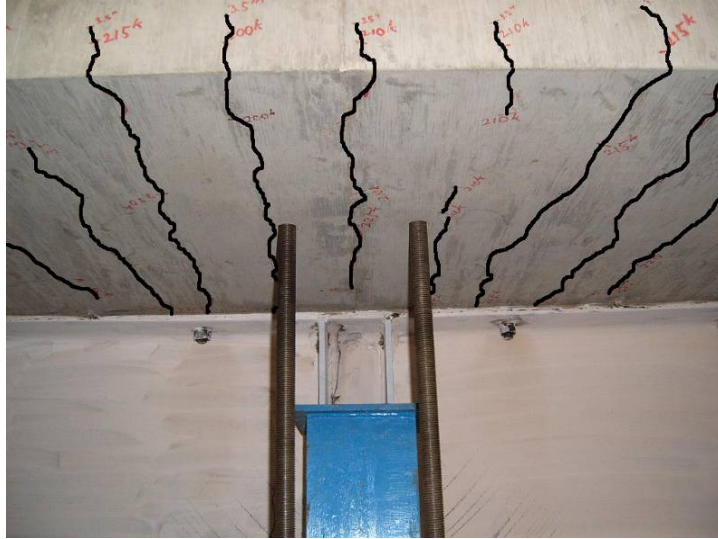


Figure 4.29: Specimen HASAA-30BS - Cracks on the bottom of the concrete slab (4.25-in deflection)



Figure 4.30: Specimen HASAA-30BS - Failed shear connectors

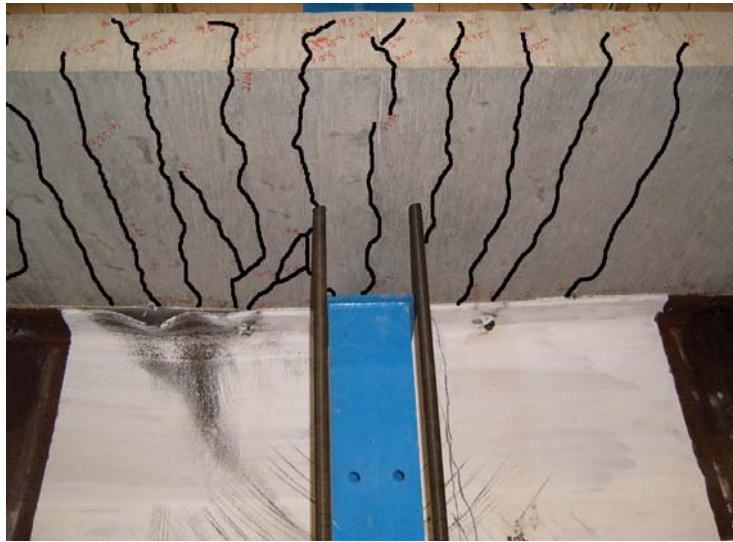


Figure 4.31: Specimen HASAA-30BS – Concrete cracks and beam local buckling (10-in. deflection)

4.3.4 Specimen HTFGB-30BS

Specimen HTFGB-30BS was a partially composite beam retrofitted using the HTFGB (high-tension friction grip bolt) connector. It was also designed with 30 percent shear connection ratio based on the specified strength of the concrete, the steel beam, and the HTFGB connector. The number and location of shear connectors were the same as for Specimens HASAA-30BS and DBLNB-30BS. For the HTFGB connector, shear force at the steel-concrete interface is first transferred through friction. Once friction is overcome, interface shear is transferred through bearing between the connector and the concrete and bearing between the connector and the beam flange.

As shown in Figure 4.22 and Figure 4.24, Specimen HTFGB-30BS was initially a little stiffer than the previous two partially composite beam specimens, and did not lose that initial stiffness until 55 kips loading. This can likely be attributed to the initial development of full composite action due to the transfer of interface shear by friction. The slip at the steel-concrete interface was less than 0.001 in. at 50 kips of loading. The

friction at the steel-concrete interface was first overcome at a load between 55 and 60 kips. With a loud noise, the load dropped by about 10 kips to 48 kips. Several similar drops in load occurred up to 150 kips loading. After each load drop, the specimen recovered the lost load, and continued to increase in strength. These load drops are attributed to the occurrence of slip at the connectors, with load recovery occurring as the connectors come into bearing. The magnitude of each load drop decreased with the increasing load. After friction was overcome, Specimen HTFGB-30BS was less stiff than Specimens DBLNB-30BS and HASAA-30BS. The first crack on the bottom of the slab was detected at a load of 150 kips, and more cracks were not detected until 195 kips. Whitewash flaking on the bottom flange and web of the beam was first observed at a load of 175 kips. At 200 kips, several cracks in the concrete propagated to the center of the slab. At 210 kips, the stiffness of the specimen reduced significantly, and the test was continued under displacement control.

At 3.5-in. deflection, maximum crack width on the bottom of the concrete slab was 0.01 in., and the crack spacing ranged from 5 to 8 in. At 4.0-in. deflection, whitewash flaking on the top flange around the shear connectors close to the loading point was observed, indicating significant bearing force at the shear connector. At 6.5-in. deflection, significant whitewash flaking was observed on the bottom flange of the beam (Figure 4.32). At 7.25-in. deflection, a single crack on the top of the concrete slab was observed, and the maximum crack width on the bottom of the slab was 0.04 in. At 8.5- and 8.75-in. deflections, multiple horizontal cracks on the side of the slab were detected indicating concrete crushing on the top of the slab.

A single shear connector at the south end failed with a loud noise at 8.84-in. deflection. No strength drop was observed, however. The maximum slip at the steel-concrete interface near the south end at this point was 0.45 in. Significant concrete crushing was observed at 9.5-in. deflection. The maximum load on the specimen was 257 kips at 9.53-in. deflection. Between 9.75- and 10.0-in. deflections, 5 shear connectors failed consecutively at intervals of about one second, and the load dropped from 255 to 225 kips. Concrete crushing was observed on the top of the slab as shown in Figure 4.33.

One shear connector failed between 10.0- and 10.25-in. deflection; two shear connectors failed between 10.5- and 10.75-in. deflection; and another shear connector failed between 10.75- and 11.0-in. deflection. Strength drops were observed at each shear connector failure except the first shear connector failure at 8.84-in. deflection. The test was stopped at 11.0-in. deflection.



Figure 4.32: Specimen HTFGB-30BS – Whitewash flaking (6.5-in. deflection)



Figure 4.33: Specimen HTFGB-30BS – Concrete crushing on the top of the slab (10-in. deflection)

4.4 DISCUSSION OF FIRST FOUR FULL-SCALE BEAM TESTS

In this section, results of the first four full-scale composite beam tests are discussed in greater detail, including observations on overall stiffness and strength, failure modes, and deformation capacity of the specimens. Comparisons with the individual shear connector test results for the corresponding shear connection methods are also provided in this section. Finally, constructability issues are discussed for each connection method.

4.4.1 Stiffness and Strength

The partially composite beams tested in this program showed much higher stiffness and strength than the reference non-composite beam, despite the low shear connection ratio. Figure 4.34 shows the load-deflection relations for the test specimens along with theoretical values based on simplified analysis. Solid lines represent the

theoretical initial stiffness and ultimate load-carrying capacity of the non-composite beam, and the dashed lines represent the values for the retrofitted composite beams.

The theoretical stiffness and strength of the non-composite Specimen NON-00BS is based on the steel beam only, using the measured yield stress for the W30x99 test beam (Table 4.2).

The theoretical stiffness of the partially composite specimens was determined using an effective moment of inertia, computed using Equation 2.17. The theoretical strength of these specimens was based on simple plastic cross-sectional analysis, as described in Section 2.3.2.2. The theoretical initial stiffness and strength of the partially composite beams were calculated based on the material properties of Specimen DBLNB-30BS. In computing the theoretical strength, the actual measured yield stress of the steel beam and compressive strength of the concrete were used. The shear connector strength was computed as $0.5A_{sc}F_u$ per Equation 2.28. In this calculation, the effective shear area, A_{sc} , of shear connectors with threads in the shear plane was calculated as 80 percent of the gross area of the unthreaded connectors, that is, $A_{sc} = 0.80 \times \pi (0.875/2)^2 = 0.48 \text{ in}^2$. For the ultimate tensile strength of the shear connector material, F_u , the measured value of 147 ksi was used.

The behavior of Specimen NON-00BS, which represents an existing non-composite bridge girder without any shear connectors, basically reflected the behavior of a bare steel beam. Specimen NON-00BS shows only slightly higher stiffness and strength than the bare beam. By comparing the theoretical strength and stiffness (which are based on the steel beam only) with the measured load-deflection response, the contribution of the concrete slab toward the stiffness and strength of the girder appears to be negligible. Note also that load-deflection response of Specimen NON-00BS exhibited excellent deformation capacity, a desirable attribute for a bridge girder.

The composite beams retrofitted with the post-installed shear connectors showed much higher stiffness and strength than the non-composite Specimen NON-00BS as expected. Recall that the shear connection ratio of the specimens was relatively low (30

percent) and the spacing between the connectors was 28.5 in., much larger than the spacing required for a fully composite beam. Despite the relatively small number of shear connectors provided in these specimens, a 40 percent increase in strength was achieved compared to the non-composite specimen, demonstrating the efficiency of partially composite design.

The measured ultimate strength of the test specimens showed good agreement compared to the theoretical values. Specimen HASAA-30BS showed slightly higher strength and deformation capacity than Specimen DBLNB-30BS. Specimen HTFGB 30-BS showed superior deformation capacity than the other two partially composite beam specimens with uniformly distributed shear connectors as shown in Figure 4.34. It is considered that the oversized hole in the concrete resulted in larger slip capacity of the HTFGB connector. It is believed that the higher slip capacity of the HTFGB connectors enabled a greater degree of load redistribution among the shear connectors, resulting in higher strength and ductility of this beam. Deformed HTFGB connectors can be seen in Figure 4.35 which shows the bottom of the concrete slab after the test.

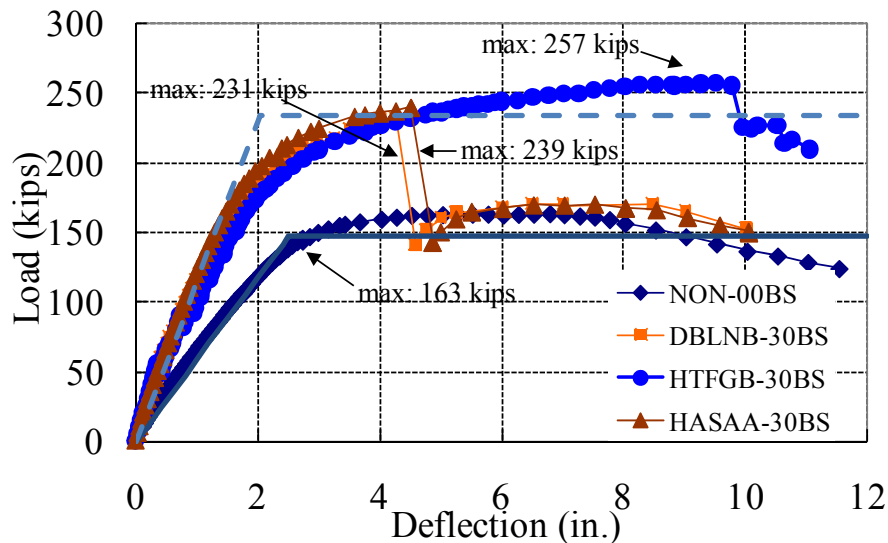


Figure 4.34: Test results compared with theoretical values of stiffness and strength



Figure 4.35: Specimen HTFGB-30BS – shear connectors after the test (slab bottom)

4.4.2 Failure Modes

As mentioned in Section 4.3.1, Specimen NON-00BS showed very ductile behavior without any sudden loss of strength during the test. Cracks occurred on the bottom of the concrete slab at low load levels, suggesting the lack of significant composite action between the concrete slab and the steel beam. In the partially composite beams, cracks were observed on the bottom of the concrete slab at much higher loads than for the non-composite beam. After shear connectors failed, Specimen DBLNB-30BS and HASAA-30BS showed concrete cracking patterns similar to those of Specimen NON-00BS. In these two specimens, there was no concrete crushing even at large deflections, although cracks on the side of concrete slab propagated transversely across the slab, which suggests imminent concrete crushing on the top of the slab. Specimen HTFGB-30BS, in contrast, showed significant concrete crushing on the top of the slab as shown in Figure 4.36. It is considered that composite action at large deflections required high strain on the top of the concrete slab and this high strain demand caused crushing in the top concrete.



Figure 4.36: Specimen HTFGB-30BS – concrete crushing on the top (10.5-in. deflection)

For non-composite Specimen NON-00BS, the ultimate strength of the beam was controlled by achieving the fully plastic moment of the W30x99 beam. This section is compact for local buckling. That is, the section is capable of developing its plastic moment prior to the occurrence of local flange or web buckling. Further, the compression flange was well braced against lateral torsional buckling. Consequently, because the beam section is compact and the beam was well braced, it was capable of developing its plastic moment, and maintaining its plastic moment capacity through large inelastic deformations. The ultimate loss of strength of this specimen, which occurred at very large deflections, was due to local flange and web buckling. Note that the presence of the slab did not prevent local buckling of the top flange, although it may have delayed it. Typical local buckling at large deflections is shown in Figure 4.37.

In contrast to Specimen NON-00BS, the two retrofitted partially composite beams, Specimen DBLNB-30BS and HASAA-30BS, showed a sudden strength drop when the shear connectors failed. After failure of the shear connectors, both of the

retrofitted partially composite beams behaved very much like the non-composite beam specimen. Thus, while the retrofitted beam specimens showed a sudden strength drop when the shear connectors failed, the specimens had substantial residual strength and deformation capacity, as they reverted back to non-composite beams.

Specimen HTFGB-30BS showed a significantly larger deformation capacity than the other two retrofitted beams, due to higher slip capacity of the HTFGB connectors. This allowed the beam to behave compositely at large deflections and to keep the neutral axis close to the top flange resulting in only minor local flange buckling, as shown in Figure 4.38.



Figure 4.37: Specimen NON-00BS – Typical beam local flange and web buckling at large displacements



Figure 4.38: Specimen HTFGB-30BS – flange local buckling (11.0-in. deflection)

4.4.3 Interface Slip and Neutral Axis Locations

All of the test specimens showed an increase in slip at the interface between the concrete slab and the steel beam as the deflection increased. Figure 4.17 shows the interface slip of Specimen NON-00BS. Slip increased linearly with the midspan deflection at the early stages of loading. After local buckling of the web and flange occurred, slip on the south end increased continuously, whereas the slip on the north end decreased.

The partially composite beams retrofitted with post-installed shear connectors showed much less slip at the early stages of loading as shown in Figure 4.39. After shear connector failure occurred in Specimens DBLNB-30BS and HASAA-30BS, the end slip-deflection behavior closely resembled that of the non-composite specimen.

Specimens DBLNB-30BS and HASAA-30BS showed beam end slip values, at the point of connector failure and sudden strength loss, of 0.23 in. and 0.27 in. respectively. These values are 26 percent and 31 percent of the connector diameter (7/8 in.), less than the values from the single shear connector tests. The first shear connector

failure occurred at 0.45-in. end slip for Specimen HTFGB-30BS, which is much larger than the other two partially composite beam test specimens, and also less than the values measured in the single shear connector tests. It appears that single shear connector tests overestimate slip capacities of the shear connectors tested in this study. However, the ultimate strength predicted with Equation 2.28 based on the single shear connector tests appears to adequately predict the strength of the partially composite beam specimens retrofitted with post-installed shear connectors.

Specimen HTFGB-30BS showed almost zero slip at the early stages of loading before the friction at the steel-concrete interface was overcome at a load of approximately 55 kips on the beam, as shown in Figure 4.40. First significant slip occurred at the steel-concrete interface with a load noise between 55 and 60-kips loading when the friction at the interface due to pretensioning of the shear connectors was overcome and connector slip occurred in the oversized holes in the concrete and the steel beam. Although Specimen HTFGB-30BS showed almost zero slip at low load levels, slip at the interface was larger than for the other two composite test specimens after friction was overcome.

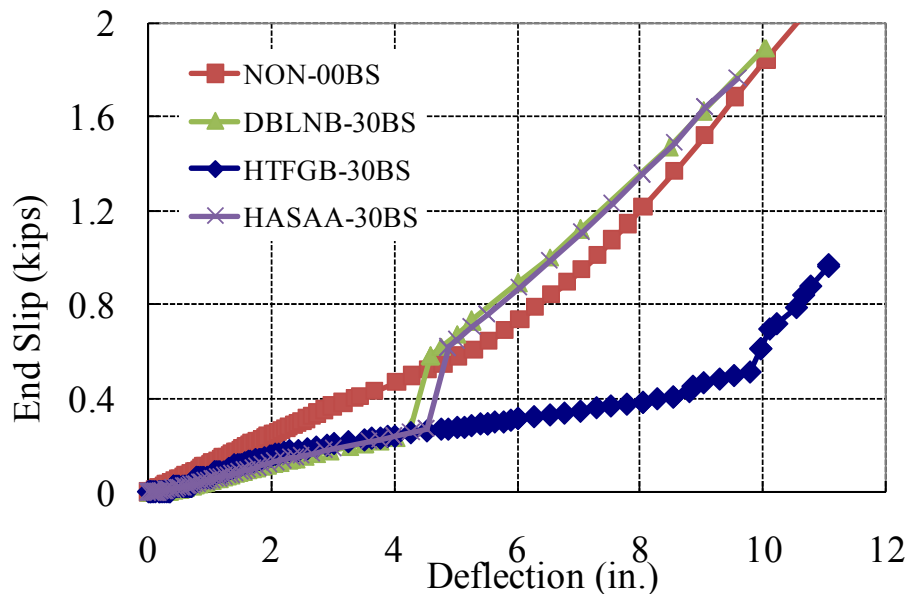


Figure 4.39: Slip at the ends of test specimens

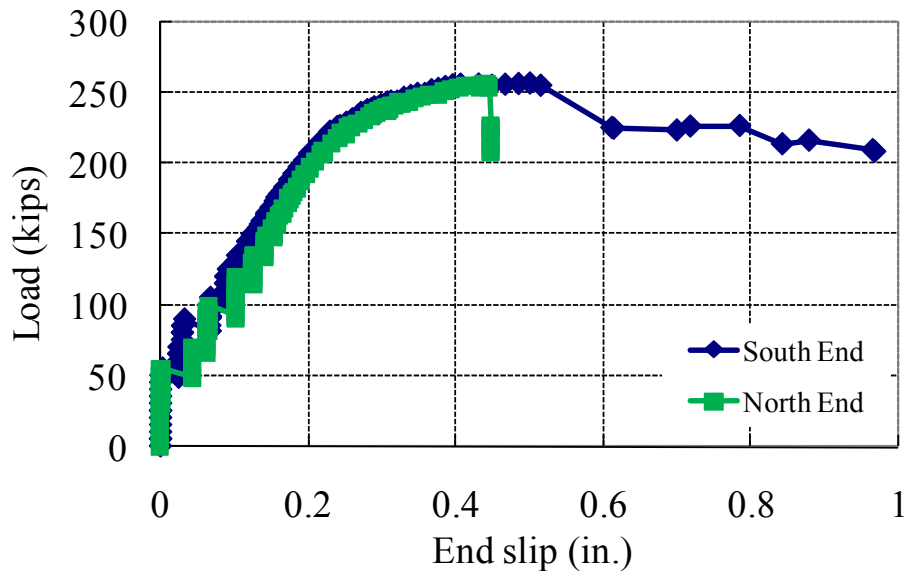


Figure 4.40: Slip at the ends of Specimen HTFGB-30BS

Composite action in the retrofitted partially composite beams can be further evaluated by locating the neutral axis in the steel beams from strain gage data. For non-composite beams, the neutral axis is expected to be at mid-height of the steel beam section. For composite beams, the neutral axis moves toward the top flange due to the composite action between the concrete slab and the steel beam. Figure 4.41 shows the measured neutral axis location at midspan of the girder with increasing midspan deflection. Neutral axis locations were obtained by interpolating data from the strain gages on the beam section.

For Specimen NON-00BS, the neutral axis was located near mid-height of the steel section, as expected. At very low load levels at the start of the test, the neutral axis was located higher up in the cross-section, suggesting some degree of composite action, perhaps due to combinations of bond and friction between the steel and concrete. However, as indicated in Figure 4.41, this composite action only occurred at the very early stage of loading. Once the load exceeded about 10% of the full capacity, this composite action ended, and the girder subsequently behaved in an almost purely non-

composite manner. When evaluating existing non-composite bridges, it is sometimes surmised that some degree of composite action can be considered when load rating the girders, resulting from bond and friction between the steel and concrete. However, the test results for Specimen NON-00BS suggest that such “unintended” composite action should not be relied upon in evaluating the strength of existing non-composite girders. Bowen and Engelhardt (2003) reached a similar conclusion after an extensive series of field load tests on non-composite steel girders.

For the retrofitted partially composite beams, the neutral axis stayed above mid-height of the steel section at all load levels, as indicated in Figure 4.41. All of the partially composite beam specimens showed almost full composite action in the early stages of loading, likely due to the friction at the steel-concrete interface. However, the neutral axis moved down as the midspan deflection increased, indicating partial composite interaction between the steel beam and the concrete slab.

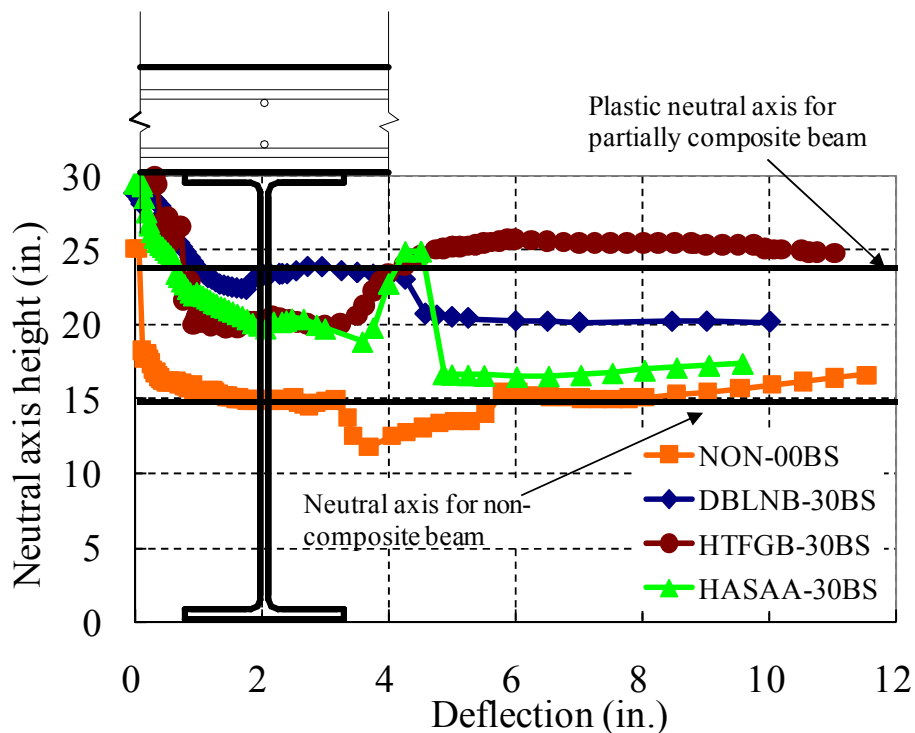


Figure 4.41: Neutral axis locations of test specimens

4.4.4 Constructability

In addition to assessing the structural performance of the retrofitted girders, constructability of the three shear connection methods was also evaluated during the full-scale beam tests. Procedures used to install the shear connectors in the test specimens are similar to the procedures that could be used on an actual bridge, allowing for some assessment of potential construction-related difficulties.

4.4.4.1 Double-Nut Bolt (DBLNB) Method

For the DBLNB connection method, access from both the top and the bottom of the concrete slab is needed to install the shear connectors. For each connector, a 2.5-in. diameter hole was made in the slab, using a core drilling machine from the top of the slab. In the laboratory, it took 5 to 10 minutes to complete a hole. The core drill bit sometimes hit and cut through transverse reinforcing bars during the drilling operation. The top transverse reinforcing bars function to resist negative moment in the transverse direction of the slab, and cutting a number of these bars may adversely affect the structural integrity of the slab. Cutting transverse reinforcing bars might also be detrimental to the fatigue performance of shear connectors as discussed in the previous chapter. The longitudinal reinforcing bars function primarily as temperature reinforcement, so cutting these bars is less consequential. In field applications, a reinforcing bar locator can potentially be used to help avoid cutting through reinforcing bars.

After completing the 2.5-in. diameter holes in the slab, a 15/16-in. diameter hole was drilled through the top flange of the steel beam, centered in the 2.5-in. hole in the slab. The holes in the top flanges were also made from the top of the slab using a magnetic drill with a long drill bit. In the laboratory, a 1-in. thick steel plate was anchored on the concrete slab to hold the magnetic drill. A hollow round bar was also placed inside the cored hole in the concrete to serve as a guide for the steel drill bit. Tightening of a connector using an impact wrench from the bottom of the slab generally

took less than 30 seconds. Load indicator washers were used to control the pretension on the connector. The hole in the concrete slab was then filled with grout having a specified strength of 2000 psi at 2 hours and 5100 psi at 24 hours. Traffic may need to be stopped until the grout gains sufficient strength.

4.4.4.2 High-Tension Friction-Grip Bolt (HTFGB) Method

This method also requires access from both the top and the bottom of the slab to install the shear connectors. For each connector, two different size holes were drilled in the concrete slab. A rotary hammer drill was first used to drill 2-in. diameter hole, and a core drilling machine was then used to drill a 1-in. diameter hole. It took 5 to 10 minutes to drill the 1-in. diameter hole. In the laboratory, about 10 holes could be finished with a coring bit before it wore out.

After completing drilling and coring in the concrete slab, a 15/16-in. diameter hole was drilled through the top flange of the steel beam, centered in the hole in the concrete slab. Before the drilling, the inside of the hole in the concrete was cleaned carefully of any concrete debris which had been produced during the drilling of the concrete slab. During the drilling through the steel beam flange, care was taken to not let the drill bit touch the inside surface of 1-in. diameter hole in the concrete slab. Otherwise, the drill bit for steel wore out rapidly.

After placing an ASTM A325 high strength bolt from the top, the connector was tightened from the bottom of the slab using an impact wrench. Finally, the same grout as before was used to fill the hole on the concrete surface.

More operations were needed on the top of the slab to install the HTFGB shear connector, indicating that traffic may need to be disrupted longer than for the DBLNB connection method.

4.4.4.3 Adhesive Anchor (HASAA) Method

Compared to the DBLNB and HTFGB connection methods, installation of the HASAA connectors can be completed entirely from the underside of the slab. As a first step, 15/16-in. diameter holes were drilled through the top flange of the steel beam. These holes were drilled from underneath the slab, using a magnetically mounted Jancy Slugger Cutter Mag Drill. It took 1 to 2 minutes to complete a hole. Only 6 to 8 holes were drilled with one new annular slugger cutter bit because the drill bit was easily worn when it hit the concrete. However, the drill bit can be used repeatedly after sharpening. After some experience, more than 30 holes were drilled with a single drill bit.

As the next step, a 5-in. deep hole was drilled into the concrete from beneath the slab, using a hammer drill. In the laboratory, a Hilti TE-55 hammer drill was used for this purpose. As a 15/16-in. diameter, carbide-tipped drill bit did not fit into the 15/16-in. diameter hole in the steel beam flange, a 7/8-in. diameter drill bit was used for the drilling, and was worked to make the hole bigger. To simplify the construction process, it may be possible to drill 1-in diameter holes in the steel flange, and then use the 15/16-in hammer drill for the concrete. However, the larger hole in the steel beam flange may require greater slip before the anchor bears against the beam flange, and may adversely affect the overall strength and ductility of the retrofitted beam. The effect of the hole size on the structural behavior of composite beams retrofitted with post-installed shear connectors is investigated in Chapter 5.

Hilti HY 150 adhesive was used to install the HASAA connectors. A potential drawback of this installation process is the cure time for the adhesive. For a 68°F temperature a 50 min. curing time is required for the adhesive used in the tests. During this time the adhesive should not be disturbed, which may require traffic to be stopped on the bridge.

4.5 NUMERICAL MODELING OF THE FOUR BEAM TEST SPECIMENS

The four full-scale beam specimens described above were modeled and analyzed using the finite element program ABAQUS. The intent of these analyses was to determine how well the model could capture various aspects of the measured and observed behavior of the test specimens. The ultimate objective was to develop ABAQUS models that reasonably predict the behavior of the test specimens, and then use these models to investigate the behavior of strengthened partially composite beams over a wider range of variables than could be considered in the tests. This section describes the ABAQUS models of the test specimens.

4.5.1 Finite Element Model

A three-dimensional finite element model was developed in this study to simulate the behavior of composite beams retrofitted with post-installed shear connectors. To develop the numerical model, various modeling issues were considered including element types, material behavior, numerical solution controls, boundary conditions, and interaction between the concrete slab and steel beam.

4.5.1.1 Material Modeling

A modified Hognestad (1951) stress-strain relationship was used to model the concrete stress-strain curve in compression. It is assumed that concrete is in the elastic range when f_c is less than $0.45f_c'$, where f_c is the compressive stress in concrete and f_c' is the ultimate concrete strength. In this model, the initial modulus of elasticity of the concrete, E_c , is taken as $1.8 \times 10^3 + 460f_c'$ (ksi). In tension, a smeared cracking model was used to model the concrete behavior (ABAQUS, 2007). In this model, cracking is assumed to occur when the stress reaches a failure surface. The concrete model, however, does not track individual macro cracks. Instead, the presence of cracks affects the stress

and material stiffness of the corresponding integration points. To include the effects of reinforcement on the bottom of the concrete slab (tension side), tension stiffening behavior was defined. In ABAQUS, tension stiffening can be defined by a post-failure stress-strain relationship of concrete material. The concrete material model used in this study is shown in Figure 4.42.

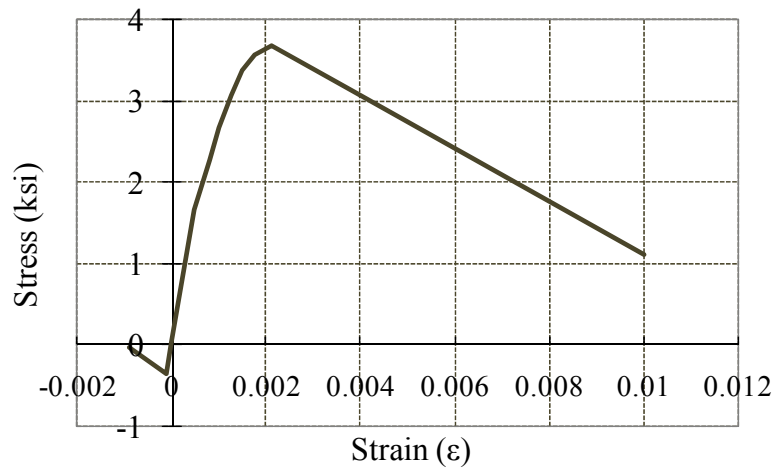


Figure 4.42: Concrete model in ABAQUS

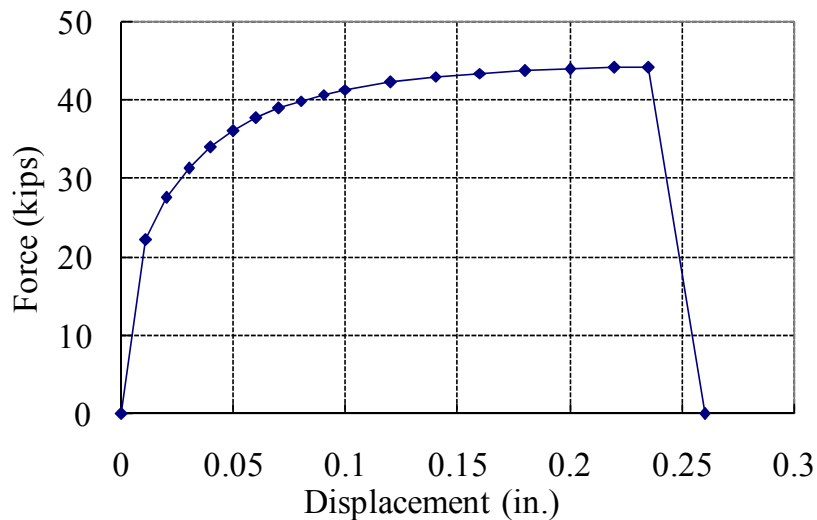


Figure 4.43: Connector load-slip relationship

To model the stress-strain relationship of the steel beams and reinforcing bars, an elastic-perfectly plastic model was used. The modulus of elasticity of the steel beams and the reinforcing bars, E_s , is taken as 29,000 ksi. Strain hardening was not included in this model.

The test specimens in this research program were unshored during construction. For unshored composite construction, the dead load of the beam (weight of the concrete slab and steel beam) is resisted by the steel beam alone, and not by the composite section. Further, the post-installed shear connectors also do not resist the beam dead load. To simulate this condition in the ABAQUS model (that is, to keep the concrete slab and the shear connectors unloaded under girder dead load), the yield stress of the steel beam was reduced to account for the dead load of the concrete slab and the steel beam instead of applying a uniformly distributed dead load on the composite beam. The moment induced by the dead load of the 38-ft long beam was 124.7 ft-kips. Therefore, the yield stress of the steel beam was reduced by $124.7 \times 12 / 312 = 4.80 \text{ ksi}$. The plastic section modulus of W30x99 beam is 312 in^3 .

Equation 2.3, proposed by Ollgaard et al. (1971) was adopted to model the load-slip relationship of the post-installed shear connectors. This load-slip relationship was developed by Ollgaard et al. (1971) for conventional welded shear studs and was used here as an approximation of the load-slip behavior of the post-installed shear connectors. The ultimate strength of the post-installed shear connectors measured in tests was used in the model. An example of a load-slip curve for a post-installed shear connector is shown in Figure 4.43.

4.5.1.2 Element Selections

A finite element analysis model developed in this study is shown in Figure 4.44. A 4-node shell element (S4) was selected for both the steel beam and the concrete slab. Element type S4 in ABAQUS is a fully integrated, finite membrane strain shell element. Simpson's rule is used to calculate the cross-sectional behavior of the shell elements

(ABAQUS 2007). In ABAQUS, one or multiple layers of reinforcement can be specified in the shell element. The reinforcing bar layers are smeared in the shell element.

Connector elements were used to model the shear connectors. ABAQUS provides several types of connector elements to impose constraints between two elements. Among these various types of connectors, CARTESIAN connectors were used to simulate the behavior of the shear connectors. This connector is a “spring-like” element defined in a local Cartesian coordinate system, and capable of deforming in the coordinate system. Elastic and inelastic behavior can be defined for the element. Connector failure can also be specified with limit values for force or relative displacement. If the specified failure criterion is met, the connector is removed and is no longer effective in the analysis.

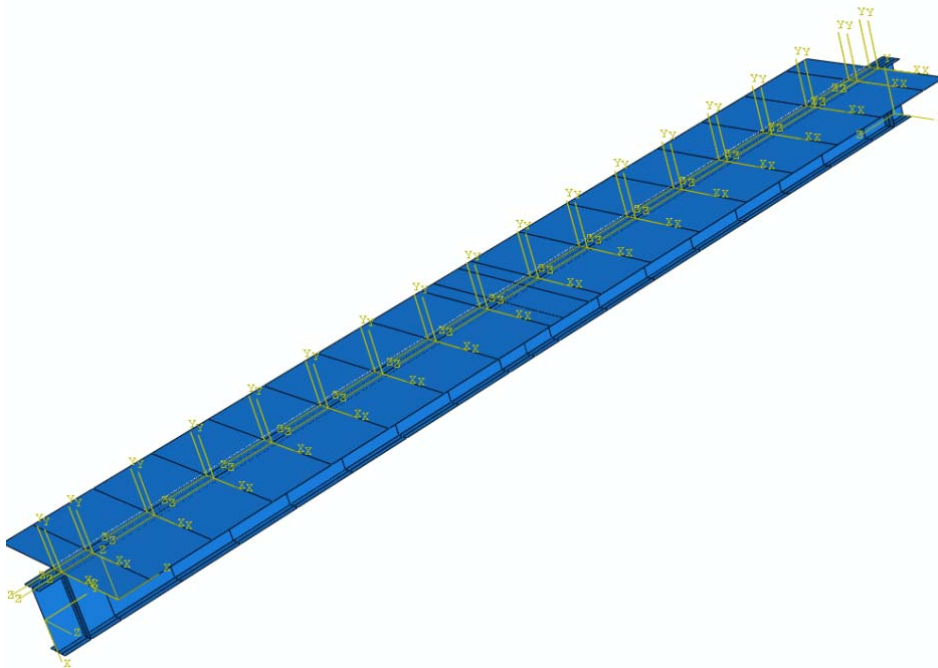


Figure 4.44: Finite element model for full-scale beam specimen

Contact interactions in ABAQUS were defined to simulate the interaction between the steel beam and the concrete slab. There is no limit on the magnitude of pressure that can be transmitted between the two surfaces. Separation of contacted surfaces was not allowed after contact occurs, since separation of the steel beam flange and the concrete slab was not detected for the full scale beam tests, except for one specimen at a large deflection. Bond and friction at the interface was not considered in the finite element model.

The connector elements were connected to the shell elements that represent the concrete slab and the steel beam. The stiffness of the connector element is affected by the stiffness of the shell elements to which the connector element is connected. To obtain load-slip relations of individual shear connector in composite beams, the single shear connector specimen described in Chapter 3 was modeled in ABAQUS. In the finite element model, slip was measured at the same location as in the single shear connector test specimens. The finite element model for the single shear connector tests is shown in Figure 4.45.

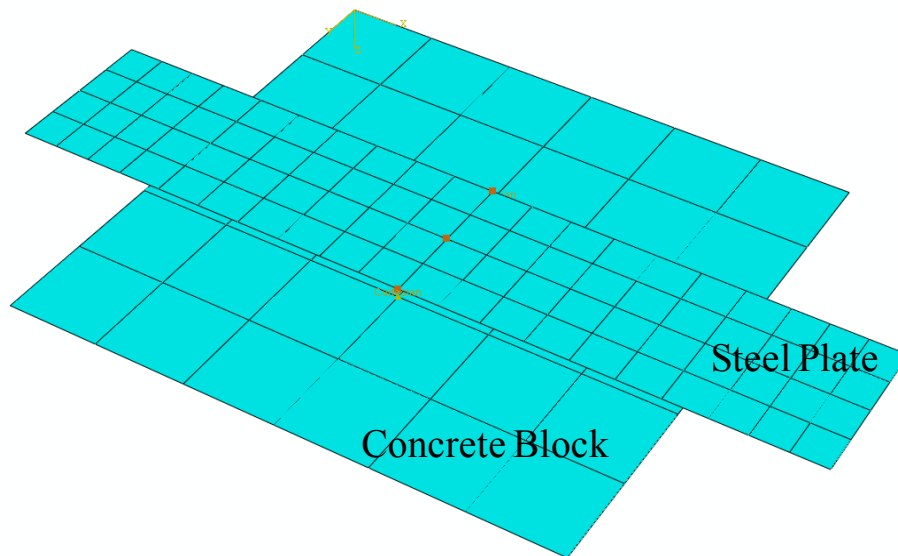


Figure 4.45: Finite element model for single shear connector specimen

4.5.1.3 Analysis Procedure

A pressure load was applied at mid-span of the beam to simulate the point load applied during the full-scale beam tests. Both geometric and material nonlinearities were considered during the analysis. Local buckling and lateral torsional buckling of the steel beam are not considered in this model.

The General Static method in ABAQUS is not appropriate to predict negative stiffness during the analysis. To simulate possible negative stiffness during the analysis, the Riks method was used for the static analysis (ABAQUS 2007). This method is generally used for predicting nonlinear collapse and post-buckling analysis including strain softening. This method uses load as unknown and seeks load and displacement simultaneously (ABAQUS 2007).

From the finite element analysis, information about load-deflection relations, neutral axis locations of non-composite beams and composite beams, and slip at the steel-concrete interface was gathered and the results were compared with the full-scale beam test results.

4.5.2 Analysis Results

4.5.2.1 Non-Composite Specimen NON-00BS

The baseline non-composite Specimen NON-00BS showed very ductile behavior which is expected in a well-braced compact steel beam. ABAQUS analysis results for the specimen are shown in Figure 4.46 to Figure 4.48. As shown in Figure 4.46, the load-deflection curve from ABAQUS shows good agreement with the test results before the beam experienced local buckling at large deflections. The analysis model in this study did not simulate local buckling of the beam flange and the web. Slip at the steel-concrete interface in the ABAQUS model was also compared to the test results as shown in Figure 4.47. The model predictions matched well with the measured slip up to a midspan deflection of about 5 to 6 in. The analysis model did not simulate the difference in slip

after local buckling at the beam flange. In the test, the slip at south end increased continuously, whereas the slip at north end decreased after the local buckling in the steel beam flange occurred.

The measured neutral axis location in the steel beam stayed near mid-height of the beam during the test, since there was little composite action at the steel-concrete interface for Specimen NON-00BS. Figure 4.48 shows longitudinal stress distribution of Specimen NON-00BS in ABAQUS. It can be seen that the neutral axis was located at the mid-height of the beam.

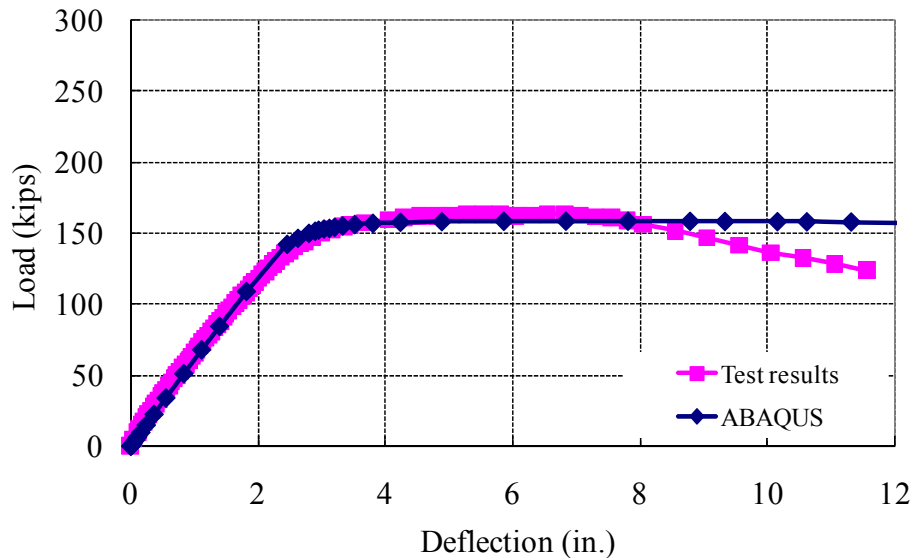


Figure 4.46: Load vs. midspan deflection curves (Specimen NON-00BS)

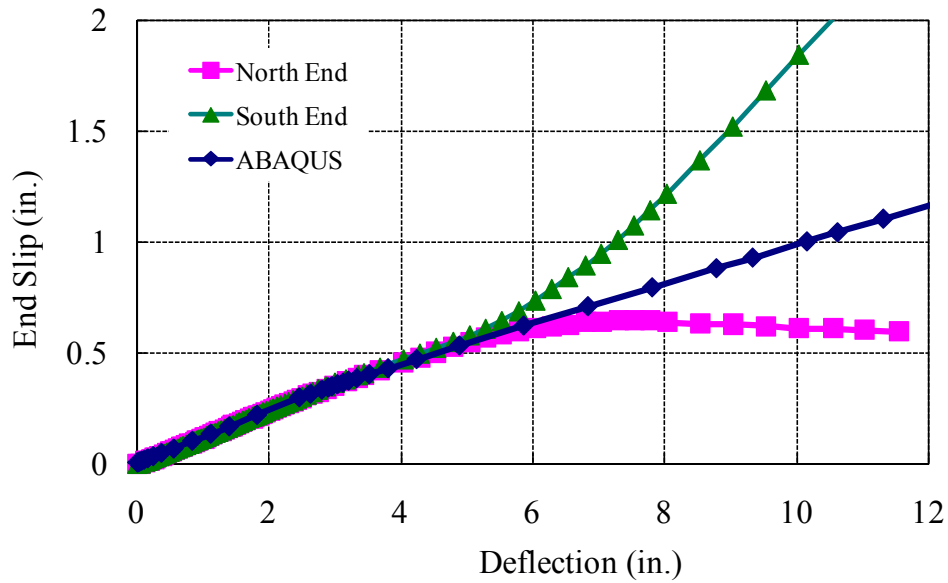


Figure 4.47: Deflection vs. end slip curves (Specimen NON-00BS)

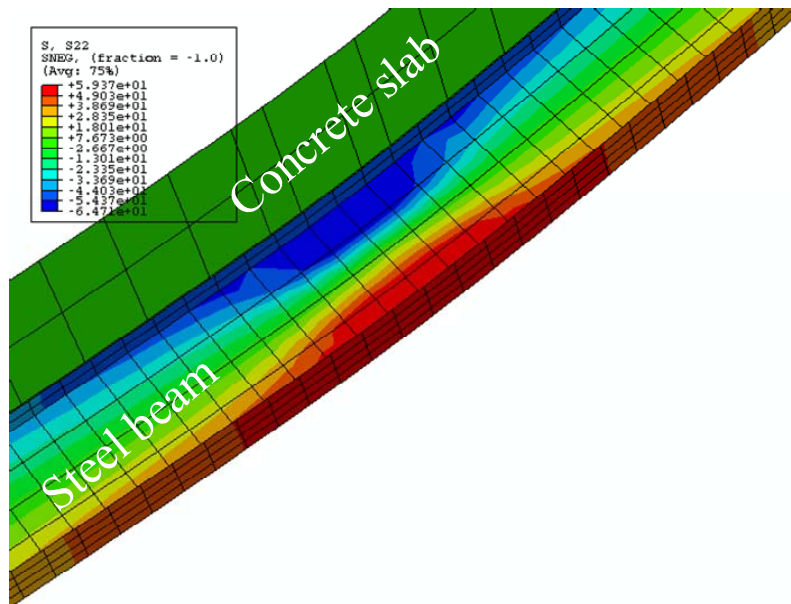


Figure 4.48: Longitudinal stress distribution (Specimen NON-00BS)

4.5.2.2 Composite Specimens DBLNB-30BS and HASAA-30BS

These two specimens showed similar behavior during the full-scale beam tests in the laboratory. The maximum measured slip at the steel-concrete interface before shear connector failure was 0.23 in. and 0.27 in. for Specimens DBLNB-30BS and HASAA-30BS respectively. The shear connectors in ABAQUS were modeled to fail when these maximum slip values were reached. Figure 4.49 shows the behavior of the DBLNB connector in the single shear connector test specimens in ABAQUS (Figure 4.45). The shear connector followed load-slip curve developed by Ollgard et al. (1971), and failed at 0.23-in. slip.

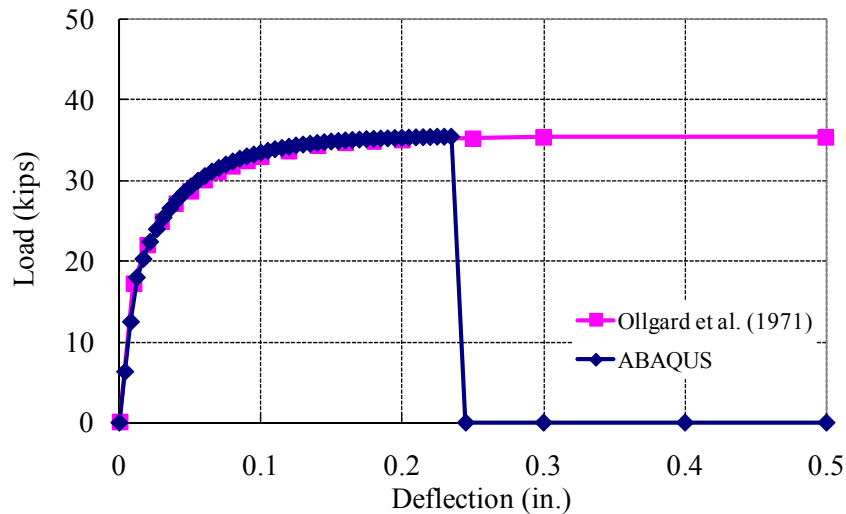


Figure 4.49: Load-slip behavior of the DBLNB connector (ABAQUS)

The measured load-deflection relations for Specimens DBLNB-30BS and HASAA-30BS are shown in Figure 4.50 and Figure 4.51, along with the corresponding ABAQUS predictions. The overall agreement between the predicted and measured curves is quite good up through failure of the shear connectors. The load-deflection curve from ABAQUS for Specimen DBLNB-30BS showed a little higher initial stiffness than the test results. However, the finite element model predicts the maximum load-carrying

capacity and the failure of shear connectors well. Note that the shear connector slip in the oversized holes in the steel beam flange was not considered for the modeling of the shear connector behavior of the DBLNB connectors. This might have resulted in a little higher stiffness in the load-deflection relations in the finite element model than the test results.

Deflection-end slip relations from the finite element model were compared to the test results of Specimens DBLNB-30BS and HASAA-30BS in Figure 4.52 and Figure 4.53. It is believed that the finite element models show good agreement with the test results before shear connector failure.

Due to the composite action between the concrete slab and the steel beam, the neutral axis of composite beams is expected to be located higher in the beam section than for the non-composite beam. Figure 4.54 shows longitudinal stress distribution of Specimen DBLNB-30BS in the ABAQUS model. Movement of neutral axis can be observed due to the composite action between the two structural components compared to non-composite beam model in Figure 4.48.

As shown in the analysis results with ABAQUS, the finite element model did not simulate the behavior of the retrofitted composite beams after shear connector failure. It was not possible to obtain convergence of the models beyond the points indicated in the plots. However, the ABAQUS model provided a good approximation of the measured behavior of the composite beam specimens up through and including shear connector failure, which is the range of behavior of primary interest in this study.

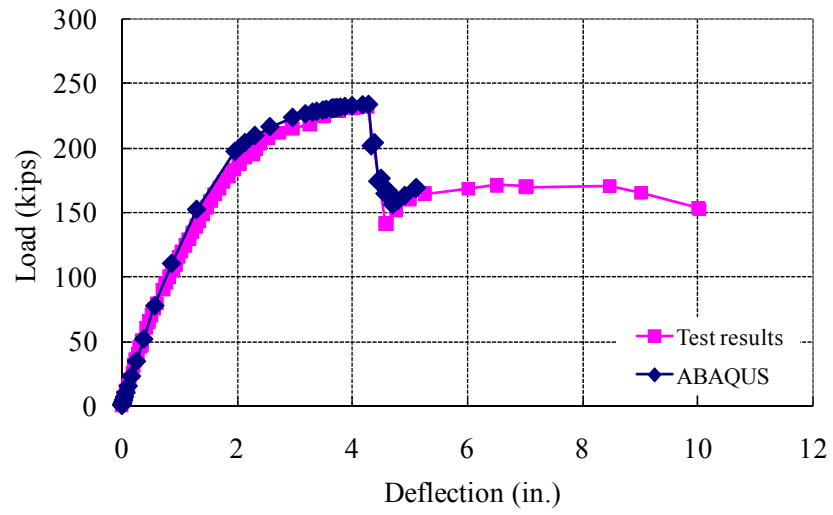


Figure 4.50: Load vs. midspan deflection curves (Specimen DBLNB-30BS)

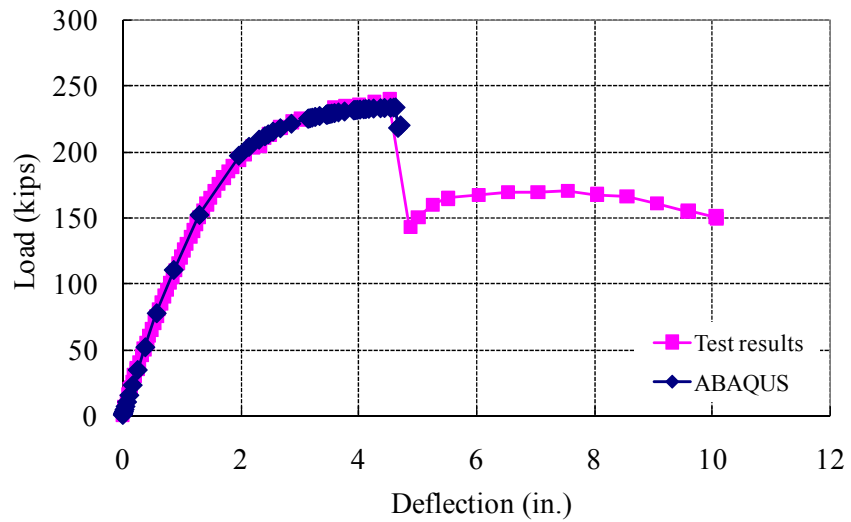


Figure 4.51: Load vs. midspan deflection curves (Specimen HASAA-30BS)

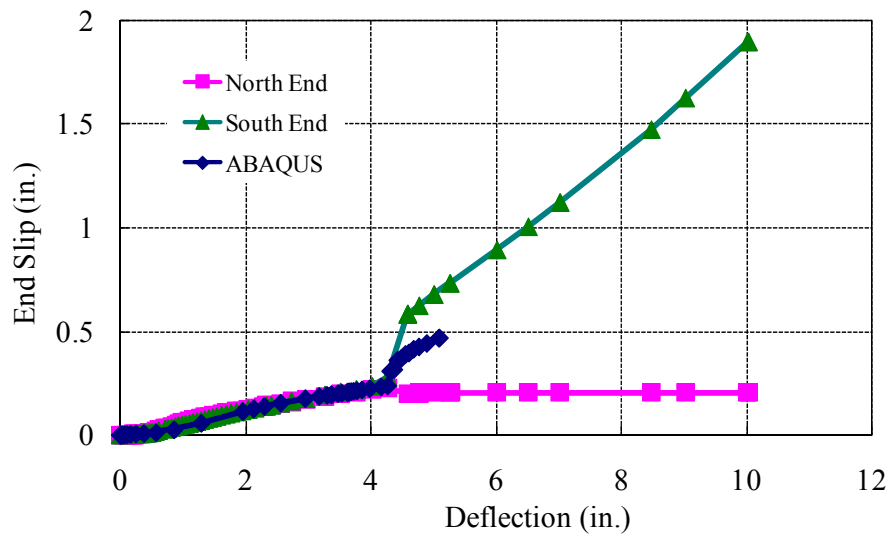


Figure 4.52: Deflection vs. end slip curves (Specimen DBLNB-30BS)

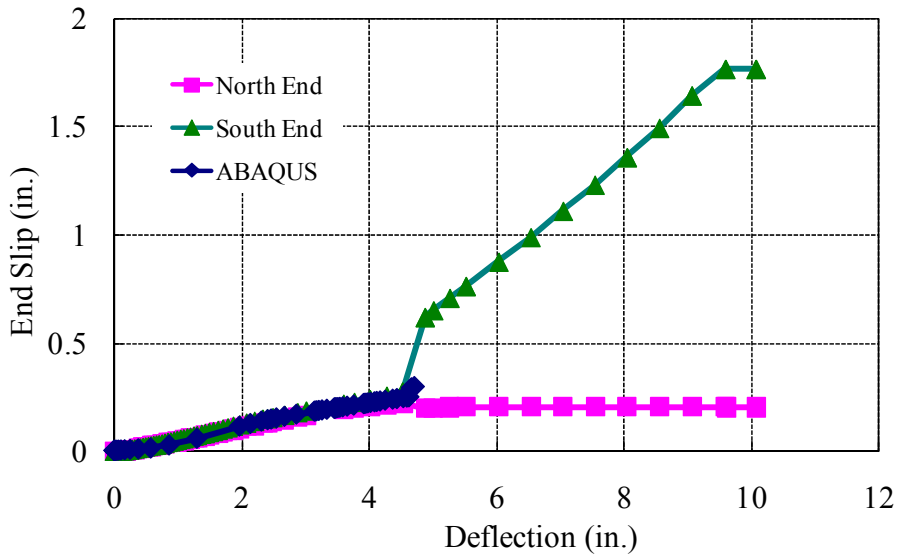


Figure 4.53: Deflection vs. end slip curves (Specimen HASAA-30BS)

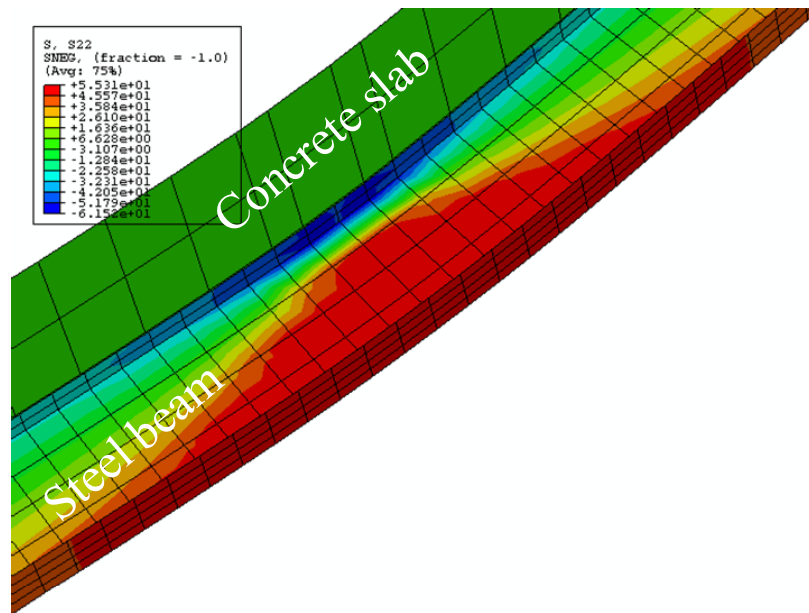


Figure 4.54: Longitudinal stress distribution (Specimen DBLNB-30BS)

4.5.2.3 Composite Specimen HTFGB-30BS

Specimen HTFGB-30BS showed significantly higher deformation capacity than Specimens DBLNB-30BS and HASAA-30BS. As shown in Figure 4.55, the finite element model predicted somewhat higher overall stiffness and lower strength than the test results. The shear connector model used in the finite element model did not include the slip due to the oversized hole in the concrete and the steel beam flange, and therefore may have overestimated the initial stiffness of the connector. The deflection-end slip relations for Specimen HTFGB-30BS in the ABAQUS model generally predicted less slip under the same deflection than the test results as shown in Figure 4.56. Nonetheless, the ABAQUS model captured the overall strength, stiffness and deformation capacity of the test specimen reasonably well.

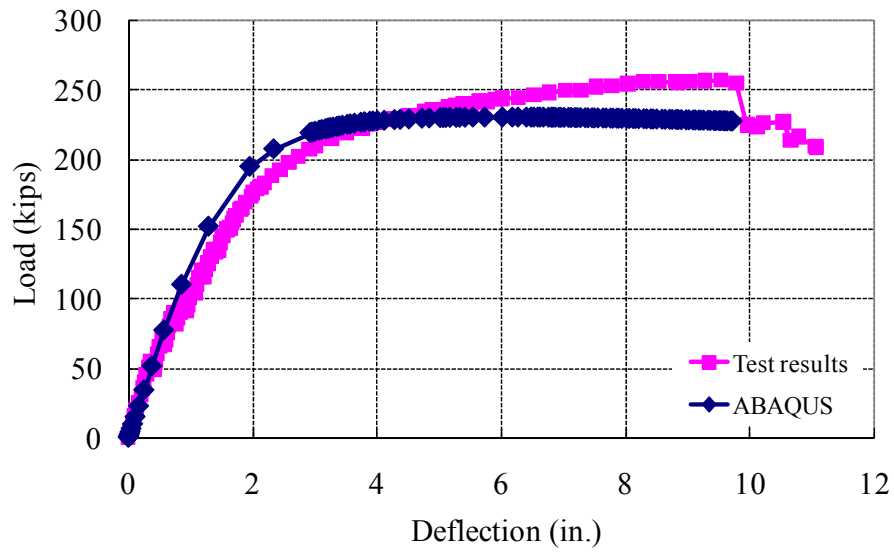


Figure 4.55: Load vs. midspan deflection curves (Specimen HTFGB-30BS)

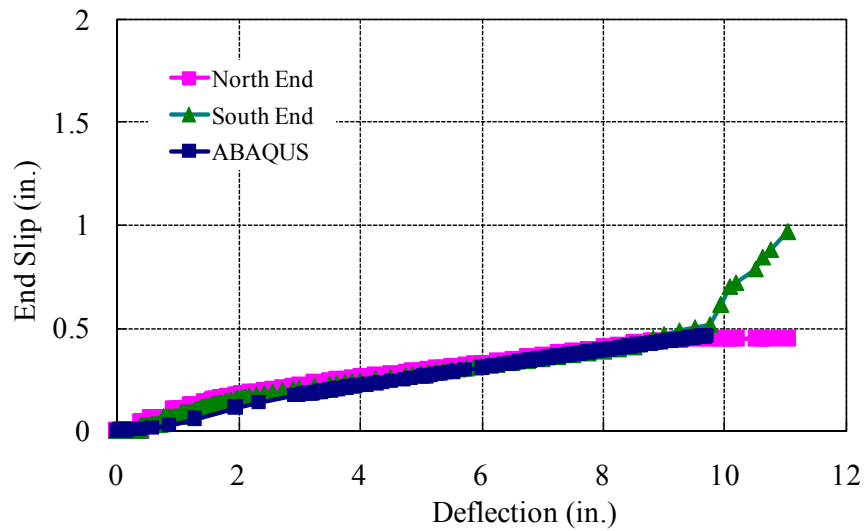


Figure 4.56: Deflection vs. end slip curves (Specimen HTFGB-30BS)

4.6 IMPROVING DEFORMATION CAPACITY OF RETROFITTED COMPOSITE BEAMS

Shear connectors at the steel-concrete interface are required to have enough slip capacity to redistribute interface shear among the connectors. Specimens DBLNB-30BS and HASAA-30BS showed limited deformation capacity due to the limited slip capacity of the high strength connector materials and due to the low shear connection ratio. Specimen HTFGB-30BS showed significantly higher deformation capacity in its overall load-deformation response due to the higher slip capacity of this connector. However, the HTFGB connectors are more difficult and time-consuming to install than the HASAA and DBLNB connectors. Because of the easier installation characteristics of the HASAA and DBLNB connectors, an approach was developed to increase the deformation capacity of beams retrofitted with these connectors.

4.6.1 Effect of Locating Shear Connectors near Supports

Oehlers and Sved (1995) developed equations to predict the maximum slip at the steel-concrete interface of partially composite beams when the beam reaches its full flexural capacity, M_{\max} . Those authors indicate that concentrating shear connectors near zero-moment regions can reduce the slip at the steel-concrete interface at M_{\max} . This suggests that simply supported beams with shear connectors concentrated near the supports can likely show higher deformation capacity than beams with uniformly distributed shear connectors along the span before the shear connectors fail.

According to Equation 4.1 (repetition of Equation 2.24), the maximum slip at the steel-concrete interface at M_{\max} is 0.15 in. for the composite beam specimen with uniformly distributed shear connectors. The minimum specified material properties were used for this calculation.

$$s_{\max} = A_m K_1 - A_{sh} K_2 \quad (4.1)$$

where, A_m = Area under moment diagram in a shear span

A_{sh} = Area under interface shear force diagram in a shear span

Interface shear force diagrams for the beams with uniformly distributed shear connectors and the shear connectors concentrated near the supports are shown in Figure 4.57. When the shear connectors are moved closer to the supports, the area of the interface shear force diagram (A_{sh}) increases, resulting in an increase of the second parameter in Equation 4.1, as shown in Figure 4.57(c). If the shear connectors are installed near the supports at a 12-in. spacing, Equation 4.1 predicts a maximum slip of 0.01 in. This value seems unrealistic, because the shear connectors need to be deformed to resist the interface shear. The maximum slip of 0.01 in. is too small for the shear connectors resist the load. Oehlers and Sved (1995) assumed that all of the shear connectors at the interface are plastic, that is resisting their ultimate load, during the analysis. Nonetheless, Equation 4.1 suggests that installing shear connectors near the supports can reduce slip at the steel-concrete interface, resulting in larger deformation capacity before shear connector failure than the composite beam with uniformly distributed shear connectors.

Finite element analysis was also conducted to evaluate the effect of moving shear connectors near the supports. The finite element model developed for Specimen HASAA-30BS was used to evaluate the performance of partially composite beams with shear connectors concentrated near the support. In the finite element model, shear connectors were moved near the supports and were located at a 12-in. spacing. The total number of shear connectors and the material properties in the analysis were not changed in the model.

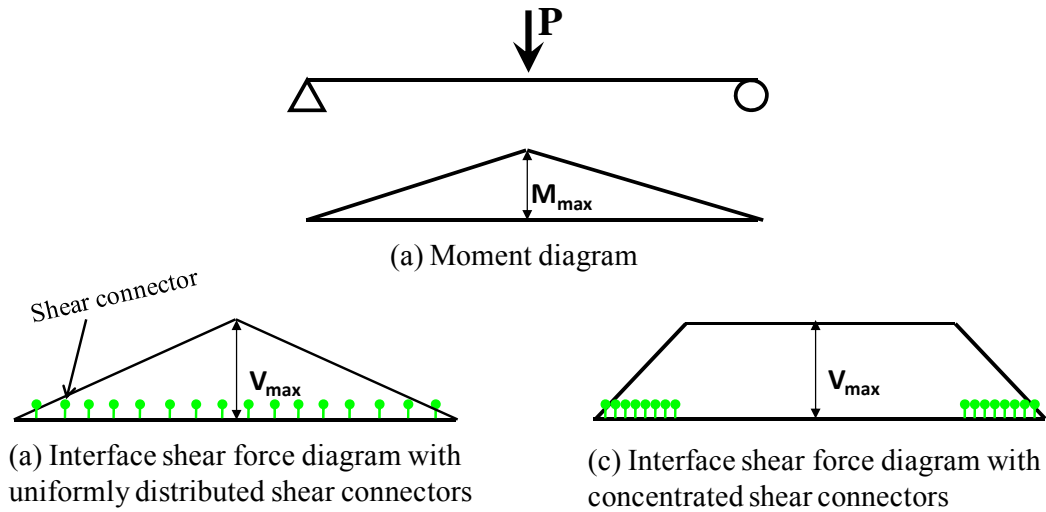


Figure 4.57: Concentrating shear connectors

The load-deflection curve predicted from finite element analysis is shown in Figure 4.58. Compared to Specimen HASAA-30BS with uniformly distributed shear connectors, the deformation capacity of the partially composite beam with shear connectors relocated near the supports was increased significantly. Figure 4.59 shows the deflection-end slip relations of the composite beams with uniformly distributed shear connectors and with shear connectors concentrated near the supports. Both results were obtained from the finite element analysis. The figure indicates that interface slip can be reduced by moving shear connectors near the supports. The graph also indicates that the composite beam with shear connectors concentrated near the supports can deflect more than the beam with uniformly distributed shear connectors before any shear connector fails.

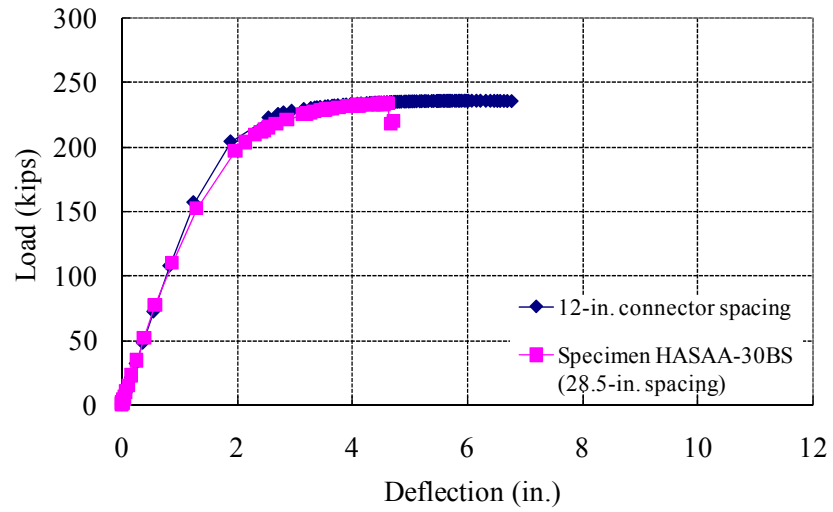


Figure 4.58: Load-deflection relations for the composite beam with concentrated shear connectors

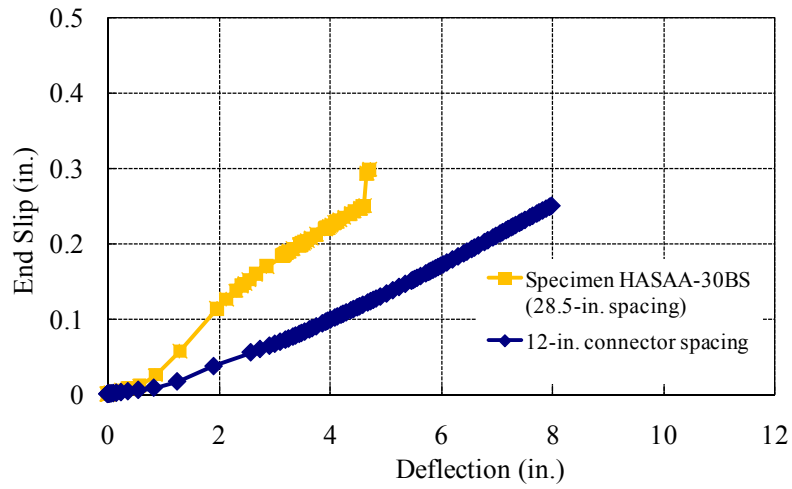


Figure 4.59: End slip for the composite beam with concentrated shear connectors

4.6.2 Test Results of Partially Composite Beam with Shear Connectors Concentrated near Supports

One additional partially composite beam specimen retrofitted with post-installed shear connectors was tested to evaluate the changes in behavior caused by concentrating shear connectors near the supports. Specimen HASAA-30BS1 was retrofitted with the HASAA connectors. It was also designed as 30 percent composite, but shear connectors were not distributed uniformly along the span at a 28.5-in. spacing. Rather, they were concentrated near the support and installed from the support at a 12 in. spacing. The total number of shear connectors installed in the beam was the same as with the other three partially composite specimens. Six out of 32 shear connectors installed had a 4-in. deep embedment depth instead of 5 in., because transverse reinforcement or reinforcing bar chairs were in the way.

Figure 4.60 and Figure 4.61 show the load-deflection and midspan deflection-slip response for Specimen HASAA-30BS1 with shear connectors concentrated near the support.

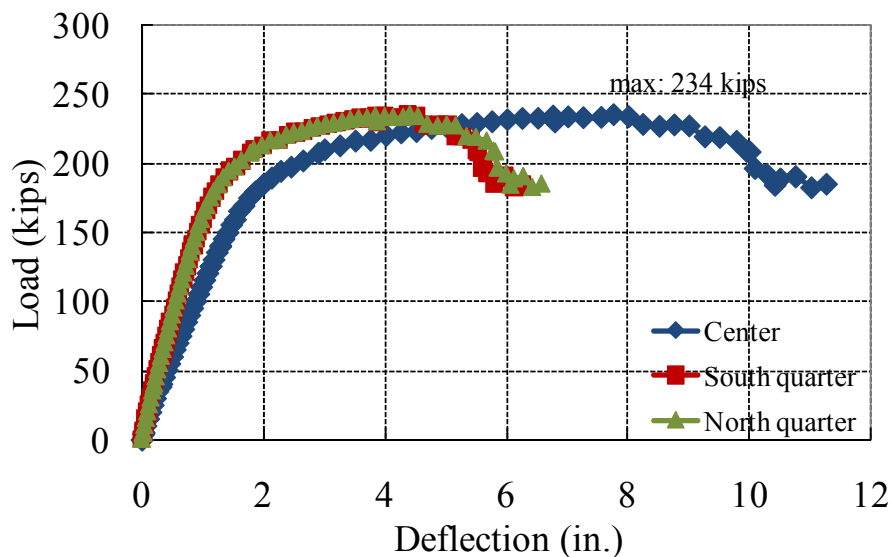


Figure 4.60: Load vs. deflection curves (Specimen HASAA-30BS1)

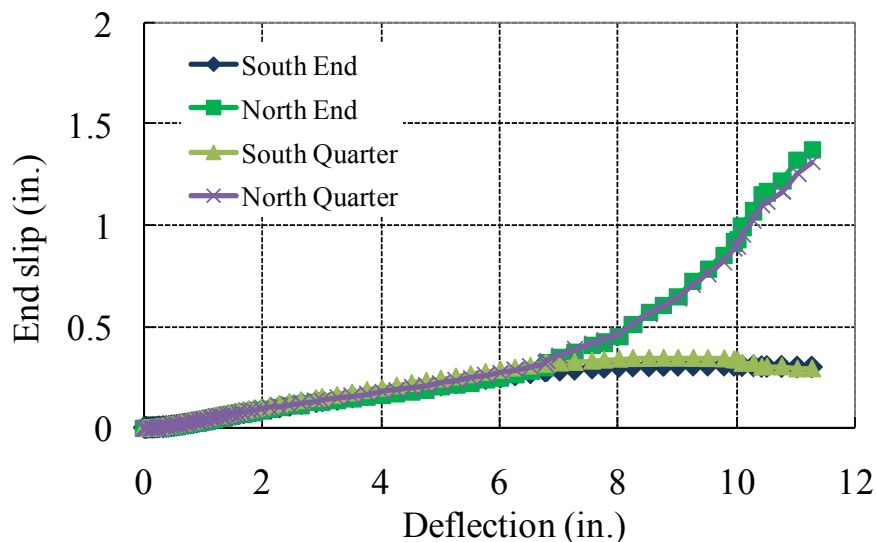


Figure 4.61: Deflection vs. slip curves (Specimen HASAA-30BS1)

4.6.2.1 Test Results for Specimen HASAA-30BS1

The load-deflection response for Specimen HASAA-30BS1 is shown in Figure 4.62 along with the test results of Specimens HASAA-30BS and NON-00BS. As shown in the figure, more ductile behavior was observed by moving the shear connectors toward the support compared to Specimen HASAA-30BS.

Specimen HASAA-30BS1 behaved very much like Specimen HASAA-30BS in the elastic range. The slightly lower strength of Specimen HASAA-30BS1 compared to Specimen HASAA-30BS can be attributed to the lower yield strength of the steel beam for Specimen HASAA-30BS1. Friction at the interface due to pretension (150 lb-ft with torque wrench) of the anchors was overcome at a load of 40 kips with a loud noise, at which point the load dropped less than 5 kips. It is believed that the concentration of shear connectors near the support induced a somewhat larger friction force at the steel-concrete interface at the early stages of the test. At a load of 160 kips, whitewash flaked on the bottom flange of the beam. At 190 kips, several cracks were observed in the

concrete slab. It appeared that the first cracks in the concrete occurred somewhat earlier than in Specimen HASAA-30BS. After reaching a load of 210 kips, displacement control was used in the test due to the reduction of stiffness in the specimen. At this point, crack width in the concrete was still less than 0.01 in.

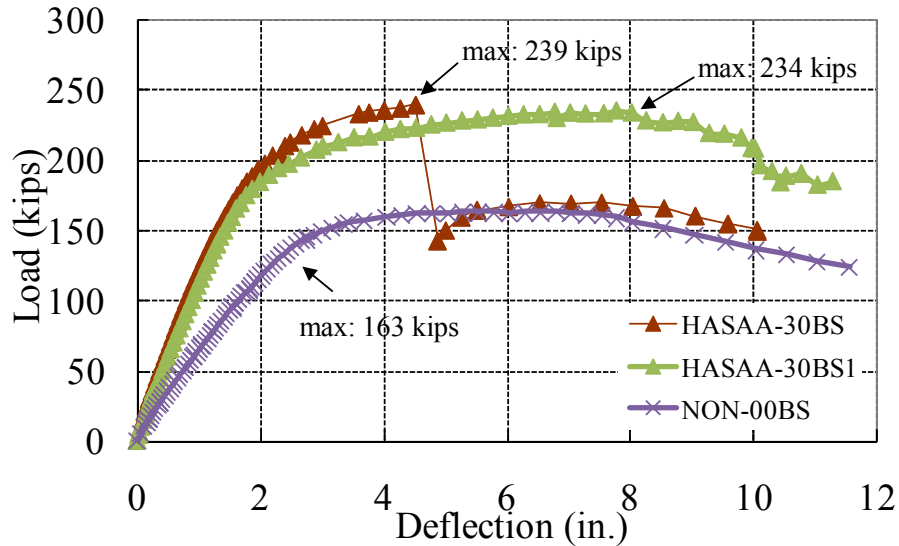


Figure 4.62: Load-deflection relations for Specimen HASAA-30BS1

At 3.5-in. deflection, top flange whitewash flaking was detected. At 5.75-in. deflection, significant whitewash flaking on the top flange was observed, indicating imminent top flange local buckling as shown in Figure 4.63. However, no gap at the interface was visually observed. One shear connector near the north support failed at 6.75-in. deflection. Load dropped less than 5 kips. Even after the first shear connector failure, the applied load increased slightly before another shear connector failure at 8.25-in. deflection. Maximum load was 234.4 kips at 7.75-in. deflection. Three more shear connectors failed during subsequent loading to 11.25-in. deflection. At 8.5-in. deflection, concrete around the shear connectors with 4-in. embedment depth showed cracks (Figure 4.64). A gap of about 0.03 in. between the concrete slab and steel beam was also

observed near the north support. At 9.0-in. deflection, flange local buckling was visually detected with a gap at the steel-concrete interface. Cracks on the top of the concrete slab near the loading point were also detected. The test stopped at 11.25-in. deflection due to safety reasons. The maximum gap at the steel-concrete interface near the north support was 0.25 in. Figure 4.65 shows concrete cracks around the shear connectors and the gap at the steel-concrete interface at the end of the test.



Figure 4.63: Specimen HASAA-30BS1 - Flange white wash flaking (5.75-in. deflection)



Figure 4.64: Specimen HASAA-30BS1 - Cracks around shear connector (8.5-in. deflection)



Figure 4.65: Specimen HASAA-30BS1 - Concrete cracks and gap at the interface near the north support (11.25-in. deflection)

4.6.2.2 Discussion of the Test Results (Specimen HASAA-30BS1)

The test results of Specimen HASAA-30BS1 show that the deformation capacity of partially composite beams can be improved by concentrating shear connectors near zero-moment regions. As shown in Figure 4.62, the deformation capacity of Specimen HASAA-30BS1 was comparable to that of Specimen NON-00BS, the non-composite baseline specimen.

Figure 4.66 shows deflection-end slip curves for Specimens HASAA-30BS and HASAA-30BS1. Slip at the interface between the steel beam and the concrete slab reduced significantly by placing the shear connectors near the supports. Specimen HASAA-30BS1 did not show a sudden increase in slip from multiple shear connector failures occurring at the same time. This might be attributed to the redistribution of the interface shear force among the shear connectors close to each other. Figure 4.67 shows the neutral axis locations during the tests, and indicates composite action was maintained even at large deflections after some shear connectors failed. The test results of Specimen HASAA-30BS1 suggest that installation of shear connectors near the zero moment regions reduces slip at the steel-concrete interface and is also beneficial for the redistribution of the interface shear, which prevent sudden loss of strength.

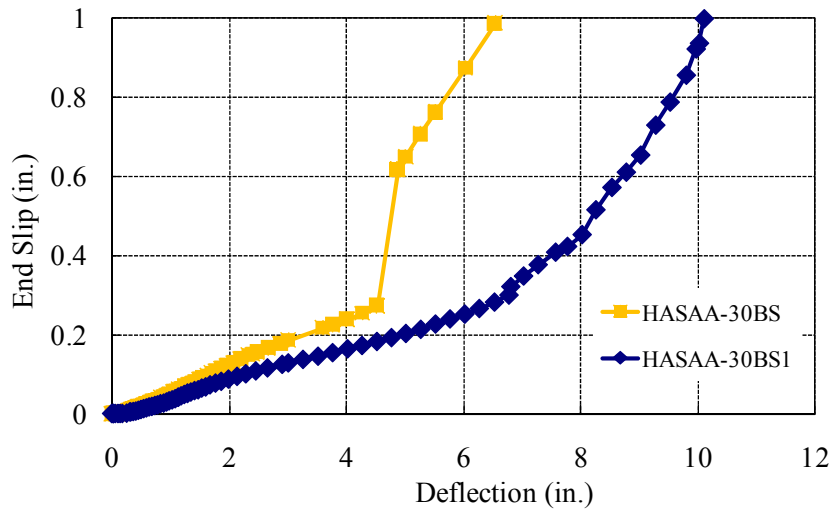


Figure 4.66: Deflection vs. end slip curves for test specimens

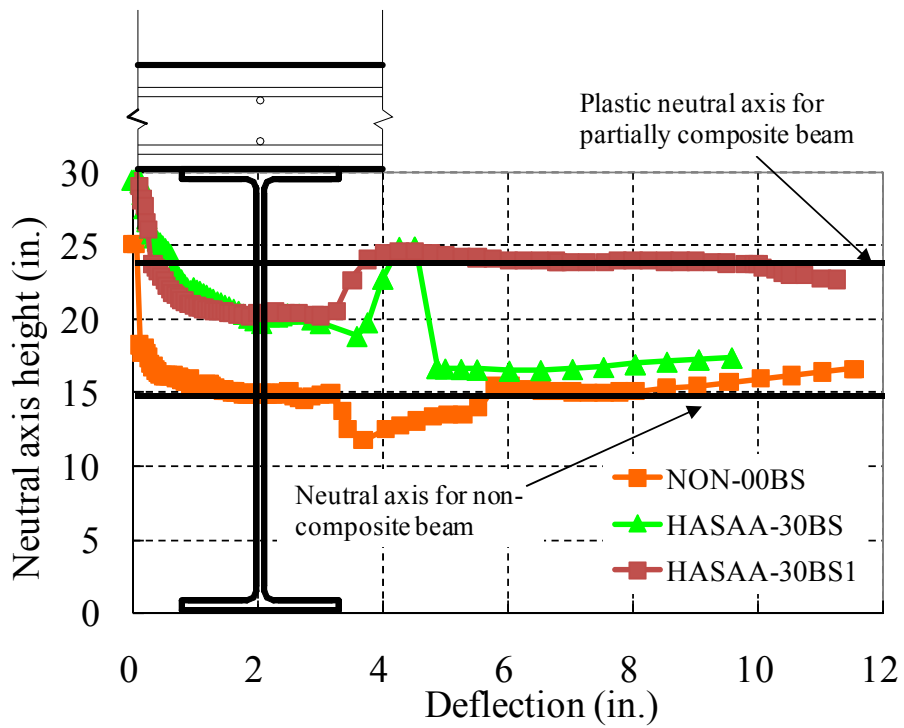


Figure 4.67: Neutral axis locations of test specimens

4.7 SUMMARY

In this chapter, static tests on four steel-concrete composite beams retrofitted with post-installed shear connectors are described. One non-composite beam was also tested for comparison with the behavior of the retrofitted composite beams. The number of post-installed shear connectors used in the retrofitted specimens was based on the concept of partially composite design. Partial composite design is not normally used for new composite bridge girders, because fatigue typically controls the required number of shear connectors. Because of the superior fatigue characteristics of the post-installed shear connectors tested in this study, however, fatigue is not likely to control the required number of shear connectors, and partial composite design is therefore possible. With partial composite design, 50 to 70 percent of the shear connectors normally needed for full composite design can be eliminated, while still achieving a 40- to 50-percent increase in load-carrying capacity in positive-moment regions of a girder.

The performance of bridge girders retrofitted with post-installed shear connectors was evaluated with a series of large-scale beam tests, supplemented with finite element analysis. Finite element analysis indicated that installation of shear connectors concentrated near zero moment regions can reduce slip at the steel-concrete interface, resulting in larger deformation capacity compared to the composite beams with uniformly distributed shear connectors. This analysis result was verified by a test on the last of four full-scale steel-concrete composite beam specimens.

CHAPTER 5

Parametric Finite Element Study

5.1 INTRODUCTION

Full-scale composite beam tests give valuable insight into the structural behavior of the beams retrofitted with post-installed shear connectors. Given the practical limits on laboratory testing, however, it is practically not possible in the laboratory to test the range of variables needed for complete design recommendations (Lam *et al.* 2000). In this study, the finite element method was adopted to study the behavior of many composite beams with different geometries, and to investigate the effects of various parameters on the behavior of composite beams.

Beam depth, span length, and shear connection ratio were selected as the main variables for the parametric study, along with the effects of oversized holes in the steel beam flange. Results from the parametric studies, combined with test results, were used to develop preliminary design recommendations in Chapter 7.

5.2 PARAMETRIC STUDY OF COMPOSITE BEAMS

Using the analytical model developed in Chapter 4, parametric studies were conducted to evaluate the effects of beam depth, span length, and shear connection ratio. Sixty composite beams were modeled with steel beam depths from W27 to W36, span lengths from 30 ft to 50 ft, and shear connection ratios from 10 to 50 percent. The beams were simply supported, and were intended as variants on the full-scale beam specimens tested for this study. The beam sections and span lengths were determined based on the field investigation conducted by Hungerford (2004). In that investigation, typical span lengths of continuous steel girder bridges ranged from 50 ft to 60 ft. Since the parametric study involved simply supported beams, it was desired to use simply supported spans

equal in length to the approximate distance between the points of inflection of those continuous girders. For end spans of multi-span continuous bridges, the distance between points of inflection is about 75 percent of the span. Relatively low shear connection ratios were selected for the composite beam design because the high fatigue strength of post-installed shear connectors permits the use of significantly fewer shear connectors than conventional welded shear studs for new construction. As shown in the full-scale beam tests, the strength of non-composite beams can be improved significantly even with low shear connection ratios.

From the analysis of composite beams using the finite element program ABAQUS, the maximum strength, stiffness, and deformation capacity were evaluated and the maximum strength and stiffness were compared with the results from current design equations in the AASHTO and AISC provisions. Deformation capacities were compared in terms of an equivalent ductility factor (defined later in this chapter), and that ductility factor was also used to recommend a minimum shear connection ratio for strengthening existing bridge girders using post-installed shear connectors.

To evaluate the effect of oversized holes in the steel beam flange, six more composite beams were modeled in this study. In the single shear connector tests and full-scale beam tests, 15/16-in. diameter holes were drilled through the steel beam flange to install 7/8-in. diameter shear connectors. Field engineers in TxDOT recommended the use of 1-in. diameter holes in the steel beam flange for the HASAA connector to facilitate the installation process. Although the gap between the oversized hole and the shear connector was filled with adhesive, slip without load may occur due to poor workmanship or weathering of the adhesive. Shear connectors in the six composite beam models were designed to slip without load until the gap closed and then to follow the load-slip curves proposed by Ollgaard et al. (1971). As shown in Figure 5.1, the shear connectors were assumed to fail at 0.23-in. slip after the initial gap closed. For the DBLNB and HTFGB connectors, recall that 7/8-in. diameter holes in the steel beam flange are recommended for 7/8-in. diameter shear connectors, so that significant slip without load can be prevented.

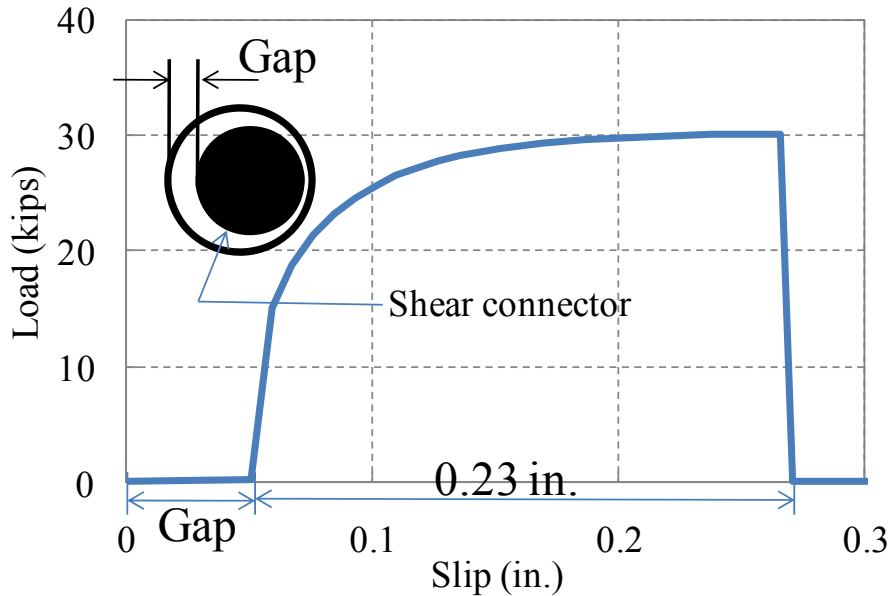


Figure 5.1: Idealized load-slip behavior of a shear connector with an initial gap

In the parametric studies, slab details and material properties were kept constant. The concrete slab, 7-in. deep and 84-in. wide, had the same details as the full-scale beam test specimens discussed in the previous chapter. The yield stress of the steel beam and the ultimate strength of the concrete were taken as 50 ksi and 3,000 psi, respectively. Assuming 7/8-in. diameter shear connectors with 125-ksi ultimate strength and the threads in the shear plane, the shear connectors had an ultimate strength of 30.1 kips. All shear connectors were installed near the support with 12-in. spacing. To impose higher slip demands on the post-installed shear connectors, self-weight of the steel beam and concrete slab was not considered.

5.3 RESULTS OF PARAMETRIC STUDY

5.3.1 Composite Beams with Different Geometries

Load-deflection relations of composite beams with W36x160 beam and 50-ft long span are shown in Figure 5.2. As expected, the strength, stiffness, and deformation capacity of the composite beams increased with increasing shear connection ratio. Load-deflection curves of all of the sixty composite beams modeled in ABAQUS are shown in Appendix A. Failure of the composite beams was taken as coinciding with the failure of the first shear connector. For some composite beams, the solution did not converge before the first shear connector failure. These composite beams were used only for evaluation of strength and stiffness, not for evaluation of deformation capacity. The maximum strength and initial stiffness of the composite beams from the finite element method are listed in Table 5.1 to Table 5.3 along with the values computed from current design provisions (AASHTO 2007, AISC 2005), as discussed in the following section.

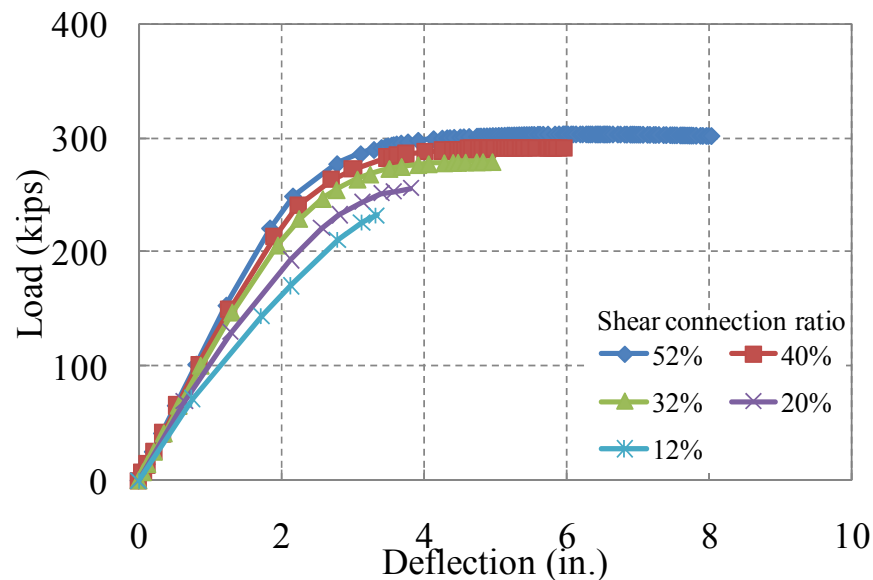


Figure 5.2: Load-deflection relations of composite beams (W36x160 beam, 50-ft span)

Table 5.1: Analysis results for composite beams with 30-ft span

Section	Shear connection ratio (%)	Number of connectors in a shear span	Max. load (kips)		Initial stiffness (kips/in.)		Ductility
			AASHTO AISC	ABAQUS	AISC	ABAQUS	
W27x94	47	22	244	252	217	213	7.6
	39	18	237	245	206	208	5.2
	30	14	226	235	193	199	4.2
	22	10	210	222	178	187	3.3
	13	6	191	201	160	169	2.8
W30x99	50	24	280	292	266	266	*
	41	20	272	285	253	261	4.7
	29	14	252	266	231	246	3.6
	21	10	235	248	214	230	3.0
	12	6	213	226	193	209	2.3
W33x130	48	24	385	398	405	388	*
	40	20	373	388	387	381	4.0
	32	16	357	373	367	369	3.4
	20	10	327	342	332	340	2.7
	12	6	302	317	303	311	2.1
W36x160	52	26	495	513	567	517	*
	40	20	473	491	533	507	*
	32	16	454	473	507	492	2.8
	20	10	420	439	462	455	2.4
	12	6	393	413	423	418	2.2

*: Convergence was not achieved before shear connector failed.

Table 5.2: Analysis results of composite beams with 40-ft long span

Section	Shear connection ratio (%)	Number of connectors in a shear span	Max. load (kips)		Initial stiffness (kips/in.)		Ductility
			AASHTO AISC	ABAQUS	AISC	ABAQUS	
W27x94	47	22	183	190	92	98	*
	39	18	178	185	87	94	4.9
	30	14	169	178	82	89	3.2
	22	10	158	166	75	84	2.5
	13	6	143	151	68	74	2.1
W30x99	50	24	210	216	112	119	*
	41	20	204	212	107	116	4.5
	29	14	189	197	98	108	3.0
	21	10	176	184	90	101	2.5
	12	6	160	168	81	93	2.2
W33x130	48	24	289	297	171	176	*
	40	20	279	287	163	171	3.4
	32	16	268	276	155	165	2.8
	20	10	245	253	140	152	2.2
	12	6	227	235	128	140	1.9
W36x160	52	26	371	386	239	238	3.9
	40	20	355	366	225	230	2.6
	32	16	341	352	214	222	2.5
	20	10	315	325	195	206	1.9
	12	6	295	300	179	190	1.6

*: Convergence was not achieved before shear connector failed.

Table 5.3: Analysis results of composite beams with 50-ft long span

Section	Shear connection ratio (%)	Number of connectors in a shear span	Max. load (kips)		Initial stiffness (kips/in.)		Ductility
			AASHTO AISC	ABAQUS	AISC	ABAQUS	
W27x94	47	22	147	151	47	50	*
	39	18	142	147	44	48	4.5
	30	14	135	141	42	46	2.9
	22	10	126	132	39	44	2.4
	13	6	115	117	35	41	1.7
W30x99	50	24	168	172	57	62	*
	41	20	163	168	55	60	4.4
	29	14	151	157	50	56	2.6
	21	10	141	146	46	53	2.2
	12	6	128	132	42	49	1.9
W33x130	48	24	231	235	87	92	*
	40	20	224	228	84	89	2.8
	32	16	214	219	79	86	2.1
	20	10	196	199	72	80	1.7
	12	6	182	180	65	74	**
W36x160	52	26	297	304	122	126	3.4
	40	20	284	291	115	121	2.5
	32	16	272	279	110	117	2.1
	20	10	252	256	100	108	1.6
	12	6	236	232	91	97	**

*: Convergence was not achieved before shear connector failed.

** : Max. load was less than simple plastic analysis result.

5.3.1.1 Comparisons with Current Design Provisions (Strength and Stiffness)

The post-installed shear connection methods introduced in this dissertation are unconventional, and the shear connectors are recommended to be installed only near the supports or zero-moment regions. This is in contrast to conventional welded shear studs which are typically installed along the entire span of composite beams. Therefore, it is necessary to determine whether the equations used to calculate the maximum strength and initial stiffness of composite beams in the current design provisions (AISC 2005, AASHTO 2007) can also be used to determine the maximum strength and initial stiffness of composite beams retrofitted with post-installed shear connectors.

For this purpose, the maximum load-carrying capacity of the composite beams modeled in ABAQUS was compared with the results from simple plastic analysis, as described in Section 2.3.2.2. Figure 5.3 shows the maximum strength of the sixty composite beams from ABAQUS along with the maximum strength from simple plastic analysis. The straight line at 45 degrees indicates complete agreement between the two sets of predicted capacities. Analysis results lying below the straight line correspond to cases in which the strength computed from simple plastic analysis is less than the strength predicted by the ABAQUS model, that is where simple plastic analysis provides a conservative estimate of strength. As shown in Figure 5.3, the strength predicted by simple plastic analysis agreed very well with the strength predicted by ABAQUS, for all of the analytical models with various span lengths, beam depths, and shear connection ratios. In cases where there were discrepancies, simple plastic analysis gave conservative results, except for two composite beams. The composite beams with W33x130 and W36x160 beam sections, 50-ft span length, and 10-percent shear connection ratio did not reach their maximum strengths based on the current design provisions. Those specimens did, however, reach over 98 percent of the maximum strength from simple plastic analysis.

Stiffness of the composite beams retrofitted with post-installed shear connectors in the elastic range, as predicted by ABAQUS, were also compared with stiffness

predictions based on the *AISC Specification*. As described in Section 2.3.2.2, the *AISC Specification* provides an equation for the effective moment of inertia for a partially composite beam. As shown in Figure 5.4, the ABAQUS-predicted stiffnesses of most of the composite beams were generally within 10 percent or less of the values given by the AISC equation. The ABAQUS-predicted stiffness values were usually greater than the AISC values. Because the ABAQUS-predicted stiffnesses were based on analytical models calibrated against the full-scale tests described here, they are presumably more accurate than the AISC values. This implies that using the AISC equations, which give slightly smaller stiffnesses and hence greater deflections, would be conservative for the composite beams studied here. Some specimens with short spans, large beam depths, and high shear connection ratios showed slightly lower stiffness in ABAQUS than that predicted by the equation in the *AISC Specification*.

The post-installed shear connectors investigated in this study are intended for use in strengthening existing non-composite steel bridge girders. Due to the high fatigue strengths of these post-installed shear connectors, partially composite design is possible. Further, because of the high cost of post-installing shear connectors, there is a strong incentive to minimize the number of connectors. For this reason, the shear connection ratios used in this study are lower than the ratios typically used for new construction in building applications (AISC 2005). In the AISC Specification, Equations 2.17 and 2.18 are not recommended for use with composite beams with a shear-connection ratio less than 25 percent. As shown in Figure 5.3 and Figure 5.4, however, even with very low shear connection ratio, the strength and stiffness of composite beams retrofitted with post-installed shear connectors can be determined quite accurately by the equations widely used for new constructions in the AISC and AASHTO provisions.

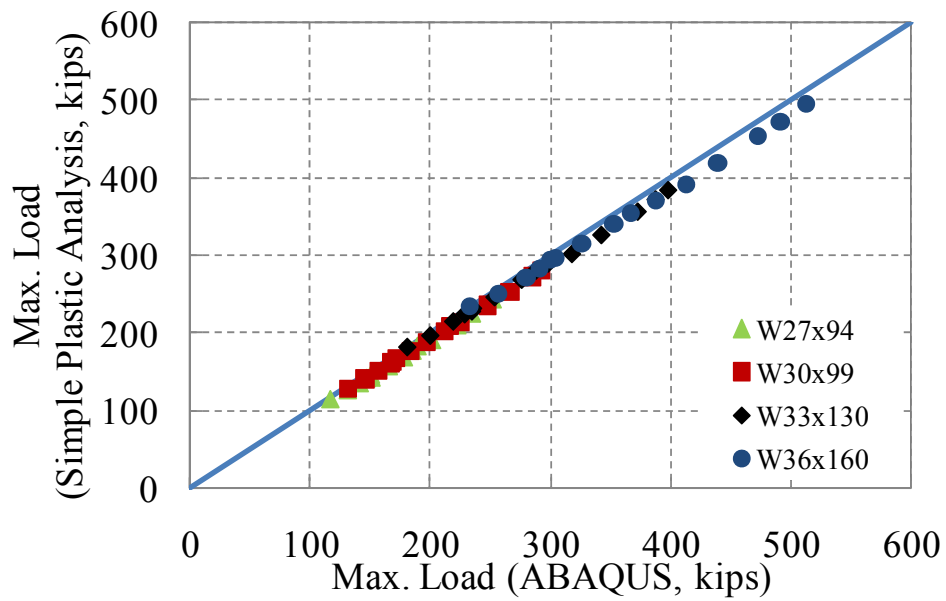


Figure 5.3: Comparison of strength of composite beams (ABAQUS versus simple plastic analysis)

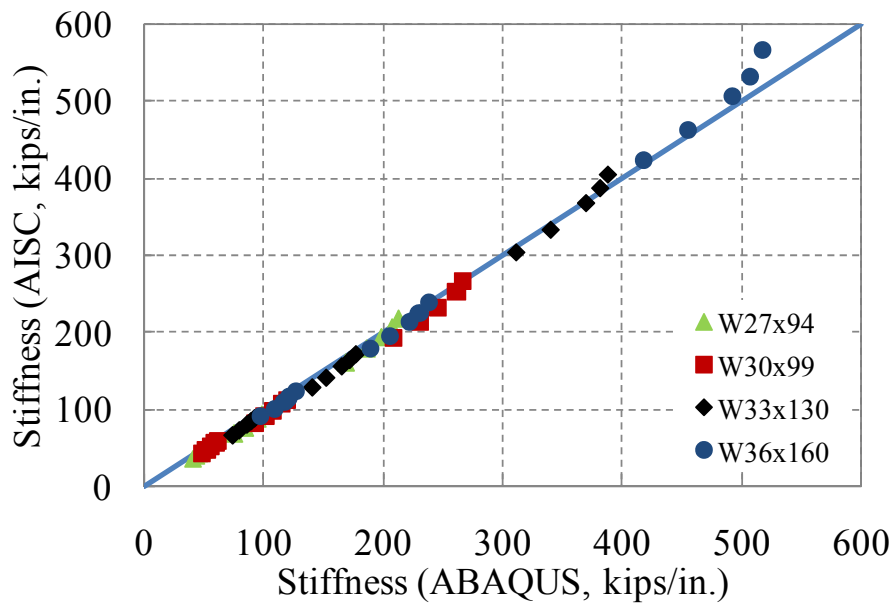


Figure 5.4: Comparison of stiffness of composite beams (ABAQUS versus simple plastic analysis)

5.3.1.2 Deformation Capacity of Composite Beams with Post-Installed Shear Connectors

Current AASHTO and AISC design provisions have no specific requirements for inelastic deformation capacity of composite beams. These provisions provide quantitative design criteria only for stiffness and strength of composite beams. Although not specifically addressed by AASHTO or AISC, some degree of inelastic deformation capacity, i.e. ductility, is desirable. Ductility enhances safety by providing warning of impending failure, and by allowing redistribution of loads to adjacent beams. The load-deformation response curves of the sixty composite beams modeled using the finite element program ABAQUS provides the opportunity to assess the ductility of these beams. From the response curves, the ductility of the beams was evaluated using a ductility factor, μ , defined in terms of an equivalent elasto-plastic load-deflection curve, as shown in Figure 5.5. The analytically predicted load-deflection curve of a composite beam was idealized by two straight lines representing the initial stiffness calculated using ABAQUS and the maximum strength calculated using simple plastic analysis. The intersection of those two lines was taken as an equivalent yield displacement, Δ_y . The maximum deflection, Δ_{\max} , was defined as the deflection at which the first shear connector failed. The corresponding ductility factor was then calculated as Δ_{\max} / Δ_y .

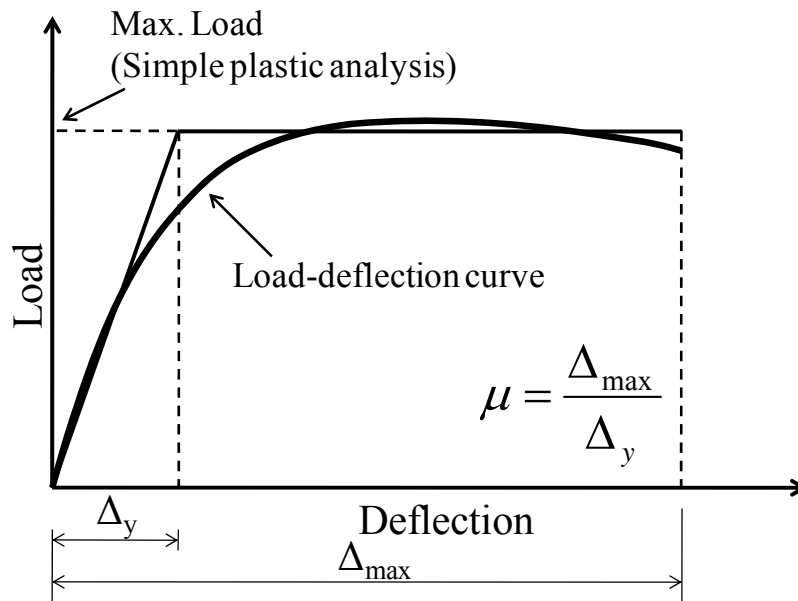


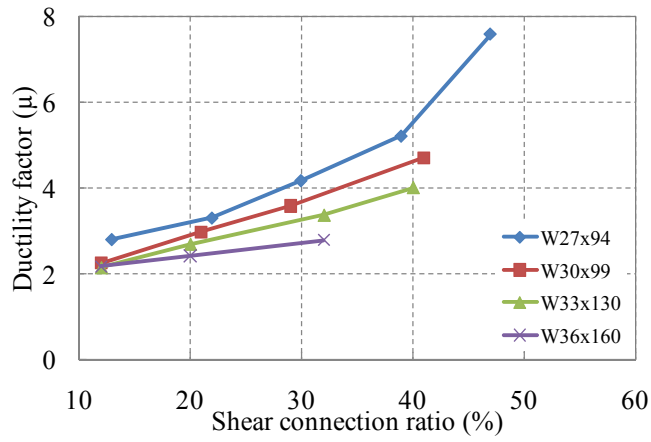
Figure 5.5: Definition of ductility factor

The calculated ductility factor for each composite beam is plotted in Figure 5.6, and listed in Table 5.1 through Table 5.3. Composite beams for which the analyses stopped before shear connector failure are not plotted in the figure, nor are composite beams which did not reach the maximum load calculated from simple plastic analysis. As shown in Figure 5.6, the ductility factor of composite beams increases with increasing shear connection ratio. It is also obvious that deep steel beam sections lower the ductility of composite beams. Equations 2.22 and 2.23 indicate that increased span length increases the slip demand at the steel-concrete interface at M_{\max} . As expected, the increased slip demand at the steel-concrete interface causes composite beams with long spans to have lower ductility factors than composite beams with short spans.

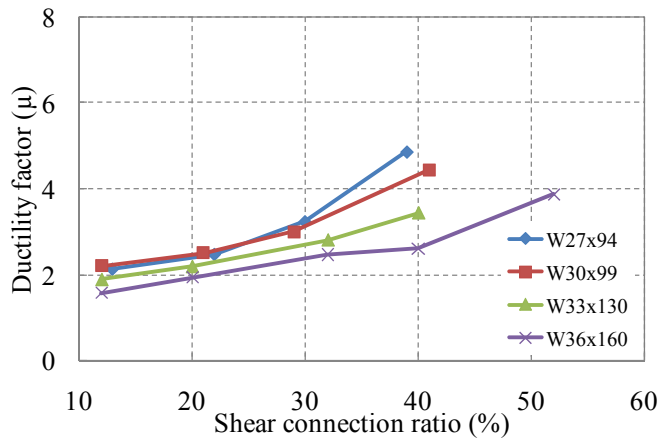
In general, the greater the ductility factor for a particular beam, the greater the amount of inelastic redistribution of applied loads. For this parametric study, it was judged useful to select a minimum acceptable ductility factor. Examination of Figure 4.34 and Figure 4.62 shows that all full-scale composite beam specimens in this study had a ductility factor of at least 2.0. All specimens showed substantial deflection, over 4 in.,

before any shear connector failed. Therefore, that value could be considered a lower (conservative) limit for composite beams retrofitted with post-installed shear connectors. For this reason, a ductility factor of 2 was taken as the minimum allowable ductility factor for this parametric study.

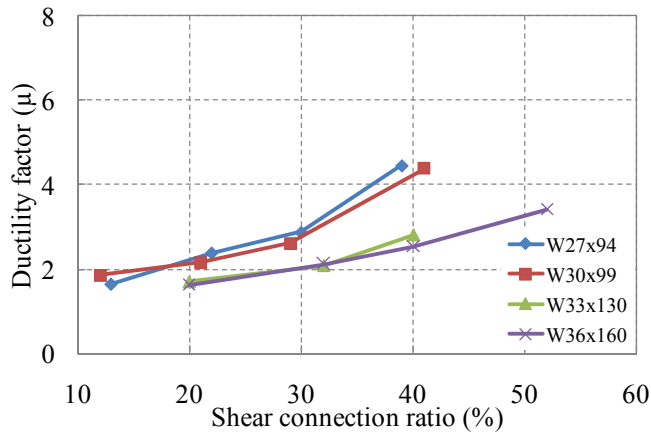
Most composite beams investigated in this parametric study had ductility factors higher than 2. Some composite beams with low shear connection ratios, deep beam sections, and long spans had the ductility factors less than 2 (Figure 5.6), however. In this study a minimum shear connection ratio 30 percent is recommended for strengthening of existing non-composite steel bridge girders using post-installed shear connectors. All composite beams modeled in ABAQUS with shear connection ratios exceeding 30 percent showed ductility factors higher than 2. In these parametric studies, as in the full-scale composite beam Specimen HASAA-30BS1 in Chapter 4, the post-installed shear connectors were concentrated near the support to reduce slip at the steel-concrete interface.



(a) *Span: 30 ft*



(b) *Span: 40 ft*



(c) *Span: 50 ft*

Figure 5.6: Ductility of composite beams

5.3.2 Effect of Oversized Holes

The effect of oversized holes in the steel beam flange was evaluated for composite beams having the same geometry as the full-scale test specimens described in Chapter 4. Figure 5.7 shows the ABAQUS load-deflection curves for six composite beams with 38-ft spans, along with the analysis results for an otherwise identical non-composite beam. The composite beams addressed in the figure had shear connection ratios of 30 percent, corresponding to 16 shear connectors in a shear span. Composite beam Model HASAA-30BS2 in Figure 5.7 had no gap between the holes in the steel beam flange and the connectors. That model showed the highest stiffness, strength, and ductility factor of all the composite beams in Figure 5.7. In the other composite beam models, slip occurred in the shear connectors without any load, using the load-slip relationship shown in Figure 5.1.

Model HASAA-30BS3 was designed so that the two shear connectors near the support would resist load without any gap, and the other 14 shear connectors in the same shear span would have the maximum gap of 0.125 in., assumed to be unfilled with adhesive, so that these shear connectors would not resist load until 0.125-in. slip was reached. This model was developed because shear connectors near a support have the maximum slip demand, and generally govern the deformation capacity of the composite beam. Because the other shear connectors would not begin to resist load until experiencing a slip of 0.125 in., very low initial stiffness was expected for this composite beam. It did in fact have lower initial stiffness and lower deformation capacity than Model HASAA-30BS2. It still showed higher strength than the result from simple plastic analysis, however, and its ductility factor was still higher than 2.

The other four analytical models, Models HASAA-30BS4 to HASAA-30BS7, had shear connectors with initial gaps that were assumed to vary randomly. For each composite beam, 32 random numbers between 0 and 1 were generated, and those numbers were multiplied by 0.125 in. which is the maximum slip that shear connectors can experience without any load. This method was considered to be a realistic reflection

of the gaps associated with shear connectors in real construction. The four composite beam models with arbitrary shear-connector gaps at oversized holes in the beam flange differed little with each other with respect to initial stiffness and maximum strength. As shown in Table 5.4, initial stiffness of these composite beams is lower than that of Model HASAA30BS2 which had no gaps. Their maximum strength, however, differs little from that of Model HASAA-30BS2. These four composite beam models also show ductility factors higher than 2.

From the finite element analysis involving different shear connector locations in oversized holes, one can conclude that oversized holes in the steel beam flange do not significantly affect the behavior of composite beams retrofitted with post-installed shear connectors. If the gaps happen to be filled during construction (as was the case with Specimens HASAA-30BS and HASAA-30BS1 in Chapter 4), stiffness, strength and ductility are increased.

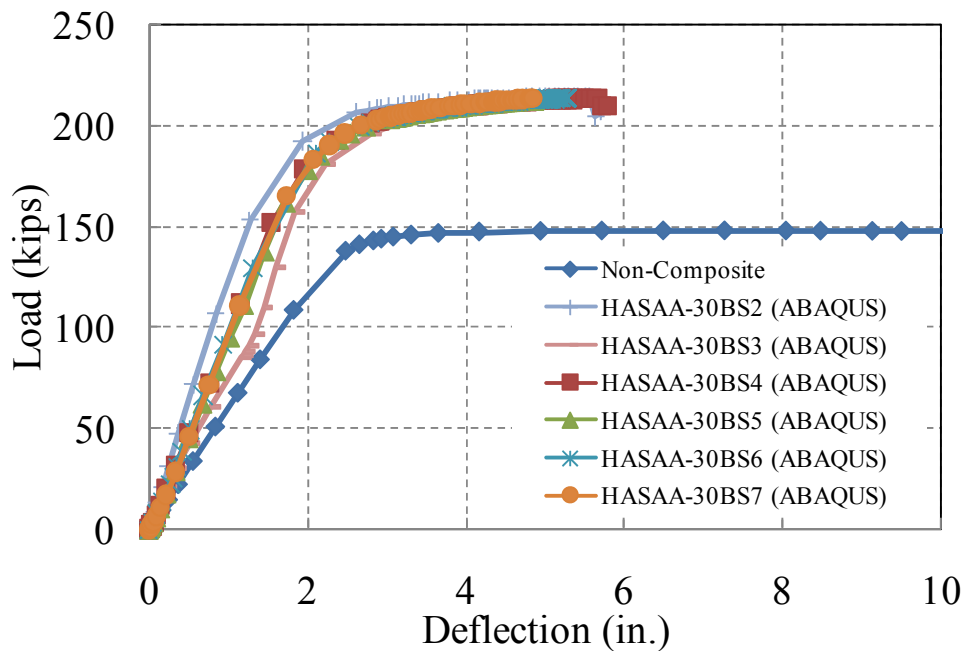


Figure 5.7: Load-deflection graphs considering the effects of oversized holes

Table 5.4: Analysis results of composite beams with oversized holes in the beam flange

Model	Max. load (kips)		Ductility factor
	AISC, AASHTO	ABAQUS	
HASAA-30BS2	205	214	3.3
HASAA-30BS3	205	211	2.3
HASAA-30BS4	205	213	2.8
HASAA-30BS5	205	212	2.2
HASAA-30BS6	205	214	2.5
HASAA-30BS7	205	213	2.3

5.4 SUMMARY

In this chapter, results are described for parametric studies conducted to supplement the full-scale beam test results obtained in this study, and to investigate the behavior of composite beams retrofitted with post-installed shear connectors with various beam depths, span lengths, and shear connection ratios. The effect of oversized holes in the steel beam flange was also investigated.

From the analytical study of 60 composite beam models, it was concluded that current design equations (AASHTO 2007, AISC 2005) accurately predict the maximum strength and elastic stiffness of partially composite beams with post-installed shear connectors concentrated near the supports or the zero-moment regions.

The deformation capacity of the composite beams was also evaluated using a ductility factor, defined in terms of an elasto-plastic approximation to calculated load-deflection curves. Based on previous experimental results, a minimum acceptable value

of 2 was suggested for that ductility. Based on the finite element analysis results, a minimum shear connection ratio of 30 percent is recommended for composite beams retrofitted with post-installed shear connectors. Because the behavior of real, multi-girder bridges is more complex than that of the single-girder bridges addressed by this parametric study, more research should be conducted on the relationship between ductility demands and available ductility for bridges made of composite beams with partial composite design.

The parametric study shows that the gap between the oversized holes in the steel beam flange and the shear connector does not affect the system behavior of composite beams significantly. It is better to eliminate such gaps if possible, however, because doing so increases strength, stiffness and ductility. In this study, the gap between the hole in the beam flange and the shear connector was minimized by filling the gap with adhesive for the HASAA connector as in the full-scale beam tests. For the DBLNB and HTFGB connectors, it is recommended to drill matched holes to minimize slip without resisting load.

CHAPTER 6

Strengthening an Existing Bridge with Post-Installed Shear Connectors – Case Study

6.1 INTRODUCTION

From the single shear connector tests, full-scale beam tests, and parametric finite element studies presented in the previous chapters, it appears that post-installed shear connectors can be an effective means for strengthening existing non-composite bridge girders. To further evaluate the feasibility of this retrofitting technique, a detailed case study was undertaken on an actual bridge located near San Antonio, Texas. For this case study, a complete design was undertaken for strengthening the bridge using post-installed shear connectors. The case study evaluated the number of shear connectors needed to achieve various target levels of strength increase considering both static and fatigue design checks on the connectors. The case study was also intended to identify potential difficulties that may arise in the design process, and to suggest possible solutions for these difficulties. This case study was undertaken with the advice and assistance of Texas Department of Transportation engineers to select the case study bridge, to provide drawings and other data on the bridge, and to identify target load rating levels for the retrofitted bridge.

6.2 DESCRIPTION OF THE CASE STUDY BRIDGE

The specific bridge chosen for this case study is located on a two-lane rural road near the city of Hondo, Texas, and crosses a small creek. Hondo is located approximately 40 miles west of San Antonio. For purposes of this case study, the bridge will be referred to as the Hondo Bridge. Figure 6.1 shows several photographs of the bridge. The bridge was built in 1950 and the measured Average Daily Traffic (ADT) in 2006 was 900

vehicles. The bridge consists of three simple spans, and the superstructure is constructed with a non-composite concrete floor slab over rolled steel wide-flange girders. The current load ratings for this bridge were sufficiently low that load posting of the bridge may be needed. Consequently, TxDOT was interested in improving the load rating to maintain the bridge in continued service, without the need to limit vehicle weights through load posting. Because the existing concrete deck and steel girders were still in good condition, and because all spans were simply supported, this bridge was chosen as a case study for strengthening with post-installed shear connectors.

The Hondo Bridge is a steel-girder bridge with three spans, each is about 40-ft long, with simply supported girders. The bridge is skewed at an angle of 30 degrees and consists of four girders in the transverse direction (Figure 6.2). The girders are connected by periodic cross-frames. Figure 6.3 and Figure 6.4 show a typical section through the girders and slab. The steel sections used for the bridge are W26x85 and the concrete slab is 6.25-in. deep. The W26x85 section is no longer produced and does not appear in modern steel manuals. The cross-section dimensions are available in older steel manuals, and are shown in Figure 6.4.

The girders are located at a 7-ft spacing. The concrete slab was cast on top of the slab without any shear connectors at the steel-concrete interface, meaning the superstructure was designed non-compositely. No. 4 reinforcing bars were placed longitudinally at an 18-in. spacing. In the transverse direction, No.6 reinforcing bars were placed at a 9-in. spacing.

The material properties of the concrete slab and the steel girders were not reported in the drawing provided by TxDOT. The *AASHTO Manual for Evaluation* provides the yield stress of the steel girders and the ultimate strength of the concrete slab based on the year built. The suggested yield stress of the steel girders and the ultimate strength of the concrete slab for load-rating were 33 ksi and 2.5 ksi, respectively (AASHTO 2003).



Figure 6.1: The Hondo case-study bridge

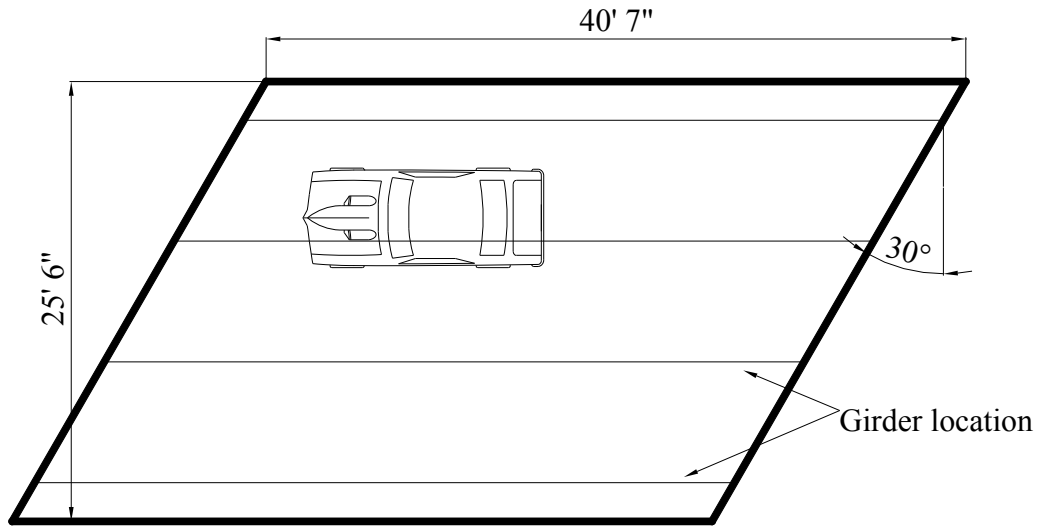


Figure 6.2: Top view of a typical span of the Hondo Bridge

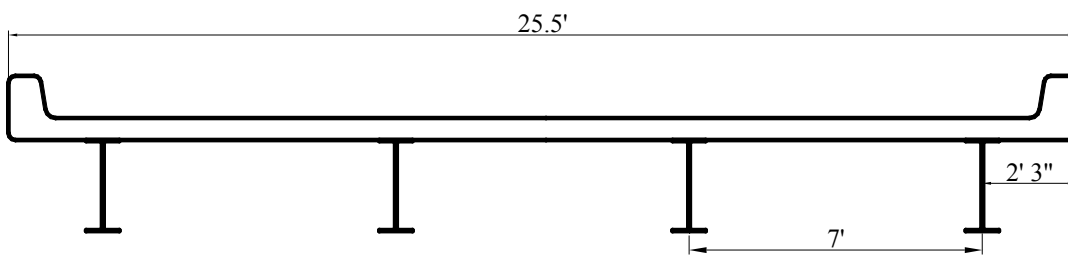


Figure 6.3: Section details for the Hondo Bridge

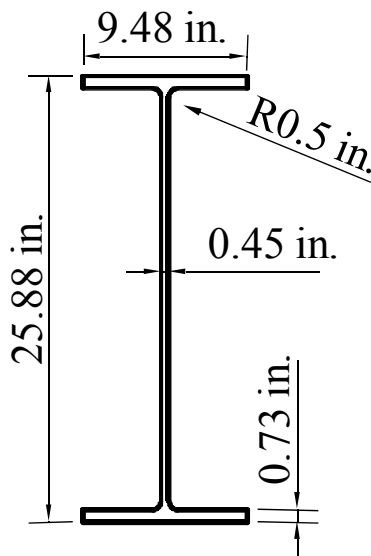


Figure 6.4: Cross-section dimensions of W26x85 bridge girder

6.3 AASHTO LOAD-RATING FOR EXISTING NON-COMPOSITE BRIDGE GIRDERS

6.3.1 General AASHTO Load Rating Approach

The Hondo Bridge was load-rated, using an HS 20 truck load, to assess the need for strengthening. In addition to the truck load, the *AASHTO Manual for Evaluation* requires evaluation of the bridge with the Standard AASHTO HS lane load. However, the truck load controlled in all cases for this relatively short span bridge. Only the interior girders were load-rated since the interior girders were more severely loaded than the exterior girders.

The Hondo Bridge was load-rated using the load factor method in the *AASHTO Manual for Evaluation*. As required by that method, the bridge was evaluated for both strength and serviceability criteria. As further required by that method, ratings were computed at both the Inventory and the Operating levels. The rating results shown in Table 6.1 are based on girder moments and stresses computed using conventional load

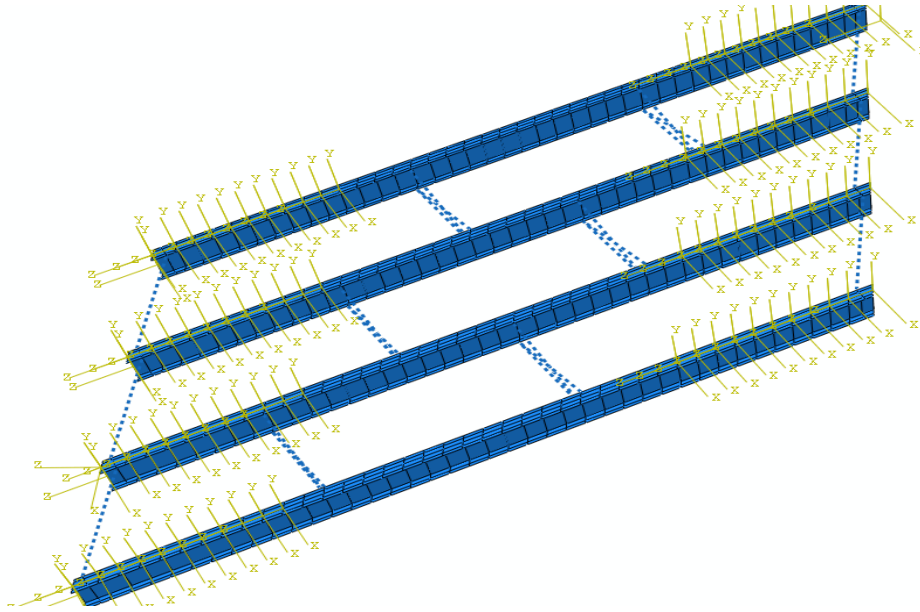
rating calculation methods. Details of these calculations are presented in Appendix B. The Operating rating level is less than HS 20, indicating that the bridge is required to be posted for load.

Table 6.1: Load rating of Hondo bridge (non-composite bridge girders)

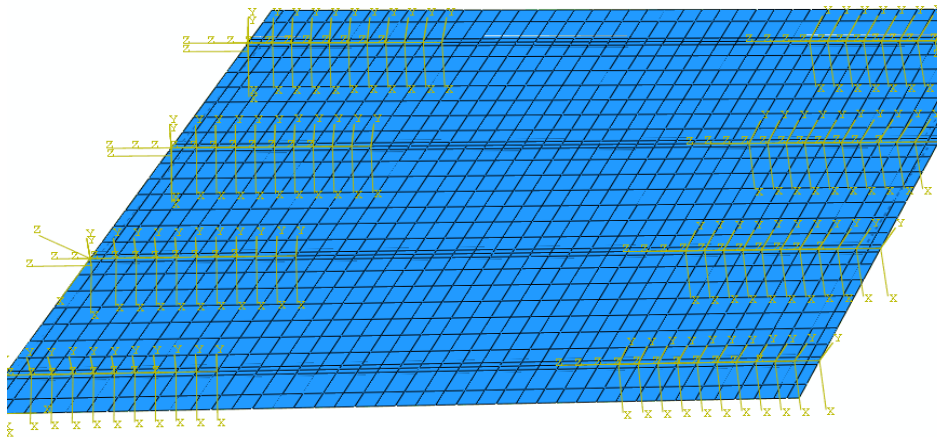
Rating level		Rating results
Inventory rating	Strength	HS 12.0
	Serviceability	HS 10.6 (Controls)
Operating rating	Strength	HS 20.0
	Serviceability	HS 17.6 (Controls)

6.3.2 Load Rating based on Finite Element Analysis

Previous research (Bowen and Engelhardt 2003) has shown that conventional load rating calculations often overestimate girder moments and stresses. A more accurate assessment of bridge structural response can be obtained by developing detailed finite element models of the bridge floor system. The more accurate analysis provided by finite element models can result in higher load ratings. In the case of the Hondo Bridge, a finite element model was developed to investigate if a significantly improved load rating is possible through more accurate prediction of structural response. The superstructure of the bridge was modeled using ABAQUS. The modeling techniques were similar to those used to model the full-scale test specimens in Chapter 4. Figure 6.5(a) shows the ABAQUS model of four girders in a span without the slab. The girders were modeled using ABAQUS shell elements and the diaphragms and the cross-frames connecting the girders were modeled using the ABAQUS connector elements. Figure 6.5(b) shows the concrete slab, which was modeled using shell elements.



(a) Steel girders, cross-frames and diaphragms



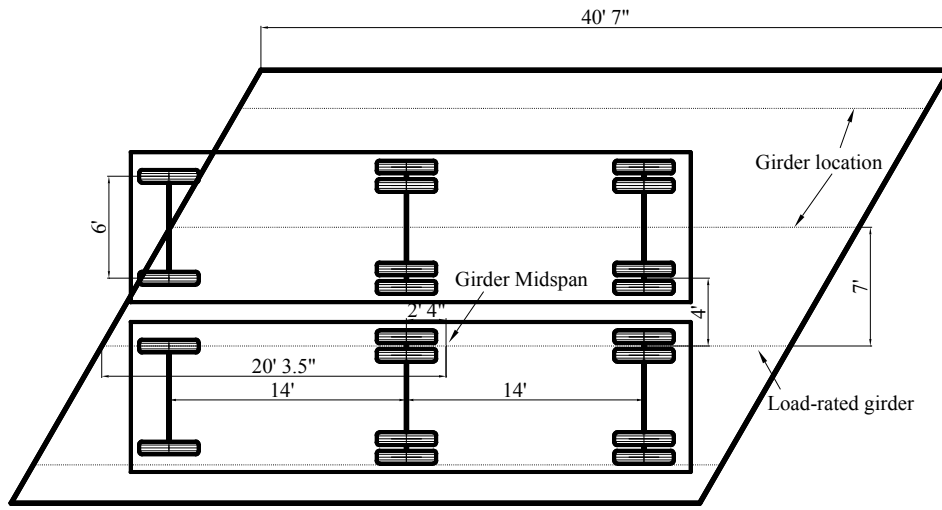
(b) Concrete slab

Figure 6.5: ABAQUS model of the Hondo Bridge

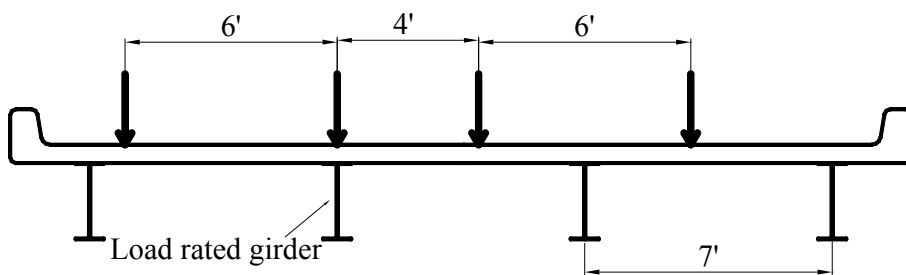
For purposes of load rating, the transverse locations of the design trucks in the ABAQUS model were determined by the lever rule. In the transverse direction, the two design trucks were placed at a 4-ft spacing. One wheel line was placed on top of the girder to be load-rated, as shown in Figure 6.6. In the longitudinal direction, the second wheel of the design truck was placed 28 in. away from the midspan of the load-rated girder. For a simply supported beam, to produce the maximum moment in the girder, the wheel loads are placed so that the centerline of the span bisects the line between the centroid of the wheel loads and the point where the central wheel load is applied (Taly 1998). To account for the effect of the dead load, the yield stress was reduced in proportion to the dead load. The maximum moment due to dead load was 146.7 ft-kips as shown in Appendix B. The load factor A_1 for load-rating is 1.3 and the plastic section modulus of the girder is 245 in.³. In ABAQUS, the yield stress of the steel girder was reduced to $33 - 1.3 \times 146.7 \times 12 / 245 = 23.7 \text{ksi}$. This method was also used to model the full-scale beam specimens in Chapter 4 and the model showed good agreement with the test results.

From the ABAQUS analysis, load-deflection plots of the Hondo Bridge before retrofitting are shown in Figure 6.7. The deflection was measured under the center wheel of the load-rated girder. The load factor ($A_2 \cdot (1 + I) \cdot RF$) on the vertical axis is the ratio of the applied load to the standard HS 20 design truck load. The load factor 1 means the bridge is loaded with the two standard HS 20 design trucks as shown in Figure 6.6(a). The ABAQUS analysis was stopped after widespread cracking in the elements comprising the slab, beyond which point the solution could not converge. This point was taken as the analytical equivalent of failure. Longitudinal stresses predicted by ABAQUS are shown in Figure 6.8. As expected, the neutral axis of each girder is located near mid-depth. The maximum load factor is 2.64. The load factor A_2 is 2.17 for the Inventory rating level and 1.3 for the Operating rating level. The impact factor I is 0.3 for the bridge. Based on the ABAQUS analysis, the load rating results for the AASHTO strength

criteria are therefore $2.64/2.17/1.3 \times (HS20) = HS18.7$ for the Inventory rating level and $2.64/1.3/1.3 \times (HS20) = HS31.3$ for the Operating rating level.



(a) Top view



(b) Section view

Figure 6.6: Standard design truck locations for load rating using ABAQUS

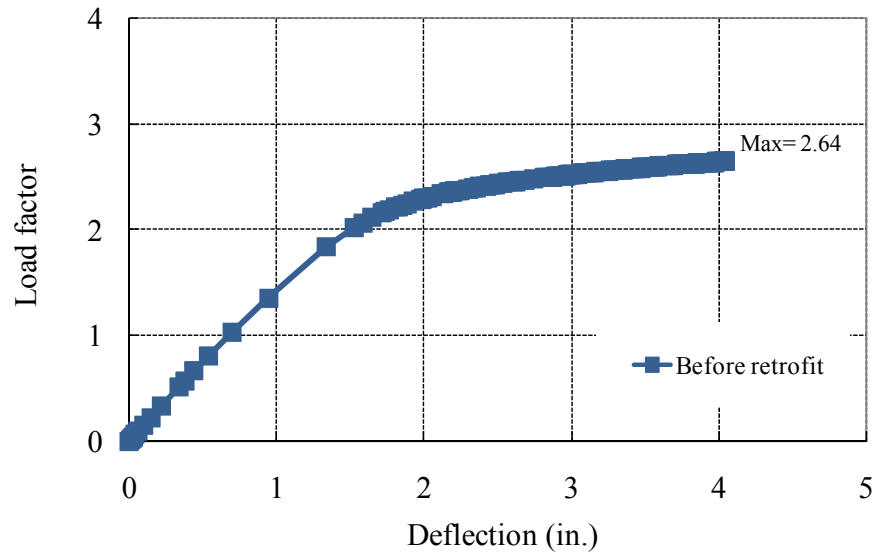


Figure 6.7: Load-deflection relations for the Hondo Bridge (before retrofitting)

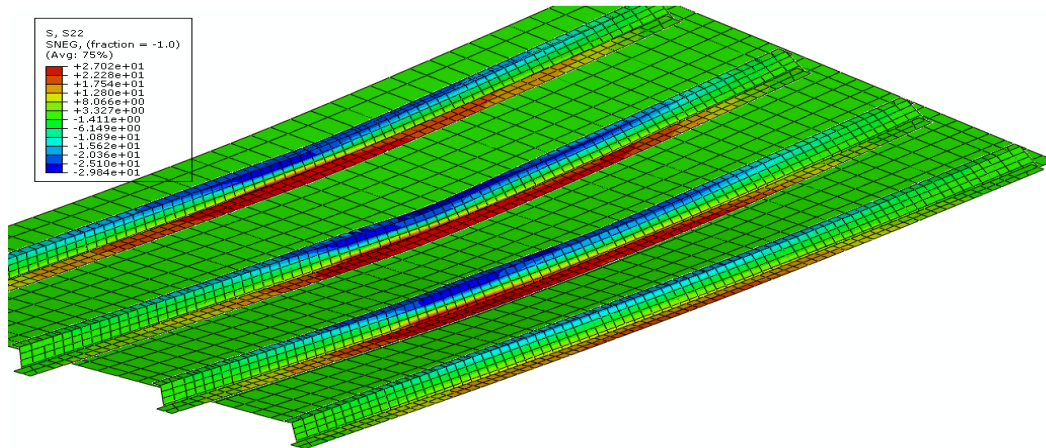


Figure 6.8: Longitudinal stress distribution of the Hondo Bridge (non-composite)

Serviceability of the bridge was also checked for overload vehicles. The *AASHTO Standard Specifications* require that the maximum stress in the beam flange not exceed $0.8F_y$ for non-composite beams. Since the dead load was resisted only by the steel girders, the four steel girders without the concrete slab were modeled in ABAQUS and distributed loads were applied on the steel beams representing the dead loads of the steel girders and the concrete slab. The maximum stress due to the dead loads was 8.76 ksi. Figure 6.9 shows the longitudinal stress distribution due to the dead loads in the girders. Then the live load, including the impact factor, was applied on the whole bridge model. The maximum stress due to the live load was 18.10 ksi and the structure remained in the elastic range. The rating factor for the serviceability criterion for the Operating rating level can be determined as shown below.

$$\frac{C - D}{L(1 + I)} = \frac{0.8 \times 33 - 8.76}{18.10} = 0.97 \quad (6.1)$$

where, C = the capacity of the member

D = the effect of dead load

L = the effect of live load

I = the impact factor for live load

With the overload $1.67L(1 + I)$ for the Inventory rating level, the sum of the stresses due to dead load and the live load was over 33 ksi, which is not acceptable. Therefore, the rating factor for the Inventory level was determined by dividing Eq. 6.1 by 1.67, which resulted in 0.58. The rating results for the serviceability criteria were HS 11.7 and HS 19.5 for the Inventory level and the Operating level, respectively. Table 6.2 compares the rating results from the general AASHTO approach with the finite element method. It is worth noting that the serviceability criterion controls the rating results. As indicated by the data in Table 6.2, by going from the standard AASHTO calculation approach to the finite element analysis, the Inventory rating increased from HS 10.6 to HS 11.7, and the Operating rating increased from HS 17.6 to HS 19.5. Thus, both the

Inventory and Operating ratings increased by about 10 percent by using finite element analysis. However, even with the improved load ratings derived by the finite element analysis, the Operating rating is still below HS 20, and some strengthening measures are still needed to avoid load posting the bridge.

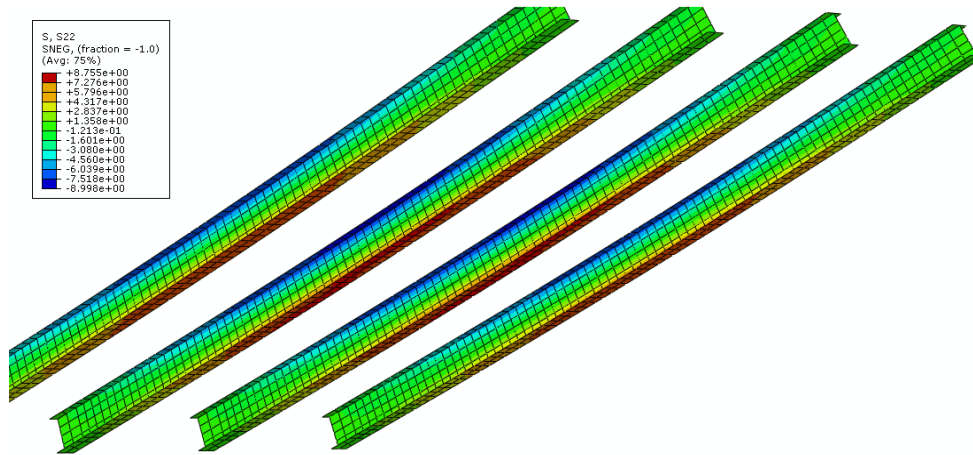


Figure 6.9: Longitudinal stress distribution due to dead load

Table 6.2: Load rating results before retrofitting

Rating method	Rating level		Rating results
Standard AASHTO approach	Inventory rating	Strength	HS 12.0
		Serviceability	HS 10.6 (Controls)
	Operating rating	Strength	HS 20.0
		Serviceability	HS 17.6 (Controls)
ABAQUS analysis	Inventory rating	Strength	HS 18.7
		Serviceability	HS 11.7 (Controls)
	Operating rating	Strength	HS 31.3
		Serviceability	HS 19.5 (Controls)

6.4 STRENGTHENING THE HONDO BRIDGE BY POST-INSTALLED SHEAR CONNECTORS

6.4.1 General Design Approach

As noted above, according to the general AASHTO load-rating method as well as the ABAQUS analysis, the bridge showed rating results lower than HS 20 even at the Operating rating level. Consequently, an increase in the load rating was desired for this bridge, and a system of post-installed shear connectors was designed to provide an increased load rating. This section describes the procedures used to determine the number and location of post-installed shear connectors required for retrofitting. Based on discussions with TxDOT personnel, the goal of this retrofit was, as a minimum, increase the Operating level rating above HS 20. It was also desired to substantially increase the

Inventory level rating, although there was no specific target for the Inventory level rating, and an HS 20 Inventory level rating was not required.

For purposes of this retrofit design, it is assumed that the post-installed shear connectors are 7/8-in. in diameter and made of high strength steel with a specified ultimate tensile strength F_u of 125 ksi. The ultimate shear strength of the connector is taken as 50 percent of the specified tensile strength, and the effective shear area is taken as 80 percent of the gross area, as recommended in Section 3.5.1. This results in a specified ultimate shear strength for each connector of 30.1 kips. Details of this strength calculation are provided in Appendix B.

Based on simple plastic cross-section analysis, it is possible to determine the moment capacity of a partially composite girder as a function of the shear connection ratio. Figure 6.10 shows the results for this analysis for the Hondo Bridge girders. A maximum 70-percent increase in flexural capacity can be achieved by installing shear connectors for full composite design (shear connection ratio of 1.0). To achieve this fully composite design, 56 shear connectors are required for each girder (28 shear connectors in a shear span). For a preliminary design, it was decided to provide a sufficient number of shear connectors to achieve a 50-percent shear connection ratio, and then determine the resulting increase in the bridge load rating. A 50-percent shear connection ratio requires 28 shear connectors in a bridge girder (14 shear connectors in a shear span), and will result in an approximately 55 percent increase in its flexural capacity. The shear connectors will be installed near the supports at a 12-in. spacing to reduce slip at the steel-concrete interface, and thereby increase the ductility of the retrofitted partially composite bridge girders, as discussed in Chapter 4. The layout and the numbering of the post-installed shear connectors are shown in Figure 6.11.

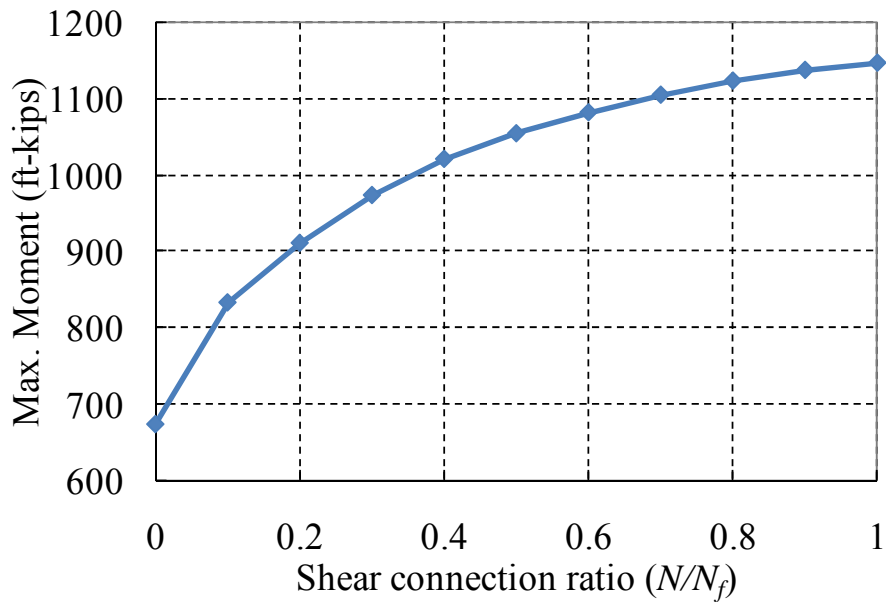


Figure 6.10: Load-carrying capacity vs. shear connection ratio for Hondo Bridge

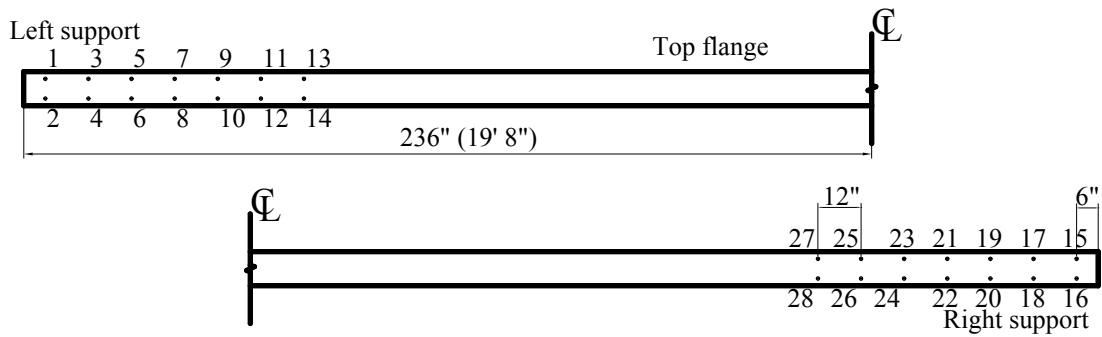


Figure 6.11: shear connector layout for Hondo Bridge

The strengthened bridge girders were then load-rated, using procedures presented step-by-step in Appendix B. The ultimate strength of the retrofitted girder was calculated using simple plastic analysis. The flexural capacity of the girder was increased by 57 percent. Based on the AASHTO strength criterion, the load rating of the strengthened bridge girders was HS 21.5 for the Inventory rating level and HS 35.9 for the Operating rating level.

The AASHTO serviceability criterion was also checked to load-rate the strengthened bridge girders. To evaluate the serviceability of the bridge girders, it is required to calculate the beam flange stress under overload vehicles. The current AASHTO provisions (AASHTO 2002, AASHTO 2005) do not address partially composite design, and so no guidelines are available for checking the stress in the steel beam flange for partially composite beams.

In building construction, partially composite design is very common practice. The commentary of the *AISC Specification for Structural Steel Buildings* (AISC 2005) provides an equation for the effective section modulus, S_{eff} , for partially composite beams. This equation (shown as Equation 2.18 in this dissertation) can be used to compute the maximum stress in the steel beam flange under service load. Using the effective section modulus, the maximum stress in the steel beam flange under overload vehicles was determined for the load rating. For the serviceability criterion, the rating results were HS 17.4 for the Inventory rating level and HS 29.1 for the Operating rating level. For the original non-composite bridge, the corresponding ratings were compares to HS 10.6 and HS 17.6 for the Inventory and Operating level ratings for the existing bridge, based on standard AASHTO load rating techniques.

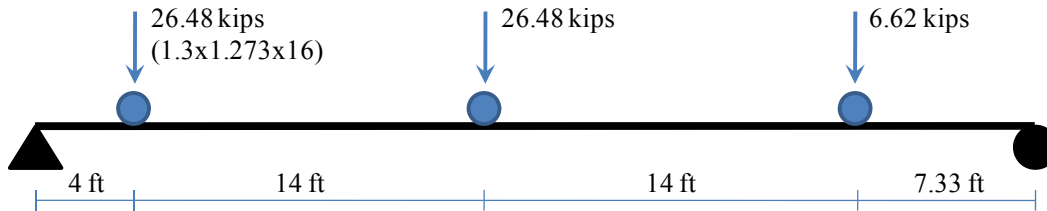
Fatigue strength of the shear connectors was also checked under the standard HS 20 design truck loading. For this case study, TxDOT requested that the shear connectors resist at least 2,000,000 loading cycles. For the DBLNB and HTFGB connectors, the fatigue endurance limit, 35 ksi, as shown in Equation 3.1 was used for the design check of the shear connectors under fatigue loads. For the HASAA connector, the S-N curve

proposed in Equation 3.2 was used, which resulted in an allowable stress range of 23.4 ksi for 2 million cycles.

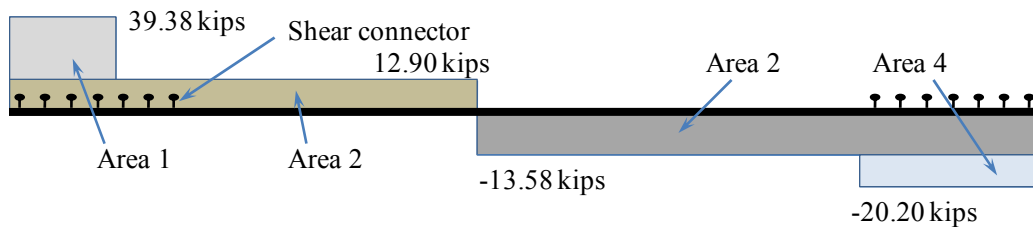
For new bridge construction, shear connectors are typically installed along the full span of the girders. To compute the stress range on the shear connectors for the fatigue design check, the HS 20 truck loads are moved along the bridge span and the shear flow is determined at various locations of the beam. Shear flow is normally calculated based on a transformed fully composite cross-section. From the shear flow, the stress on the shear connector can be computed.

For the retrofitted partially composite bridge girders, the calculation of the shear force on the connectors is not as straightforward as for conventional fully composite bridge girders, for two reasons. First, it is unclear if the conventional calculation of shear flow based on a transformed fully composite section is appropriate for a partially composite girder. Second, the shear connectors are installed only near the supports, resulting in uncertainty regarding the manner in which the shear flow is converted to shear force on the connectors. In order to provide a simple estimate of the shear force on the connectors in the partially composite girders, the shear flow was computed using a fully composite transformed section. Interface shear force at the steel-concrete interface is then computed from shear flow multiplied by the length over which the shear flow acts. The shear flow can be obtained from the shear force diagram using the transformed section. The interface shear force where shear connectors are installed is assumed to be distributed equally among the shear connectors. The interface shear force where shear connectors are not installed is assumed to be equally resisted by the shear connectors in the same shear span. Figure 6.12(a) shows the bridge girder loaded with the HS 20 design wheel load located 4 ft away from the left support. The wheel loads in Figure 6.12(a) include the impact factor and distribution factor. The corresponding shear force diagram is also shown in Figure 6.12(b) along with the shear connector locations. In the left shear span, the interface shear force corresponding to Area 1 is resisted by the 8 shear connectors under the shear force diagram. The shear force corresponding to Area 2 is equally distributed to the 14 shear connectors in the shear span. In the right shear span,

the same design approach is applied. Full details of the procedures used to compute shear force on the connectors and to evaluate the fatigue strength of the connectors in the strengthened partially composite bridge girders are shown in Appendix B.



(a) HS 20 truck wheel locations



(b) Shear force diagram and connector locations

Figure 6.12: Connector force calculation for fatigue loading

The shear force on the connectors computed based on the simplified assumptions described above were compared with the shear force on the connectors predicted by the ABAQUS model of the retrofitted girder. In ABAQUS, a simply supported composite beam with the same geometry as the Hondo Bridge was modeled. Twenty-eight shear connectors were included in the ABAQUS model using the connector element. The HS 20 truck load was applied on the beam, 4 ft away from the left support. The load was cyclically applied 20 times.

Table 6.3 shows the force in each shear connector obtained from the finite element analysis and from the hand calculation method described above.

The shear force in the connectors based on the simplified hand calculations significantly exceeded the connector shear force computed in ABAQUS for connectors near the supports. For connectors further away from the supports, the hand calculations and the ABAQUS predictions matched reasonably well. Further studies are needed to establish simple methods for computing the shear force in the connectors of a partially composite girder with connectors located only near the ends. Nonetheless, it appears that the simple hand calculations provide a conservative prediction of connector shear force.

Under fatigue loading for the Hondo Bridge, the maximum stress range that the shear connectors experienced was 30.62 ksi based on the hand calculations. Details of the calculations are provided in Appendix B. The computed value of 30.62 ksi is less than the endurance limit of 35 ksi, meaning that the 14 shear connectors in a shear span satisfy fatigue strength requirement for the DBLNB and HTFGB connectors under the HS 20 design truck loading. For the HASAA connector, the maximum stress range is higher than 23.40 ksi. Thus, more shear connectors are needed to reduce the stress range in the HASAA connectors. Several iterations showed that fifty-two HASAA connectors are needed for each bridge girder to satisfy the fatigue load requirements. Note that more than 120 conventional welded shear connectors in a bridge girder would be needed to satisfy the fatigue requirements for the Hondo Bridge.

Table 6.3: Connector force (kips) under cyclic loading

Connector Number		1, 2	3, 4	5, 6	7, 8	9, 10	11, 12	13, 14
Number of cycles	1	8.12	8.09	7.97	7.55	6.87	6.77	7.34
	5	8.10	8.10	7.97	7.52	6.75	6.74	7.35
	10	8.10	8.10	7.97	7.51	6.73	6.70	7.26
	15	8.09	8.10	7.96	7.51	6.71	6.67	7.19
	20	8.09	8.09	7.96	7.50	6.70	6.65	7.15
Hand Calculation		13.13	13.13	13.13	13.13	7.30	7.30	7.30

27, 28	25, 26	23, 24	21, 22	19, 20	17, 18	15, 16	Connector Number	Number of cycles
10.33	8.80	7.71	6.99	6.53	6.25	6.09	1	
8.97	8.86	8.08	7.26	6.73	6.41	6.22	5	
7.90	8.71	8.41	7.50	6.91	6.56	6.36	10	
7.27	8.47	8.64	7.68	7.05	6.67	6.46	15	
6.89	8.18	8.81	7.81	7.15	6.76	6.53	20	
10.62	10.62	10.62	10.62	10.62	10.62	10.62	Hand Calculation	

6.4.2 Load Rating of Retrofitted Hondo Bridge based on Finite Element Analysis

ABAQUS was also used to load-rate the strengthened girders of the Hondo Bridge. As in the simulation of the full-scale composite beams in Chapter 4, the connector element in ABAQUS was used to model the shear connectors installed in the bridge girders. The three criteria, static strength, serviceability, and fatigue strength, were taken into account to load-rate the strengthened bridge girders as in the hand calculation procedure in the previous section.

Load-deflection graph for the strengthened bridge is shown in Figure 6.13 along with the graph of the non-composite bridge before the strengthening. A load factor ($A_2 \cdot (1 + I) \cdot RF$) instead of the applied load value was used in the vertical axis. Failure of the loaded ABAQUS model was also defined as the development of widespread cracks in the concrete slab, resulting in failure to achieve convergence of the solution. No shear connector failure was detected in the analysis model, meaning that the load could have been increased further past the point of non-convergence. As shown in Figure 6.13, the strength of the bridge was improved significantly by installing post-installed shear connectors. The maximum load factor obtained from the analysis was 3.62, which resulted in the rating results of $3.62/2.17/1.3 \times HS20 = HS25.7$ for the Inventory rating level and $3.62/1.3/1.3 \times HS20 = HS42.9$ for the Operating rating level. Figure 6.14 shows the longitudinal stress distribution in the composite girders after the strengthening. As expected, the neutral axis is located near the top flange of the beam due to partial composite action.

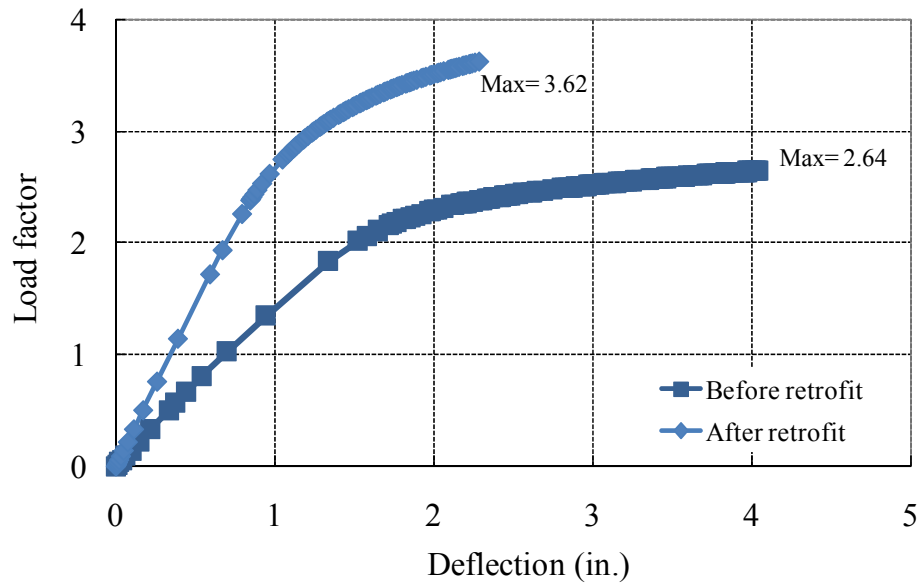


Figure 6.13: Analytically predicted load-deflection relations for Hondo Bridge (after retrofitting)

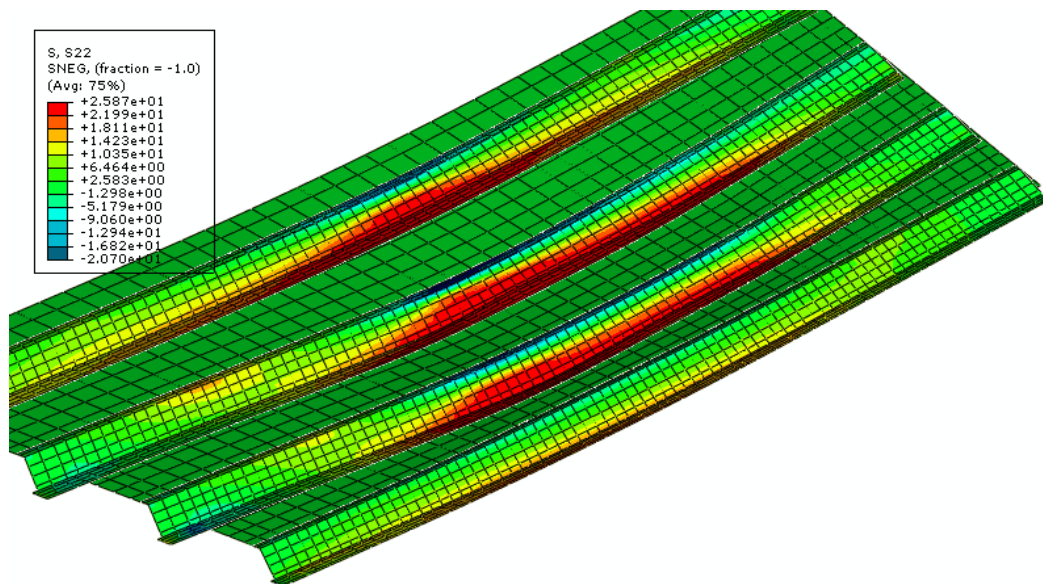


Figure 6.14: Longitudinal stress distribution of the Hondo Bridge (after retrofit)

Table 6.4: Load rating of strengthened composite bridge girders

Rating method	Rating level		Rating results
Standard AASHTO approach	Inventory rating	Strength	HS 21.5
		Serviceability	HS 17.4 (Controls)
	Operating rating	Strength	HS 35.9
		Serviceability	HS 29.1 (Controls)
ABAQUS analysis	Inventory rating	Strength	HS 25.7
		Serviceability	HS 18.4 (Controls)
	Operating rating	Strength	HS 42.9
		Serviceability	HS 30.7 (Controls)

For serviceability, the *AASHTO Standard Specifications* require that the maximum stress in the steel beam flange be less than $0.95F_y$ for overload vehicles. To load-rate the Hondo Bridge for this serviceability criterion, the HS 20 truck loading without load factor was applied to obtain the maximum stress in the steel beam flange. The maximum stress in the beam flange under the dead loads was 8.76 ksi as derived for the non-composite bridge girders. The maximum stress in the steel beam flange under the AASHTO HS 20 standard truck loads was 14.7 ksi, which resulted in a rating of $(0.95 \times 33 - 8.76) / 14.69 \times HS20 = HS30.7$ for the Operating rating level and $HS30.7 / 1.67 = HS18.4$ for the Inventory rating level. The load rating results of the strengthened bridge girders are summarized in Table 6.4.

6.5 SUMMARY

The results of this case study indicate that the load rating for an existing non-composite bridge can be increased substantially by the use of post-installed shear connectors. By taking advantage of partial composite design and the high strength of the post-installed shear connectors, a relatively small number of shear connectors can be highly effective in increasing the strength of the bridge. In the case study example, 28 post-installed shear connectors were added to each 40-ft long girder. Based on standard AASHTO load rating techniques, this resulted in an increase of the Inventory level rating from HS 10.6 to HS 17.4, and an increase in the Operating level rating from HS 17.6 to HS 29.1.

A key issue when using partial composite design is the effect of fatigue design requirements on the required number of shear connectors. Because of the low fatigue life of conventional welded shear studs, partial composite design is generally not possible, since fatigue will normally control the number of required connectors. However, because of the higher fatigue life of the post-installed connectors, it is expected that fatigue will not normally control the required number of shear connectors. And even in cases where fatigue does control, the required number of shear connectors will still be substantially less than would be required with conventional welded studs.

The effect of fatigue on the required number of shear connectors was also evaluated in this case study. The results of this evaluation showed that fatigue did not control the required number of connectors for the DBLNB and HTFGB connectors. For these cases, the required number of connectors was controlled by static strength requirements, and the 28 post-installed shear connectors per girder, based on partial composite design, were adequate to achieve the load-rating increase noted above.

In the case of the HASAA connectors, fatigue controlled the required number of connectors. This is because the fatigue life of the HASAA connector is less than that for the DBLNB and HTFGB connectors, although it is still substantially better than for conventional welded studs. In the case of the HASAA connector, satisfying fatigue

design requirements, 52 connectors were needed, as compared to 28 based on static strength requirements. Note that for conventional welded studs, approximately 120 shear studs per girder would be needed to satisfy AASHTO fatigue requirements. So, even though fatigue controlled the number of HASAA connectors, the required number is substantially less than for welded studs. For this case study bridge, the use of the DBLNB or HTFGB connectors may be preferred, since only 28 post-installed connectors are needed for each girder, compared to 52 HASAA connectors per girder. On the other hand, the HASAA connector can be completely installed from underneath the bridge, minimizing traffic disruptions. The DBLNB and HTFGB connectors require drilling from the top of the slab. Further, experience with the post-installed connectors in the laboratory suggests that the HASAA connectors are simpler and faster to install than the DBLNB and HTFGB connectors. The advantages of minimizing traffic disruptions and potentially reduced installation time and cost will at least partially offset the disadvantage of the larger number of required connectors.

An issue that requires further study is the manner in which shear force on the connector is computed in the elastic range of response, for purposes of checking fatigue. For conventional fully composite bridge girders, shear flow at the steel-concrete interface is computed based on a transformed fully composite cross-section. In the case of a partially composite girder, the use of a transformed cross-section may not provide an accurate estimate of shear flow. Further, the post-installed shear connectors are installed near the girder ends only, with no connectors in the center portion of the girder. For this arrangement of connectors, it is unclear how to compute connector shear force from the shear flow.

For the bridge of this case study, shear flow was computed using a transformed cross-section, and a simplified method was adopted for computing the resulting shear force on each connector. Comparisons with an ABAQUS model of the bridge indicated that the actual shear force on the connectors was significantly less than that calculated by this simplified procedure. Further studies are needed to develop a more accurate method of computing connector shear force for fatigue design.

CHAPTER 7

Summary, Conclusions, and Design Recommendations

7.1 SUMMARY

This dissertation was a continuation of a study on the use of post-installed shear connectors to develop composite action in existing non-composite steel bridge girder systems. Previous work conducted by Schaap (2004), Hungerford (2004), and Kayir (2006) identified various post-installed shear connectors and conducted tests on these connectors, and evaluated their performance. Based on these single shear connector tests, Kayir (2006) recommended three types of post-installed shear connectors, which are referred to as the Double-Nut Bolt (DBLNB), the High-Tension Friction-Grip Bolt (HTFGB), and the Adhesive Anchor (HASAA).

In this study, these three types of post-installed shear connectors were tested using a direct shear test setup to evaluate the structural behavior of 7/8-in. diameter post-installed shear connectors under static and fatigue loadings. From the static tests, the ultimate strength, initial stiffness, and slip capacity of the shear connectors were investigated. Fatigue tests were conducted to identify fatigue strength of the shear connectors under various stress ranges. Based on the tests, equations to predict the ultimate strength and fatigue strength of the post-installed shear connectors were developed.

Five full-scale non-composite beams were constructed, and four of them were retrofitted with post-installed shear connectors. The full-scale composite beams were tested under static loading to evaluate system performance of the retrofitted composite beams. Constructability issues for the post-installed shear connectors were also evaluated during the installation of the connectors in the full-scale beams. One non-composite beam

was also tested as a baseline specimen. To supplement the test results, a finite element model was developed and parametric studies were conducted using the finite element model to evaluate the effects of various parameters including beam depth, span length, and shear connection ratio on the overall stiffness, strength and ductility of the composite beams with post-installed shear connectors.

Finally, to further evaluate the feasibility of strengthening existing non-composite bridges with post-installed shear connectors, a detailed design for strengthening an actual case study bridge was undertaken. Potential design and construction difficulties were identified and solutions to these difficulties are suggested.

7.2 CONCLUSIONS

Overall, the results of this study indicate that the addition of post-installed shear connectors can significantly increase the strength of existing non-composite bridge girders. By using partial composite design, the addition of a relatively small number of post-installed shear connectors can increase the flexural capacity of an existing girder in positive moment regions by 40 to 50 percent. The use of post-installed shear connectors can therefore provide an effective means for strengthening existing non-composite bridges. Some specific conclusions are as follows:

- ✓ Static tests on the three types of post-installed connectors (DBLNB, HTFGB and HASAA) show strength levels that are similar or greater than those of conventional welded studs. Fatigue tests on these post-installed connectors show significantly better fatigue lives than conventional welded studs. The excellent fatigue performance of these three post-installed shear connectors is attributed, in large part, to the fact that no welds are involved in their installation.

- ✓ Preliminary recommendations were developed for computing the static strength of the post-installed shear connectors. The static strength can be estimated as one-half of the tensile strength of the connector (Equation 2.28), which was proposed by Kayir (2006). The effective shear area of the connectors with threads in a shear plane can be taken as 80 percent of gross area of unthreaded connectors.

- ✓ A limited number of fatigue tests on post-installed shear connectors showed fatigue strengths significantly higher than those of conventional welded shear studs. However, not enough fatigue tests were conducted to confidently recommend S-N relationships for all of the post-installed shear connectors. Due to the intrinsic variability of fatigue test results, additional fatigue tests would be desirable to better identify an S-N curve and fatigue endurance limit for each type of shear connectors. Nonetheless, based on the limited available data, preliminary recommendations were made. For the HASAA connector with either ISO 898 Class 5.8 threaded rods or ASTM A193 B7 threaded rods, Equation 3.2 was developed as a design S-N curve. For the DBLNB connector with ASTM A193 B7 threaded rods and HTFGB connector with ASTM A325 high-strength bolts, 35 ksi was proposed as fatigue endurance limit.

- ✓ It is recommended that partial composite design be used as a basis for determining the number of post-installed shear connectors that will be used to strengthen an existing bridge girder. Current *AASHTO Standard Specifications* and *AASHTO LRFD Specifications* only recognize fully composite design for steel bridge girders, and do not include provisions for partially composite design. The absence of partially composite design provisions in AASHTO likely reflects the fact that fatigue design requirements, rather than static strength requirements, normally control the

required number of welded shear studs on a composite girder. However, because of the higher fatigue strength of the post-installed shear connectors, fatigue is less likely to control the required number of shear connectors, thereby enabling partially composite design. The cost of post-installed shear connectors for an existing bridge is likely to be higher than the cost of welded shear studs for new construction. Fully composite design will therefore likely be very costly for strengthening existing bridges. Thus, the economic viability of strengthening existing non-composite bridges by post-installing shear connectors depends largely on the use of partially composite design.

- ✓ To evaluate overall system performance of composite beams retrofitted with post-installed shear connectors, five full-scale beam tests were conducted under static loads. For one of the five specimens, no shear connectors were installed, to provide baseline data on the strength and stiffness of a non-composite girder. The other four specimens were retrofitted with post-installed shear connectors using a 30-percent shear connection ratio. Three of the specimens had shear connectors uniformly distributed along the span. The composite beams retrofitted with post-installed shear connectors showed a significant increase in strength and stiffness compared to the non-composite beam specimen. The composite beams retrofitted with the DBLNB and HASAA connectors showed less ductility than the baseline non-composite beam. The composite beam retrofitted with the HTFGB connector showed significantly larger deformation capacity than the beams retrofitted with the DBLNB and HASAA connectors.

- ✓ From analytical solutions and finite element analysis, it was found that the slip at the steel-concrete interface can be reduced by concentrating shear

connectors near the supports, resulting in a larger deformation capacity for the retrofitted beam, compared to the case with uniformly distributed shear connectors. One last full-scale composite beam with shear connector concentrated near the beam ends was tested under static load, and showed a significant increase in deformation capacity over the otherwise identical specimen with uniformly distributed shear connectors.

- ✓ A finite element model was developed and parametric studies were conducted to investigate the effects of steel beam depth, span length, and shear connection ratio on the overall system performance of the strengthened partially composite beams. The analysis results showed that an increase in beam depth and span length resulted in reduced deformation capacity of composite beams. Composite beams with a high shear-connection ratio showed better deformation capacity than composite beams with a low shear-connection ratio. All of the composite beams with a shear-connection ratio of at least 30 percent showed a global ductility factor of at least two. Based on this analysis, a minimum shear connection ratio of 30 percent is recommended. Based on the analysis results, it was also shown that the strength and stiffness of composite beams retrofitted with post-installed shear connectors can be calculated using the current AASHTO and AISC design equations.

- ✓ A complete design example to strengthen a case study bridge located near San Antonio using post-installed shear connectors was provided in this study. The bridge consists of three simple spans. For the DBLNB and HTFGB connectors, 28 shear connectors in each bridge girder were required to satisfy the load rating requirements established by TxDOT. For the HASAA connector, more shear connectors were required due to its lower fatigue strength than the DBLNB and HTFGB connectors.

7.3 PRELIMINARY DESIGN RECOMMENDATIONS

The results of this study clearly demonstrate that the strength and stiffness of existing non-composite steel bridge girders can be increased significantly by post-installing shear connectors. Based on the research results from laboratory tests and analytical studies, a preliminary design approach for strengthening existing steel bridge girders by using post-installing shear connectors can be proposed. Preliminary design recommendations are as follows:

- ✓ Three types of post-installed shear connectors were thoroughly investigated in this study and are recommended for use in strengthening existing non-composite bridge girders. The three types of post-installed shear connectors are the Double-Nut Bolt (DBLNB), the High-Tension Friction-Grip Bolt (HTFGB), and Adhesive Anchor (HASAA). These connectors consist of high strength bolts or threaded rods placed in holes that are drilled in the concrete slab and top flange of the steel girder. The holes are filled with high strength grout (double-nut bolt and high tension friction grip bolt) or structural adhesive (adhesive anchor). Installation of the double-nut bolt and high tension friction grip bolt require construction operations on both the top and bottom sides of the concrete slab. The adhesive anchor, in contrast, can be completely installed from underneath the slab, thereby minimizing traffic disruptions on the bridge.
- ✓ Use of either 3/4-in. or 7/8-in. diameter shear connectors is recommended, as these are the tested in this research project. The use of larger diameter shear connectors can reduce the number of shear connectors needed to achieve the same level of shear connection ratio. Other diameters may be suitable, although test data would be desirable to evaluate their performance.

- ✓ For the DBLNB and HASAA connectors, the use of ASTM A193 B7 threaded rods is suggested. For the HTFGB connector, the use of ASTM A325 high-strength bolt or equivalent is suggested.
- ✓ The use of partial composite design is recommended as an overall basis for strengthening steel bridge girders with post-installed shear connectors. Use of a shear connection ratio less than 30 percent is not recommended to avoid non-ductile behavior of the strengthened girder. The flexural strength and elastic stiffness of retrofitted partial composite beams can be computed using current AASHTO and AISC design provisions (AASHTO 2007, AISC 2005).
- ✓ The use of Equation 2.28 is recommended for computing the strength of post-installed shear connectors. This equation can be applied to all three types of post-installed shear connectors.
- ✓ Pending the availability of additional fatigue tests, it is recommended to use 35 ksi as a fatigue endurance limit for the DBLNB and HTFGB connectors. Equation 3.2 is recommended to calculate the fatigue strength of the HASAA connector.
- ✓ It is recommended that general requirements concerning clear cover, edge distance, and minimum transverse spacing between shear connectors in AASHTO provisions be followed. A minimum 5-in. embedment depth is recommended for the post-installed shear connectors, because this was the minimum embedment depth used for the shear connectors in the tests described here.

- ✓ It is recommended that post-installed shear connectors be concentrated near zero moment regions, rather than being distributed uniformly along the length of the beam. This increases the overall ductility of the strengthened partially composite beams. The minimum longitudinal spacing of the shear connectors used for the full-scale beam tests was 12 in.

- ✓ Installation procedures used for the post-installed shear connectors in the full-scale beam tests are described in detail in this dissertation, and can be used as a guide for actual field installation.

- ✓ Recommended design steps for determining the number and location of post-installed shear connectors are shown in flowchart form in Figure 7.1. Detail design procedures and calculations are illustrated by the case study reported in Chapter 6.

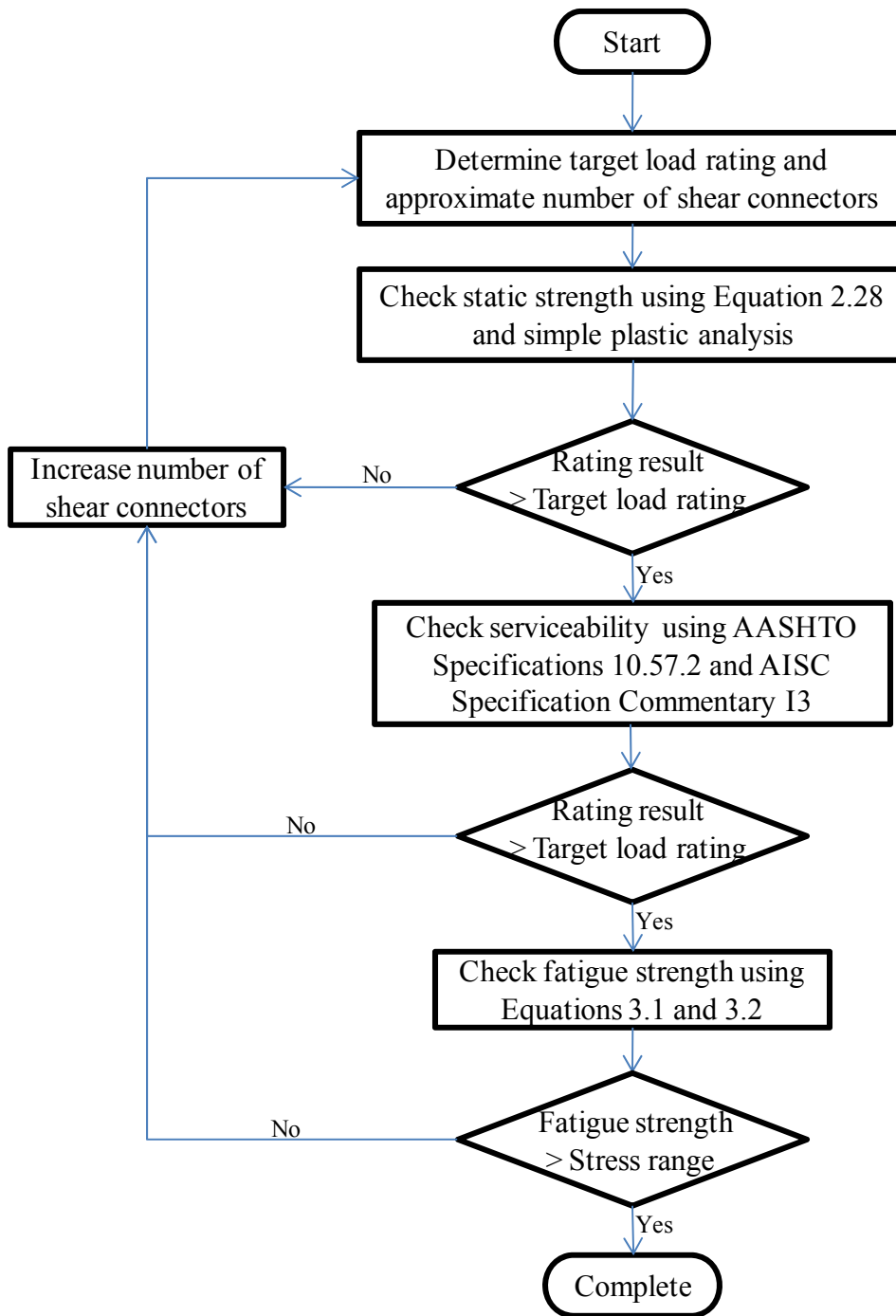


Figure 7.1: Design procedure using post-installed shear connectors

7.4 RECOMMENDATIONS FOR FURTHER RESEARCH

Following are recommendations for further research related to strengthening existing non-composite beams using post-installed shear connectors:

- ✓ Additional single shear connector tests under fatigue loading are needed to better characterize the S-N relationship for the post-installed shear connectors, as well as to characterize the variability in fatigue performance.
- ✓ Further studies are needed to develop methods for computing the forces on post-installed shear connectors under service level loading, for purposes of fatigue design. For conventional fully composite bridge girders, shear flow at the steel-concrete interface is computed based on a transformed fully composite cross-section. In the case of a partially composite girder, the use of a transformed cross-section may not provide an accurate estimate of shear flow. Further, the post-installed shear connectors are installed near the girder ends only, with no connectors in the center portion of the girder. For this arrangement of connectors, it is unclear how to compute connector shear force from the shear flow.
- ✓ This study investigated the use of post-installed shear connectors for increasing the positive moment capacity of girders, and is most useful for simple spans. Additional research is needed to extend the results in this study to continuous multi-span steel girders that have inadequate flexural capacity in negative moment regions. Possible approaches may include post-installing shear connectors in negative moment regions to develop composite action in these regions. Alternatively, post-installed shear connectors could be added to positive moment regions, with an increase in

load capacity achieved through plastic redistribution of moment from the negative moment regions to the strengthened positive moment regions.

- ✓ Further studies would be desirable to identify additional types of post-installed shear connectors that are economical, easy to install, and structurally effective.

Appendix A

Analysis Results of Composite Beams

A.1 COMPOSITE BEAMS WITH W27x94 SECTION

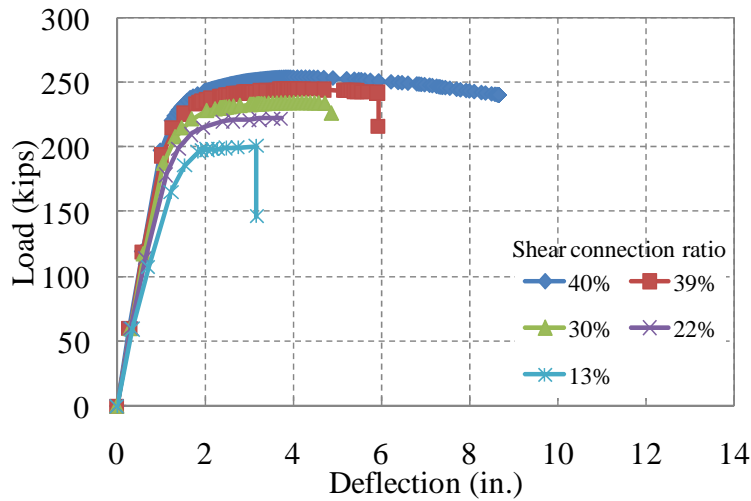
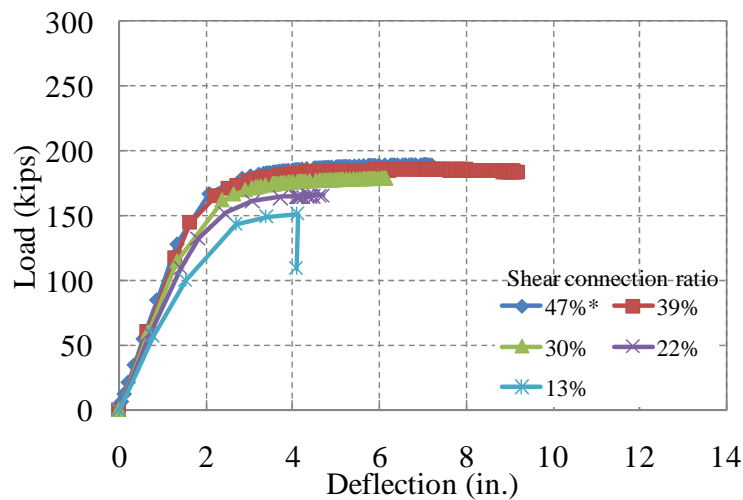
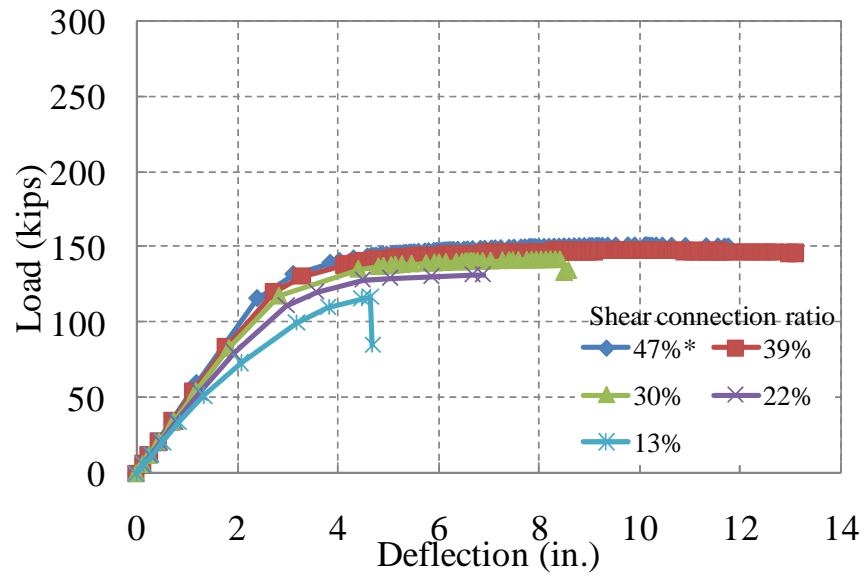


Figure A.1: Load-deflection relations of composite beams (W27x94, 30-ft span)



*: Convergence was not achieved before shear connector failed.

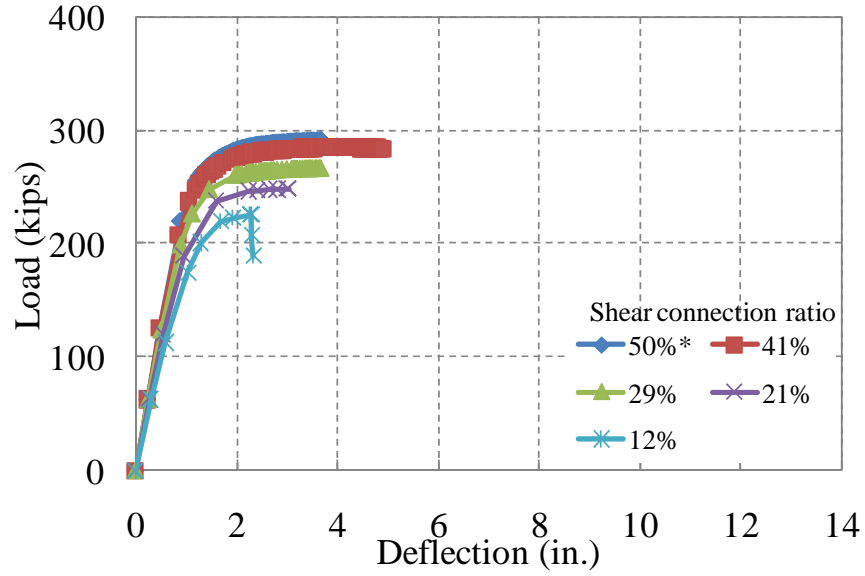
Figure A.2: Load-deflection relations of composite beams (W27x94, 40-ft span)



*: Convergence was not achieved before shear connector failed.

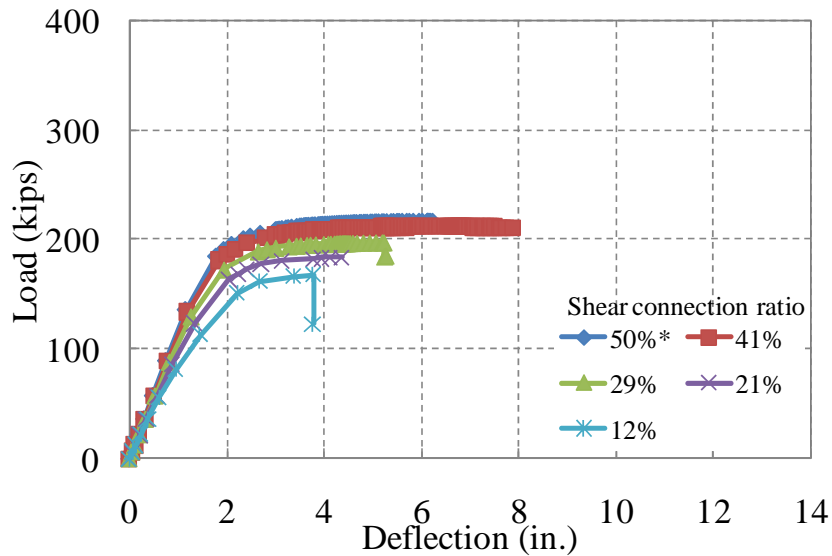
Figure A.3: Load-deflection relations of composite beams (W27x94, 50-ft span)

A.2 COMPOSITE BEAMS WITH W30x99 SECTION



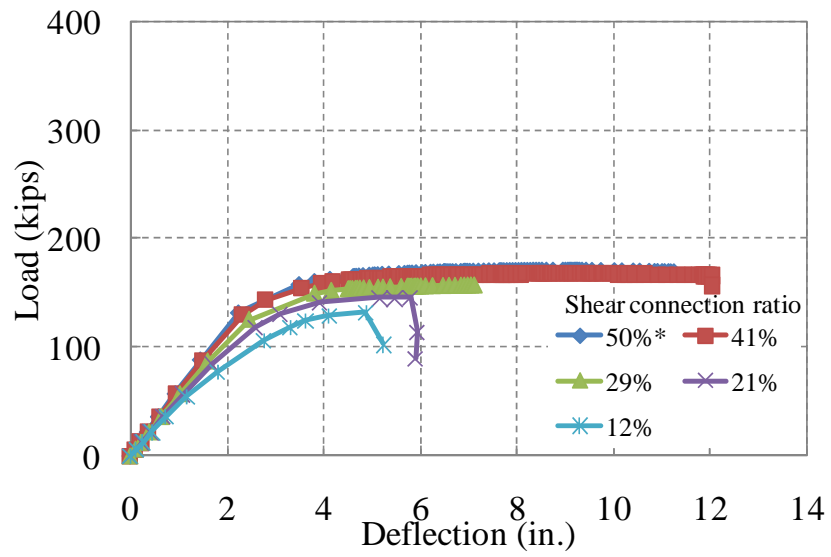
*: Convergence was not achieved before shear connector failed.

Figure A.4: Load-deflection relations of composite beams (W30x99, 30-ft span)



*: Convergence was not achieved before shear connector failed.

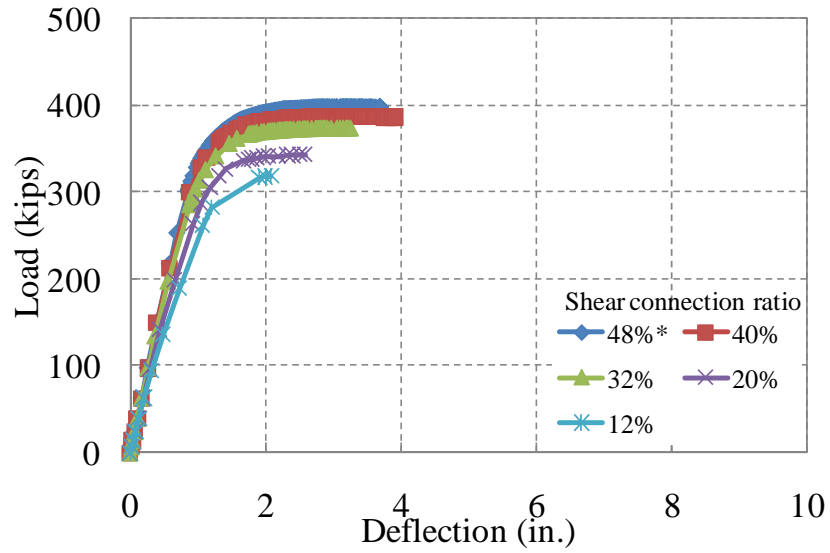
Figure A.5: Load-deflection relations of composite beams (W30x99, 40-ft span)



*: Convergence was not achieved before shear connector failed.

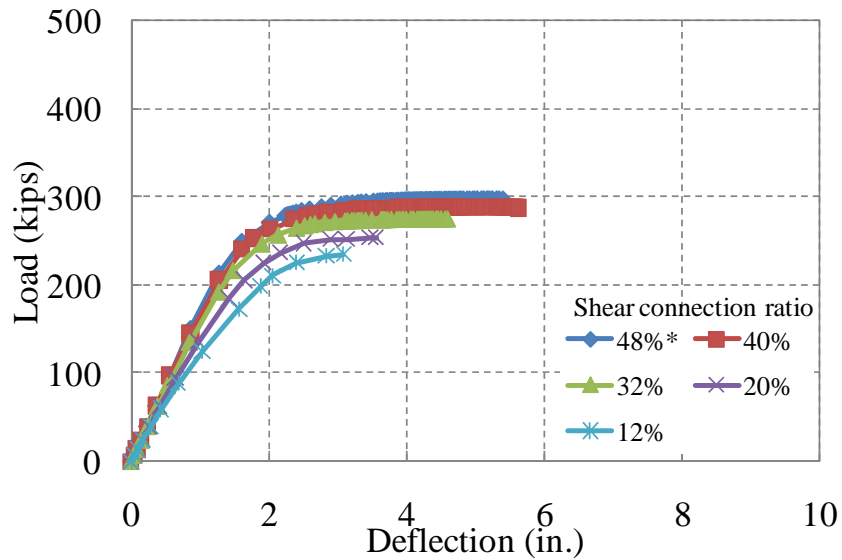
Figure A.6: Load-deflection relations of composite beams (W30x99, 50-ft span)

A.3 COMPOSITE BEAMS WITH W33x130 SECTION



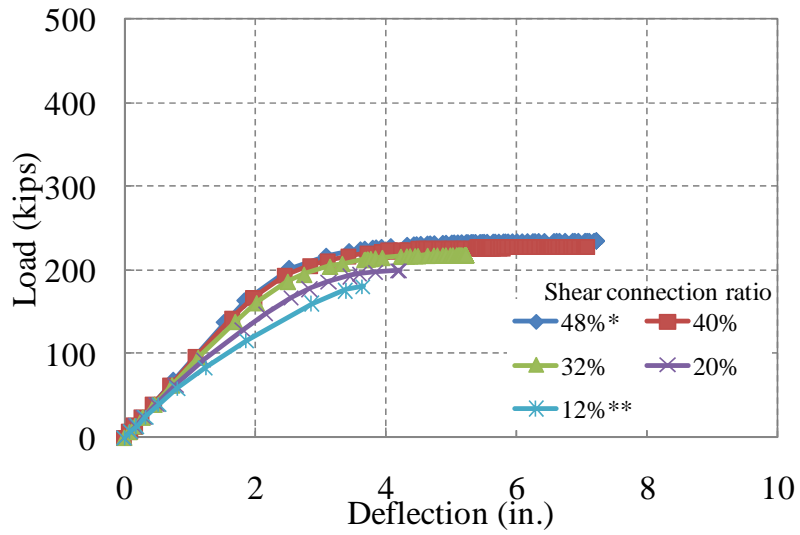
*: Convergence was not achieved before shear connector failed.

Figure A.7: Load-deflection relations of composite beams (W33x130, 30-ft span)



*: Convergence was not achieved before shear connector failed.

Figure A.8: Load-deflection relations of composite beams (W33x130, 40-ft span)

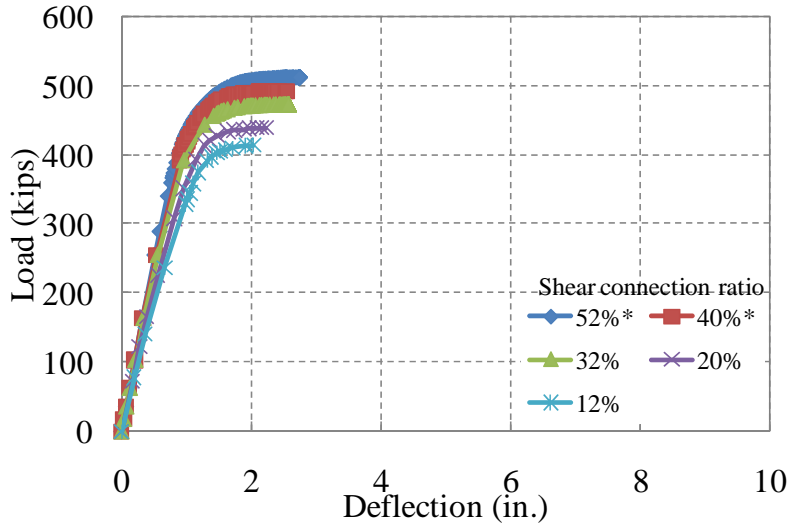


*: Convergence was not achieved before shear connector failed.

** : Max. load was less than simple plastic analysis result.

Figure A.9: Load-deflection relations of composite beams (W33x130, 50-ft span)

A.4 COMPOSITE BEAMS WITH W36x160 SECTION



*: Convergence was not achieved before shear connector failed.

Figure A.10: Load-deflection relations of composite beams (W36x160, 30-ft span)

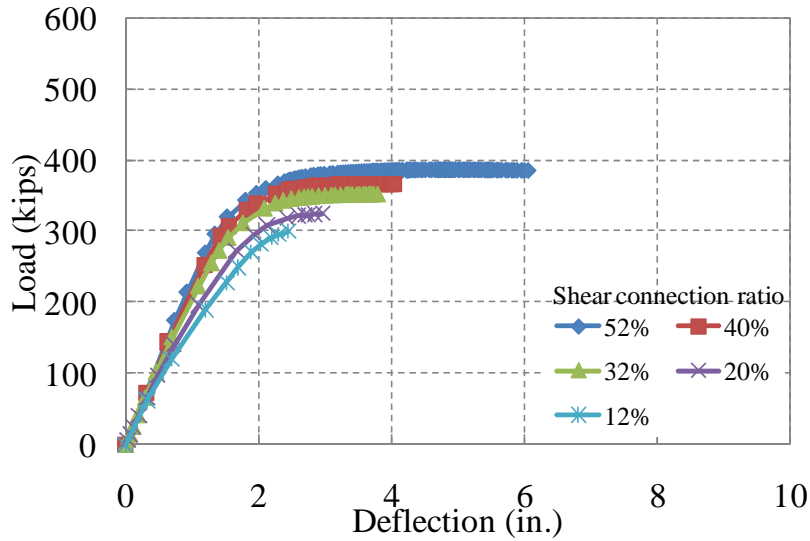
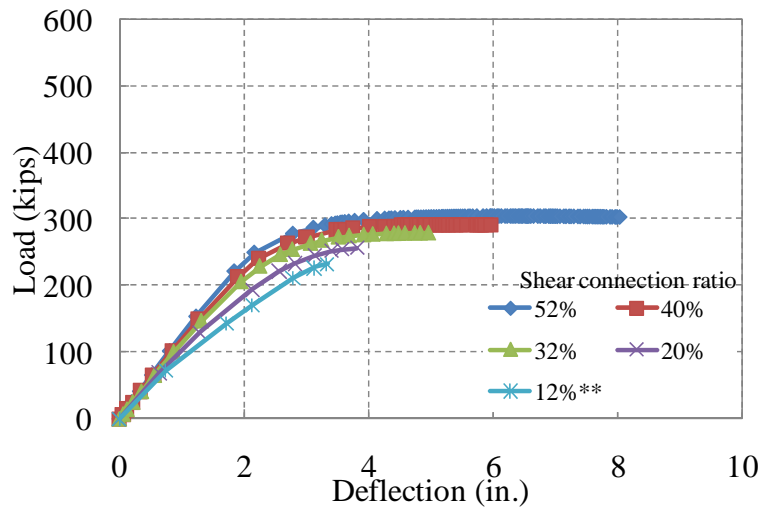


Figure A.11: Load-deflection relations of composite beams (W36x160, 40-ft span)



** : Max. load was less than simple plastic analysis result.

Figure A.12: Load-deflection relations of composite beams (W36x160, 50-ft span)

Appendix B

Load Rating For Hondo Bridge

B.1 NON-COMPOSITE BEAM LOAD RATING

B.1.1 Geometry

- Span length: 39.33 ft (bearing length deducted)

- Materials: Steel $F_y = 33 \text{ ksi}$ (year built: 1950)

AASHTO Manual 6.6.2.1

Concrete $f'_c = 2.5 \text{ ksi}$

AASHTO Manual 6.6.2.4

Steel section dimensions are shown in Figure B.1.

For the bare steel beam,

$$\bar{y} = 12.94 \text{ in.}$$

$$I_x = 2782.7 \text{ in.}^4$$

$$S_t = S_b = 215 \text{ in.}^3$$

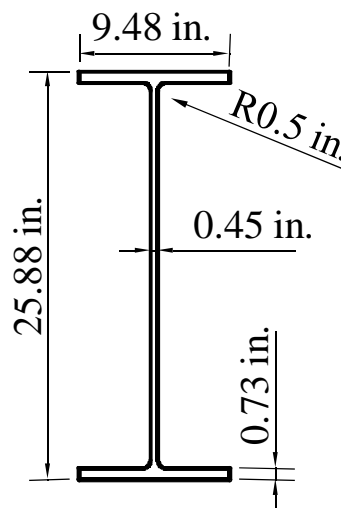


Figure B.1: Steel beam section

B.1.2 Load Calculation

- Dead loads

$$\text{Deck: } 7 \times \frac{6.25}{12} \times 0.15 = 0.547 \text{ kips / ft}$$

$$\text{Stringer: } 0.085 \text{ kips / ft} \quad \text{Diaphragm: } 0.012 \text{ kips / ft}$$

Moment due to dead load, M_{DL}

$$M_{DL} = \frac{wL^2}{8} = \frac{(0.547 + 0.085 + 0.012) \times 39.33^2}{8} = 124.52 \text{ ft} - \text{kips}$$

- Superimposed dead loads

In AASHTO, it is specified that “Curbs, railings, and wearing surface, if placed after the slab has cured, may be distributed equally to all roadway stringer beams.”

$$\text{Curb: } 1 \times \frac{10}{12} \times 0.15 / 2 = 0.063 \text{ kips / ft}$$

AASHTO Specifications 3.23.2.3.1.1

$$\text{Railing: } \frac{20 \text{ lb / ft}}{2} = 0.01 \text{ kips / ft}$$

$$\text{Wearing surface: } 7 \times \frac{0.5}{12} \times 0.144 = 0.042 \text{ kips / ft}$$

Moment due to superimposed dead load

$$M_{SDL} = \frac{wL^2}{8} = \frac{(0.0625 + 0.010 + 0.042) \times 39.33^2}{8} = 22.14 \text{ ft} - \text{kips}$$

$$M_{DL} + M_{SDL} = 146.66 \text{ ft} - \text{kips}$$

- Live Loads

$$M_L = 219 \text{ ft} - \text{k} \text{ (without impact and distribution factor)}$$

AASHTO Manual Appendix A3

$$\text{Impact factor } I = \frac{50}{L+125} \leq 0.3 \quad \text{AASHTO Specifications 3.8.2.1}$$

$$= \frac{50}{39.33+125} = 0.304 \quad \therefore I = 0.3$$

$$\text{Distribution factor } DF = \frac{S}{5.5} = \frac{7}{5.5} = 1.273 \quad \text{AASHTO Specifications 3.23.2.3.1.5}$$

$$M_{L+I} = 219 \times 1.3 \times 1.27 = 371 \text{ ft} - \text{kips} \quad (\text{with impact and distribution factor})$$

B.1.3 Section Capacity

- Check compact section criteria AASHTO Specifications 10.48.1.1

$$\text{Compression flange: } \frac{b}{t} \leq \frac{4110}{\sqrt{F_y}} \quad \text{O.K.}$$

$$\text{Web thickness: } \frac{D}{t_w} \leq \frac{19230}{\sqrt{F_y}} \quad \text{O.K.}$$

$$Z = 245 \text{ in.}^3$$

$$M_u = F_y Z = 3085 \text{ in.} - \text{kips} = 673.75 \text{ ft} - \text{kips}$$

B.1.4 Load Rating

$$RF = \frac{C - A_1 D}{A_2 L(1 + I)} \quad \text{AASHTO Manual 6.5.1}$$

For the Load Factor Method, $A_1 = 1.3$ for both Inventory and Operating level,
 $A_2 = 2.17$ for Inventory level and 1.3 for Operating level.

- Strength criterion

$$\text{Inventory level } RF = \frac{673.75 - 1.3 \times 146.66}{2.17 \times 371} = 0.60$$

$$\text{Operating level } RF = \frac{673.75 - 1.3 \times 146.66}{1.3 \times 371} = 1.00$$

- Serviceability criterion ($f_s \leq 0.8F_y$) AASHTO Specifications 10.57.1

AASHTO Specifications require that bridge girders remain elastic for overload vehicles.

$$\text{Inventory level } RF = \frac{0.8 \times 33 \times 215 / 12 - 146.66}{1.67 \times 371} = 0.53 \quad \text{Control}$$

$$\therefore RT = 0.53 \times HS20 = HS10.6$$

$$\text{Operating level } RF = 0.53 \times 1.67 = 0.88 \quad \text{Control}$$

$$\therefore RT = 0.88 \times HS20 = HS17.6$$

B.2 LOAD RATING FOR STRENGTHENED COMPOSITE BEAM

B.2.1 Geometry

Composite beam section is shown in Figure B.2.

$$\text{Modular ratio } n = \frac{29000}{1820\sqrt{2.5}} = 10.08$$

Effective slab width $b_{eff} = 75 \text{ in.}$

AASHTO Specifications 10.38.3.1

Partial composite design is used for the retrofit of the currently non-composite steel bridge girders. Fourteen shear connectors in a shear span (total 28 shear connectors in a beam) are used to retrofit the bridge. As a reference, 56 post-installed shear connectors in a beam are required for fully composite beam design.

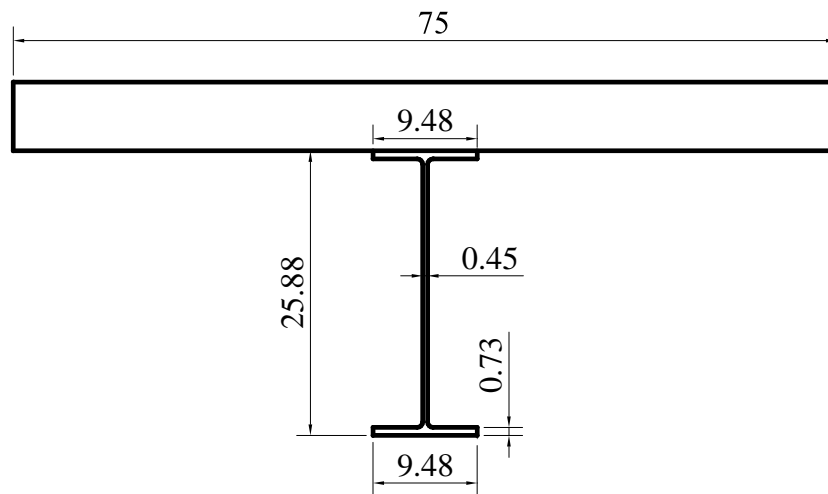


Figure B.2: Composite beam section (unit: in.)

B.2.2 Ultimate Strength

The ultimate strength of individual shear connectors can be calculated using the equation below.

$$Q_n = 0.5A_{sc}F_u = 0.5 \times 0.8 \times \pi \times \left(\frac{0.875}{2}\right)^2 \times 125 = 30.07 \text{ kips}$$

The effective shear area, A_{sc} , of the threaded part of the connectors can be calculated as 80% of the unthreaded area.

$$\sum Q_n = 30.07 \times 14 = 420.92 \text{ kips}$$

Simple plastic analysis is used to determine the ultimate strength of the partial composite beam retrofitted with post-installed shear connectors.

Plastic N.A. $\bar{y} = 6.58 \text{ in.}$ from the top of the slab

$$M_{ult} = 1056.73 \text{ ft} - \text{kips}$$

- Strength criterion

$$\text{Inventory level: } RF = \frac{1056.73 - 1.3 \times 146.66}{2.17 \times 371} = 1.08$$

$$\text{Operating level: } RF = \frac{1056.73 - 1.3 \times 146.66}{1.3 \times 371} = 1.80$$

- Serviceability criterion ($f_s \leq 0.95F_y$) AASHTO Specifications 10.57.2

For overload vehicles, the bridge girders are required to behave elastically. *AASHTO Specifications* do not address any methods to determine the beam stress for partial composite bridge girders. The effective section modulus of a partially composite beam, as given in the commentary of the *AISC Specification*, is used to calculate stress in the beam flange.

$$S_{eff} = S_s + \sqrt{\left(\sum Q_n / C_f\right)} \cdot (S_{tr} - S_s) = 215 + \sqrt{420.92 / 829.95} \cdot \left(\frac{7147.03}{23.37} - 215\right)$$

$$= 279.68 \text{ in}^3$$

AISC Specification Commentary I3

$$\text{Inventory level: } RF = \frac{33 \times 0.95 - \frac{146.66 \times 12}{215}}{1.67 \times \frac{371 \times 12}{279.68}} = 0.87 \quad \text{Controls}$$

$$\therefore RT = 0.87 \times HS20 = HS17.4$$

$$\text{Operating level: } RF = 0.87 \times 1.67 = 1.45 \quad \text{Controls}$$

$$\therefore RT = 1.45 \times HS20 = HS29.1$$

B.2.3 Fatigue Strength

Shear connectors are numbered as shown in Figure B.3. The HS20 design truck, including impact factor and distribution factor, was moved from the left support to the right support and the right to the left. The shear force in each shear connector was calculated at each location of the truck and the maximum stress range was determined for each connector. Two examples are shown below. It was assumed that horizontal shear force where shear connectors are installed is resisted by the connectors at the section. The horizontal shear force where shear connectors are not installed was assumed to be resisted equally by the shear connectors in the shear span.

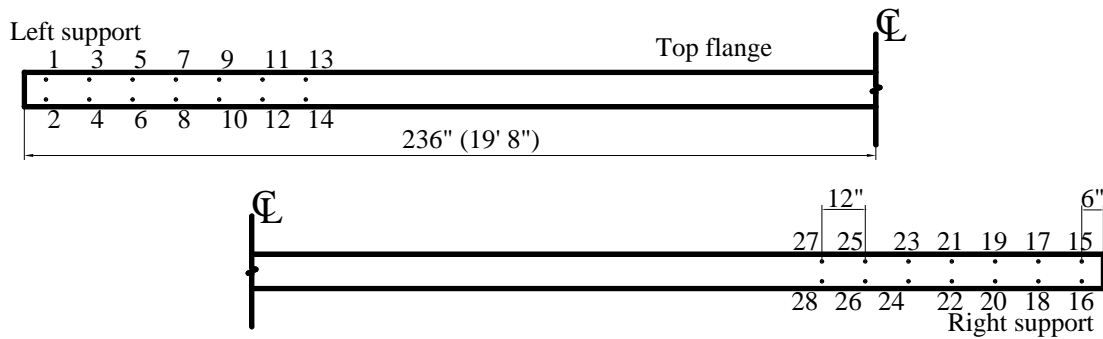


Figure B.3: Shear connector numbering

- Case I: Rear wheel is located 4 ft from the left support

Figure B.4 and Figure B.5 show truck wheel locations and the corresponding shear force diagram.

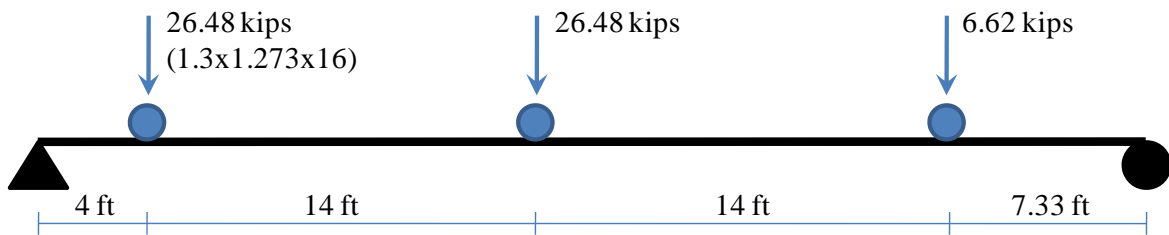


Figure B.4: Truck wheel locations

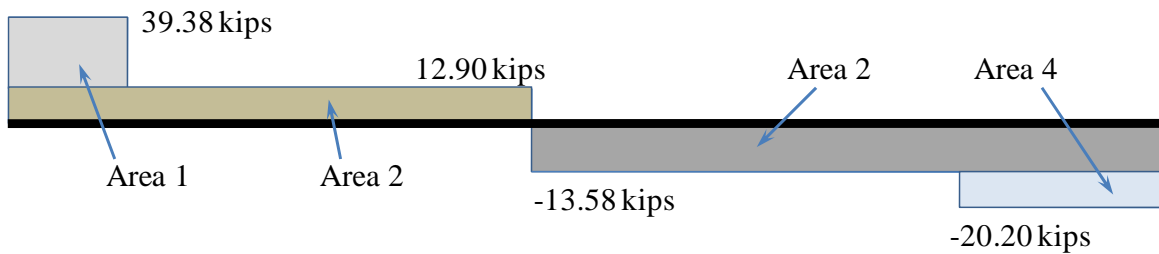


Figure B.5: Shear force diagram

For Area 1

$$V = 39.38 - 12.90 = 26.48 \text{ kips}, \quad I_{rr} = 7147.03 \text{ in}^4, \quad Q = 262.03 \text{ in}^3$$

$$\text{Shear flow } f = \frac{VQ}{I_{rr}} = \frac{26.48 \times 262.03}{7147.03} = 0.97 \text{ kips/in} = 11.65 \text{ kips/ft}$$

Total horizontal shear force, V_h , can be obtained by multiplying the shear flow with the applied span length in the beam.

$$V_h = 11.65 \text{ kips/ft} \times 4 \text{ ft} = 46.6 \text{ kips}$$

The number of shear connectors loaded in the span is 8.

$$Q_1 = Q_2 \cdots = Q_8 = 46.6 \text{ kips} / 8 = 5.825 \text{ kips}$$

For Area 2

$$V = 12.90 \text{ kips}$$

$$\text{Shear flow } f = \frac{12.90 \times 262.03}{7147.03} = 0.47 \text{ kips/in} = 5.68 \text{ kips/ft}$$

Total horizontal shear force V_h

$$V_h = 5.68 \times 18 = 102.16 \text{ kips}$$

The number of shear connectors loaded is 14.

$$Q_1 = Q_2 = \cdots = Q_{14} = 102.16 \text{ kips} / 14 = 7.30 \text{ kips}$$

For Area 3

$$V = -13.58 \text{ kips}$$

$$\text{Shear flow } f = \frac{13.58 \times 262.03}{7147.03} \times 12 = 5.97 \text{ kips/ft}$$

Total horizontal shear force V_h

$$V_h = 5.97 \times 21.33 = 127.34 \text{ kips}$$

The number of shear connectors loaded is 14.

$$Q_{15} = Q_{16} = \cdots = Q_{28} = 127.34 / 14 = 9.10 \text{ kips}$$

For Area 4

$$V = -20.20 + 13.58 = -6.62 \text{ kips}$$

$$\text{Shear flow } f = \frac{6.62 \times 262.03}{7147.03} \times 12 = 2.91 \text{ kips / ft}$$

Total horizontal shear force V_h

$$V_h = 2.91 \times 7.33 = 21.33 \text{ kips}$$

The number of shear connectors loaded is 14.

$$Q_{15} = Q_{16} = \dots = Q_{28} = 1.52 \text{ kips}$$

The shear connector forces for Case I loading are shown in Table B.1.

Table B.1: Connector shear forces for Case I loading

Connector	1	3	5	7	9	11	13
	2	4	6	8	10	12	14
Shear force (kips)	13.13	13.13	13.13	13.13	7.30	7.30	7.30

27	25	23	21	19	17	15	Connector
28	26	24	22	20	18	16	
10.62	10.62	10.62	10.62	10.62	10.62	10.62	Shear force (kips)

Case II: Rear wheel is located 36 ft from the left support

Figure B.6 and Figure B.7 show truck wheel locations and the shear force diagram for Case II loading.

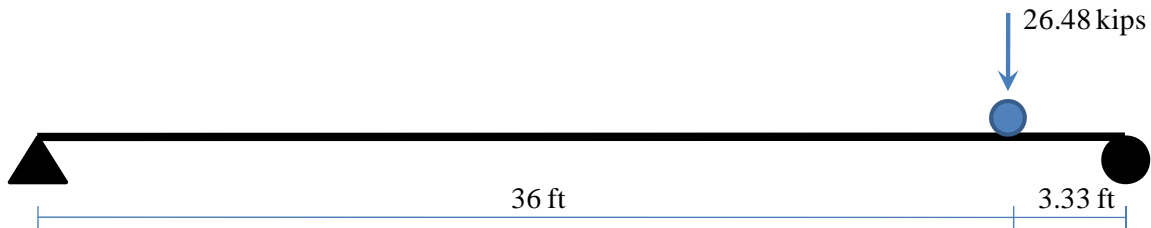


Figure B.6: Truck wheel locations

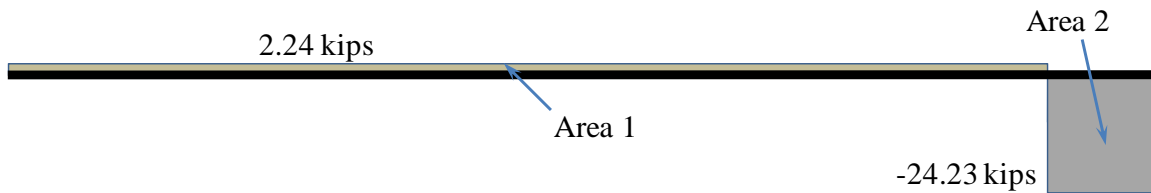


Figure B.7: Shear force diagram

For Area 1

$$V = 2.24 \text{ kips}$$

$$\text{Shear flow } f = \frac{2.24 \times 262.03}{7147.03} \times 12 = 0.9872 \text{ kips / ft}$$

Total horizontal shear force V_h

$$V_h = 0.9872 \times 36 = 35.54 \text{ kips}$$

The number of shear connectors loaded is 22 (14 in the left shear span and 8 in the right shear span)

$$Q_5 = Q_2 = \dots = Q_{14} = 1.62 \text{ kips}$$

$$Q_{21} = Q_{22} = \dots = Q_{28} = -1.62 \text{ kips}$$

Connector force is positive when the connector head deforms toward the nearest support.

For Area 2

$$V = -24.23 \text{ kips}$$

$$\text{Shear flow } f = \frac{24.23 \times 262.03}{7147.03} \times 12 = 10.66 \text{ kips / ft}$$

Total horizontal shear force V_h

$$V_h = 10.66 \times 3.33 = 35.54 \text{ kips}$$

The number of shear connectors loaded is 6.

$$Q_{15} = Q_{16} = \dots = Q_{20} = 5.92 \text{ kips}$$

Connector shear forces are summarized in Table B.2 for Case II loading.

Table B.2: Connector shear forces for Case II loading

Connector	1	3	5	7	9	11	13
	2	4	6	8	10	12	14
Shear force (kips)	1.62	1.62	1.62	1.62	1.62	1.62	1.62

27	25	23	21	19	17	15	Connector
28	26	24	22	20	18	16	
-1.62	-1.62	-1.62	-1.62	5.92	5.92	5.92	Shear force (kips)

The HS20 truck load was moved to the both directions. Table B.3 shows shear connector force for several truck locations. Truck locations in Table 3 are the distance from a support to the rear wheel location.

- Check maximum stress range

Connector 7 and 8 experienced the maximum stress range for the truck loadings.

$$\frac{13.12 + 1.61}{0.8 \times \pi \times (0.875/2)^2} = 30.62 \text{ksi} \leq 35 \text{ksi} \quad \therefore \text{O.K.}$$

Table B.3: Shear connector force for several truck locations (kips)

Distance from left support (ft)	Shear connector number (near left support)							Shear connector number (near right support)						
	1, 2	3, 4	5, 6	7, 8	9, 10	11, 12	13, 14	27, 28	25, 26	23, 24	21, 22	19, 20	17, 18	15, 16
0	8.34	8.34	8.34	8.34	8.34	8.34	8.34	8.34	8.34	8.34	8.34	8.34	8.34	8.34
2	14.49	14.49	8.01	8.01	8.01	8.01	8.01	9.68	9.68	9.68	9.68	9.68	9.68	9.68
4	13.12	13.12	13.12	13.12	7.30	7.30	7.30	10.63	10.63	10.63	10.63	10.63	10.63	10.63
10	11.19	11.19	11.19	11.19	11.19	11.19	11.19	10.92	10.92	10.92	10.92	10.92	10.92	12.85
16	11.06	11.06	11.06	11.06	11.06	11.06	11.06	11.06	11.06	11.06	11.06	11.06	11.06	11.06
20	10.44	10.44	10.44	10.44	10.44	10.44	10.44	6.00	6.00	12.20	12.20	12.20	12.20	12.20
30	5.92	5.92	5.92	5.92	5.92	5.92	5.92	5.92	5.92	5.92	5.92	5.92	5.92	5.92
36	1.61	1.61	1.61	1.61	1.61	1.61	1.61	-1.61	-1.61	-1.61	-1.61	5.92	5.92	5.92
38	0.63	0.63	0.63	0.63	0.63	0.63	0.63	-0.63	-0.63	-0.63	-0.63	-0.63	9.37	9.37

Distance from right support (ft)	Shear connector number (near left support)							Shear connector number (near right support)						
	1, 2	3, 4	5, 6	7, 8	9, 10	11, 12	13, 14	27, 28	25, 26	23, 24	21, 22	19, 20	17, 18	15, 16
0	8.34	8.34	8.34	8.34	8.34	8.34	8.34	8.34	8.34	8.34	8.34	8.34	8.34	8.34
2	9.68	9.68	9.68	9.68	9.68	9.68	9.68	8.01	8.01	8.01	8.01	8.01	14.49	14.49
4	10.63	10.63	10.63	10.63	10.63	10.63	10.63	7.30	7.30	7.30	13.12	13.12	13.12	13.12
10	12.85	10.92	10.92	10.92	10.92	10.92	10.92	11.19	11.19	11.19	11.19	11.19	11.19	11.19
16	11.06	11.06	11.06	11.06	11.06	11.06	11.06	11.06	11.06	11.06	11.06	11.06	11.06	11.06
20	12.20	12.20	12.20	12.20	12.20	6.00	6.00	10.44	10.44	10.44	10.44	10.44	10.44	10.44
30	5.92	5.92	5.92	5.92	5.92	5.92	5.92	5.92	5.92	5.92	5.92	5.92	5.92	5.92
36	5.92	5.92	5.92	-1.61	-1.61	-1.61	-1.61	1.61	1.61	1.61	1.61	1.61	1.61	1.61
38	9.37	9.37	-0.63	-0.63	-0.63	-0.63	-0.63	0.63	0.63	0.63	0.63	0.63	0.63	0.63

References

- AASHTO (2007). "LRFD Bridge Design Specifications Interim Customary U.S. Units, 4th Edition." American Association of State Highway and Transportation Officials, Washington, D.C.
- AASHTO (2002). "Standard Bridge Design Specifications (2002) 17th Edition." American Association of State Highway and Transportation Officials, Washington, D.C.
- AASHTO (2005). "Guide Manual for Condition Evaluation and Load and Resistance Factor Rating (LRFR) of Highway Bridges." American Association of State Highway and Transportation Officials, Washington, D.C.
- AASHTO (2003). "Manual for Condition Evaluation of Bridges, Second Edition." American Association of State Highway and Transportation Officials, Washington, D.C.
- ABAQUS (2007). "ABAQUS Analysis User's Manual (Ver. 6.7)." ABAQUS, Inc, Pawtucket, RI.
- ACI (2005). "Building Code Requirements for Structural Concrete (ACI 318-05) and Commentary (ACI 318R-05)." American Concrete Institute, Farmington Hills, Michigan, 2005.
- AISC (2005). "Steel Construction Manual Thirteenth Edition." American Institute of Steel Construction, U.S.A., 2005.
- Benac, D. J. (2007). "Technical Brief: Avoiding Bolt Failures." Journal of Failure Analysis and Prevention, Vol. 7, No. 2, pp79-80.
- Bowen, C.M. and Engelhardt, M.D. (2003). "Analysis, Testing, and Load Rating of Historic Steel Truss Bridge Decks." Center for Transportation Research Report, CTR 1741-2, University of Texas at Austin.
- Daniels, J.H. and Fisher, J.W. (1966). "Fatigue Behavior of Continuous Composite Beams." Fritz Engineering Laboratory Report No. 324.1, Lehigh University.
- Dallam, L.N. (1970). "Static and Fatigue Properties of High-Strength Bolt Shear Connectors." Missouri Cooperative Highway Research Program Report 70-2, Engineering Experiment Station, University of Missouri-Columbia.

- Dedic, D.J. and Klaiber, F.W. (1984). "High-Strength Bolts as Shear Connectors in Rehabilitation Work." *Concrete International*, Vol. 6, No. 7, pp41-46.
- El-Lobody, E. and Lam, D. (2003). "Finite Element Analysis of Steel-Concrete Composite Girders." *Advances in Structural Engineering*, Vol. 6, No. 4, pp267-281.
- Hungerford, B.E. (2004). "Methods to Develop Composite Action in Non-Composite Bridge Floor Systems: Part II." MS Thesis, Department of Civil, Architectural and Environmental Engineering, University of Texas at Austin.
- Johnson, R.P., May, I.N. (1975). "Partial-Interaction Design of Composite Beams." *The Structural Engineer* 53(8), 305-311.
- Kalfas, C., Pavlidis, P., and Galoussis, E. (1997), "Inelastic Behavior of Shear Connection by a Method Based on FEM." *Journal of Constructional Steel Research*, Vol. 44, pp107-114.
- Kayir, H. (2006). "Methods to Develop Composite Action in Non-Composite Bridge Floor Systems: Fatigue Behavior of Post-Installed Shear Connectors." MS Thesis, Department of Civil, Architectural and Environmental Engineering, University of Texas at Austin.
- Klaiber, F. W., et al. (1983). "Strengthening of Existing Single Span Steel Beam and Concrete Deck Bridges." Final Report, Part I, Engineering Research Institute, Iowa State University.
- Lam, D. and El-Lobody, E. (2005). "Behavior of Headed Stud Shear Connectors in Composite Beam." *Journal of Structural Engineering*, 123(2), pp145-150.
- Lam, D., Elliott, K.S., and Nethercot, D.A. (2000). "Parametric Study on Composite Steel Beams with Precast Concrete Hollow Core Floor Slabs." *Journal of Constructional Steel Research*, Vol 54, pp283-304.
- Lehman, H.G., Lew, H.S., Toprac, A.A. (1965). "Fatigue Strength of 3/4 in. Studs in Lightweight Concrete." Center for Highway Research, The University of Texas at Austin.
- McGarraugh, J.B., Baldwin, J.W. (1971). "Lightweight Concrete-Steel Composite Beams." *Engineering Journal*, American Institute of Steel Construction, 8(3), 90-98.
- MTS Systems Division (2000). "Model 407 Controller Product Manual." Firmware Version 5.3.

- Oehlers, D.J., Coughlan, C.G. (1986). "The Shear Stiffness of Stud Shear Connections in Composite Beams." *Journal of Constructional Steel Research*, (6), 273-284.
- Oehlers, D.J., Johnson, R.P. (1987). "The Strength of Stud Shear Connections in Composite Beams." *Structural Engineering* 65B.2, 44-48.
- Oehlers, D.J., Sved, G. (1995) "Composite Beams with Limited-Slip-Capacity Shear Connectors." *Journal of Structural Engineering*, 121(6), 932-938.
- Ollgaard, J.G., Slutter, R.G., Fisher, J.W. (1971). "Shear Strength of Stud Shear Connectors in Lightweight and Normal-Weight Concrete." *AISC Engineering Journal*, 8, 55-64.
- Queiroz, F.D., Vellasco, P.C.G.S., and Nethercot, D.A. (2007). "Finite Element Modeling of Composite Beams with Full and Partial Shear Connection." *Journal of Constructional Steel Research*, Vol. 63, pp 505-521.
- Schaap, B. A. (2004). "Methods to Develop Composite Action in Non-Composite Bridge Floor Systems: Part I." MS Thesis, Department of Civil, Architectural and Environmental Engineering, University of Texas at Austin.
- Slutter, R.G., Fisher, J.W. (1966). "Fatigue Strength of Shear Connectors." *Highway Research Record* 147, 65-88.
- Taly, N. (1998). "Design of Modern Highway Bridges." McGraw-Hill, New York, NY.
- Thurlimann, B. (1959). "Fatigue and Static Strength of Stud Shear Connectors." *Journal of the American Concrete Institute*, 1287-1301.
- Toprac, A. A. (1965). "Fatigue Strength of ¾-Inch Stud Shear Connectors." *Highway Research Record*. 103, 53-77.
- TxDOT (2004). "Standard Specifications for Construction and Maintenance of Highways, Streets, and Bridges." Texas Department of Transportation, Austin, TX.
- Viest, I.M. et al. (1997). "Composite Construction: Design for Buildings." McGraw-Hill, New York, NY.
- Viest, I.M., Fountain, R. S., Siess, C.P. (1958). "Development of the New AASHTO Specification for Composite Steel and Concrete Bridges." *HRB Bull.* 174, 1-17.

VITA

Gun Up Kwon was born on February 2, 1977, in Seoul, South Korea, the son of Kee Eun Kwon and Myeong Ja Kim. He attended Hanyang University, Korea where he obtained his Bachelor of Science in Architectural Engineering in February 2002. He also received a Master of Science from Hanyang University in February 2004. In August 2004, he entered the Ph.D. program in the Department of Civil, Architectural and Environmental Engineering at the University of Texas at Austin.

Permanent address: 465-7 Guseo 1-dong, Geumjung-gu,

Busan 609-311 South Korea

This dissertation was typed by the author.